

Sol-Gel Synthesis of Phosphate-Based Glasses for Biomedical Applications

Thesis submitted by

Farzad Foroutan

For the degree of

DOCTOR OF PHILOSOPHY

Division of Biomaterials and Tissue Engineering
UCL Eastman Dental Institute, University College London
256 Gray's Inn Road, London, WC1X 8LD, UK.

-2015-

Declaration

I, Farzad Forouran, confirm that the work presented in this thesis is my own. Where information has been derived from other sources, I confirm that this has been included in the thesis.

**Dedicated to My Mother and
in Memory of My Father**

Acknowledgements

I would like to convey my sincere thanks and deep appreciation to those who have supported and inspired me during my PhD. First and foremost, special thanks to my supervisors Prof. Jonathan Knowles and Prof. Nora De Leeuw. I would not be able to complete my project without their invaluable guidance, encouragement and support. It has been an honour and a pleasure to work with them.

I am most thankful to the UCL Industrial Doctorate Centre in Molecular Modelling & Materials Science and UCL Graduate School for their financial support. This work was also supported by the WCU program through the National Research Centers Program funded by the Ministry of Education, Science and Technology, Republic of Korea.

I would like to thank Drs. George Georgiou, Graham Palmer, and Nicola Mordan for their advice and technical support. My colleague and friends specifically Nick Walter and Dr. Gareth Owens for their guidance and help with cell culture and ion chromatography studies. Those PhD students who graduated before me, including Nilay and In-Ho for their precious guidance during my PhD. I would also like to thank Omaer, Mustafa, and Piyaphong who made my time memorable and enjoyable in the office and the other students in our department who have been very helpful.

Outside the department, I would like to gratefully acknowledge Dr. Jesse Jokerst from the Department of Radiology at Stanford University for performing cell culture and ultrasound imaging studies. Dr. Richard Martin from the School of Engineering at Aston University for his guidance with XANES study at Diamond Light Source Centre. EPSRC NMR Service at Chemistry Department-Durham University and Dr. David Apperley for performing MAS NMR measurements.

Special thanks go to my wife, Mitra. Her understanding and encouragement helped me to move forward throughout this journey.

Most importantly, I would especially like to thank to my mother for her encouragement throughout the years in my life and I would not be able to succeed without her support. Last but not least, thanks to my sisters Farnaz and Farnoush for their support during my PhD.

Abstract

This thesis concerns the development of a new and facile sol-gel synthesis route for production of phosphate-based glasses for biomedical applications including; tissue engineering, imaging contrast agents and drug delivery systems. The structure of the prepared samples was probed by XRD, ^{31}P MAS-NMR, EDX and FTIR spectroscopy that confirmed successful synthesis and production of phosphate-based glasses *via* the sol-gel method. In this study, for the first time, quaternary phosphate-based sol-gel derived glasses in the $\text{P}_2\text{O}_5\text{--CaO--Na}_2\text{O--TiO}_2$ system with a high TiO_2 content of up to 30 mol% were synthesised. While incorporating a high percentage of titanium into the phosphate network is non-trivial *via* traditional melt-quench methods. Investigation of quaternary glasses with the general formula of $(\text{P}_2\text{O}_5)_{55}\text{--}(\text{CaO})_{25}\text{--}(\text{Na}_2\text{O})_{(20-x)}\text{--}(\text{TiO}_2)_x$, where $X = 0, 5, 10$ or 15 revealed, substituting titanium in place of sodium significantly improves the stability and prolongs the degradation of these glasses, which opens up a number of potential biomedical applications. Cell studies on titanium-stabilised glasses suggested glasses containing 5 or 10 mol% TiO_2 have optimal potential for bone tissue engineering applications. Electrospinning was used to prepare $(\text{P}_2\text{O}_5)_{55}\text{--}(\text{CaO})_{30}\text{--}(\text{Na}_2\text{O})_{15}$ glass nanospheres with a diameter size range of 200-500 nm. These glass nanospheres were used as a transient contrast agent for ultrasound imaging to label mesenchymal stem cells and it was determined *in vitro* and *in vivo* that these nanospheres had a detection limit of 5 and 9 $\mu\text{g.mL}^{-1}$, respectively. Cell counts down to 4000 could be measured with ultrasound imaging with no cytotoxicity at doses required for imaging. Glass nanospheres were also used as a carrier for drug delivery applications with a linear release of tetracycline hydrochloride molecules within the first 4 hours of the study period. Importantly, ion release studies confirmed these glass nanospheres biodegrade into an aqueous medium with degradation products that can be easily metabolised in the body. To the knowledge

of the author, this is the first report of sol-gel synthesis and electro spraying to prepare glass nanospheres at low processing temperature and the first use of such a system for both diagnostic and therapeutic purposes.

Table of Contents

CHAPTER 1.	Introduction and Literature Review	22
1.1.	Biomaterials	23
1.2.	Biomaterials classifications	24
1.2.1.	Bioinert materials	24
1.2.2.	Bioactive materials	25
1.2.2.1.	Bioactive glasses	26
1.2.3.	Bioresorbable materials	28
1.2.3.1.	Bioresorbable glasses	30
1.3.	Phosphate-based glasses	30
1.3.1.	Structure	30
1.3.2.	Synthesis methods	32
1.3.2.1.	Melt-quench	32
1.3.2.2.	Sol-gel	33
1.3.2.2.1.	Preparation of sol	35
1.3.2.2.2.	Colloid formation	36
1.3.2.2.3.	Gel formation	36
1.3.2.2.4.	Ageing and drying	37
1.3.2.2.5.	Preparation of bulk sol-gel derived glasses	38
1.3.3.	Solubility and degradation rate of phosphate-based glasses	39
1.4.	Biomaterial applications	41
1.4.1.	Orthopaedics	41
1.4.2.	Tissue engineering	42
1.4.3.	Drug delivery	45
1.4.3.1.	Therapeutic nanoparticles	46
1.4.4.	Diagnostic contrast agents	49
1.4.4.1.	Diagnostic nanoparticles	49
1.5.	Potential biomedical applications of phosphate-based glass systems	51
1.5.1.	Binary P ₂ O ₅ -TiO ₂ glasses	51
1.5.2.	Ternary P ₂ O ₅ -CaO-TiO ₂ glasses	52
1.5.3.	Ternary P ₂ O ₅ -CaO-Na ₂ O glasses	53
1.5.4.	Quaternary P ₂ O ₅ -CaO-Na ₂ O-TiO ₂ glasses	53

	References	56
CHAPTER 2.	Sol-Gel Synthesis and Characterisation of Phosphate-Based Glasses Using Triethyl Phosphate as a Phosphorus Precursor	70
2.1.	Introduction	71
2.2.	Materials and methods	72
2.2.1.	Materials	72
2.2.2.	Sol-gel synthesis methods	74
2.2.2.1.	Binary P ₂ O ₅ -TiO ₂ glasses	74
2.2.2.2.	Ternary P ₂ O ₅ -CaO-TiO ₂ glasses	75
2.2.2.3.	Ternary P ₂ O ₅ -CaO-Na ₂ O glasses	76
2.2.2.4.	Quaternary P ₂ O ₅ -CaO-Na ₂ O-TiO ₂	77
2.2.3	Drying procedure	78
2.2.4.	Structural characterisation	79
2.2.4.1.	X-ray diffraction	79
2.2.4.1.1.	XRD analysis method	80
2.2.4.2.	Energy dispersive X-ray	80
2.2.4.2.1.	EDX analysis method	81
2.2.4.3.	Nuclear magnetic resonance	81
2.2.4.3.1.	³¹ P MAS-NMR analysis method	83
2.2.4.4.	Fourier transform infrared spectroscopy	83
2.2.4.4.1.	FTIR analysis method	84
2.3.	Results	85
2.3.1.	Sample preparation	85
2.3.2.	XRD	87
2.3.2.1.	Binary P ₂ O ₅ -TiO ₂ glasses	87
2.3.2.2.	Ternary P ₂ O ₅ -CaO-TiO ₂ and P ₂ O ₅ -CaO-Na ₂ O glasses	90
2.3.2.3.	Quaternary P ₂ O ₅ -CaO-Na ₂ O-TiO ₂ glasses	91
2.3.3.	EDX	92
2.3.4.	³¹ P MAS-NMR	94
2.3.4.1.	Binary P ₂ O ₅ -TiO ₂ and ternary P ₂ O ₅ -CaO-TiO ₂ and P ₂ O ₅ -CaO-Na ₂ O glasses	94
2.3.4.2.	Quaternary P ₂ O ₅ -CaO-Na ₂ O-TiO ₂ glasses	97
2.3.5.	FTIR spectroscopy	98
2.4.	Discussion	102

	References	107
CHAPTER 3.	Sol-Gel Synthesis and Characterisation of Ternary P_2O_5-CaO-Na_2O and Quaternary P_2O_5-CaO-Na_2O-TiO_2 Glass Systems Using n-butyl Phosphate as a Phosphorus Precursor.	110
3.1.	Introduction	111
3.2.	Materials and methods	112
3.2.1.	Materials	112
3.2.2.	Sol-gel synthesis methods	113
3.2.3.	Drying procedure	114
3.2.4.	Structural characterisation methods	115
3.2.4.1.	XRD and EDX	115
3.2.4.2.	^{31}P MAS-NMR and FTIR	115
3.3.	Results	115
3.3.1.	Sample preparation	115
3.3.2.	XRD	117
3.3.3.	EDX	118
3.3.4.	^{31}P MAS-NMR	119
3.3.5	FTIR	122
3.4.	Discussion	124
	References	126
CHAPTER 4.	Bone Tissue Engineering Applications of Titanium-Stabilised Sol-Gel Derived Glasses	128
4.1.	Introduction	129
4.2.	Aims	130
4.3.	Materials and methods	131
4.3.1.	Sol-gel synthesis	131
4.3.2.	pH change measurement	131
4.3.3.	Ion release measurement	132
4.3.3.1.	Cation release	132
4.3.3.2.	Anion release	133
4.3.4.	Cell studies	133
4.3.4.1.	Cell culture	133
4.3.4.2.	Cytocompatibility assay	134

4.3.4.3.	Cell and particle imaging	135
4.4.	Results	136
4.4.1.	pH change measurement	136
4.4.2.	Ion release measurement	137
4.4.3.	Cytocompatibility	139
4.4.4.	Cell and particle imaging	140
4.5.	Discussion	144
	References	147
CHAPTER 5.	Sol-gel Synthesis and Electro spraying of Ternary (P₂O₅)_{0.55}-(CaO)_{0.30}-(Na₂O)_{0.15} Glass Nanospheres for Diagnostic and Therapeutic Applications.	149
5.1.	Introduction	150
5.2	Aims	152
5.3.	Materials and methods	153
5.3.1.	Design of electro spraying	153
5.3.2.	Synthesis of the sol for subsequent electro spraying	154
5.4.	Structural characterisation methods	155
5.4.1.	SEM	155
5.4.2.	XRD and EDX	156
5.4.3.	³¹ P MAS-NMR and FTIR	156
5.4.4.	Cell culture, labelling, and cytotoxicity	156
5.4.5.	Biodegradation monitoring	158
5.4.6.	<i>In vitro</i> ultrasound imaging	159
5.4.7.	<i>In vivo</i> ultrasound imaging	159
5.4.8.	Drug release measurement	160
5.5.	Results	160
5.5.1.	SEM and EDX	160
5.5.2.	XRD	162
5.5.3.	³¹ P MAS-NMR	163
5.5.4.	FTIR	164
5.5.5.	Ion release study	165
5.5.6.	Cytotoxicity study	166
5.5.7.	<i>In vitro</i> ultrasound imaging	168
5.5.8.	<i>In vivo</i> ultrasound imaging	171

5.5.9	Ultrasound cellular imaging	173
5.5.10.	Drug release measurement	177
5.6.	Discussion	178
	References	182
CHAPTER 6.	General Discussion and Future Directions	187
	References	192
APPENDICIES		193
	Appendix I	194
	Appendix II: List of publications	199
	Appendix III: List of conferences	200

List of Tables

CHAPTER 1

Table 1.1.	Surface tension and boiling points of various solvents.	39
------------	---	----

CHAPTER 2

Table 2.1.	Theoretical compositions of sol-gel synthesised phosphate-based glasses using triethyl phosphate as a phosphorus precursor.	72
------------	---	----

Table 2.2.	Effect of heat treatment on phosphate-based sol-gel derived glasses using triethyl phosphate as a phosphorus precursor.	87
------------	---	----

Table 2.3.	Intended compositions and measured values of sol-gel derived glasses using triethyl phosphate as a phosphorus precursor determined by EDX (in parentheses).	93
------------	---	----

Table 2.4.	³¹ P MAS-NMR peak parameters of binary and ternary phosphate-based sol-gel derived glasses using triethyl phosphate as a phosphorus precursor.	96
------------	---	----

Table 2.5.	³¹ P MAS-NMR peak parameters of quaternary P ₂ O ₅ -CaO-Na ₂ O-TiO ₂ sol-gel derived glasses using triethyl phosphate as a phosphorus precursor.	98
------------	---	----

Table 2.6.	Infrared band assignment of phosphate-based sol-gel derived glasses using triethyl phosphate as a phosphorus precursor. (ν, stretching; s, symmetric; as, asymmetric).	101
------------	--	-----

CHAPTER 3

Table 3.1.	Compositions of starting solution for ternary P ₂ O ₅ -CaO-Na ₂ O and quaternary P ₂ O ₅ -CaO-NaO-TiO ₂ sol-gel derived samples using n-butyl phosphate as a phosphorus precursor.	112
------------	--	-----

Table 3.2.	The effect of drying procedure in ternary P ₂ O ₅ -CaO-Na ₂ O and quaternary P ₂ O ₅ -CaO-Na ₂ O-TiO ₂ sol-gel derived samples using n-butyl phosphate as a phosphorus precursor.	116
------------	--	-----

Table 3.3.	Intended compositions and measured values of sol-gel derived glasses using n-butyl phosphate as a phosphorus precursor determined by EDX (in parentheses).	119
------------	--	-----

Table 3.4.	³¹ P MAS-NMR peak parameters of ternary P ₂ O ₅ -CaO-Na ₂ O	121
------------	---	-----

and quaternary P_2O_5 -CaO- Na_2O - TiO_2 sol-gel derived glasses using n-butyl phosphate as a precursor.

Table 3.5.	Infrared band assignment of phosphate-based sol-gel derived glasses using n-butyl phosphate as a phosphorus precursor.	122
------------	--	-----

CHAPTER 4

Table 4.1.	The theoretical compositions of phosphate-based sol-gel derived glasses using n-butyl phosphate as a phosphorus precursor.	131
------------	--	-----

CHAPTER 5

Table 5.1.	Intended composition and measured values of sol-gel derived glasses determined by EDX (in parentheses).	162
Table 5.2.	^{31}P MAS-NMR peak parameters of phosphate-based glass nanospheres.	169

List of Figures

CHAPTER 1

- Figure 1.1. Schematic phosphate structure as a function of composition. 32
- Figure 1.2. Four types of aggregated colloids that are coacervates, tactoid, crystalloids, and flocks. 36
- Figure 1.3. Tissue engineering concept includes; (a) isolating patients' cells, (b) *in vitro* cultivation of cells on a two-dimensional surface, (c) seeding cells in a porous scaffold and adding growth factors, small molecules and etc., (d) further cell cultivation in bioreactor, and (e) transplantation of the engineered tissue. 43

CHAPTER 2

- Figure 2.1. Structure of; (a) triethyl phosphate, (b) titanium isopropoxide, (c) 2-methoxyethanol, (d) *n*-dimethyl formamide, (e) calcium methoxyethoxide, and (f) sodium methoxide solution. 73
- Figure 2.2. Schematic of the sol-gel synthesis of binary P_2O_5 - TiO_2 glasses. 74
- Figure 2.3. Flow diagram of the sol-gel synthesis of ternary P_2O_5 - TiO_2 -CaO glasses. 75
- Figure 2.4. Schematic of the sol-gel synthesis of ternary P_2O_5 -CaO- Na_2O glasses. 76
- Figure 2.5. Schematic of the sol-gel synthesis of quaternary P_2O_5 -CaO- Na_2O - TiO_2 glasses. 77
- Figure 2.6. Heat treatment diagram for the sol-gel synthesised phosphate-based glasses. 78
- Figure 2.7. Representations of PO_4 tetrahedra with various polymerisation. 83
- Figure 2.8. Photographs of heat treated; (A) $EP_{55}T_{45}$, (B) $EP_{50}T_{50}$, (C) $EP_{55}CT_{30}$, and (D) $EP_{55}CNT_{15}$ sol-gel derived glasses. 86
- Figure 2.9. XRD patterns of binary sol-gel derived samples in P_2O_5 - TiO_2 system using triethyl phosphate as a phosphorus precursor. Crystalline patterns were observed for $EP_{65}T_{35}$ and $EP_{70}T_{30}$ 88

	sol-gel derived samples.	
Figure 2.10.	XRD patterns of; (a) EP ₆₅ T ₃₅ and (b) EP ₇₀ T ₃₀ sol-gel derived samples. Crystalline phases were identified using the Crystallographica Search-Match software which are corresponded to TiP ₂ O ₇ crystalline structure.	89
Figure 2.11.	XRD patterns of ternary sol-gel derived glasses in the P ₂ O ₅ -CaO-TiO ₂ system using triethyl phosphate as a phosphorus precursor. All patterns are free from any detectable crystalline phases.	90
Figure 2.12.	XRD patterns of ternary sol-gel derived glasses in the P ₂ O ₅ -CaO-Na ₂ O systems using triethyl phosphate as a phosphorus precursor which showed no evidence of any detectable crystalline phases.	91
Figure 2.13.	XRD patterns of the quaternary sol-gel derived samples in P ₂ O ₅ -CaO-Na ₂ O-TiO ₂ system using triethyl phosphate as a phosphorus precursor which are free from any detectable crystalline phase.	92
Figure 2.14.	³¹ P MAS-NMR spectra of binary P ₂ O ₅ -TiO ₂ sol-gel derived glasses using triethyl phosphate as a phosphorus precursor. The peaks correspond to mainly Q ¹ and Q ² phosphate units.	94
Figure 2.15.	³¹ P MAS-NMR spectra of ternary sol-gel derived glasses using triethyl phosphate as a phosphorus precursor in; (a) P ₂ O ₅ -CaO-TiO ₂ and (b) P ₂ O ₅ -CaO-Na ₂ O systems. The peaks correspond to mainly Q ¹ and Q ² phosphate units.	95
Figure 2.16.	³¹ P MAS-NMR spectra of quaternary P ₂ O ₅ -CaO-Na ₂ O-TiO ₂ sol-gel derived glasses using triethyl phosphate as a phosphorus precursor. The peaks correspond to mainly Q ¹ and Q ² phosphate units.	97
Figure 2.17.	FTIR spectra of binary P ₂ O ₅ -TiO ₂ sol-gel derived glasses using triethyl phosphate as a phosphorus precursor.	99
Figure 2.18.	FTIR spectra of ternary sol-gel derived glasses using triethyl phosphate as a phosphorus precursor in; (a) P ₂ O ₅ -CaO-TiO ₂ and (b) P ₂ O ₅ -CaO-Na ₂ O systems.	100
Figure 2.19	FTIR spectra of quaternary P ₂ O ₅ -CaO-Na ₂ O-TiO ₂ sol-gel derived glasses using triethyl phosphate as a phosphorus precursor.	101

Figure 2.20. Schematic setup to analyse the evaporated gas from ternary EP₅₅CN₂₀ sol-gel derived sample via FTIR spectroscopy during the heat treatment cycle. 104

Figure 2.21. FTIR spectra of ternary EP₅₅CN₂₀ sol-gel derived sample during the heat treatment cycle from 100 to 220 °C. 105

CHAPTER 3

Figure 3.1. Structural formula of n-butyl phosphate; a mixture of (a) mono butyl phosphate (C₄H₁₁O₄P) and (b) di-butyl phosphate (C₈H₁₉O₄P). 113

Figure 3.2. Schematic sol-gel synthesis of; (A) ternary P₂O₅-CaO-Na₂O and (B) quaternary P₂O₅-CaO-Na₂O-TiO₂ samples using n-butyl phosphate as a phosphorus precursor. 114

Figure 3.3. Photographs of; A) BP₄₀CNT₂₅, B) BP₄₀CNT₃₀, and C) BP₅₅CNT₁₅ sol-gel derived glasses using n-butyl phosphate as a phosphorus precursor. The scale bar for A, B, and C is 1 cm. 116

Figure 3.4. XRD patterns of ternary P₂O₅-CaO-Na₂O sol-gel derived samples using n-butyl phosphate as a phosphorus precursor that are free from any detectable crystalline phase. 117

Figure 3.5. XRD patterns of quaternary P₂O₅-CaO-Na₂O-TiO₂ sol-gel derived samples using n-butyl phosphate as a phosphorus precursor that showed no evidence of any detectable crystalline phase. 118

Figure 3.6. ³¹P MAS-NMR spectra of; (a) ternary P₂O₅-CaO-Na₂O and (b) quaternary P₂O₅-CaO-Na₂O-TiO₂ sol-gel derived glasses using n-butyl phosphate as a phosphorus precursor. The peaks correspond to mainly Q¹ and Q² phosphate units. 120

Figure 3.7. FTIR spectra of; (a) ternary P₂O₅-CaO-Na₂O and (b) quaternary P₂O₅-CaO-Na₂O-TiO₂ sol-gel derived glasses using n-butyl phosphate as a phosphorus precursor. 123

CHAPTER 4

Figure 4.1. pH measurement after 0, 1, 3 and 7 days immersion of sol-gel derived glass microparticles in deionised water that 137

	shows significant decrease in pH after 24 hours. Error bars represent the standard deviation of 3 samples.	
Figure 4.2.	Cumulative release of (a) Ca^{2+} and (b) Na^+ cations and (c) $\text{P}_2\text{O}_7^{4-}$, (d) $\text{P}_3\text{O}_{10}^{5-}$, (e) $\text{P}_3\text{O}_9^{3-}$ and (f) PO_4^{3-} anions from sol-gel derived glass microparticles after 1, 3 and 7 days storage in deionised water. Error bars represent the standard deviation of 3 samples.	138
Figure 4.3.	Cytocompatibility of sol-gel glass microparticles containing 0, 5, 10 or 15 mol% Ti with MG-63 at 1, 3 and 7 days. Dotted line represents initial seeding density. Error bars represent the standard deviation of 3 samples.	139
Figure 4.4.	Scanning electron micrographs showing particles morphology and cell attachment. (A, B) Control (cells on cell culture support), (C, D) Ti0, (E, F) Ti5, (G-I) Ti10, and (J, K) Ti15.	142
Figure 4.5.	Confocal micrographs showing cells attached to sol-gel glass microparticles containing (A, B) 5 or (C, D) 10 mol% TiO_2 . The green fluorescent stain (phalloidin) shows filamentous actin and red (propidium iodide) shows nuclei.	143
CHAPTER 5		
Figure 5.1.	Schematic of the electrospraying setup including; syringe pump, nozzle (stainless steel needle), high voltage supply, collection substrate, and hot plate. The high voltage between the nozzle and the ground creates nanospheres from the needle tip and these are propelled toward the heated silicone oil as a substrate to obtain dried gel nanospheres.	154
Figure 5.2.	SEM image of (A, B) washed and heat-treated PGNs (the scale bars represent 5 and $2\mu\text{m}$) and (C, D) dispersed PGNs in ethanol solution after heat-treatment (the scale bars represent $2\mu\text{m}$). The PGNs have an approximate size distribution of 200 - 500 nm with a mean diameter of 320 nm based on measurement of more than 100 particles.	161
Figure 5.3.	The XRD pattern of PGNs which is free from any detectable crystalline phase.	162
Figure 5.4.	^{31}P MAS-NMR spectrum of PGNs that correspond to mainly	163

	Q ¹ and Q ² phosphate units.	
Figure 5.5.	FTIR spectrum and band assignment for PGNs (ν , stretching; s, symmetric; as, asymmetric).	164
Figure 5.6.	Cumulative release of phosphorus, calcium, and sodium in deionized water as a function of time for the investigated PGNs. Error bars represent the standard deviation of 3 samples.	165
Figure 5.7.	Increasing concentrations of PGNs were used to label MSCs for 4 hours followed by treatment with different markers of cytotoxicity. All experiments were validated with a positive control (POS). A) Cells were plated, tagged with DCFDA, and then perturbed with PGNs. Any ROS generation resulted in fluorescence from the DCFDA probe. Only the 1000 $\mu\text{g.mL}^{-1}$ sample significantly upregulated ROS. A hydrogen peroxide positive control validated the assay. The negative control was wells with no cells. B) The MTS reagent measures cell metabolism and showed no decrease at any concentration studied. Here, we used both freshly dissolved PGNs (fresh) and PGNs that had been in solution for 24 hours (degraded). No concentration decreased metabolism. Error bars represent the standard deviation of 6 wells.	167
Figure 5.8.	Ultrasound images in the z-axis for inclusions with 0 mg.mL^{-1} PGNs (A) and 1 mg.mL^{-1} PGNs at 40 MHz (B). The increased backscatter results from the increasing number of particles that was further quantified for multiple fields of view in (C). PGNs (0.25 mg.mL^{-1}) at various time points were imaged with ultrasound to understand how signal changes as a function of time (D). These data indicate that ultrasound signal decreases as the PGNs degrades because of decreased acoustic impedance. The imaging window is within the first four hours of dissolution.	169
Figure 5.9.	Panel A is an ultrasound image in the z-axis for 1 mg.mL^{-1} PGNs at 16 MHz, and B is signal and signal-to-background for both 16 and 40 MHz. Here, the signal was defined as echogenicity of the sample and background was adjacent	170

agar. While the signal was higher at 40 MHz, the signal-to-background at 16 MHz was 4.6-fold higher than 40 MHz because of a lower background signal. These data indicate that the PGNs are suitable for imaging at both clinical and pre-clinical frequencies.

- Figure 5.10. Nude mice received 100 μL boluses of 2 $\text{mg}\cdot\text{mL}^{-1}$ PGNs in 1:1 matrigel:PBS and imaged at 40 MHz immediately after implantation (A) and 1 day after (B). Red outlines in A and B indicate the region of implantation. 172
- Figure 5.11. Decreasing concentrations of PGNs were also implanted to calculate the limit of detection and variance between animals (A). Error bars represent the standard error of measurement. Changes in ultrasound backscatter for PGNs indicate a 3.5-fold decrease in signal-to-background ratio (SBR) (B). Error bars represent the standard deviation. 173
- Figure 5.12. The optimal labeling conditions were tested empirically including starting concentration of PGNs (A) and incubation time (B). We found a nearly linear relationship between starting concentration and cell fluorescence (A). These concentrations used 2 hours of labeling. In B, we studied the effect of time and found that incubation times beyond 2 hours offered no additional signal. (C) MSCs labelled with these conditions (500 $\mu\text{g}\cdot\text{mL}^{-1}$ and 2 hours) were imaged with 40 MHz ultrasound—the limit of detection is 4000 MSCs. 175
- Figure 5.13. Phase contrast/fluorescence microscopy of naive MSCs (A) and MSCs labelled with PGNs shows that fluorescence only corresponds to the cells (low non-specific binding) (B). Panel C is ultrasound image of blank agarose phantom (no cells), panel D is the ultrasound backscatter from 225,000 MSCs, and panel E is the same number MSCs labelled with PGNs in an agar phantom. The PGNs increased the backscatter two-fold versus unlabelled cells. Panel F is a confocal image through the medial slice of adherent cells labelled with fluorescently tagged PGNs. The image shows that the nanoparticles are located throughout the cell and 176

are localized in the cytoplasm and are not simply on the cell surface.

- Figure 5.14. TCH release measurement of drug-loaded PGNs determined *via* UPLC. Highest release occurred within the first 4 hours of the entire study. Error bars represent the standard deviation of 3 samples. 177

APPENDICES

- Figure A.1. Schematic of sol-gel synthesis of phosphate-based glasses to prepare thin film coating, glass nanospheres *via* electro spraying and subsequent heat-treatment or to obtain bulk glasses *via* carefully controlled heat-treatment of the gel over three weeks. 195
- Figure A.2. Various electro spraying modes (A) and steps of nanospheres production *via* electro spraying (B) 196
- Figure A.3. SEM images of sol-gel derived glasses (after heat-treatment) created by electro spraying at; A) voltage of 12 kV and flow rate of 1 mL.h⁻¹, B) voltage of 15 kV and flow rate of 0.5 mL.h⁻¹, C) voltage of 18 kV and flow rate of 0.5 mL.h⁻¹, D) voltage of 20 kV and flow rate of 0.4 mL.h⁻¹, and voltage of 20 kV and flow rate of 0.2 mL.h⁻¹ (E and F). 197
- Figure A.4. Photographs of; electro spray deposition of quaternary (P₂O₅)₅₅-(CaO)₂₅-(Na₂O)₁₀-(TiO₂)₁₀ glass on (A) aluminium foil and (B) titanium disc. C) SEM image of coated titanium disc after heat-treatment at 250 °C. 198

Abbreviations

HA	Hydroxyapatite
SBF	Simulated Body Fluid
PLLA	Poly-L-Lactic Acid
PGA	Polyglycolic Acid
PLA	Poly(lactic Acid)
HCA	carbonated hydroxyapatite
PCA	Poly Cyanoacrylate
PCL	Poly (ϵ -Caprolactone)
XRD	X-Ray Diffraction
FTIR	Fourier Transform Infrared
EDX	Energy Dispersive X-Ray
^{31}P MAS-NMR	^{31}P Magic Angle Spinning Nuclear Magnetic Resonance
<i>n</i> -DMF	<i>n</i> -Dimethyl Formamide
SEM	Scanning Electron Microscopy
CLSM	Confocal Laser Scanning Microscopy
IC	Ion Chromatography
ICP-MS	Inductively Coupled Plasma Mass Spectroscopy
PGN	Phosphate-based Glass Nanospheres
UPLC	Ultra Performance Liquid Chromatography
DCFDA	2',7' -Dichlorofluorescein Diacetate
MSC	Human mesenchymal stem cell
MTS	3-(4,5-dimethylthiazol-2-yl)-5-(3-carboxymethoxyphenyl)- (4-sulfophenyl)-2H-tetrazolium
DMSO	Dimethyl Sulfoxide
HBSS	Hanks Buffered Saline Solution
SB	Signal-to-Background
TCH	Tetracycline Hydrochloride
POS	Positive Control
NEG	Negative Control
ROS	Reactive Oxygen Species

CHAPTER 1

Introduction and Literature Review

1.1. Biomaterials

Over the past 50 years, medical care has been developed and human life expectancy has increased dramatically. Since the mean age of the population of developed countries is continuously increasing, there is a significant and growing need for materials to replace diseased or damaged human tissues. These materials are required to be compatible with the body, that is related to the behaviour of the material in various contexts. They must have the ability to perform with an appropriate host response in a specific situation which considered to be one of the most specific properties of biomaterials and is called biocompatibility. A biocompatible material must elicit minimal immune response and should not disturb the blood flow (Cook et al., 2003).

Ceramics have shown great potential as biomaterials, due to their physicochemical properties. Almost any ceramic material that is not toxic can be potentially used as a biomaterial and can be defined as substances that augment the function of soft and hard tissues such as repair and reconstruction of bone defects and diseased or damaged musculoskeletal system (Ben-Nissan, 2004). Bioceramic materials are inorganic and usually contain both metallic and non-metallic elements where the atomic bonding is almost entirely ionic and can be subclassified as amorphous and crystalline. Amorphous bioceramics show order only on a very short length scale and are called glasses, but crystalline bioceramics show regular atomic arrays over large distances.

Bioceramics have a long history but only since the 1960s with the improvement of surgical techniques, the replacement of body parts has become more commonplace (Hench and Wilson, 1991, Peppas and Langer, 1994). Undoubtedly, bioceramics have had a great impact on the practice of contemporary medicine and patient care in both saving, and improving the quality of the lives of humans and

animals. Some of their major clinical applications are in dentistry, orthopaedics, maxillofacial surgery, and more recently drug delivery and imaging contrast agents (Jones and Hench, 2003, Vallet-Regi and Ruiz-Hernandez, 2011, Jokerst et al., 2013, Foroutan et al., 2015).

1.2. Biomaterial classifications

Biomaterials can be derived either from natural or synthetic components and can be classified into two main categories: *biological* with a natural origin or *biomedical* with an artificial origin. The main problems with the biological materials are their limitation of the amount that can be collected and increasing the risk of viral and bacterial infections (Chai et al., 2011) as well as control of sample to sample and batch to batch variability. While artificial materials can be supplied from a variety of materials (polymers, ceramics, and metals) and can be sterilised to reduce the risk of bacterial infections.

One of the main material groups being developed are bioceramics, since they show very good interaction with their surrounded tissues. According to their biological response, bioceramics can be classified as (Hulbert et al., 1982); 1) bioinert (alumina and zirconia), 2) bioactive or surface reactive (sintered HA and bioglass), and 3) bioresorbable (phosphate-based glasses).

1.2.1. Bioinert materials

Up to a few decades ago, bioceramics were expected to have appropriate physical properties to suit the function of the replaced tissue with minimal cytotoxicity (Hench, 1980). Bioinert materials belong to the first generation of bioceramics and are characterised to be accepted by the body with minimal or low interaction with

the physiological environment. These materials do not elicit a significant response from the body and a mechano-chemical bond is formed with the bone and tissue. They are typically based on dense or porous ceramics such as alumina or zirconia. Alumina ceramics have proven their bioinertness with high hardness and abrasion resistance mainly for dental and orthopaedic applications. According to the American Society for Testing and Materials (ASTM), alumina implants should contain 99.5 % pure alumina and other alkali oxides with less than 0.1 % of SiO_2 (Park, 2003). Zirconia ceramics are in clinical use in total hip replacement because of their inertness, high mechanical strength and fracture toughness (Hentrich et al., 1969).

1.2.2. Bioactive materials

The second generation of bioceramics is defined as bioactive with a surface that has a spontaneous capability to interact with physiological fluids in the human body and form a bone-like layer which is very similar to the mineral phase of the bone. The bone-like layer made of hydroxyapatite (HA) and can exhibit fast reaction kinetics that results in the formation of a good chemical bond between the material and the tissue at the interface (Kokubo et al., 2003). This property makes these materials ideal for various biomedical applications such as orthopaedics and dental prosthetics to induce regeneration of the damaged bone and tissue. As research developed from bioinert toward bioactive ceramics, scientists focused on their different structures (crystalline, glass, and glass-ceramic). They found that the compositions that mimicked the inorganic component of bone, could form a good interaction with hard and soft tissues (Urist et al., 1994). One of the most widely used crystalline bioactive ceramic is dense HA (hydroxyapatite). However, it shows poor mechanical properties which limit its application to space filling or use as a

coating for other biomaterials with good mechanical properties. Meanwhile, among amorphous bioactive ceramics, silicate-based glasses have been more popular, with good interaction with the bone and surrounding tissues (Hench and Wilson, 1991, Hench, 1998).

1.2.2.1. Bioactive glasses

Generally, the term glass includes every solid that possesses a non-crystalline structure and exhibits a glass transition when heated towards the liquid state. Bioactive glasses have been defined as materials that induce a specific biological activity and show specific surface reaction when implanted into the body (Rahaman et al., 2011). Indeed, one of the most attractive features of glasses is their non-stoichiometry and thus compositional flexibility, which allows researchers to tailor the properties to the end application. These glasses also have the potential to initiate a range of biological responses by releasing ions into the local environment (Hench and Wilson, 1984). The most applicable bioactive glasses are silicate-based glasses that have been used extensively in non-load bearing applications and there is a possibility to design these glasses with specific clinical properties, mainly for tissue regeneration applications (Hench and Wilson, 1991). The first silicate-based bioactive glass was discovered by Hench *et al.* (Hench and Wilson, 1991, Hench, 1998) as a second generation of biomaterials with a reactive surface which could exhibit reaction kinetics to bond with the bone at the interface (Hench and Polak, 2002). The base components of these bioactive glasses are usually SiO_2 (silicate is the main component), Na_2O , CaO , and P_2O_5 . These glasses are stable to hydrolysis because of their high silica content, but they can promote direct osteoblast cell attachment and proliferation. Studies have shown that the content of Si cations in the human body varies, around 100 ppm in bone and ligaments to

around 200-600 ppm in cartilage and other connective tissues. Release of Si^{4+} ions in an aqueous medium has been demonstrated to promote osteoblast proliferation, differentiation and collagen production (Carlisle, 1970, Pietak et al., 2007). However, glasses with a significantly lower molar ratio of Ca and P do not generate direct bonding with the bone.

The most studied silica-based glass composition is 45S5 bioglass[®], which contains 45% SiO_2 , 24.5% Na_2O , 24.5% CaO and 6% P_2O_5 in weight. The bioactivity and bone bonding of the 45S5 bioglass[®] is attributed to the formation of a carbonate-substituted hydroxyapatite-like (HCA) layer on the glass surface in contact with the body fluid. This layer is similar to the mineral constituent of the bone and bonds firmly with the living bone and tissue (Hench, 1998). *In vitro* studies on the bioactivity of these glasses is typically performed in simulated body fluid (SBF), which is an aqueous solution whose composition of inorganic ions is almost equal to blood plasma. This method is an easy way to evaluate the surface reactivity of a material and if a layer of HCA is formed on the material surface, then the material is considered as bioactive and can bond with the living tissue on implantation (Kokubo and Takadama, 2006). The presence of silanol groups and the textural properties, such as porosity and pore volume, seem to play a significant role in the formation of the apatite layer on their surfaces (Cho et al., 1998, Pereira et al., 1995). Presumably, the adsorption of PO_4^{3-} by hydrogen bonding and Ca^{2+} ions on the silica surface induce the precipitation of the apatite-like layer (Li et al., 1992, Andersson and Karlsson, 1991). These bioglasses have been used to repair jaw defects caused by periodontal disease or hard tissue replacement such as the small bone in the middle ear (Rust et al., 1996). The main advantage of these glasses is rapid connection to the tissue, however, there are some questions raised regarding their slow degradation, the long term effects of silica in the body, and the

poor mechanical properties that may limit the application of these glasses for bone replacement purposes.

1.2.3. Bioresorbable materials

Different terms (e.g. degradable, resorbable, absorbable) are used to indicate that a given material will gradually disappear after being introduced into a living organ and is defined as a third generation of biomaterials. These materials react and dissolve in the physiological fluid and can be replaced by bone and tissue cells over a specific period of time (Vallet-Regi, 2001). Bioresorbable materials offer a potential solution to complications such as tissue irritation and inflammation that may require secondary surgery to remove the implant. The degradation rate of these materials should not exceed the rate of tissue formation and to ensure a gradual stress transfer from implant to tissue, the rate at which the implant weakens should be matched with the increase in tissue strength. The newly replaced tissue is completely biological and should have very similar properties to the surrounding tissue.

A good bioresorbable material should have the following properties:

- I. Dissolution rate matches with the regeneration rate of the damaged tissue
- II. The interface between tissue and implant remains stable during the regeneration
- III. The break-down components are easily metabolised in the body

The use of polymers as bioresorbable materials has been extensively studied. One of the earliest studies on bioresorbable materials was done by Kulkarni *et al.* (Kulkarni et al., 1966) who studied the application of poly-L-lactic acid (PLLA) with

the slow degradation rate in animals and no serious tissue reactions. Later, the use of various bioresorbable materials such as polyglycolic acid (PGA) and polylactic acid (PLA) led to materials with better biodegradation (Rokkanen et al., 2000). However, the degradation of these polymer-based systems could result in polymer fragments with heterogeneous chain-lengths that may lead to toxicity (Suuronen et al., 2004).

Calcium phosphate ceramics are generally bioactive and have been widely used in medicine as bone substitutes, maxillofacial reconstruction, dental implant coatings, and orthopaedic prostheses. These ceramics show excellent biocompatibility because of their chemical and structural similarities to the inorganic phase of human bone, but only some of them are bioresorbable. Bioresorbability of these ceramics depends on the composition, porosity, particle size, and preparation condition. For example, pure hydroxyapatite sintered at high temperature is minimally resorbable, whereas, it is resorbable if sintered at lower temperatures (900 °C) (LeGeros, 2008). Tricalcium phosphate ceramics are also known as bioresorbable materials with a greater dissolution rate in comparison to the hydroxyapatite and are usually resorbed within one month of implantation (Suzuki et al., 1997). These bioresorbable ceramics have been used clinically as a bone filler to repair periodontal defects, augmentation, and have been formed into a number of different geometries, to be used as a drug delivery system (Park, 2003, Damien and Parsons, 1991). Phosphate-based glasses may also offer a great potential for soft and hard tissue regeneration since they are bioresorbable with a controllable solubility by altering their compositions (Franks et al., 2000, Knowles, 2003).

1.2.3.1. Bioresorbable glasses

Phosphate-based glasses seem to be an attractive material for biomedical applications since they are highly biocompatible with controllable degradation rate and break-down components that can easily be metabolised in the body (Knowles, 2003, Kiani et al., 2012). Studies confirmed that these glasses show a controllable degradation rate in aqueous medium (from a few days to several months) and can be used when the implant is needed for a certain length of time (mostly short term and non-load bearing applications) to promote healing or growth surrounding damaged tissue or to enhance and promote tissue regeneration through the delivery of cells and bone growth factors (Knowles, 2003, Navarro et al., 2003b). The addition of metal oxides such as TiO_2 and Fe_2O_3 to these glasses can increase their durability to make them more applicable to be used as a third generation of biomaterials in the field of tissue engineering (Knowles, 2003, Pickup et al., 2008b, Ahmed et al., 2004a, Lakhkar et al., 2012).

1.3. Phosphate-based glasses

1.3.1. Structure

Phosphate-based glasses are inorganic polymers based upon the tetrahedral phosphate anion, which is linked to form a three-dimensional network (Brow, 2000). These glasses are formed of sp^3 hybrid orbitals by the phosphorus outer electrons ($3s^23p^3$). The fifth electron is promoted to the 3d orbital where strong molecular bonding orbitals are obtained with oxygen 2p electrons, which is charge balanced by polymerisation or the presence of metallic ions (Cruickshank, 1961). The tetrahedra are classified using the Q^i terminology originally devised for silicate-based glasses, but has been applied to phosphates where (i) represents the

number of bridging oxygen atoms per tetrahedron (Lippmaa et al., 1980, Abou Neel et al., 2009).

The prevalence of any particular Q^i species depends on the cation content of the glass composition. If phosphorus pentoxide is heated without adding any cation then the PO_4 tetrahedra can be attached to a maximum of three neighbouring tetrahedra forming a three-dimensional network (Q^3 species) that is named ultraphosphate (Navarro et al., 2003a, Jager et al., 2000). The Q^3 species will be the only phosphate group within highly cross-linked phosphate network. Adding metal cations such as Li^+ , Na^+ , and K^+ change the Q^3 to Q^2 species (Brow, 2000). The positive charge for every phosphate anion, with theoretically infinite phosphate chain lengths, and when the concentration of cations is equal to anions, only Q^2 species are present and is named a meta-phosphate composition (Engelhar.G, 1972, Vanwazer and Holst, 1950, Martin, 1991). The addition of further cations will form terminating Q^1 species that decrease the possible chain length and when the concentration of cations is twice the anions, only Q^1 species dominate. As this anion can only form on oxygen bridges, it is termed a chain terminator, producing only phosphate dimers, or pyrophosphate, when it is the only species present and increasing the amount of cations up to three times higher the number of anions changes the Q^1 to Q^0 species and is denoted orthophosphate (Engelhar.G, 1972, Vanwazer and Holst, 1950, Martin, 1991). Contamination with water can also cause compositional anomalies when making phosphate glasses. Water has a similar role to alkali oxides, which reduces the polymerisation by the formation of hydroxyl groups (Brow et al., 1990). **Figure 1.1** shows the schematic phosphate structure as a function of composition.

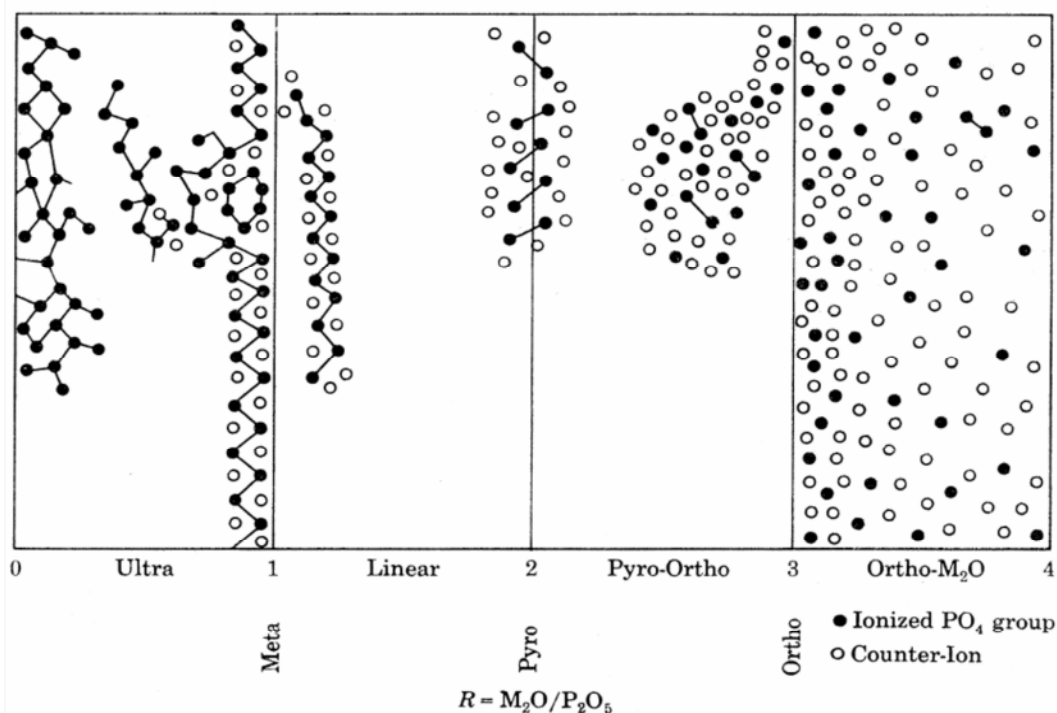


Figure 1.1. Schematic phosphate structure as a function of composition (Vanwazer and Griffith, 1955).

1.3.2. Synthesis methods

1.3.2.1. Melt-quench

In the melt-quench method a mixture of oxide precursors is melted in a furnace at temperatures of usually over 1000 °C (the exact melting temperature depends on the glass composition) and amorphous solid can be obtained by rapid quenching of the melt obtained by the fusion of one or more precursors (Lakhkar et al., 2011, Abou Neel et al., 2009). When the cooling rate is sufficiently high to suppress nucleation and crystal growth, the melt's disordered state is maintained in the solid state. To achieve a high cooling rate the melt is usually spread on a solid surface of a high thermally conductive material like steel. Alternatively, the molten glass can be poured into a preheated mould to form different shapes such as plates or rods. In this case, the mould with the molten glass is placed in an annealing furnace and

the glass is cooled down gradually to the room temperature to remove any residual stress.

Since the main component in the phosphate-based glasses (phosphorus pentoxide) is highly hygroscopic, the presence of small amounts of water can promote crystallisation (Brow et al., 1990). To overcome this problem some proportion of phosphorus can be added in the form of a stable oxides such as CaHPO_4 or NaH_2PO_4 and then adding any remaining minimal amount as pure P_2O_5 or melting the glass in ampoules or covered crucibles. For instance, to synthesise ternary P_2O_5 - CaO - Na_2O glass systems; P_2O_5 , NaH_2PO_4 , and CaCO_3 powders can be used as the sources of phosphorus, sodium and calcium. The solid mixture is melted for 0.5-2 hour in a Pt/Rh crucible in a range of 800-1550 °C depending on the composition. The melt is then poured into a metal or graphite mould and annealed to the room temperature from 350-500 °C with a cooling rate of 5-10 °C.min⁻¹ to remove any residual stresses (Franks et al., 2001, Abou Neel et al., 2009).

1.3.2.2. Sol-gel

The sol-gel method serves as a useful alternative (depending on the end application) to the conventional melt-quench method and refers to a low-temperature synthesis method by using chemical precursors in liquid form to produce ceramics and glasses with high purity and homogeneity. The interest in producing glasses *via* sol-gel routes has been increasing very rapidly since the processing temperature is usually below the crystallisation temperature of the oxide elements that allows for the production of novel glass compositions (Carta et al., 2005). Another advantage of sol-gel synthesis over the other methods is the tunable structure that allows control over the morphology, porosity, size, and the

ability to modify the surface that is not achievable *via* the melt-quench route. Such examples include spraying methods and spin casting as processing methods which allow structures such as ultra-thin and uniform coatings to be achieved.

The main advantages of the sol-gel synthesis are;

- I. High purity
- II. Homogeneity
- III. Low processing temperature that allows to incorporate different kinds of inorganic, organic, and biomolecules during the formation of a gel matrix
- IV. Low energy required in comparison with the melt-quench method
- V. A variety of shapes and morphologies can be obtained

The sol-gel process occurs where one or many elements are used to form a sol from which is obtained a homogeneous and amorphous gel solid by the transition from a liquid sol to a solid gel (Gupta and Kumar, 2008). In this process, choosing the right precursors, temperature of the precursor solutions, and appropriate ageing time have been found to be critical processing factors (Hench and West, 1990). At a very early stage of the development of sol-gel technology, the need for precursor compounds that have high solubility in an organic solvent that can easily transform into chemically reactive forms are essential. Studies have shown phosphoric acid (H_3PO_4) cannot be used as a phosphorus precursor because it is too reactive and leads to precipitation rather than gelation and more convenient precursors could be obtained by dissolving P_2O_5 into alcohol solutions (Livage et al., 1992, Christensen et al., 1990).

The interest in phosphate-based sol-gel materials has been increased by the availability of $\text{PO}(\text{OH})_{3-x}(\text{OR})_x$ (R=alkyl group) as a better phosphate precursor choice (Noda et al., 1997). Tang *et al.* (Tang et al., 2005) successfully synthesised

transparent titanophosphate sol-gel derived glasses with high refractive index for optical applications by using triethyl phosphate as a phosphorus precursor. In another study by Carta *et al.* (Carta *et al.*, 2005), quaternary phosphate-based glasses in the P_2O_5 -CaO- Na_2O - SiO_2 system with low silica content were successfully prepared by using P_2O_5 dissolved in anhydrous ethanol. Following that silicate free sol-gel glasses in the P_2O_5 -CaO- Na_2O system were successfully synthesised for biomedical application purposes (Carta *et al.*, 2007a, Lee *et al.*, 2013). The process of reacting from the liquid may allow these sol-gel derived glasses to be drawn into fibres, micro/nano-sized glass spheres, or as a thin film on a substrate. Low processing temperatures also have direct and positive implications for biomedical applications, specifically in drug delivery systems that offer molecular control over the incorporation of active biological ingredients such as antibiotics and chemotherapeutic molecules into the glass structure (Pickup *et al.*, 2012). A comparison between sol-gel and melt-derived glasses with similar compositions also appear to have similar structure and atomic correlations (Carta *et al.*, 2007b).

1.3.2.2.1. Preparation of the sol

The first step involves the mix of components in the solution and consists of a series of successive reactions. Generally, a sol is a colloidal suspension of solid particles in a liquid and since the particles do not adhere to adjacent particles, each particle remains completely dispersed (Zelinski and Uhlmann, 1984, Kendall and Stainton, 2001). Sols are the simplest colloid dispersion and can be formed with different kinds of structure depending on the suspension.

1.3.2.2.2. Colloid formation

When the particles of the sol grow through further aggregation a colloid is formed. Colloids are solid particles with a diameter size range of 1-100 nm that can mimic the behaviour of atoms in the dispersed liquid with an amorphous or crystalline structure (Hench and West, 1990). Colloids can be classified into four main types: coacervates, tactoids, crystalloids, and flocks (**Figure 1.2**) (Heller, 1980). Coacervates are particles that attach to one another, but are not bonded together by surface charges or van der Waals attraction. Tactoids are particles that are regularly arranged, but not bonded with one another, and if slowly dried or a repulsive barrier is gradually reduced, the particles will be irreversibly bonded in an ordered arrangement known as a crystalloid. However, if particles rapidly aggregate, they form disordered clusters termed flocks.

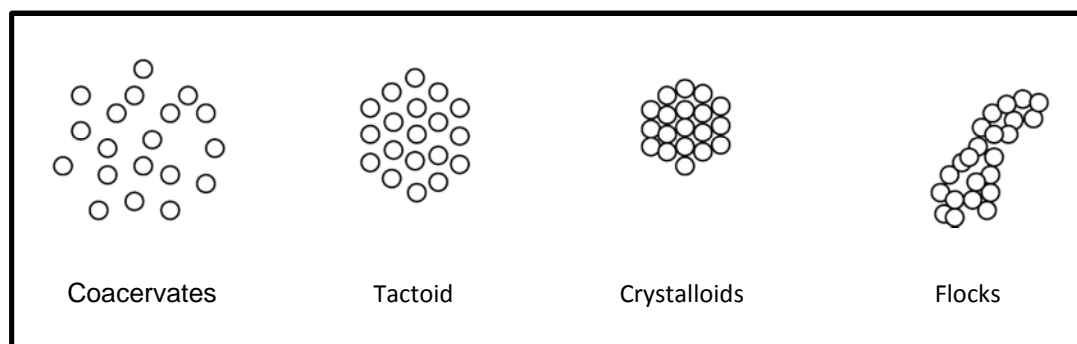


Figure 1.2. Four types of aggregated colloids that are coacervates, tactoid, crystalloids, and flocks (Heller, 1980).

1.3.2.2.3. Gel formation

A gel is a colloidal or polymeric solid containing a fluid component which has an internal network to make a three dimensional network (Hench and West, 1990). The sol and gel are distinguished by the degree of adhesion, as particles of a gel adhere

strongly, whereas sol particles disperse discretely (Kendall and Stainton, 2001). The high coordination number (the number of adhesive points with gel particles) of a gel determines the gel structure and if it is strong enough, it does not crack when the liquid is removed, but the gel may collapse when it is less well connected. The strength of a gel depends on whether the bonding between the solid phase is permanent or reversible, which depends on the mechanism of gelation. During gelation, aggregated particles grow into clusters and then these clusters link together to produce a gel. The gel point is identified as the moment when the last bond is formed in the cluster that causes a sharp increase in the viscosity.

1.3.2.2.4. Ageing and drying

Ageing is essential to increase the strength of the gel against cracking. This can occur during the drying stage (Hench and West, 1990). At this stage, more bond formation occurs and polymer or particles continue to attach themselves and this increases the interparticle necks and decreases the porosity. Shrinkage of the gel occurs while the liquid is removed from the pores that can affect the strength of the network and also plays an important role in the gel structure.

Drying can be divided into three main stages (Hench and West, 1990): In the first stage, the reduction of gel volume is equal to the volume of evaporated liquid and generally changes of structure such as volume, weight, and density occurs. The second stage starts when the critical point is reached with highest capillary pressure and the gel resists further shrinkage. Consequently, cracking is likely to occur at this stage and because of the decreased rate of evaporation, it is called the first falling rate period. In the third stage, the liquid ceases to flow to the surface and

is removed only by diffusion of its vapour and is named the second falling rate period.

1.3.2.2.5. Preparation of bulk sol-gel derived glasses

In the final heat treatment stage, the remaining solvent evaporates and a bulk glass can be obtained. A bulk glass is defined here as a glass piece, the smallest dimension of which is in the order of several millimeters or larger. The preparation of bulk glasses from bulk gels dated back to several decades ago. Dislich (Dislich, 1971) prepared small pieces of transparent borosilicate glass *via* the sol-gel method. Later, Yamane *et al.* (Yamane *et al.*, 1979) reported the preparation of large-size pieces of silica glasses. However, the preparation of large pieces of bulk glasses is not an easy task and according to the author's knowledge, there has been no study on the preparation of bulk phosphate-based glasses *via* the sol-gel method. Cracks and fracture are often generated when wet gels consisting of pores filled with solvent, start drying. The reason for cracking during the drying stage is related to the generation of a capillary pressure gradient in the liquid phase of the gel. The difference in pressure leads to differential shrinkage of the gel network, since the exterior of the gel usually contracts faster than the interior and this causes cracking (Hench and West, 1990). The capillary force is expressed in **Equation 1.1** by Zarzycki *et al.* (Zarzycki *et al.*, 1982):

$$(1.1) \quad \Delta P = \frac{4\gamma \cos \theta}{D}$$

Where ΔP is the capillary force, γ is the surface tension of the solvent, θ is the contact angle between the capillary wall and the solvent and D is the diameter of the capillaries. To suppress capillary pressure, solvents with low surface tension can be chosen in order to obtain bulk sol-gel derived glasses (Sakka et al., 1993). **Table 1.1** shows the surface tension and boiling points of various solvents (Sakka et al., 1993).

Solvent	Surface tension at 25 °C (dyne. cm ⁻¹)	Boiling point (°C)
Diethylether	17.1	334.6
Acetone	23.7	56.2
Dimethylformamide	36.8	153
2-methoxy ethnaol	42.8	125.5
Ethylene glycol	46.5	244.3
Water	72.8	100

1.3.3. Solubility and degradation rate of phosphate-based glasses

As mentioned previously, phosphate-based glasses have the potential to dissolve completely in an aqueous medium and offer real advantages for various biomedical applications. A significant amount of work has been focused on ternary phosphate-based glasses in the P₂O₅-CaO-Na₂O system and it was found that the solubility of these glasses is very sensitive to the glass composition (Bunker et al., 1984, Franks et al., 2000, Ahmed et al., 2004c). The results confirmed that increasing CaO content decreases the solubility, meanwhile, increasing Na₂O content increases the

solubility. Franks *et al.* (Franks *et al.*, 2002) investigated the solubility of quaternary glasses in the P_2O_5 -CaO-MgO- Na_2O system. In these quaternary glasses, substituting MgO for CaO, reduced the solubility and even pH changes at longer periods of time because of the smaller ionic radius of magnesium. Knowles *et al.* (Knowles *et al.*, 2001) developed quaternary phosphate-based glasses in the P_2O_5 -CaO- K_2O - Na_2O system and K_2O was used as Na_2O substitutes with the concentration of 0 to 25 mol%. Solubility results showed an increase in solubility with increasing K_2O content because of the larger ionic radius of potassium in comparison to sodium that causes a larger disrupting effect on the structure and weakens the network. Navarro *et al.* (Navarro *et al.*, 2003a, Navarro *et al.*, 2003b) investigated quaternary glasses in the P_2O_5 -CaO- Na_2O - TiO_2 system. Results showed the solubility was greatly decreased as the titanium content increased, even with the incorporation of only 3 mol% TiO_2 . Environmental scanning electron microscopy (ESEM) experiments also revealed much higher surface degradation occurred for the glasses with 0 mol% TiO_2 . In other studies, sodium oxide was partially replaced by Fe_2O_3 that resulted in lower dissolution rates (Ahmed *et al.*, 2004a, Lin *et al.*, 1994). The decrease in solubility was attributed to the strong cross-linking effects of the titanium and iron ions and replacement of P-O-P bonds in the glass by Ti-O-P and Fe-O-P bonds.

It should be noted that all the above solubility and degradation studies were done on phosphate-based glasses obtained by the traditional melt-quench technique and to date, there has been no study performed on the degradation of phosphate-based glasses obtained by the sol-gel technique. The reasons can be related to the limited research regarding synthesis and also the limitation in preparing bulk phosphate-based glasses.

1.4. Biomaterial applications

1.4.1. Orthopaedics

Biomaterials can be a good alternative for tissue replacement and nowadays almost every part of the body can be assisted by synthetic implants. It has been calculated that around 20 million people have an implanted medical device which costs more than 8% of the total health care budget worldwide (Lysaght and O'Loughlin, 2000). To take the case of bone, approximately 2.2 million bone graft procedures are performed worldwide at a cost of around \$2.5 billion each year (Giannoudis et al., 2005). Implantable biomaterials were the main focus of attention in orthopaedics that includes the anatomical replacement of parts of the body. For example the diseased hip joint has been replaced with a simple ball and socket device (usually metal-on-plastic) designed to reduce wear and inflammatory responses (Charnley, 1982 1976). The main attention for orthopaedic devices has been focused on various calcium-phosphate bioceramics, such as hydroxyapatite and tricalcium phosphate ceramics, because they show a degree of chemical similarity to the apatite phase of bone itself. However, they have poor mechanical properties that severely restrict their applications in orthopaedics. Meanwhile, these bioceramics can be excellent candidates for coating medical implants, usually metallic prosthesis, that result in a combination of both bioactivity of the bioceramics and good mechanical properties of the metals. These bioceramics are osteoconductive and bond directly to the bone. Also, they have been used to fill small bone defects, guide the bone growth and bond firmly to the bone.

1.4.2. Tissue engineering

The demand of patients who need to replace damaged hard or soft tissues is continuously increasing and we know that natural tissue does not behave like, or even look like a combination of ceramic, metal, and polymer. Although autograft (a tissue graft transferred from one part of the patient's body to another part) is preferable, supply is limited and lacks mechanical integrity. Alternative sources of tissue can be obtained from other humans (allograft) or animals (xenograft). These resolve the difficulties of supply, however, there is an increased risk of immunological rejection and disease transmission.

Development of a new and more efficient biomaterial to regenerate new tissue is a human challenge as it can have a great effect on everyday life of people worldwide. An effective approach can be growing specific cells from a patient on a three-dimensional scaffold under controlled culture conditions (Langer and Vacanti, 1993). As an example, bone has a considerable ability to regenerate following injury and highly porous-three dimensional scaffolds are needed to accommodate cells and guide them to regenerate the bone that may be indistinguishable from the normal healthy bone. A desirable strategy to repair bone tissue, is to induce osteogenesis *in situ*. Stem cells can be utilised to differentiate to form bone tissue, and seed those cells into an injectable scaffold, resulting in bone tissue formation (Dvir et al., 2011). Alternatively the implant can be implanted in direct contact with the cells with the purpose to stimulate and to direct tissue formation (Suchanek and Yoshimura, 1998). The ideal scaffold should have appropriate mechanical properties, controllable degradation, high bioactivity, and the ability to deliver cells for tissue regeneration (Hench and Polak, 2002, Jones and Boccaccini, 2005). It should also be conducive to supply oxygen, nutrient, and biomolecules to the growing cells to regenerate new tissues (Williams, 2004). **Figure 1.3** shows the

general tissue engineering concept of using biodegradable scaffolds to promote the reorganisation of the cells to form a functional tissue (Dvir et al., 2011).

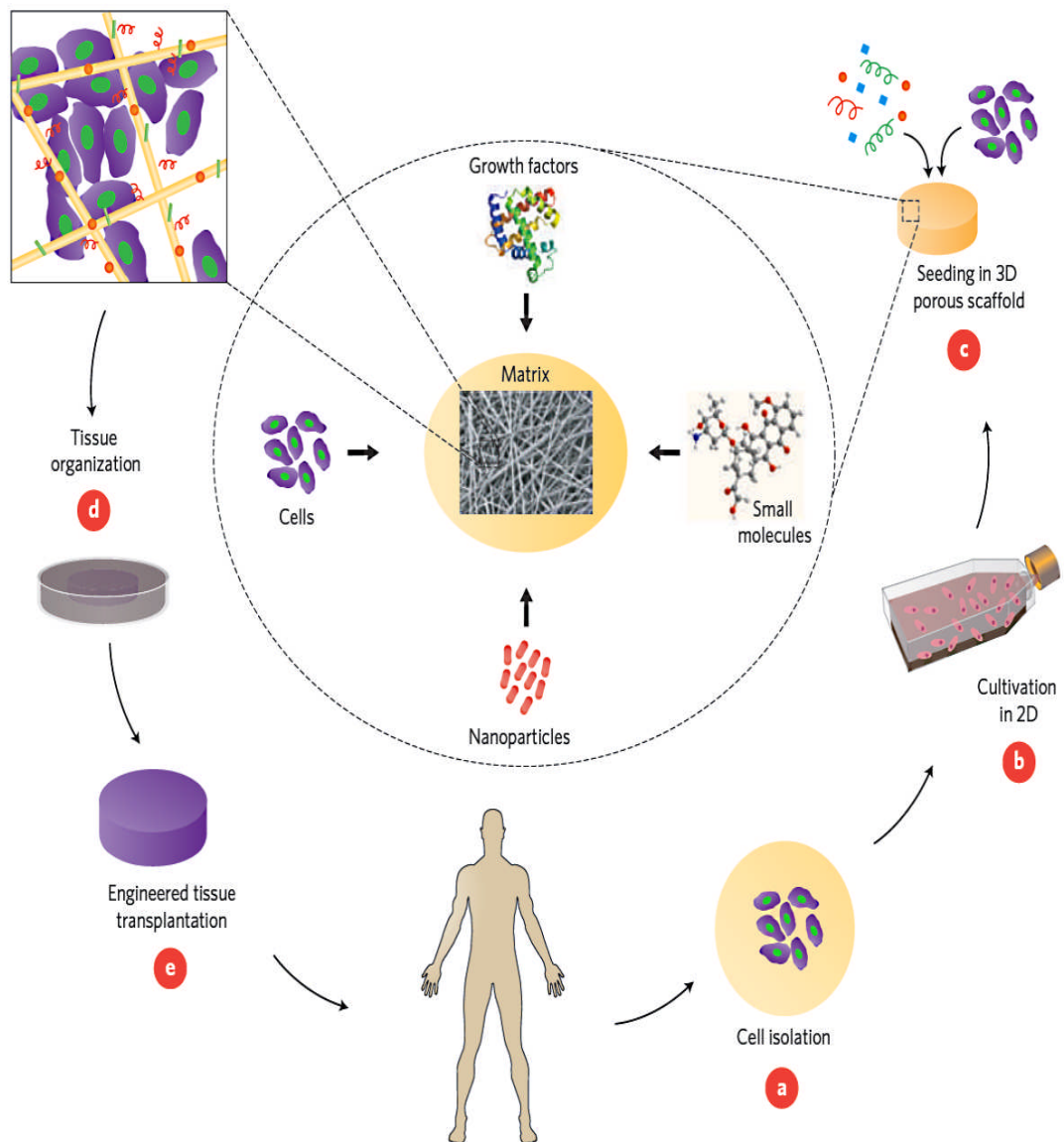


Figure 1.3. Tissue engineering concept includes; **(a)** isolating patients' cells, **(b)** *in vitro* cultivation of cells on a two-dimensional surface, **(c)** seeding cells on a porous scaffold and adding growth factors, small molecules and etc., **(d)** further cell cultivation in bioreactor, and **(e)** transplantation of the engineered tissue (Dvir et al., 2011).

Bioceramics are one of the most promising scaffold materials in bone tissue engineering. Hydroxyapatite (HA) exhibits excellent biocompatibility due to its close chemical and crystal resemblance to the mineral phase of bone. However, the lack of biodegradation of HA in the body is generally undesirable and limits its potential tissue engineering applications (Marcacci et al., 2007).

Bioactive silicate-based glasses can be a good choice with a long history of applications as biomedical implants (Hench, 1998). However, they should be synthesised in a way to be resorbable, with high interconnected porous structure in three-dimensions. It has been also found that 45S5 Bioglass[®] can partially crystallise when heated up to high temperature (around 950 °C) during scaffold fabrication which increases the mechanical property of the glass and the crystalline phase can transform to a biodegradable, amorphous calcium phosphate in a biological environment (Boccaccini et al., 2007, Chen et al., 2006). However, the long term effect of silica in the body is still unknown and the degradation rate of these bioglasses is very slow in comparison to biological tissues and often takes 1–2 years to fully dissolve (Lenza et al., 2002, Tadjoeidin et al., 2002, Hamadouche et al., 2001). This may limit their potential application as scaffolds for tissue regeneration, which benefit from having a similar degradation rate to the host tissue.

Phosphate-based glasses seem to be an attractive choice with a more controllable degradation rate for tissue engineering applications, in which the presence of a scaffold is only required to support cells/tissue in the short term (Knowles, 2003, Ahmed et al., 2004a). The degradation rate of phosphate glasses which is typically relatively rapid, can be easily altered *via* addition of various modifier oxides, such as calcium oxide (CaO) and sodium oxide (Na₂O). This enables the design of materials that release ions such as Ca²⁺ and Na⁺, which can stimulate cellular

behaviours such as cell proliferation and bone formation (Knowles, 2003, Navarro et al., 2003b, Franks et al., 2000). The degradation rate of phosphate-based glasses can also be prolonged by the addition of other oxide elements such as titanium dioxide (TiO_2), which forms stable Ti-O based cross-links in the phosphate network (Kiani et al., 2012).

1.4.3. Drug delivery

Conventional drug delivery modes such as injection of a dose or taking a pill, exhibit some drawbacks such as, when it is taken, the drug concentration in blood rises dramatically up to a peak, which is generally at a toxic level and then rapidly declines to below the minimum effective drug level. Also, specialised drugs to treat specific diseases, can injure other tissues (Xue and Shi, 2004). Drug delivery is a technique of designing a system to release a drug over a specific period of time in a controlled manner. Controlled drug delivery has several advantages in comparison with conventional dosage methods which includes; improving efficiency, continuous action, targeting specific diseased cells, and reduce patient toxicity (Vallet-Regi et al., 2007, Pickup et al., 2012). Designing a carrier system for drug delivery applications is quite challenging in terms of targeting the drug to a specific site and continuous release over a specific period of time. Several studies have been focused on drug delivery systems to provide enhanced efficacy, higher stability, solubility, and administer at much lower dosage of drugs (E-Sherbiny and Smyth, 2010, Xue and Shi, 2004).

Drug delivery carriers have the potential to deliver low-molecular-weight drugs, as well as large bio macromolecules such as genes and proteins, either in a localised or a targeted manner. Many newly designed drugs based on biomolecules such as proteins, peptides, and DNA are chemically very unstable or sensitive and therefore

encapsulating these biomolecules seems to be essential to deliver them to the diseased tissue. The drug delivery carriers should be non-toxic, non-immunogenic, and preferably biodegradable to deliver the therapeutic agent to the proper site of action.

In recent years, several drug delivery systems such as micelles, dendrimers, liposomes, emulsions, and porous materials have been developed to improve the efficiency of drugs and minimize their toxic side effects (Benita and Lambert, 2004, Manzano and Vallet-Regi, 2010, Torchilin, 2005). The size of the carrier is also an important variable that determines how it can be applied to the body and development of novel processing to prepare size-controllable carriers with high encapsulation efficiency, is a major challenge in drug delivery systems (Vallet-Regi and Ruiz-Hernandez, 2011).

1.4.3.1. Therapeutic nanoparticles

Nanotechnology has provided new avenues for engineering biomaterials that can revolutionise health care in therapeutic technologies. Significant evidence exists that highlights the promise nanotechnology has for biological applications, particularly in drug delivery systems. Nanotechnology has accelerated the development of novel drug delivery systems for strict control over the temporal release of a drug (LaVan et al., 2002). It may also provide an ideal solution and promote a new concept of chemotherapy; that may include sustained, controlled, and targeted chemotherapy. The drug can be either physically dispersed in nanoparticle matrices or surrounded by a vesicle like membrane.

The size of nanoparticles has an important effect on its interaction with its environment. Nanoparticles can accumulate in the tumour tissue with the upper limit

of approximately 400 nm to allow diffusion through the tumour (Alexis et al., 2008, Yuan et al., 1995). They must also be larger than 10 nm in diameter to avoid clearance by first renal filtration pass (Davis et al., 2008). Also, targeting is especially relevant in the context of cancer therapies, since most of the commonly used anticancer drugs have several side-effects due to nonspecific action on healthy cells (Qian et al., 2012). Nanoparticles can be taken up by cells that mean the potential for cell targeting is widely applicable.

Various types of nanocarriers for cancer chemotherapy to deliver concentrated drug payloads to the diseased tissue have been developed and have the potential to drastically improve the way cancer is treated (Strebhardt and Ullrich, 2008, Peer et al., 2007). Commonly used nanocarriers include but are not limited to; polymeric nanoparticles, carbon nanotubes, lipid-based nanocarriers, gold nanoparticles, and silica-based nanoparticles. The primary goals in designing these nanoparticles are to control the particle size, surface property, and release of drug at the therapeutically optimal rate and dose regimen. Polymeric nanoparticles have been used for drug delivery research to increase the therapeutic benefits, while minimizing side effects. Polymeric nanoparticles such as poly lactic-acid (PLA) and poly lactide co-glycolides have been used as drug delivery carriers, because of their good biodegradability and low toxicity (Reddy, 2005). Solvent evaporation is a common technique used to prepare biodegradable nanoparticles from poly lactic acid (PLA), poly (D,L-glycolide) (PLG), and poly cyanoacrylate (PCA). The electrospraying technique has been considered as promising technique for nanoparticle synthesis because it is a simple and cost effective method to prepare particles in a controlled way, with a specific size and narrow distribution and has been used to encapsulate drug molecules into biodegradable polymers such as poly (ϵ -caprolactone) PCL for controlled drug delivery devices (Ding et al., 2005).

Bioceramics have been the subject of intense interest for drug delivery applications. Kortesuo *et al.* (Kortesuo *et al.*, 2000) reported a sustained release of toremifene citrate from implanted silica glass discs with no tissue irritation at the site of the implantation over 42 days. Grun *et al.* (Grun *et al.*, 1997) developed mono-dispersed mesoporous silica microspheres based on the Stöber reaction for drug delivery applications. Following that mesoporous silica nanospheres (MSNs) with narrow size distribution were successfully synthesised by fine-tuning the reaction conditions and using surfactants (Unger *et al.*, 2000, Kosuge and Singh, 2001). MSNs have the ability to encapsulate different kinds of therapeutic agent within their pore channels and protect them from enzymatic degradation. The drug molecules are usually incorporated through adsorption and the uptake capacities of MSNs are correlated to the specific surface area and the pore size of the material (Andersson *et al.*, 2004). In order to minimize premature release and control the drug delivery at the targeted site, the pores can be mechanically blocked with polymers and nanocrystals or chemical bonds directly over the opening pores (Mal *et al.*, 2003, Fu *et al.*, 2003, Vivero-Escoto *et al.*, 2010). Cancer cells could also be targeted by surface functionalisation of MSNs with specific ligands (Wang *et al.*, 2010). However, it was confirmed that intravenous or intraperitoneal injection into mice at high doses appear to be lethal and toxic that can be related to deformation of the red blood cells and eventually hemolysis (Zhao *et al.*, 2011). Another study on intravenous injection of MSNs with different particle sizes into mice at lower doses confirmed that the MSNs were mainly located in the liver and spleen and could degrade gradually up to after 1 month of injection (He *et al.*, 2011).

Phosphate-based glasses can be a useful alternative, since studies on these glasses showed a linear dissolution rate in an aqueous medium with the degradation products that can be easily metabolised in the body (Bitar *et al.*, 2004, Knowles, 2003). A few studies show these glasses can be synthesised at low

temperature and have significant potential as a carrier in a drug delivery system (Pickup et al., 2012, Lee et al., 2013). However, the slow synthesis reactions and the difficulty to tailor the shape of these glasses may limit their potential drug delivery applications.

1.4.4. Diagnostic contrast agents

Detection of a disease at an early stage is a critical issue in medicine and the earlier it is diagnosed, the better is the chance for a successful treatment. Many diagnostic imaging techniques are currently available such as X-ray, ultrasound imaging, positron emission tomography, and magnetic resonance imaging. Molecular imaging techniques have also proven to be of great value for cancer, cardiovascular diseases, and neurological disorders (Weissleder and Mahmood, 2001). The resolution can be enhanced by using specific contrast agents for different imaging techniques. However, to diagnose a disease successfully, a combination of these techniques may be applied together and development of multimodal probes that can be detected by different imaging techniques has been considered to improve imaging instruments for diagnosis applications (Lim et al., 2010).

1.4.4.1. Diagnostic nanoparticles

The current progress of nanotechnology has the potential to improve detection in diagnostic imaging and targeting specific disease areas compared to conventional contrast agents. Nano-size particles can carry more than two imaging agents to provide more detailed information on the target site (Jennings and Long, 2009).

Silica-based nanoparticles are the most commonly used materials for multimodal imaging. For example, optical imaging probes like dye doped silica nanoparticles can be coupled with MRI contrast agents that are ferromagnetic nanoparticles (Malvindi et al., 2011, Jokerst et al., 2013). Silica nanoparticles also have good acoustic backscatter properties and can be used as a contrast agent for ultrasound molecular imaging (Jokerst et al., 2013, Liberman et al., 2013).

In medical diagnostics, there is a great potential to monitor biological molecules of interest, while, delivering therapeutic agents with nanoscale materials. These nanomaterials called “theranostic” and have the potential to serve dual roles as diagnostic and therapeutic agents (Janib et al., 2010). This concept moves us closer to personalised medicine where therapies are directed towards an individual patient and detected by the physician by an integrated imaging agent. Silica-based nanoparticles can be promising candidates for theranostic applications. Studies on MSNs showed the ability to encapsulate magnetic nanoparticles and drug molecules within the silica matrices for imaging and targeting drug delivery applications (Ruiz-Hernandez et al., 2007). Moreover, they have the potential to be used as a contrast agent for molecular imaging and luminescent molecules such as organic dyes can be encapsulated for biological assays (Sharma et al., 2006). Recently, Lu *et al.* (Lu et al., 2010) synthesised MSN-based theranostic particles containing luminescent molecules and an anticancer therapeutic agent that can suppress tumour growth in mice. Phosphate-based glasses can also be a good choice with a controllable degradation rate, however, according to the author’s knowledge, there has been no study on the potential diagnostic applications of these glasses, which might be related to the difficulty of tailoring their structure.

1.5. Potential biomedical applications of phosphate-based glass systems

1.5.1. Binary P_2O_5 - TiO_2 glasses

The addition of TiO_2 to phosphate glasses can stabilise the phosphate network, since Ti^{4+} ion has a small ionic radius and a large electrical charge that can penetrate into the phosphate network (Kiani et al., 2012). Thus, the bonding between different chains can become stronger and the vitreous network will be fortified. When titanium with its high charge/diameter ratio (6.1) is incorporated into the phosphate network, it can easily attract oxygen from the PO_4 tetrahedron and create Ti-O-P bonds (Brauer et al., 2010). Other studies confirmed that TiO_2 improves the glass forming ability, chemical durability, modulus of elasticity and raises the glass viscosity, which was shown by an increase in the glass transition temperature (T_g), and consequently strengthens the glass network (Navarro et al., 2003a, Lee and Hsu, 1999). In addition, the Ti^{4+} cation has been investigated extensively for killing or growth inhibition of bacteria when it is combined with UV light (Jacoby et al., 1998, Linkous et al., 2000, Sunada et al., 2003).

Binary P_2O_5 - TiO_2 (PT) glasses were produced by the conventional melt-quench method at a relatively high melting temperature (range of 1300-1500 °C) and were usually coloured deep purple because of the remaining Ti^{3+} ions in the glass network (Hashimoto et al., 2012). Synthesis of binary P_2O_5 - TiO_2 glass systems *via* a sol-gel route allowed the preparation of glassy thin films for a variety of applications such as humidity sensors and proton conducting materials (Makita et al., 1997b, Makita et al., 1997a). However, according to the previous studies on the sol-gel preparation of these glasses, high heat treatment temperatures were applied

in order to remove solvents and other organic molecules that may limit their potential biomedical application (Pickup et al., 2008b).

1.5.2. Ternary P_2O_5 -CaO-TiO₂ glasses

The addition of CaO to binary P_2O_5 -TiO₂ glasses can make these glasses more suitable for various biomedical applications with the release of Ca²⁺ ions that can stimulate cell proliferation (Navarro et al., 2003b). Ternary glasses in the P_2O_5 -CaO-TiO₂ (PCT) system are bioresorbable and can host human bone derived cells and enzyme delivery devices. Titanium reduces the dissolution rate of these glasses and can also cause significant gene up regulation (Abou Neel et al., 2007, Knabe et al., 2004, Ribeiro et al., 2004). These glasses are defined as materials that can react and dissolve over time in physiological fluid and can be replaced by regeneration of hard or soft tissues. The replaced tissue may have a similar properties to the original surrounding tissues.

Ternary PCT glasses have been prepared *via* melt-quench methods previously, however, preparation of these glasses *via* the sol-gel method have some significant advantages in comparison with the melt-quench method. The low-temperature nature of the sol-gel method can offer the potential to use these glasses as a carrier in drug delivery systems and also biocompatible glassy films can be prepared for coating biomedical implants. Recently, Pickup *et al.* (Pickup et al., 2008a) successfully synthesised sol-gel derived $(P_2O_5)_{0.50}-(TiO_2)_{0.25}-(CaO)_{0.25}$ glass composition. However, according to the author's knowledge, there are no other studies on sol-gel preparation of glasses with related compositions to those described above.

1.5.3. Ternary P_2O_5 -CaO- Na_2O glasses

Ternary P_2O_5 -CaO- Na_2O (PCN) glasses have a near linear dissolution rate in aqueous media and the degradation rate can be finely tuned through subtle variations in composition (Franks et al., 2000, Knowles, 2003). These glasses have a high degradation rate and can be used for biomedical applications such as imaging contrast agents and drug delivery systems. Their biocompatibility may also offer numerous advantages over the current polymer-based systems where their degradation can result in polymer fragments with heterogeneous chain-lengths that could lead to toxicity (Vemula et al., 2009). However, these ternary glasses are too soluble for cell attachment and proliferation in tissue engineering applications (Ahmed et al., 2004b).

For several years, these glasses have been used for the controlled release of ions (Driver and Telfer, 1988), however, few studies have been carried out on the synthesis of these glasses *via* the sol-gel route and even fewer on the potential drug delivery applications of these glasses. The reasons can be related to the high synthesis temperature and complicated morphological trait (Carta et al., 2009). Recently, Pickup *et al.* (Pickup et al., 2012) showed these materials can be synthesised at lower temperatures with the sustained release of the drug within a week. The results suggested the potential drug delivery applications of these materials and a focus on these materials would be of interest.

1.5.4. Quaternary P_2O_5 -CaO- Na_2O - TiO_2 glasses

Quaternary phosphate-based glasses of the general formula P_2O_5 -CaO- Na_2O - TiO_2 (PCNT) synthesised *via* the melt-quench route, have shown a variety of interesting properties which make them suitable for various biomedical applications (Navarro et

al., 2003b, Navarro et al., 2002, Ribeiro et al., 2004). Studies on these glasses confirmed that the addition of titania to the P_2O_5 -CaO- Na_2O glass systems can improve glass-forming ability and chemical durability of these glasses (Navarro et al., 2003a, Kishioka et al., 1974). Moreover, it was shown that the incorporation of TiO_2 into phosphate-based glasses not only decreases the solubility of these glasses, but also decreases the crystallisation tendency by the formation of cross links between TiO_4 and TiO_6 structural groups and phosphate tetrahedra (Brauer et al., 2007). In another study, quaternary phosphate-based glasses in the P_2O_5 -CaO- Na_2O - TiO_2 system with up to 15 mol% TiO_2 were successfully produced *via* the melt-quench route and have shown that TiO_2 can increase the bulk density of the glass (Abou Neel et al., 2008). The degradation rate of these quaternary glasses can be increased by substituting Na_2O for TiO_2 (Navarro et al., 2005, Navarro et al., 2003b, Kiani et al., 2012). Because of the controllable degradation rate of these glasses, they have the potential to be used as a scaffold for tissue regeneration, or as a host matrix for embedding pharmaceutical molecules that could be useful in clinical practice (Kiani et al., 2012, Vallet-Regi et al., 2007). Recently, Lakhkar *et al.* (Lakhkar et al., 2012) reported the application of the melt-derived titanium-stabilised phosphate-based glass microspheres with the ability to provide a stable surface for cell attachment, growth, and proliferation as a scaffold for tissue engineering. However, high synthesis temperatures, low surface area, and very small porosity of these glasses may limit their potential applications as a scaffold in tissue engineering.

Sol-gel synthesis of these PCNT glasses can be a good alternative due to the low synthesis temperature in comparison with the melt-quench method. The low processing temperature of the sol-gel synthesis leads to the opportunity to incorporate bioactive molecules for drug delivery application, along with the ease of

releasing homogeneous mixing of the reactants that gives high quality amorphous glassy-like materials (Makita et al., 1997a, Pickup et al., 2008b). For their potential tissue regeneration applications high specific surface area and more porosity would be expected for the synthesised glasses *via* the sol-gel method, that could lead to increase their bioactivity compare to those obtained by the melt-quench method with the same composition (Perez-Pariente et al., 2000, Vallet-Regi et al., 2000). In addition, since the sol-gel process starts with the liquid form of precursors, there is a possibility to produce nano/micrometer sized particles. However, there has been no study on the sol-gel synthesis of the PCNT glasses for potential biomedical applications.

References

- ABOU NEEL, E. A., CHRZANOWSKI, W. & KNOWLES, J. C. 2008. Effect of increasing titanium dioxide content on bulk and surface properties of phosphate-based glasses. *Acta Biomaterialia*, 4, 523-534.
- ABOU NEEL, E. A., MIZOGUCHI, T., ITO, M., BITAR, M., SALIH, V. & KNOWLES, J. C. 2007. In vitro bioactivity and gene expression by cells cultured on titanium dioxide doped phosphate-based glasses. *Biomaterials*, 28, 2967-2977.
- ABOU NEEL, E. A., PICKUP, D. M., VALAPPIL, S. P., NEWPORT, R. J. & KNOWLES, J. C. 2009. Bioactive functional materials: a perspective on phosphate-based glasses. *Journal of Materials Chemistry*, 19, 690-701.
- AHMED, I., COLLINS, C. A., LEWIS, M. P., OLSEN, I. & KNOWLES, J. C. 2004a. Processing, characterisation and biocompatibility of iron-phosphate glass fibres for tissue engineering. *Biomaterials*, 25, 3223-3232.
- AHMED, I., LEWIS, M., OLSEN, I. & KNOWLES, J. C. 2004b. Phosphate glasses for tissue engineering: Part 1. Processing and characterisation of a ternary-based P(2)O(5)-CaO-Na(2)O glass system. *Biomaterials*, 25, 491-499.
- AHMED, I., LEWIS, M., OLSEN, I. & KNOWLES, J. C. 2004c. Phosphate glasses for tissue engineering: Part 2. Processing and characterisation of a ternary-based P(2)O(5)-CaO-Na(2)O glass fibre system. *Biomaterials*, 25, 501-507.
- ALEXIS, F., RHEE, J. W., RICHIE, J. P., RADOVIC-MORENO, A. F., LANGER, R. & FAROKHZAD, O. C. 2008. New frontiers in nanotechnology for cancer treatment. *Urologic Oncology-Seminars and Original Investigations*, 26, 74-85.
- ANDERSSON, J., ROSENHOLM, J., AREVA, S. & LINDEN, M. 2004. Influences of material characteristics on ibuprofen drug loading and release profiles from ordered micro- and mesoporous silica matrices. *Chemistry of Materials*, 16, 4160-4167.
- ANDERSSON, O. H. & KARLSSON, K. H. 1991. On the Bioactivity of Silicate Glass. *Journal of Non-Crystalline Solids*, 129, 145-151.
- BEN-NISSAN, B. 2004. Nanocoated converted coral meets high structural strength requirement for load-bearing bone graft applications. *Mrs Bulletin*, 29, 611-611.

- BENITA, S. & LAMBERT, G. 2004. Ocular drug delivery by cationic emulsions. *Isopt: Proceedings of the 5th International Symposium on Ocular Pharmacology and Therapeutics*, Monte Carlo, Monaco, 7-13.
- BITAR, M., SALIH, V., MUDERA, V., KNOWLES, J. C. & LEWIS, M. P. 2004. Soluble phosphate glasses: in vitro studies using human cells of hard and soft tissue origin. *Biomaterials*, 25, 2283-2292.
- BOCCACCINI, A. R., CHEN, Q., LEFEBVRE, L., GREMILLARD, L. & CHEVALIER, J. 2007. Sintering, crystallisation and biodegradation behaviour of Bioglass (R)-derived glass-ceramics. *Faraday Discussions*, 136, 27-44.
- BRAUER, D. S., KARPUKHINA, N., LAW, R. V. & HILL, R. G. 2010. Effect of TiO₂ addition on structure, solubility and crystallisation of phosphate invert glasses for biomedical applications. *Journal of Non-Crystalline Solids*, 356, 2626-2633.
- BRAUER, D. S., RUSSEL, C. & KRAFT, J. 2007. Solubility of glasses in the system P₂O₅-CaO-MgO-Na₂O-TiO₂: Experimental and modeling using artificial neural networks. *Journal of Non-Crystalline Solids*, 353, 263-270.
- BROW, R. K. 2000. Review: the structure of simple phosphate glasses. *Journal of Non-Crystalline Solids*, 263, 1-28.
- BROW, R. K., KIRKPATRICK, R. J. & TURNER, G. L. 1990. The Short-Range Structure of Sodium-Phosphate Glasses .1. Mas Nmr-Studies. *Journal of Non-Crystalline Solids*, 116, 39-45.
- BUNKER, B. C., ARNOLD, G. W. & WILDER, J. A. 1984. Phosphate-Glass Dissolution in Aqueous-Solutions. *Journal of Non-Crystalline Solids*, 64, 291-316.
- CARLISLE, E. M. 1970. Silicon . A Possible Factor in Bone Calcification. *Science*, 167, 279-280.
- CARTA, D., KNOWLES, J. C., GUERRY, P., SMITH, M. E. & NEWPORT, R. J. 2009. Sol-gel synthesis and structural characterisation of P₂O₅-B₂O₃-Na₂O glasses for biomedical applications. *Journal of Materials Chemistry*, 19, 150-158.
- CARTA, D., KNOWLES, J. C., GUERRY, P., SMITH, M. E. & NEWPORT, R. J. 2010. *SOL-GEL AND MELT-QUENCHED BOROPHOSPHATE GLASSES FOR BIOMEDICAL APPLICATIONS*, Handbook of Borates: Chemistry, Production and Applications, Nova Science Publishers, Inc.

- CARTA, D., KNOWLES, J. C., SMITH, M. E. & NEWPORT, R. J. 2007a. Synthesis and structural characterization of P(2)O(5)-CaO-Na(2)O sol-gel materials. *Journal of Non-Crystalline Solids*, 353, 1141-1149.
- CARTA, D., PICKUP, D. M., KNOWLES, J. C., AHMED, I., SMITH, M. E. & NEWPORT, R. J. 2007b. A structural study of sol-gel and melt-quenched phosphate-based glasses. *Journal of Non-Crystalline Solids*, 353, 1759-1765.
- CARTA, D., PICKUP, D. M., KNOWLES, J. C., SMITH, M. E. & NEWPORT, R. J. 2005. Sol-gel synthesis of the P(2)O(5)-CaO-Na(2)O-SiO(2) system as a novel bioresorbable glass. *Journal of Materials Chemistry*, 15, 2134-2140.
- CHAI, F., RAOUL, G., WISS, A., FERRI, J. & HILDEBRAND, H. F. 2011. Biomaterials as bone substitute: Classification and contribution. *Revue De Stomatologie Et De Chirurgie Maxillo-Faciale*, 112, 212-221.
- CHARNLEY, J. 1976. Long-Term Wear Studies of High-Density Polyethylene in Total Hip-Replacement. *Journal of Bone and Joint Surgery-British Volume*, 58, 390-390.
- CHARNLEY, J. 1982. Evolution of Total Hip-Replacement. *Annales Chirurgiae Et Gynaecologiae*, 71, 103-107.
- CHEN, Q. Z. Z., THOMPSON, I. D. & BOCCACCINI, A. R. 2006. 45S5 Bioglass (R)-derived glass-ceramic scaffolds for bone tissue engineering. *Biomaterials*, 27, 2414-2425.
- CHO, S. B., MIYAJI, F., KOKUBO, T., NAKANISHI, K., SOGA, N. & NAKAMURA, T. 1998. Apatite formation on silica gel in simulated body fluid: effects of structural modification with solvent-exchange. *Journal of Materials Science-Materials in Medicine*, 9, 279-284.
- CHRISTENSEN, E., VONBARNER, J. H., ENGELL, J. & BJERRUM, N. J. 1990. Preparation of Cu₂Zr₂P₃O₁₂ from Alkoxide-Derived Gels - Phase Formation as a Function of Heat-Treatment. *Journal of Materials Science*, 25, 4060-4065.
- COOK, J. L., WILLIAMS, N., KREEGER, J. M., PEACOCK, J. T. & TOMLINSON, J. L. 2003. Biocompatibility of three-dimensional chondrocyte grafts in large tibial defects of rabbits. *American Journal of Veterinary Research*, 64, 12-20.
- CRUICKSHANK, D. 1961. Role of 3d-Orbitals in Pi-Bonds Between .A. Silicon, Phosphorus, Sulphur, or Chlorine And .B. Oxygen or Nitrogen. *Journal of the Chemical Society*, 5486-5504.

- DAMIEN, C. J. & PARSONS, J. R. 1991. Bone-Graft and Bone-Graft Substitutes - a Review of Current Technology and Applications. *Journal of Applied Biomaterials*, 2, 187-208.
- DAVIS, M. E., CHEN, Z. & SHIN, D. M. 2008. Nanoparticle therapeutics: an emerging treatment modality for cancer. *Nature Reviews Drug Discovery*, 7, 771-782.
- DING, L., LEE, T. & WANG, C. H. 2005. Fabrication of monodispersed Taxol-loaded particles using electrohydrodynamic atomization. *Journal of Controlled Release*, 102, 395-413.
- DISLICH, H. 1971. Preparation of Multicomponent Oxide Glasses by Polycondensation. *Angewandte Chemie-International Edition*, 10, 825-&.
- DRIVER, P. M. & TELFER, S. B. 1988. An Assessment of the Performance of a New Formulation of Soluble Phosphate-Glass Bolus on the Copper and Selenium Status of Scottish Blackface Ewes. *Animal Production*, 46, 491-491.
- DVIR, T., TIMKO, B. P., KOHANE, D. S. & LANGER, R. 2011. Nanotechnological strategies for engineering complex tissues. *Nature Nanotechnology*, 6, 13-22.
- E-SHERBINY, I. M. & SMYTH, H. D. C. 2010. Biodegradable nano-micro carrier systems for sustained pulmonary drug delivery: (I) Self-assembled nanoparticles encapsulated in respirable/swellable semi-IPN microspheres. *International Journal of Pharmaceutics*, 395, 132-141.
- ENGELHAR.G 1972. Bond Properties of Silylphosphine, Germylphosphine and Stannyphosphine on Basis of Their P-31 Nmr Shifts and Their Interpretation Using Letcher-Van-Wazer Theory. *Zeitschrift Fur Anorganische Und Allgemeine Chemie*, 387, 52-54.
- FOROUTAN, F., JOKERST, J. V., GAMBHIR, S. S., VERMESH, O., KIM, H.-W. & KNOWLES, J. C. 2015. Sol-Gel Synthesis and Electrospaying of Biodegradable (P₂O₅)₅₅-(CaO)₃₀-(Na₂O)₁₅ Glass Nanospheres as a Transient Contrast Agent for Ultrasound Stem Cell Imaging. *Acs Nano*, 9, 1868-1877.
- FRANKS, K., ABRAHAMS, I., GEORGIU, G. & KNOWLES, J. C. 2001. Investigation of thermal parameters and crystallisation in a ternary CaO-Na₂O-P₂O₅-based glass system. *Biomaterials*, 22, 497-501.

- FRANKS, K., ABRAHAMAS, I. & KNOWLES, J. C. 2000. Development of soluble glasses for biomedical use Part I: In vitro solubility measurement. *Journal of Materials Science-Materials in Medicine*, 11, 609-614.
- FRANKS, K., SALIH, V., KNOWLES, J. C. & OLSEN, I. 2002. The effect of MgO on the solubility behavior and cell proliferation in a quaternary soluble phosphate based glass system. *Journal of Materials Science-Materials in Medicine*, 13, 549-556.
- FU, Q., RAO, G. V. R., ISTA, L. K., WU, Y., ANDRZEJEWSKI, B. P., SKLAR, L. A., WARD, T. L. & LOPEZ, G. P. 2003. Control of molecular transport through stimuli-responsive ordered mesoporous materials. *Advanced Materials*, 15, 1262-1266.
- GIANNOUDIS, P. V., DINOPOULOS, H. & TSIRIDIS, E. 2005. Bone substitutes: An update. *Injury-International Journal of the Care of the Injured*, 36, 20-27.
- GRUN, M., LAUER, I. & UNGER, K. K. 1997. The synthesis of micrometer- and submicrometer-size spheres of ordered mesoporous oxide MCM-41. *Advanced Materials*, 9, 254-261.
- GUPTA, R. & KUMAR, A. 2008. Bioactive materials for biomedical applications using sol-gel technology. *Biomedical Materials*, 3, 1-15.
- HAMADOUCHE, M., MEUNIER, A., GREENSPAN, D. C., BLANCHAT, C., ZHONG, J. P. P., LA TORRE, G. P. & SEDEL, L. 2001. Long-term in vivo bioactivity and degradability of bulk sol-gel bioactive glasses. *Journal of Biomedical Materials Research*, 54, 560-566.
- HASHIMOTO, T., WAGU, M., KIMURA, K., NASU, H., ISHIHARA, A., NISHIO, Y. & IWAMOTO, Y. 2012. Titanophosphate glasses as lithium-free nonsilicate pH-responsive glasses-Compatibility between pH responsivity and self-cleaning properties. *Materials Research Bulletin*, 47, 1942-1949.
- HE, Q. J., ZHANG, Z. W., GAO, F., LI, Y. P. & SHI, J. L. 2011. In vivo Biodistribution and Urinary Excretion of Mesoporous Silica Nanoparticles: Effects of Particle Size and PEGylation. *Small*, 7, 271-280.
- HELLER, W. 1980. Polymer colloids. *Plenum, New York*.
- HENCH, L. L. 1980. Biomaterials. *Science*, 208, 826-831.
- HENCH, L. L. 1998. Bioceramics. *Journal of the American Ceramic Society*, 81, 1705-1728.
- HENCH, L. L. & POLAK, J. M. 2002. Third-generation biomedical materials. *Science*, 295, 1014-1017.

- HENCH, L. L. & WEST, J. K. 1990. The Sol-Gel Process. *Chemical Reviews*, 90, 33-72.
- HENCH, L. L. & WILSON, J. 1984. Surface-Active Biomaterials. *Science*, 226, 630-636.
- HENCH, L. L. & WILSON, J. 1991. Bioceramics. *Mrs Bulletin*, 16, 62-74.
- HENTRICH, R. L., STEIN, H. G., GRAVES, G. A. & BAJPAI, P. K. 1969. An Evaluation of Inert and Resorbable Ceramics for Future Clinical Orthopedic Applications. *American Ceramic Society Bulletin*, 48, 801-805.
- HULBERT, S. F., HENCH, L. L., FORBERS, D. & BOWMAN, L. S. 1982. History of bioceramics. *Ceramics International*, 8, 131-140.
- JACOBY, W. A., MANESS, P. C., WOLFRUM, E. J., BLAKE, D. M. & FENNEL, J. A. 1998. Mineralization of bacterial cell mass on a photocatalytic surface in air. *Environmental Science & Technology*, 32, 2650-2653.
- JAGER, C., HARTMANN, P., WITTER, R. & BRAUN, M. 2000. Neu 2D NMR experiments for determining the structure of phosphate glasses: a review. *Journal of Non-Crystalline Solids*, 263, 61-72.
- JANIB, S. M., MOSES, A. S. & MACKAY, J. A. 2010. Imaging and drug delivery using theranostic nanoparticles. *Advanced Drug Delivery Reviews*, 62, 1052-1063.
- JENNINGS, L. E. & LONG, N. J. 2009. 'Two is better than one'-probes for dual-modality molecular imaging. *Chemical Communications*, 3511-3524.
- JOKERST, J. V., KHADEMI, C. & GAMBHIR, S. S. 2013. Intracellular Aggregation of Multimodal Silica Nanoparticles for Ultrasound-Guided Stem Cell Implantation. *Science Translational Medicine*, 5.
- JONES, J. R. & BOCCACCINI, A. R. 2005. Biomedical Applications: Tissue Engineering. *Cellular Ceramics: Structure, Manufacturing, Properties and Applications*, 547-570.
- JONES, J. R. & HENCH, L. L. 2003. Regeneration of trabecular bone using porous ceramics. *Current Opinion in Solid State & Materials Science*, 7, 301-307.
- KENDALL, K. & STAINTON, C. 2001. Adhesion and aggregation of fine particles. *Powder Technology*, 121, 223-229.
- KIANI, A., LAKHKAR, N. J., SALIH, V., SMITH, M. E., HANNA, J. V., NEWPORT, R. J., PICKUP, D. M. & KNOWLES, J. C. 2012. Titanium-containing bioactive phosphate glasses. *Philosophical Transactions of the Royal Society a-Mathematical Physical and Engineering Sciences*, 370, 1352-1375.

- KISHIOKA, A., HABA, M. & AMAGASA, M. 1974. Glass Formation in Multicomponent Phosphate Systems Containing TiO_2 . *Bulletin of the Chemical Society of Japan*, 47, 2493-2496.
- KNABE, C., BERGER, G., GILDENHAAR, R., KLAR, F. & ZREIQAT, H. 2004. The modulation of osteogenesis in vitro by calcium titanium phosphate coatings. *Biomaterials*, 25, 4911-4919.
- KNOWLES, J. C. 2003. Phosphate based glasses for biomedical applications. *Journal of Materials Chemistry*, 13, 2395-2401.
- KNOWLES, J. C., FRANKS, K. & ABRAHAMS, I. 2001. Investigation of the solubility and ion release in the glass system $K(2)O-Na(2)O-CaO-P(2)O(5)$. *Biomaterials*, 22, 3091-3096.
- KOKUBO, T., KIM, H. M. & KAWASHITA, M. 2003. Novel bioactive materials with different mechanical properties. *Biomaterials*, 24, 2161-2175.
- KOKUBO, T. & TAKADAMA, H. 2006. How useful is SBF in predicting in vivo bone bioactivity? *Biomaterials*, 27, 2907-2915.
- KORTESUO, P., AHOLA, M., KARLSSON, S., KANGASNIEMI, I., YLI-URPO, A. & KIESVAARA, J. 2000. Silica xerogel as an implantable carrier for controlled drug delivery - evaluation of drug distribution and tissue effects after implantation. *Biomaterials*, 21, 193-198.
- KOSUGE, K. & SINGH, P. S. 2001. Mesoporous silica spheres via l-alkylamine templating route. *Microporous and Mesoporous Materials*, 44, 139-145.
- KULKARNI, R. K., PANI, K. C., NEUMAN, C. & LEONARD, F. 1966. Polylactic Acid for Surgical Implants. *Archives of Surgery*, 93, 839-&.
- LAKHKAR, N., ABOU NEEL, E. A., SALIH, V. & KNOWLES, J. C. 2011. Titanium and Strontium-doped Phosphate Glasses as Vehicles for Strontium Ion Delivery to Cells. *Journal of Biomaterials Applications*, 25, 877-893.
- LAKHKAR, N. J., PARK, J. H., MORDAN, N. J., SALIH, V., WALL, I. B., KIM, H. W., KING, S. P., HANNA, J. V., MARTIN, R. A., ADDISON, O., MOSSELMANS, J. F. W. & KNOWLES, J. C. 2012. Titanium phosphate glass microspheres for bone tissue engineering. *Acta Biomaterialia*, 8, 4181-4190.
- LANGER, R. & VACANTI, J. P. 1993. Tissue Engineering. *Science*, 260, 920-926.
- LAVAN, D. A., LYNN, D. M. & LANGER, R. 2002. Moving smaller in drug discovery and delivery. *Nature Reviews Drug Discovery*, 1, 77-84.
- LEE, I. H., FOROUTAN, F., LAKHKAR, N. J., GONG, M. S. & KNOWLES, J. C. 2013. Sol-gel synthesis and structural characterization of $P_2O_5-CaO-Na_2O$

- glasses. *Physics and Chemistry of Glasses-European Journal of Glass Science and Technology Part B*, 54, 115-120.
- LEE, J. S. & HSU, C. K. 1999. The devitrification behavior of calcium phosphate glass with TiO₂ addition. *Thermochimica Acta*, 333, 115-119.
- LEGEROS, R. Z. 2008. Calcium Phosphate-Based Osteoinductive Materials. *Chemical Reviews*, 108, 4742-4753.
- LENZA, R. F. S., VASCONCELOS, W. L., JONES, J. R. & HENCH, L. L. 2002. Surface-modified 3D scaffolds for tissue engineering. *Journal of Materials Science-Materials in Medicine*, 13, 837-842.
- LI, P. J., OHTSUKI, C., KOKUBO, T., NAKANISHI, K., SOGA, N., NAKAMURA, T. & YAMAMURO, T. 1992. Apatite Formation Induced by Silica-Gel in a Simulated Body-Fluid. *Journal of the American Ceramic Society*, 75, 2094-2097.
- LIBERMAN, A., WU, Z., BARBACK, C. V., VIVEROS, R., BLAIR, S. L., ELLIES, L. G., VERA, D. R., MATTREY, R. F., KUMMEL, A. C. & TROGLER, W. C. 2013. Color Doppler Ultrasound and Gamma Imaging of Intratumorally Injected 500 nm Iron-Silica Nanoshells. *Acs Nano*, 7, 6367-6377.
- LIM, E. K., YANG, J., DINNEY, C. P. N., SUH, J. S., HUH, Y. M. & HAAM, S. 2010. Self-assembled fluorescent magnetic nanoprobe for multimode-biomedical imaging. *Biomaterials*, 31, 9310-9319.
- LIN, S. T., KREBS, S. L., KADIYALA, S., LEONG, K. W., LACOURSE, W. C. & KUMAR, B. 1994. Development of Bioabsorbable Glass-Fibers. *Biomaterials*, 15, 1057-1061.
- LINKOUS, C. A., CARTER, G. J., LOCUSON, D. B., OUELLETTE, A. J., SLATTERY, D. K. & SMITHA, L. A. 2000. Photocatalytic inhibition of algae growth using TiO₂, WO₃, and cocatalyst modifications. *Environmental Science & Technology*, 34, 4754-4758.
- LIPPMAA, E., MAGI, M., SAMOSON, A., ENGELHARDT, G. & GRIMMER, A. R. 1980. Structural Studies of Silicates by Solid-State High-Resolution Si-29 Nmr. *Journal of the American Chemical Society*, 102, 4889-4893.
- LIVAGE, J., BARBOUX, P., VANDENBORRE, M. T., SCHMUTZ, C. & TAULELLE, F. 1992. Sol-Gel Synthesis of Phosphates. *Journal of Non-Crystalline Solids*, 147, 18-23.
- LU, J., LIONG, M., LI, Z. X., ZINK, J. I. & TAMANOI, F. 2010. Biocompatibility, Biodistribution, and Drug-Delivery Efficiency of Mesoporous Silica Nanoparticles for Cancer Therapy in Animals. *Small*, 6, 1794-1805.

- LYSAGHT, M. J. & O'LOUGHLIN, J. A. 2000. Demographic scope and economic magnitude of contemporary organ replacement therapies. *Asaio Journal*, 46, 515-521.
- MAKITA, K., NOGAMI, M. & ABE, Y. 1997a. Sol-gel synthesis of amorphous P₂O₅-TiO₂ films and their electrical properties. *Journal of the Ceramic Society of Japan*, 105, 595-599.
- MAKITA, K., NOGAMI, M. & ABE, Y. 1997b. Sol-gel synthesis of high-humidity-sensitive amorphous P₂O₅-TiO₂ films. *Journal of Materials Science Letters*, 16, 550-552.
- MAL, N. K., FUJIWARA, M., TANAKA, Y., TAGUCHI, T. & MATSUKATA, M. 2003. Photo-switched storage and release of guest molecules in the pore void of coumarin-modified MCM-41. *Chemistry of Materials*, 15, 3385-3394.
- MALVINDI, M. A., GRECO, A., CONVERSANO, F., FIGUEROLA, A., CORTI, M., BONORA, M., LASCIALFARI, A., DOUMARI, H. A., MOSCARDINI, M., CINGOLANI, R., GIGLI, G., CASCIARO, S., PELLEGRINO, T. & RAGUSA, A. 2011. Magnetic/Silica Nanocomposites as Dual-Mode Contrast Agents for Combined Magnetic Resonance Imaging and Ultrasonography. *Advanced Functional Materials*, 21, 2548-2555.
- MANZANO, M. & VALLET-REGI, M. 2010. New developments in ordered mesoporous materials for drug delivery. *Journal of Materials Chemistry*, 20, 5593-5604.
- MARCACCI, M., KON, E., MOUKHACHEV, V., LAVROUKOV, A., KUTEPOV, S., QUARTO, R., MASTROGIACOMO, M. & CANCEDDA, R. 2007. Stem cells associated with macroporous bioceramics for long bone repair: 6-to 7-year outcome of a pilot clinical study. *Tissue Engineering*, 13, 947-955.
- MARTIN, S. W. 1991. Review of the Structures of Phosphate-Glasses. *European Journal of Solid State and Inorganic Chemistry*, 28, 163-205.
- NAVARRO, M., CLEMENT, J., GINEBRA, M. P., MARTINEZ, S., AVILA, G. & PLANELL, J. A. 2002. Improvement of the stability and mechanical properties of resorbable phosphate glasses by the addition of TiO₂. *Bioceramics* 14, 218-2, 275-278.
- NAVARRO, M., GINEBRA, M. P., CLEMENT, J., MARTINEZ, S., AVILA, G. & PLANELL, J. A. 2003a. Physicochemical degradation of titania-stabilized soluble phosphate glasses for medical applications. *Journal of the American Ceramic Society*, 86, 1345-1352.

- NAVARRO, M., GINEBRA, M. P. & PLANELL, J. A. 2003b. Cellular response to calcium phosphate glasses with controlled solubility. *Journal of Biomedical Materials Research Part A*, 67A, 1009-1015.
- NAVARRO, M., SANZANA, E. S., PLANELL, J. A., GINEBRA, M. P. & TORRES, P. A. 2005. In vivo behavior of calcium phosphate glasses with controlled solubility. *Bioceramics* 17, 284-286, 893-896.
- NODA, K., SAKAMOTO, W., KIKUTA, K., YOGO, T. & HIRANO, S. 1997. Effect of phosphorus sources on synthesis of KTiOPO_4 thin films by sol-gel method. *Chemistry of Materials*, 9, 2174-2178.
- PARK, J. B., BRONZINO, J.D. AND KIM, Y.K. 2003. Biomaterials Principles and Applications. *CRC Press, Boca Raton, USA.*, 21-53.
- PEER, D., KARP, J. M., HONG, S., FAROKHZAD, O. C., MARGALIT, R. & LANGER, R. 2007. Nanocarriers as an emerging platform for cancer therapy. *Nature Nanotechnology*, 2, 751-760.
- PEPPAS, N. A. & LANGER, R. 1994. New Challenges in Biomaterials. *Science*, 263, 1715-1720.
- PEREIRA, M. M., CLARK, A. E. & HENCH, L. L. 1995. Effect of Texture on the Rate of Hydroxyapatite Formation on Gel-Silica Surface. *Journal of the American Ceramic Society*, 78, 2463-2468.
- PEREZ-PARIENTE, J., BALAS, F. & VALLET-REGI, M. 2000. Surface and chemical study of SiO_2 center dot P_2O_5 center dot CaO center dot (MgO) bioactive glasses. *Chemistry of Materials*, 12, 750-755.
- PICKUP, D. M., ABOU NEEL, E. A., MOSS, R. M., WETHERALL, K. M., GUERRY, P., SMITH, M. E., KNOWLES, J. C. & NEWPORT, R. J. 2008a. TiK-edge XANES study of the local environment of titanium in bioresorbable $\text{TiO}(2)$ - CaO - $\text{Na}(2)\text{O}$ - $\text{P}(2)\text{O}(5)$ glasses. *Journal of Materials Science-Materials in Medicine*, 19, 1681-1685.
- PICKUP, D. M., NEWPORT, R. J. & KNOWLES, J. C. 2012. Sol-Gel Phosphate-based Glass for Drug Delivery Applications. *Journal of Biomaterials Applications*, 26, 613-622.
- PICKUP, D. M., SPEIGHT, R. J., KNOWLES, J. C., SMITH, M. E. & NEWPORT, R. J. 2008b. Sol-gel synthesis and structural characterisation of binary $\text{TiO}(2)$ - $\text{P}(2)\text{O}(5)$ glasses. *Materials Research Bulletin*, 43, 333-342.
- PICKUP, D. M., VALAPPIL, S. P., MOSS, R. M., TWYMAN, H. L., GUERRY, P., SMITH, M. E., WILSON, M., KNOWLES, J. C. & NEWPORT, R. J. 2009. Preparation, structural characterisation and antibacterial properties of Ga-

- doped sol-gel phosphate-based glass. *Journal of Materials Science*, 44, 1858-1867.
- PIETAK, A. M., REID, J. W., STOTT, M. J. & SAYER, M. 2007. Silicon substitution in the calcium phosphate bioceramics. *Biomaterials*, 28, 4023-4032.
- QIAN, W. Y., SUN, D. M., ZHU, R. R., DU, X. L., LIU, H. & WANG, S. L. 2012. pH-sensitive strontium carbonate nanoparticles as new anticancer vehicles for controlled etoposide release. *International Journal of Nanomedicine*, 7, 5781-5792.
- RAHAMAN, M. N., DAY, D. E., BAL, B. S., FU, Q., JUNG, S. B., BONEWALD, L. F. & TOMSIA, A. P. 2011. Bioactive glass in tissue engineering. *Acta Biomaterialia*, 7, 2355-2373.
- REDDY, L. H. 2005. Drug delivery to tumours: recent strategies. *Journal of Pharmacy and Pharmacology*, 57, 1231-1242.
- RIBEIRO, C. C., BARRIAS, C. C. & BARBOSA, M. A. 2004. Calcium phosphate-alginate microspheres as enzyme delivery matrices. *Biomaterials*, 25, 4363-4373.
- ROKKANEN, P. U., BOSTMAN, O., HIRVENSALO, E., MAKELA, E. A., PARTIO, E. K., PATIALA, H., VAINIONPAA, S., VIHTONEN, K. & TORMALA, P. 2000. Bioabsorbable fixation in orthopaedic surgery and traumatology. *Biomaterials*, 21, 2607-2613.
- RUIZ-HERNANDEZ, E., LOPEZ-NORIEGA, A., ARCOS, D., IZQUIERDO-BARBA, I., TERASAKI, O. & VALLET-REGI, M. 2007. Aerosol-assisted synthesis of magnetic mesoporous silica spheres for drug targeting. *Chemistry of Materials*, 19, 3455-3463.
- RUST, K. R., SINGLETON, G. T., WILSON, J. & ANTONELLI, P. J. 1996. Bioglass middle ear prosthesis: Long-term results. *American Journal of Otology*, 17, 371-374.
- SAKKA, S., AOKI, K., KOZUKA, H. & YAMAGUCHI, J. 1993. Sol-Gel Synthesis of Silica-Gel Disc as Applied to Supports of Organic-Molecules with Optical Functions. *Journal of Materials Science*, 28, 4607-4614.
- SHARMA, P., BROWN, S., WALTER, G., SANTRA, S. & MOUDGIL, B. 2006. Nanoparticles for bioimaging. *Advances in Colloid and Interface Science*, 123, 471-485.
- STREBHARDT, K. & ULLRICH, A. 2008. Paul Ehrlich's magic bullet concept: 100 years of progress. *Nature Reviews Cancer*, 8, 473-480.

- SUCHANEK, W. & YOSHIMURA, M. 1998. Processing and properties of hydroxyapatite-based biomaterials for use as hard tissue replacement implants. *Journal of Materials Research*, 13, 94-117.
- SUNADA, K., WATANABE, T. & HASHIMOTO, K. 2003. Studies on photokilling of bacteria on TiO₂ thin film. *Journal of Photochemistry and Photobiology a-Chemistry*, 156, 227-233.
- SUURONEN, R., KONTIO, R., ASHAMMAKHI, N., LINDQVIST, C. & LAINE, P. 2004. Bioabsorbable self-reinforced plates and screws in craniomaxillofacial surgery. *Bio-Medical Materials and Engineering*, 14, 517-524.
- SUZUKI, T., HUKKANEN, M., BUTTERY, L. D. K., POLAK, J. M., YOKOGAWA, Y., NISHIZAWA, T., NAGATA, F., KAWAMOTO, Y., KAMEYAMA, T. & TORIYAMA, M. 1997. Effect of surface instability of calcium phosphate ceramics on growth and adhesion of osteoblast-like cells derived from neonatal rat calvaria. *Bioceramics*, Vol 10, 105-108.
- TADJOEDIN, E. S., DE LANGE, G. L., LYARUU, D. M., KUIPER, L. & BURGER, E. H. 2002. High concentrations of bioactive glass material (BioGran (R)) vs. autogenous bone for sinus floor elevation - Histomorphometrical observations on three split mouth clinical cases. *Clinical Oral Implants Research*, 13, 428-436.
- TANG, A. J., HASHIMOTO, T., NASU, H. & KAMIYA, K. 2005. Sol-gel preparation and properties of TiO₂-P₂O₅ bulk glasses. *Materials Research Bulletin*, 40, 55-66.
- TORCHILIN, V. P. 2005. Recent advances with liposomes as pharmaceutical carriers. *Nature Reviews Drug Discovery*, 4, 145-160.
- UNGER, K. K., KUMAR, D., GRUN, M., BUCHEL, G., LUDTKE, S., ADAM, T., SCHUMACHER, K. & RENKER, S. 2000. Synthesis of spherical porous silicas in the micron and submicron size range: challenges and opportunities for miniaturized high-resolution chromatographic and electrokinetic separations. *Journal of Chromatography A*, 892, 47-55.
- URIST, M. R., OCONNOR, B. T. & BURWELL, R. G. 1994. Bone-Grafts, Derivatives and Substitutes - Introduction. *Bone Grafts, Derivatives and Substitutes*, 1-2.
- VALLET-REGI, M. 2001. Ceramics for medical applications. *Journal of the Chemical Society-Dalton Transactions*, 97-108.

- VALLET-REGI, M., ARCOS, D. & PEREZ-PARIENTE, J. 2000. Evolution of porosity during in vitro hydroxycarbonate apatite growth in sol-gel glasses. *Journal of Biomedical Materials Research*, 51, 23-28.
- VALLET-REGI, M., BALAS, F., COLILLA, M. & MANZANO, M. 2007. Bioceramics and pharmaceuticals: A remarkable synergy. *Solid State Sciences*, 9, 768-776.
- VALLET-REGI, M. & RUIZ-HERNANDEZ, E. 2011. Bioceramics: From Bone Regeneration to Cancer Nanomedicine. *Advanced Materials*, 23, 5177-5218.
- VANWAZER, J. R. & GRIFFITH, E. J. 1955. Structure and Properties of the Condensed Phosphates .10. General Structural Theory. *Journal of the American Chemical Society*, 77, 6140-6144.
- VANWAZER, J. R. & HOLST, K. A. 1950. Structure and Properties of the Condensed Phosphates .1. Some General Considerations About Phosphoric Acids. *Journal of the American Chemical Society*, 72, 639-644.
- VEMULA, P. K., CRUIKSHANK, G. A., KARP, J. M. & JOHN, G. 2009. Self-assembled prodrugs: An enzymatically triggered drug-delivery platform. *Biomaterials*, 30, 383-393.
- VIVERO-ESCOTO, J. L., SLOWING, I. I., TREWYN, B. G. & LIN, V. S. Y. 2010. Mesoporous Silica Nanoparticles for Intracellular Controlled Drug Delivery. *Small*, 6, 1952-1967.
- WANG, L. S., WU, L. C., LU, S. Y., CHANG, L. L., TENG, I. T., YANG, C. M. & HO, J. A. A. 2010. Biofunctionalized Phospholipid-Capped Mesoporous Silica Nanoshuttles for Targeted Drug Delivery: Improved Water Suspensibility and Decreased Nonspecific Protein Binding. *Acs Nano*, 4, 4371-4379.
- WEISSLEDER, R. & MAHMOOD, U. 2001. Molecular imaging. *Radiology*, 219, 316-333.
- WILLIAMS, D. 2004. Benefit and risk in tissue engineering. *Materials Today*, 7, 24-29.
- XUE, J. M. & SHI, M. 2004. PLGA/mesoporous silica hybrid structure for controlled drug release. *Journal of Controlled Release*, 98, 209-217.
- YAMANE, M., ASO, S., OKANO, S. & SAKAINO, T. 1979. Low-Temperature Synthesis of a Monolithic Silica Glass by the Pyrolysis of a Silica-Gel. *Journal of Materials Science*, 14, 607-611.
- YUAN, F., DELLIAN, M., FUKUMURA, D., LEUNIG, M., BERK, D. A., TORCHILIN, V. P. & JAIN, R. K. 1995. Vascular-Permeability in a Human Tumor

Xenograft - Molecular-Size Dependence and Cutoff Size. *Cancer Research*, 55, 3752-3756.

ZARZYCKI, J., PRASSAS, M. & PHALIPPOU, J. 1982. Synthesis of Glasses from Gels - the Problem of Monolithic Gels. *Journal of Materials Science*, 17, 3371-3379.

ZELINSKI, B. J. J. & UHLMANN, D. R. 1984. Gel Technology in Ceramics. *Journal of Physics and Chemistry of Solids*, 45, 1069-1090.

ZHAO, Y. N., SUN, X. X., ZHANG, G. N., TREWYN, B. G., SLOWING, I. I. & LIN, V. S. Y. 2011. Interaction of Mesoporous Silica Nanoparticles with Human Red Blood Cell Membranes: Size and Surface Effects. *Ac's Nano*, 5, 1366-1375.

CHAPTER 2

Sol-Gel Synthesis and Characterisation of Phosphate-Based Glasses Using Triethyl Phosphate as a Phosphorus Precursor

2.1. Introduction

As previously mentioned, sol-gel synthesis of phosphate-based glasses is a non-trivial task as P_2O_5 is a poor gel former and choosing a suitable phosphorus precursor is essential. In this chapter, triethyl phosphate was used as a phosphorus precursor to synthesise various phosphate-based glass systems with a new and simplified sol-gel method at relatively low processing temperatures for potential use in biomedical applications such as tissue engineering, drug delivery, and imaging contrast agents.

To become familiar with the sol-gel reaction and to avoid complications of ternary and quaternary systems, the synthesis process was commenced with a simple binary titano-phosphate glasses with the general formula of $(P_2O_5)_{(100-X)}-(TiO_2)_{(X)}$, where $X=30, 35, 40, 45$ or 50 mol%. This experiment also served as a pilot study to explore the compositional limitations of such system.

The second investigated system was based on ternary phosphate-based glasses in the P_2O_5 -CaO- TiO_2 system. The phosphorus pentoxide content was kept fixed at 55 mol% (ultraphosphate region) and titanium dioxide was substituted in place of calcium oxide to prepare ternary phosphate-based sol-gel derived glasses with the general formula of $(P_2O_5)_{(55)}-(CaO)_{(45-X)}-(TiO_2)_{(X)}$, where $X=20, 25$, or 30 mol%.

The third system was based on ternary phosphate-based glasses in the P_2O_5 -CaO- Na_2O system. Similar to the previously investigated system, P_2O_5 content was kept fixed at 55 mol% and sodium oxide was substituted in place of calcium oxide to prepare ternary sol-gel derived glasses with the general formula of $(P_2O_5)_{(55)}-(CaO)_{(45-X)}-(Na_2O)_{(X)}$, where $X=10, 15$, or 20 mol%.

The final system investigated was a quaternary phosphate-based glass system with the general formula of $(P_2O_5)_{(40)}-(CaO)_{(25)}-(Na_2O)_{(35-X)}-(TiO_2)_{(X)}$ and $(P_2O_5)_{(55)}-(CaO)_{(25)}-(Na_2O)_{(20-Y)}-(TiO_2)_{(Y)}$, where $X=20, 25$, or 30 mol% and $Y=5, 10$, or 15

mol%, with fixed phosphorus pentoxide at 40 or 55 mol%, calcium oxide content of 25 mol%, and substitution of titanium dioxide in place of sodium oxide. According to the knowledge of the author, there is no study reported on the sol-gel synthesis of these quaternary phosphate-based glasses.

Table 2.1 shows the compositions of starting solutions for binary, ternary, and quaternary sol-gel derived glass systems. The structure of the prepared samples was probed using X-ray diffraction (XRD), solid-state ^{31}P magic angle spinning nuclear magnetic resonance (^{31}P MAS-NMR), and Fourier transform infrared (FTIR) spectroscopy. The elemental proportions were also measured by energy dispersive X-ray spectroscopy (EDX). Together, these methods provide detailed information on sample structural variations from the phase level to the atomic level.

Table 2.1. Theoretical compositions of sol-gel synthesised phosphate-based glasses using triethyl phosphate as a phosphorus precursor.

Sample Code	Theoretical composition	Concentration (mol%)			
		P ₂ O ₅	TiO ₂	CaO	Na ₂ O
EP ₇₀ T ₃₀	(P ₂ O ₅) ₇₀ -(TiO ₂) ₃₀	70.0	30.0	0.0	0.0
EP ₆₅ T ₃₅	(P ₂ O ₅) ₆₅ -(TiO ₂) ₃₅	65.0	35.0	0.0	0.0
EP ₆₀ T ₄₀	(P ₂ O ₅) ₆₀ -(TiO ₂) ₄₀	60.0	40.0	0.0	0.0
EP ₅₅ T ₄₅	(P ₂ O ₅) ₅₅ -(TiO ₂) ₄₅	55.0	45.0	0.0	0.0
EP ₅₀ T ₅₀	(P ₂ O ₅) ₅₀ -(TiO ₂) ₅₀	50.0	50.0	0.0	0.0
EP ₅₅ CT ₂₀	(P ₂ O ₅) ₅₅ -(CaO) ₂₅ -(TiO ₂) ₂₀	55.0	20.0	25.0	0.0
EP ₅₅ CT ₂₅	(P ₂ O ₅) ₅₅ -(CaO) ₂₀ -(TiO ₂) ₂₅	55.0	25.0	20.0	0.0
EP ₅₅ CT ₃₀	(P ₂ O ₅) ₅₅ -(CaO) ₁₅ -(TiO ₂) ₃₀	55.0	30.0	15.0	0.0
EP ₅₅ CN ₁₀	(P ₂ O ₅) ₅₅ -(CaO) ₃₅ -(Na ₂ O) ₁₀	55.0	0.0	35.0	10.0
EP ₅₅ CN ₁₅	(P ₂ O ₅) ₅₅ -(CaO) ₃₀ -(Na ₂ O) ₁₅	55.0	0.0	30.0	15.0
EP ₅₅ CN ₂₀	(P ₂ O ₅) ₅₅ -(CaO) ₂₅ -(Na ₂ O) ₂₀	55.0	0.0	25.0	20.0
EP ₄₀ CNT ₂₀	(P ₂ O ₅) ₄₀ -(CaO) ₂₅ -(Na ₂ O) ₁₅ -(TiO ₂) ₂₀	40.0	20.0	25.0	15.0
EP ₄₀ CNT ₂₅	(P ₂ O ₅) ₄₀ -(CaO) ₂₅ -(Na ₂ O) ₁₀ -(TiO ₂) ₂₅	40.0	25.0	25.0	10.0
EP ₄₀ CNT ₃₀	(P ₂ O ₅) ₄₀ -(CaO) ₂₅ -(Na ₂ O) ₅ -(TiO ₂) ₃₀	40.0	30.0	25.0	5.0
EP ₅₅ CNT ₅	(P ₂ O ₅) ₅₅ -(CaO) ₂₅ -(Na ₂ O) ₁₅ -(TiO ₂) ₅	55.0	5.0	25.0	15.0
EP ₅₅ CNT ₁₀	(P ₂ O ₅) ₅₅ -(CaO) ₂₅ -(Na ₂ O) ₁₀ -(TiO ₂) ₁₀	55.0	10.0	25.0	10.0
EP ₅₅ CNT ₁₅	(P ₂ O ₅) ₅₅ -(CaO) ₂₅ -(Na ₂ O) ₅ -(TiO ₂) ₁₅	55.0	15.0	25.0	5.0

2.2. Materials and methods

2.2.1. Materials

The following precursors were used without further purification to prepare phosphate-based sol-gel derived glasses; triethyl phosphate (C₆H₁₅O₄P, 99%, Sigma-Aldrich, Gillingham, UK), titanium (IV) isopropoxide (97%, Sigma-Aldrich, Gillingham, UK), calcium methoxyethoxide (20% in methoxyethanol, ABCR GmbH,

Karlsruhe, Germany), 2-methoxyethanol (99.8%, Sigma-Aldrich, Gillingham, UK), sodium methoxide solution (30 wt% in methanol, Sigma-Aldrich, Gillingham, UK), and *n*-dimethyl formamide (*n*-DMF, $\geq 99.8\%$, Alfa Aesar, Heysham, UK). **Figure 2.1** shows the structural formula of the used precursors.

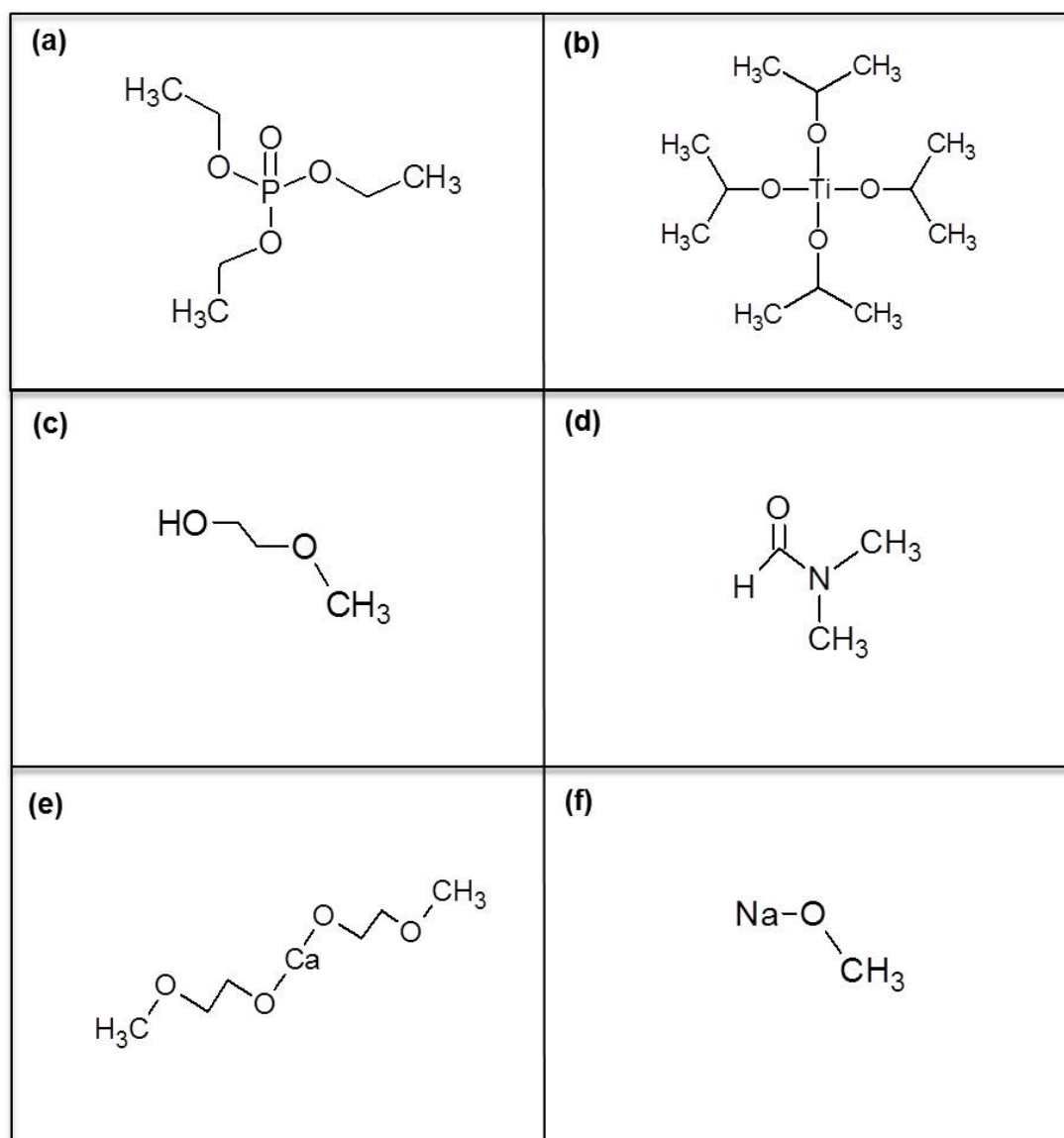


Figure 2.1. Structure of; **(a)** triethyl phosphate, **(b)** titanium isopropoxide, **(c)** 2-methoxyethanol, **(d)** *n*-dimethyl formamide, **(e)** calcium methoxyethoxide, and **(f)** sodium methoxide.

2.2.2. Sol-gel synthesis methods

2.2.2.1. Binary P_2O_5 - TiO_2 glasses

The reaction was initiated by diluting triethyl phosphate in 2-methoxyethanol at a molar ratio of 1:3 and magnetically stirred for about 10 minutes (the whole reaction was carried out in a dried vessel). The reaction vessel was then cooled in an ice bath before titanium isopropoxide was added dropwise into the vessel and mixed by stirring for 1 hour. In the final stage, *n*-DMF (with a molar ratio of 0.25) was added to the solution and a homogeneous solution was obtained after stirring for about 10 minutes. A schematic of the sol-gel synthesis of binary P_2O_5 - TiO_2 glasses is shown in **Figure 2.2**.

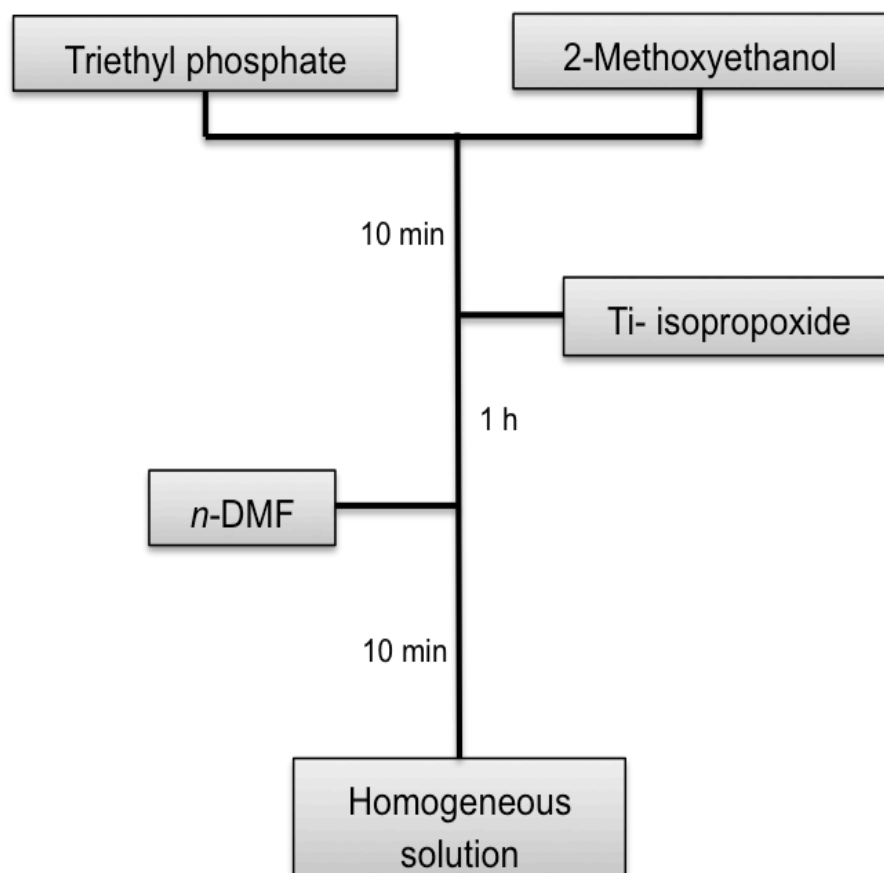


Figure 2.2. Schematic of the sol-gel synthesis of binary P_2O_5 - TiO_2 glasses using triethyl phosphate as a phosphorus precursor.

2.2.2.2. Ternary P_2O_5 -CaO- TiO_2 glasses

A similar sol-gel preparation method that was described for binary P_2O_5 - TiO_2 glasses, was used to prepare ternary P_2O_5 -CaO- TiO_2 glasses. The only difference between these two methods was in the final stage where before adding *n*-DMF, calcium methoxyethoxide was added dropwise into the vessel and allowed to react for about 1 hour. Finally, a homogeneous solution was obtained after 10 minutes of stirring. The sol-gel preparation of ternary P_2O_5 -CaO- TiO_2 glasses is outlined schematically in **Figure 2.3**.

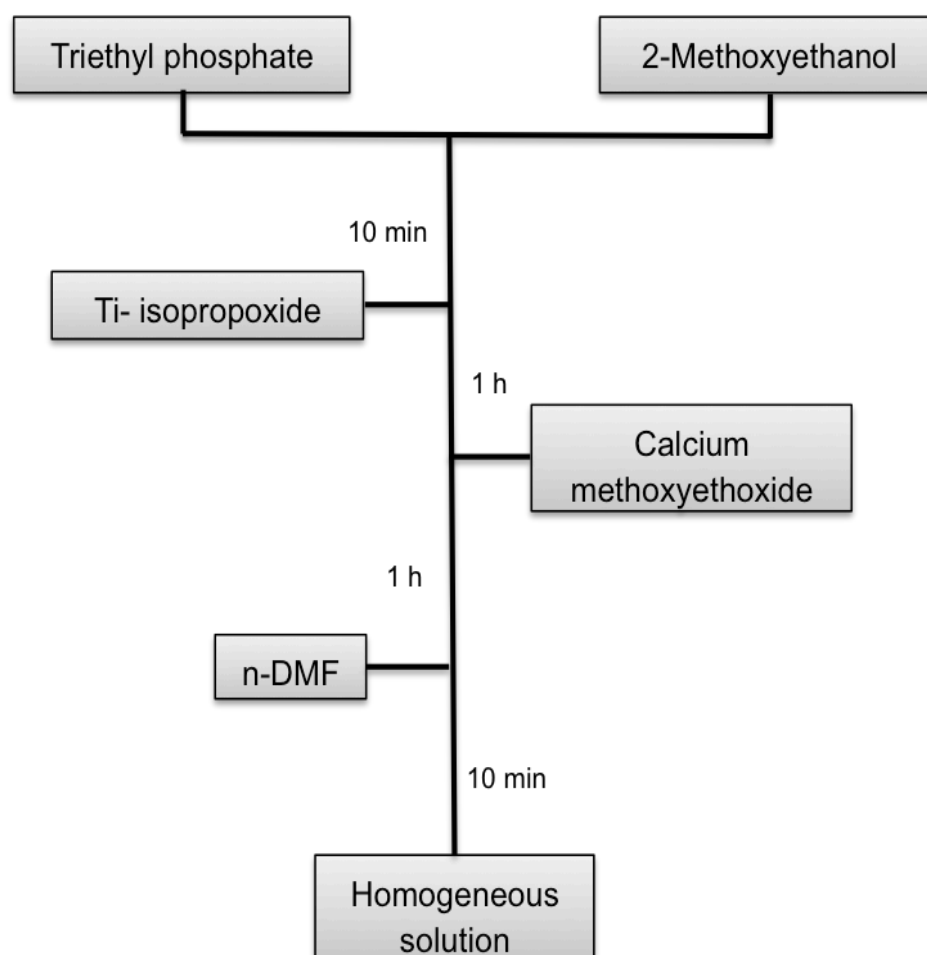


Figure 2.3. Flow diagram of the sol-gel synthesis of ternary P_2O_5 - TiO_2 -CaO glasses using triethyl phosphate as a phosphorus precursor.

2.2.2.3. Ternary P_2O_5 -CaO- Na_2O glasses

The reaction was started by diluting triethyl phosphate in 2-methoxyethanol (at a molar ratio of 1:3) and stirred for about 10 minutes. Similar to section 2.2.2.1, the reaction vessel was cooled in an ice bath and then calcium methoxyethoxide was added dropwise into the vessel and stirred for 1 hour before sodium methoxide was added gradually to the mixture. Finally, after an additional 1 hour of stirring of the mixture, *n*-DMF was added and a homogeneous solution was obtained after about 10 minutes stirring of the mixture (**Figure 2.4**).

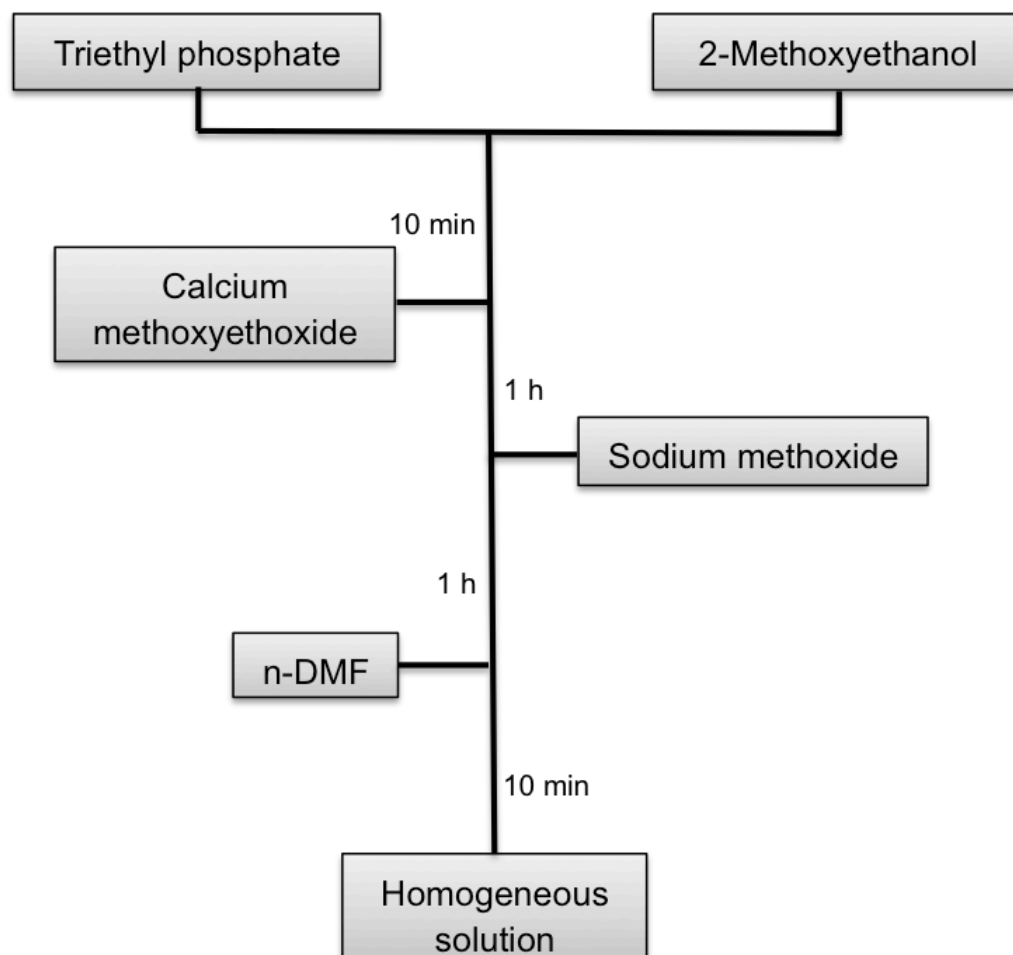


Figure 2.4. Schematic of the sol-gel synthesis of ternary P_2O_5 -CaO- Na_2O glasses using triethyl phosphate as a phosphorus precursor.

2.2.2.4. Quaternary P_2O_5 -CaO- Na_2O - TiO_2 glasses

The reaction was initiated by diluting triethyl phosphate in 2-methoxyethanol (at a molar ratio of 1:3). Using a magnetic stirrer, the components were mixed thoroughly for 10 minutes. After 10 min of stirring the reaction vessel was cooled in an ice bath before adding titanium isopropoxide dropwise into the mixture and stirring for 1 hour. Then calcium methoxyethoxide was poured slowly into the mixture and after 1 hour of stirring, sodium methoxide was added and the mixture stirred for another 1 hour. Finally, *n*-DMF (with a molar ratio of 0.25) was added to the mixture and a homogeneous solution was obtained after 10 minutes of stirring. A schematic of the sol-gel synthesis of quaternary P_2O_5 -CaO- Na_2O - TiO_2 glasses is shown in **Figure 2.5**.

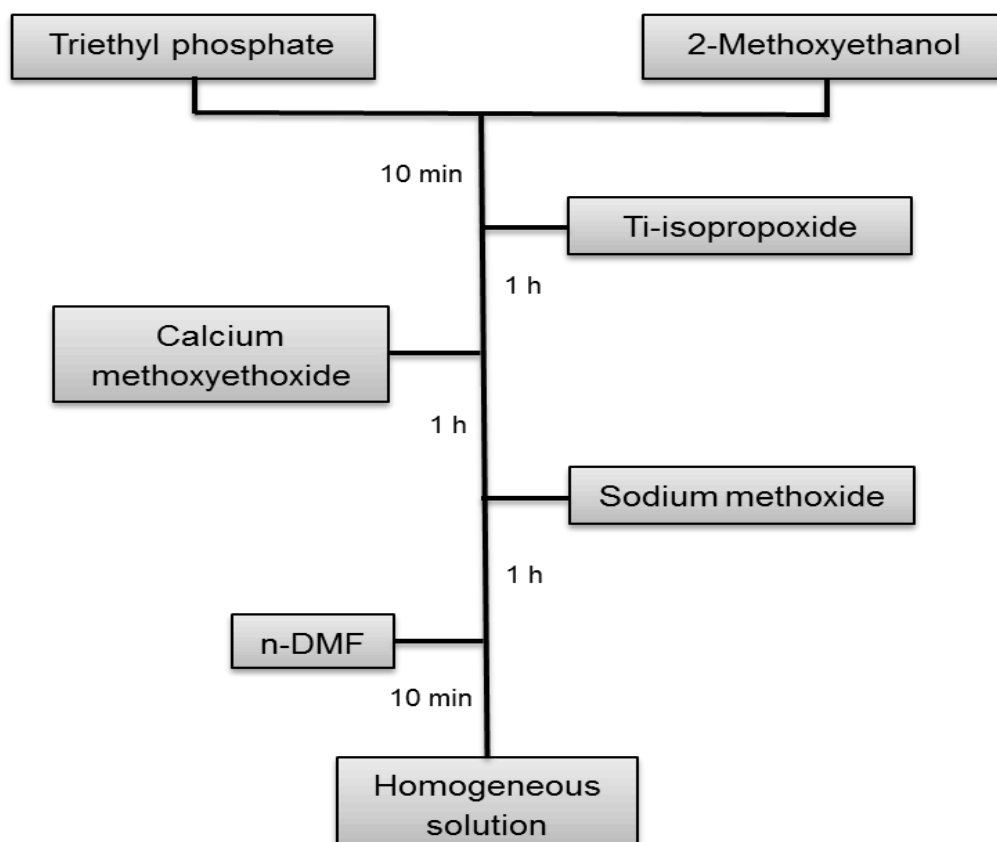


Figure 2.5. Schematic of the sol-gel synthesis of quaternary P_2O_5 -CaO- Na_2O - TiO_2 glasses using triethyl phosphate as a phosphorus precursor.

2.2.3. Drying procedure

The obtained homogeneous solutions of all four glass systems were aged at room temperature for three days in sealed glass containers before drying in an oven (EV014-Townson & Mercer, Cheshire, UK). The temperature was then increased gradually ($5\text{ }^{\circ}\text{C}\cdot\text{h}^{-1}$) to $60\text{ }^{\circ}\text{C}$ and kept for a week. Following this, samples were placed in contact with the air and the heating was continued at $120\text{ }^{\circ}\text{C}$ for an additional four days. Then the temperature was increased to $180\text{ }^{\circ}\text{C}$ and kept for two days before the heating cycle was finalised by heating the samples at $200\text{ }^{\circ}\text{C}$ for 2 hours to remove any remaining solvent and aiming to obtain bulk, glassy-like samples. After the final heating stage the oven was turned off and samples left overnight in the oven to cool down slowly. **Figure 2.6** shows the heat-treatment diagram for the sol-gel synthesised phosphate-based glasses.

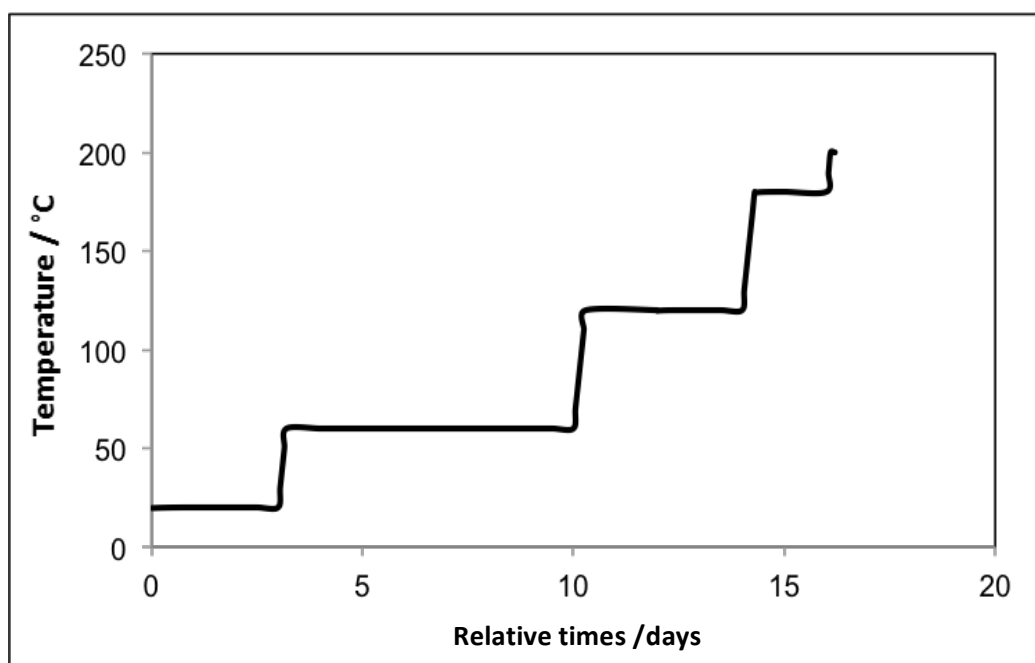


Figure 2.6. Heat treatment diagram for the sol-gel synthesised phosphate-based glasses.

2.2.4. Structural characterisation

2.2.4.1. X-ray diffraction

X-ray diffraction (XRD) has developed into one of the most powerful techniques for determining the atomic structure of solids during the past 100 years. If the atoms of a structure are arranged in a random way, such a structure is called amorphous. Otherwise, the three dimensional structure of non-amorphous materials is defined by regular, repeating planes of atoms that form a crystalline lattice. When a focused X-ray beam interacts with such atomic planes, part of the beam is transmitted or absorbed, but part of it would be scattered and diffracted back from the sample. Based on the diffracted beam orientation, the distance between the planes of atoms can be measured by applying Bragg's Law (**Equation 2.1**) (Warren, 1969).

$$(2.1) \quad \text{Bragg's Law Equation:} \quad n\lambda = 2d \sin\theta$$

Where n is the order of the diffracted beam, λ is the wavelength of the incident X-ray beam, d is the distance between the adjacent atomic planes, and the θ is the angle of incidence of the X-ray beam. The characteristic set of d -spacings and their intensity provide a unique fingerprint for the phases that are present in the sample.

Amorphous materials may be more desirable as a biodegradable material and because they are isotropic, they do not produce crystalline fragments during the degradation. The fragmented pieces can cause inflammation of the surrounding tissues that may limit the potential biomedical applications (Bostman and Pihlajamaki, 2000a, Bostman and Pihlajamaki, 2000b). In our work, XRD was performed mainly to ensure that samples were amorphous and in some cases, where crystallisation had occurred, to identify the crystalline phases.

2.2.4.1.1. XRD analysis method

XRD patterns were obtained on a Bruker-D8 Advance Diffractometer (Coventry, UK) from powder samples in a flat plate geometry using Ni-filtered Cu K α radiation. The obtained sol-gel derived samples were ground at 10 Hz to form a powder (MM301 milling machine, Retsch GmbH, Hope, UK). Data were collected using a Lynx Eye detector over an angular range of 2θ between 10 and 100° with a step size of 0.02° and a count time of 12 second per step. Crystalline phases (if present) were identified using the Crystallographica Search-Match software (Oxford Cryosystems, Oxford, UK).

2.2.4.2. Energy dispersive X-ray

Energy dispersive X-ray spectroscopy (EDX) is an analytical technique used for the elemental analysis or chemical characterisation. Each element has a unique atomic structure which would be translated into a specific set of peaks on its X-ray spectrum. EDX can determine the elemental composition of samples by identifying specific X-ray peaks for each element. The number and energy of the X-rays emitted from a specimen can be measured by an energy-dispersive spectrometer. As the emitted X-rays energy is a function of energy difference between the two electron shells and the atomic structure of the element, the elemental composition of the specimen can be measured (Goldstein, 2003). There is debate over the reproducibility of elemental data from EDX compared to methods such as X-ray fluorescence, but if performed carefully, with flat samples, a large number of data points or scan area and calibrated detector the obtained data can be reliable.

2.2.4.2.1. EDX analysis method

EDX-Inca 300 (Oxford instrument, Abingdon, UK) was used to determine the exact compositions of the prepared samples. Scanning electron microscopy XL30 (Philips, Eindhoven, Netherland) was operated at 20 kV, spot size 5 and a working distance of 10 mm to identify the particular elements and their relative proportions with EDX from the scanned area. The obtained data were converted to mol% of oxides of the elements to allow a comparison to be made with the theoretical compositions of the prepared samples.

2.2.4.3. Nuclear magnetic resonance

Solid-state nuclear magnetic resonance (NMR) offers significant opportunities to probe structure and has been widely developed and used as both spectroscopic and imaging techniques. Many atomic nuclei possess an intrinsic angular momentum or spin and when the nuclei are placed in a strong magnetic field, the nuclei align with the magnetic field. Quantum mechanics indicates that if a particle is moving with periodic motion, it can absorb electromagnetic radiation if the frequency of that motion exactly matches the frequency of the radiation. Such nuclear magnetic resonances can be recorded by the NMR spectrometer as a peak in the spectrum.

^{31}P NMR is one of the more routine and relatively easily obtained and processed type of NMR spectra due to the high sensitivity of the ^{31}P isotope (which has 100% natural abundance) and possesses a large magnetic moment and consequently a high receptivity (Mackenzie and Smith, 2002). ^{31}P is a spin 1/2 nucleus and can be strongly influenced by the chemical shielding interaction. Chemical shielding interaction is a result of the electron cloud density around the nucleus which modifies the experienced magnetic field by the nucleus. This leads to a change in

the resonance frequency of the nucleus and is termed as a chemical shift. The common approach is to use magic angle spinning (MAS) at 54.7° between the axis of rotation of the powder sample (many kHz) and the main static magnetic field direction that removes the anisotropy and greatly improves the resolution. In such spectra, the Q^n species can be identified based on their differing isotropic chemical shifts that is usually expressed in units of ppm to remove the magnetic field dependence. The static line shapes break up into the isotropic line and a series of spinning side bands that are separated from the isotropic line by multiples of the spinning rate. The intensity contribution from the spinning side bands must be taken into account in determining the relative abundance of each site.

With ^{31}P MAS-NMR analysis, there is a possibility to measure the relative quantities of the various Q^n species that comprise the glass structure. The PO_4^{3-} tetrahedron is the base component of the phosphate-based glasses. Phosphate tetrahedra are classified according to the number of oxygen atoms that they share with other phosphate tetrahedra. An oxygen atom which is shared in such a way would be referred to as bridging oxygen (BO) thereafter. According to Abou Neel *et. al* (Abou Neel et al., 2009), the different type of phosphate tetrahedra are labelled according to the number of BOs and they range from Q^0 (an isolated PO_4^{3-} tetrahedra) to Q^3 (share three covalently bonded BOs with neighbouring PO_4^{3-}) (**Fig. 2.7**).

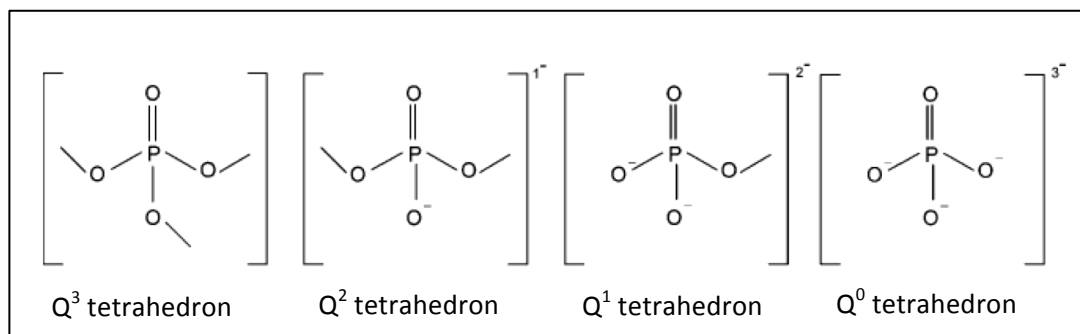


Figure 2.7. Representations of PO_4 tetrahedra with various polymerisation (Abou Neel et al., 2009).

2.2.4.3.1. ^{31}P MAS-NMR analysis method

^{31}P MAS-NMR spectra were acquired on a Varian VNMRS-400 Spectrometer (Crawley, UK) and all spectra were referenced to the resonance of the secondary reference ammonium dihydrogen phosphate ($\text{NH}_4\text{H}_2\text{PO}_4$) at 0.9 ppm (relative to 85% H_3PO_4 solution at 0 ppm). The spectra were recorded at 161.87 MHz for which ground sample powders were loaded into a 4 mm (rotor o.d.) magic angle spinning probe. The spectra were obtained using direct excitation with a 90° pulse, a 60 second recycle delay at ambient probe temperature ($\sim 25^\circ\text{C}$), and at a sample spin rate of 10 KHz and between 20 and 88 repetitions. In order to obtain the relative abundances of each of the Q^n species, the intensities of these peaks were fitted by the DM-fit software (Massiot et al., 2002).

2.2.4.4. Fourier transform infrared spectroscopy

Fourier transform infrared (FTIR) spectroscopy is a technique to obtain an infrared spectrum of transmission or absorption of a solid, liquid or gas. The absorption of

infrared radiation is related to the vibration of pairs or groups of atoms. The frequency of the incident radiation is varied and the transmission or the absorption of the radiation is measured and to be IR active a molecule must vary its electric dipole moment. The importance of the IR technique in the study of the glass is due to its ability to provide information on dynamic properties and changes in the rigidity of the network against an external infrared excitation (Moustafa and El-Egili, 1998). Peaks at various wavenumbers in an FTIR spectrum can be assigned to different chemical groups since each bond or group of atoms has different vibrational energies.

The FTIR spectroscopy is a commonly used technique for investigating the various structural units that are present in phosphate-based glasses. The FTIR spectra of phosphate-based glasses are generally obtained in a range between 600-1500 cm^{-1} (Le Saout et al., 2002, Carta et al., 2007). Peak intensities of the FTIR spectra are also in agreement with the corresponding various Q^n species observed in NMR studies, thereby implying if the phosphate chains have undergone polymerisation or depolymerisation.

2.2.4.4.1. FTIR analysis method

FTIR spectra were collected using a Perkin Elmer spectrometer 2000 (Perkin Elmer, Seer Green, UK) with an attenuated total reflectance accessory (Golden Gate, Specac, Orpington, UK). Powder samples were scanned at room temperature in an absorbance mode in the range of 600-1500 cm^{-1} at a 4 cm^{-1} resolution and the obtained data were analysed by the software supplied by Perkin Elmer Co.

2.3. Results

2.3.1. Sample preparation

Table 2.2 shows the effect of the drying procedure on the sol-gel synthesised phosphate-based glasses. Samples in the binary P_2O_5 - TiO_2 system with high titanium dioxide contents ($TiO_2 \geq 40$ mol%) turned to gel after storage for about 5 minutes at room temperature. However, for the samples with 30 and 35 mol% TiO_2 , the gelation was not observed even after storage for up to 3 days at room temperature. For these samples, the gelation occurred after overnight storage at 60 °C. Bulk, transparent and glassy-like specimens were obtained after the final heat treatment for samples with high TiO_2 content ($TiO_2 > 40$ mol%) (**Figs. 2.8A, B**). For the other compositions, however, dark brown and opaque powders were obtained.

All samples in the ternary P_2O_5 -CaO- TiO_2 system turned to gel after about two days storage at room temperature and transparent specimens were obtained after the final heat treatment. A bulk and glassy-like specimen with few cracks was obtained for a sample with TiO_2 content of 30 mol% (**Fig. 2.8C**).

For samples in the ternary P_2O_5 -CaO- Na_2O system, gelation was not observed even after storage for up to 3 days at room temperature. They turned into a gel after overnight storage at 60 °C, however, the prepared samples cracked into small fragments after the final heat treatment. The same behaviour was observed, in terms of gel formation, for samples in the quaternary P_2O_5 -CaO- NaO - TiO_2 system. A bulk and transparent specimen with a few cracks was obtained for a sample contain 15 mol% TiO_2 with phosphorus pentoxide at 55 mol% (**Fig. 2.8D**). For 40 mol% P_2O_5 quaternary glasses, however, it was not possible to make bulk samples.

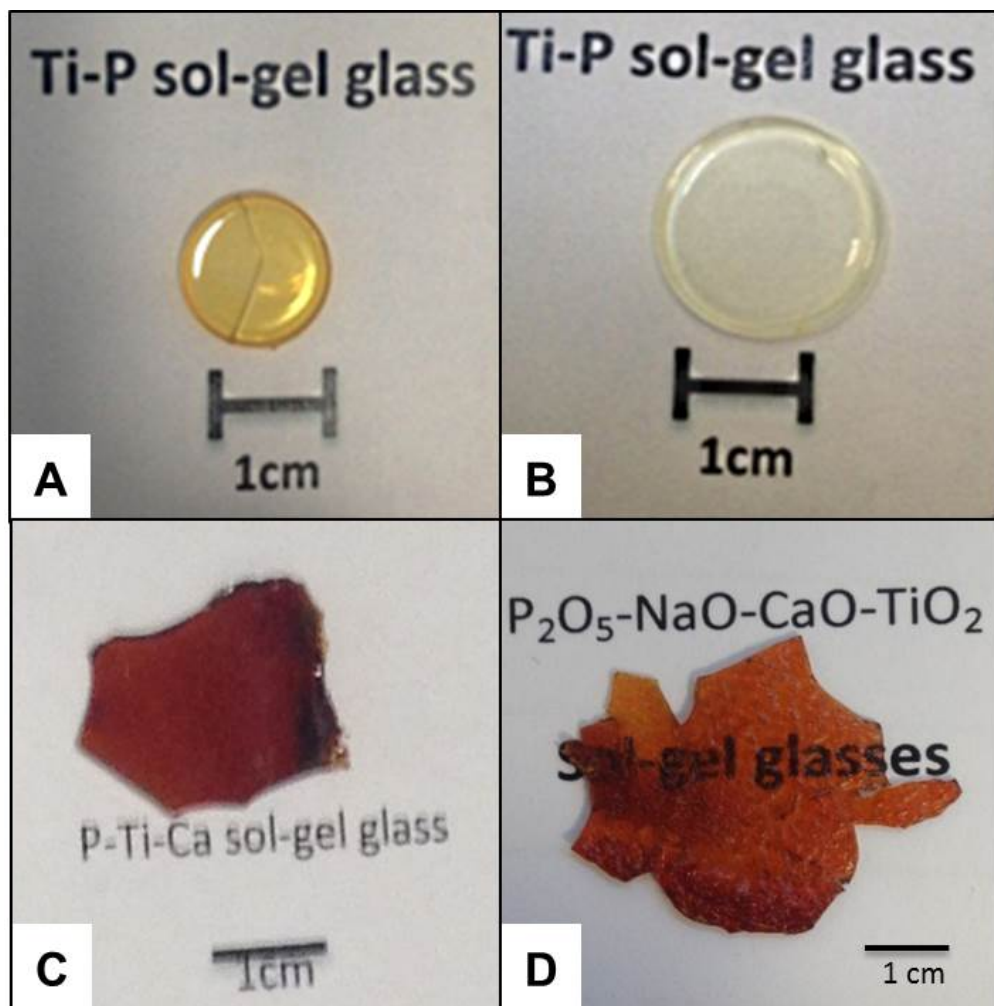


Figure 2.8. Photographs of heat treated; (A) EP₅₅T₄₅, (B) EP₅₀T₅₀, (C) EP₅₅CT₃₀, and (D) EP₅₅CNT₁₅ sol-gel derived glasses using triethyl phosphate as a phosphorus precursor.

Table 2.2. Effect of heat treatment on phosphate-based sol-gel derived glasses using triethyl phosphate as a phosphorus precursor.

Sample code	Gelation at room temperature	Transparency	Bulk and crack-free sample
EP ₇₀ T ₃₀	X	X	X
EP ₆₅ T ₃₅	X	X	X
EP ₆₀ T ₄₀	✓	✓	Heavily cracked
EP ₅₅ T ₄₅	✓	✓	Few cracks
EP ₅₀ T ₅₀	✓	✓	✓
EP ₅₅ CT ₂₀	✓	✓	Heavily cracked
EP ₅₅ CT ₂₅	✓	✓	Heavily cracked
EP ₅₅ CT ₃₀	✓	✓	Few cracks
EP ₅₅ CN ₁₀	X	✓	Heavily cracked
EP ₅₅ CN ₁₅	X	✓	Heavily cracked
EP ₅₅ CN ₂₀	X	✓	Heavily cracked
EP ₄₀ CNT ₂₀	X	✓	Heavily cracked
EP ₄₀ CNT ₂₅	X	✓	Heavily cracked
EP ₄₀ CNT ₃₀	X	✓	Heavily cracked
EP ₅₅ CNT ₅	X	✓	Heavily cracked
EP ₅₅ CNT ₁₀	X	✓	Heavily cracked
EP ₅₅ CNT ₁₅	X	✓	Few cracks

2.3.2. XRD

2.3.2.1. Binary P₂O₅-TiO₂ glasses

Figure 2.9 shows the XRD patterns of binary sol-gel derived samples in the P₂O₅-TiO₂ system. For samples containing TiO₂ ≥ 40 mol%, a broad peak at 2θ values of between 20 and 40° was observed and was free from any detectable crystalline peaks which confirmed the amorphous and glassy nature of these samples. Also,

as the TiO_2 content was increased, the intensity of these peaks increased. For the samples containing 30 and 35 mol% TiO_2 , however, crystalline patterns were observed with three main sharp peaks at 22, 25, and 28°. Crystalline phases were identified using the Crystallographica Search-Match software which corresponded to titanium pyrophosphate (TiP_2O_7) (ICDD no. 38-1468) (**Fig. 2.10a, b**) (Wang et al., 2007b). Since the aim of this study was to synthesise samples with an amorphous structure for potential biomedical applications, these samples were excluded from the rest of structural characterisation studies.

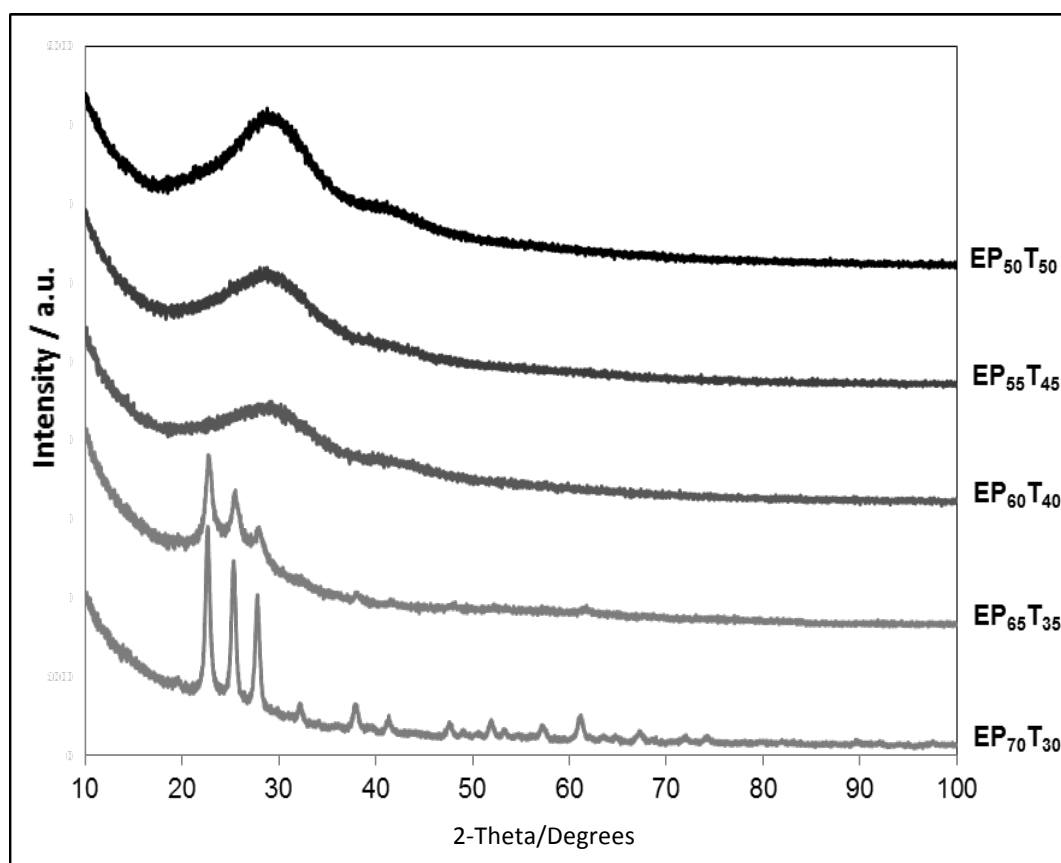


Figure 2.9. XRD patterns of binary sol-gel derived samples in the P_2O_5 - TiO_2 system using triethyl phosphate as a phosphorus precursor.

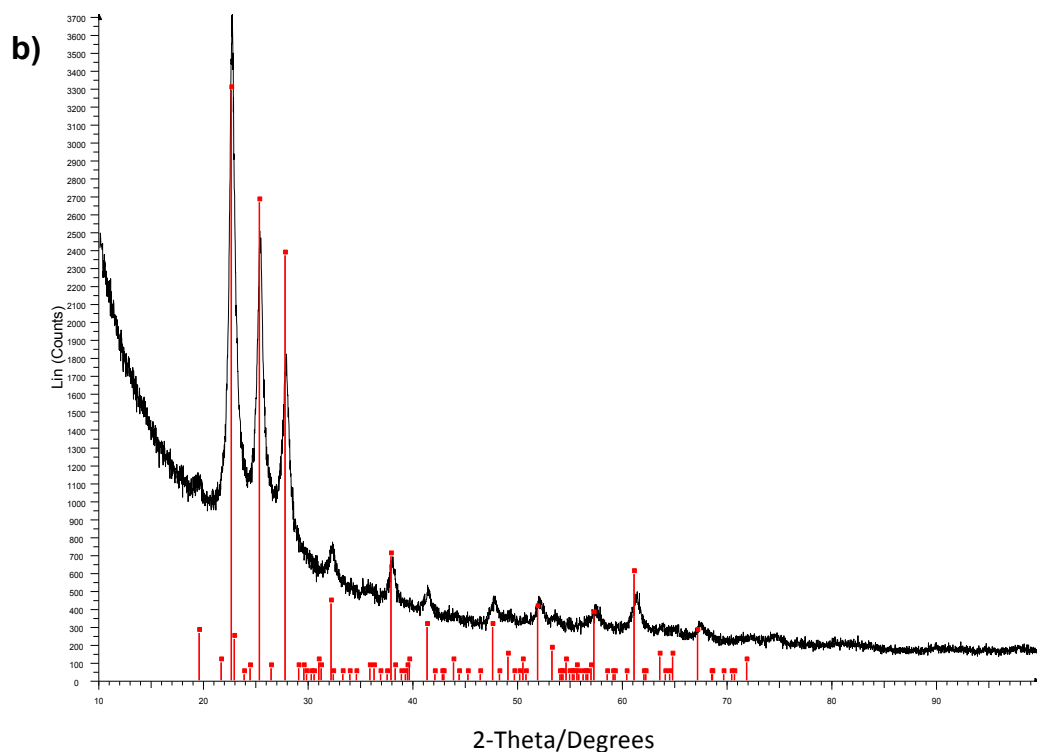
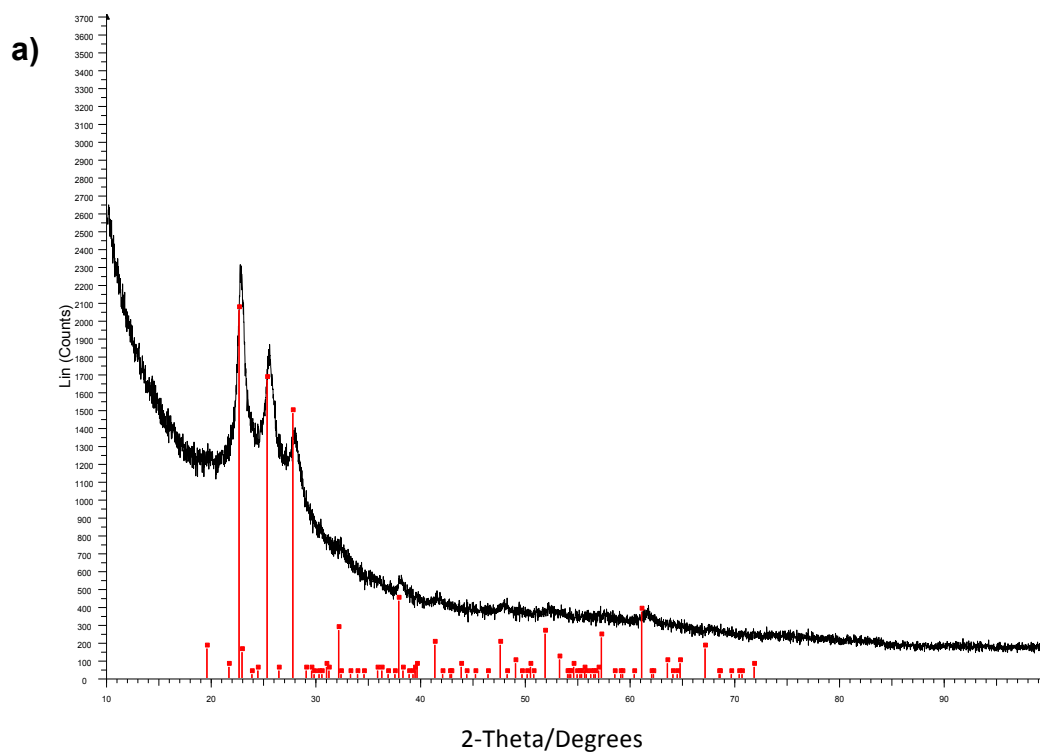


Figure 2.10. XRD patterns of; (a) EP₆₅T₃₅ and (b) EP₇₀T₃₀ sol-gel derived samples. Crystalline phases were identified using the Crystallographica Search-Match software which corresponded to TiP₂O₇ crystalline structure.

2.3.2.2. Ternary P₂O₅-CaO-TiO₂ and P₂O₅-CaO-Na₂O glasses

XRD patterns for phosphate-based glasses in the P₂O₅-CaO-TiO₂ and P₂O₅-CaO-Na₂O systems are shown in **Figures 2.11** and **2.12**. For both systems the XRD patterns were free from any detectable crystalline phase with a broad peak at 2 θ values of between 20 and 45°. These results confirmed the amorphous nature of the prepared samples in both systems.

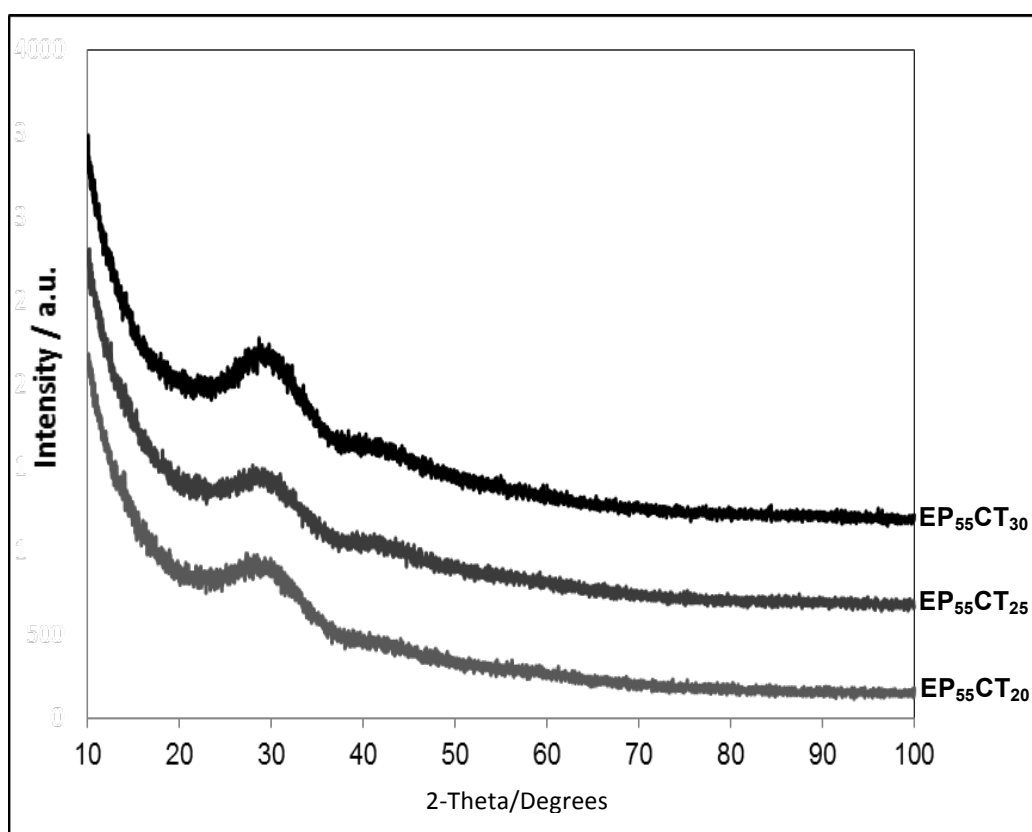


Figure 2.11. XRD patterns of ternary sol-gel derived glasses in the P_2O_5 -CaO-TiO₂ system using triethyl phosphate as a phosphorus precursor. All patterns are free from any detectable crystalline phases.

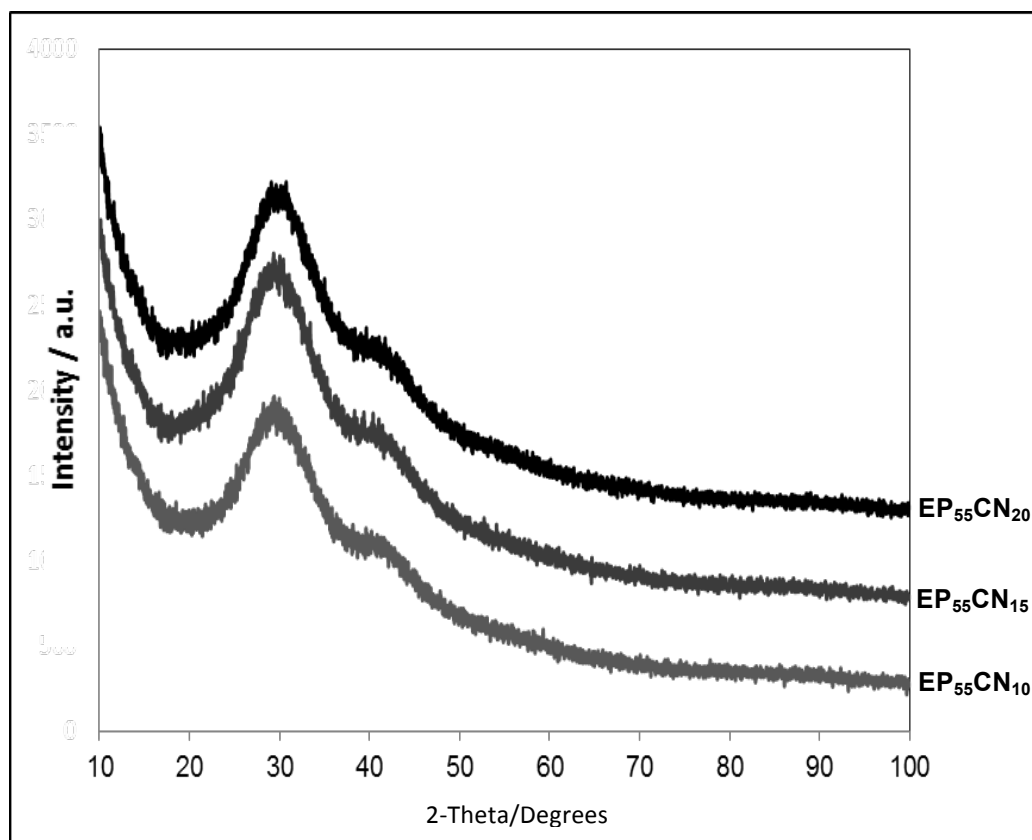


Figure 2.12. XRD patterns of ternary sol-gel derived glasses in the P_2O_5 -CaO-Na₂O system using triethyl phosphate as a phosphorus precursor which showed no evidence of any detectable crystalline phases.

2.3.2.3. Quaternary P_2O_5 -CaO-TiO₂-Na₂O glasses

Figure 2.13 shows the XRD patterns of quaternary sol-gel derived glasses in the P_2O_5 -CaO-Na₂O-TiO₂ system. For all samples, a broad peak at 2θ values of

between 20 and 40° was observed and was free from any detectable crystalline phase, confirming the amorphous and glassy nature of the prepared samples.

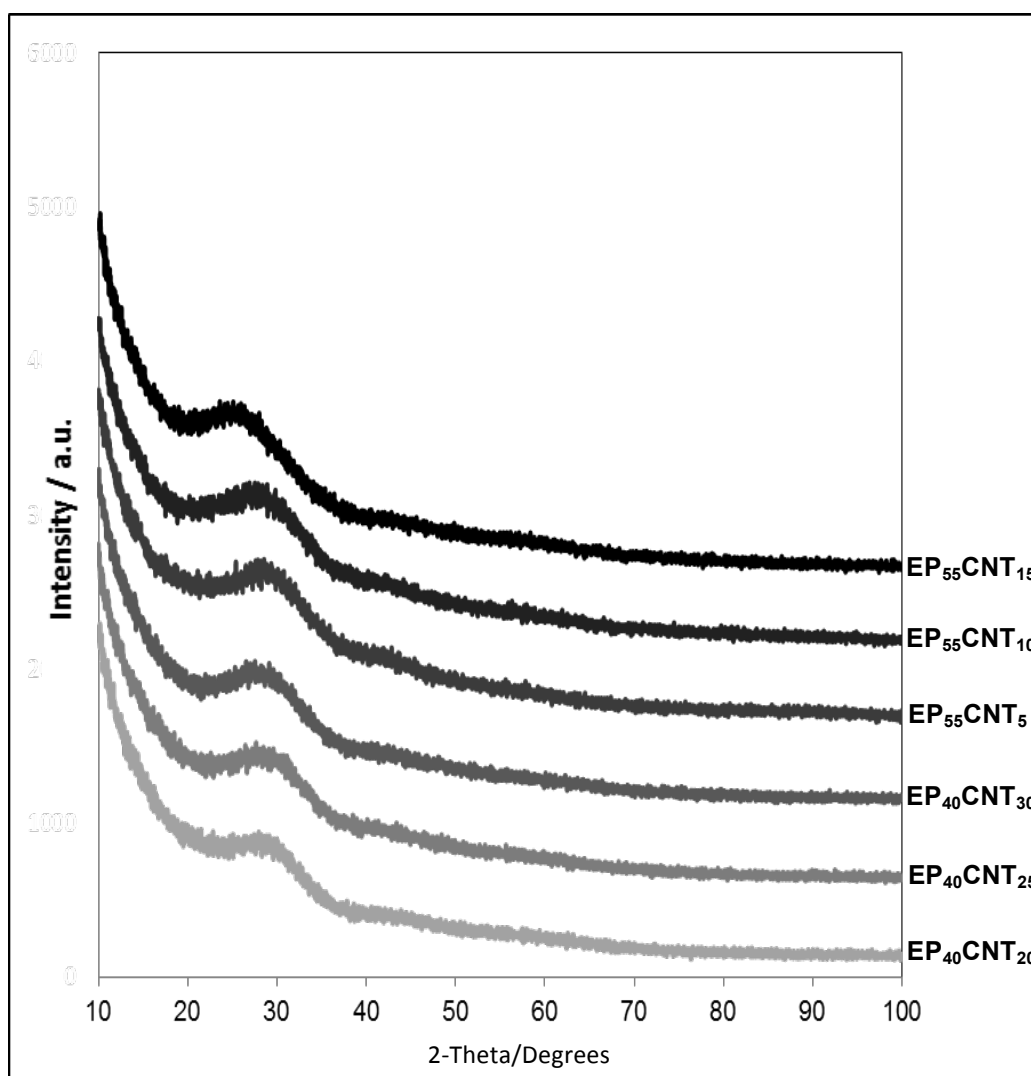


Figure 2.13. XRD patterns of the quaternary sol-gel derived glasses in the P₂O₅-CaO-Na₂O-TiO₂ system using triethyl phosphate as a phosphorus precursor that are free from any detectable crystalline phases.

2.3.3. EDX

EDX results are reported in **Table 2.3** that shows the highest deviation from the theoretical values for P_2O_5 content occurred in P_2O_5 -CaO- Na_2O sol-gel derived glasses which was 9.9-11.3 mol% lower than the theoretical values. This reduction was accompanied by a concomitant increase in the percentage content of the other oxides to compensate. While, glasses with a general formula of; P_2O_5 - TiO_2 , P_2O_5 -CaO- TiO_2 , and P_2O_5 -CaO- Na_2O - TiO_2 show 7.1-9.2, 7.4-8.7, and 7.7-9.7 mol% P_2O_5 reduction, respectively, from the theoretical values.

Table 2.3. Intended compositions and measured values of sol-gel derived glasses using triethyl phosphate as a phosphorus precursor determined by EDX (in parentheses).

Sample code	Concentration (mol%)			
	P_2O_5	TiO_2	CaO	Na_2O
EP ₆₀ T ₄₀	60.0 (50.8±1.6)	40.0 (49.2±1.4)	0.0	0.0
EP ₅₅ T ₄₅	55.0 (46.5±1.4)	45.0 (53.5±1.5)	0.0	0.0
EP ₅₀ T ₅₀	50.0 (42.9±1.5)	50.0 (57.1±1.7)	0.0	0.0
EP ₅₅ CT ₂₀	55.0 (46.3±1.9)	20.0 (24.9±1.8)	25.0 (28.8±1.3)	0.0
EP ₅₅ CT ₂₅	55.0 (47.1±1.5)	25.0 (29.7±1.6)	20.0 (23.2±1.2)	0.0
EP ₅₅ CT ₃₀	55.0 (47.6±1.4)	30.0 (34.4±1.5)	15.0 (18.0±1.3)	0.0
EP ₅₅ CN ₁₀	55.0 (45.1±1.4)	0.0	35.0 (41.5±1.0)	10.0 (13.4±1.0)
EP ₅₅ CN ₁₅	55.0 (44.6±1.0)	0.0	30.0 (36.8±0.9)	15.0 (18.6±0.8)
EP ₅₅ CN ₂₀	55.0 (43.7±1.1)	0.0	25.0 (32.0±1.0)	20.0 (24.3±0.7)
EP ₄₀ CNT ₂₀	40.0 (32.3±1.9)	20.0 (22.0±0.9)	25.0 (28.5±1.0)	15.0 (17.2±0.8)
EP ₄₀ CNT ₂₅	40.0 (32.5±2.1)	25.0 (26.8±0.8)	25.0 (27.8±1.1)	10.0 (12.9±0.9)
EP ₄₀ CNT ₃₀	40.0 (32.7±1.8)	30.0 (32.1±1.1)	25.0 (27.6±0.9)	5.0 (7.6±0.7)
EP ₅₅ CNT ₅	55.0 (45.3±1.8)	5.0 (7.9±0.8)	25.0 (29.0±1.2)	15.0 (17.8±1.0)
EP ₅₅ CNT ₁₀	55.0 (46.1±1.7)	10.0 (12.7±0.9)	25.0 (28.9±1.0)	10.0 (12.3±0.9)
EP ₅₅ CNT ₁₅	55.0 (46.7±2.0)	15.0 (17.6±1.1)	25.0 (28.4±1.3)	5.0 (7.3±0.9)

2.3.4. ^{31}P MAS-NMR

2.3.4.1. Binary $\text{P}_2\text{O}_5\text{-TiO}_2$ and ternary $\text{P}_2\text{O}_5\text{-CaO-TiO}_2$ and $\text{P}_2\text{O}_5\text{-CaO-Na}_2\text{O}$ glasses

^{31}P MAS-NMR spectra of binary and ternary phosphate-based glasses are presented in **Figures 2.15** and **2.16** and peak parameters of each spectrum are listed in **Table 2.4**. Peaks in the range of 0.8 to 1.7 ppm and -7.9 to -9.4 ppm are attributed to Q^0 and Q^1 phosphate units, respectively (Lee et al., 2013, Brow, 2000). Peaks in the range of -21.8 to -25.4 ppm are attributed to Q^2 phosphate units (Lee et al., 2013, Kirkpatrick and Brow, 1995). For titanium-containing glasses, additional peaks in the range between -14.3 and -15.7 ppm correspond to $\text{Q}^1(\text{Ti-O-P})$ phosphate units (Abrahams et al., 2004, Brauer et al., 2010, Foroutan et al., 2015).

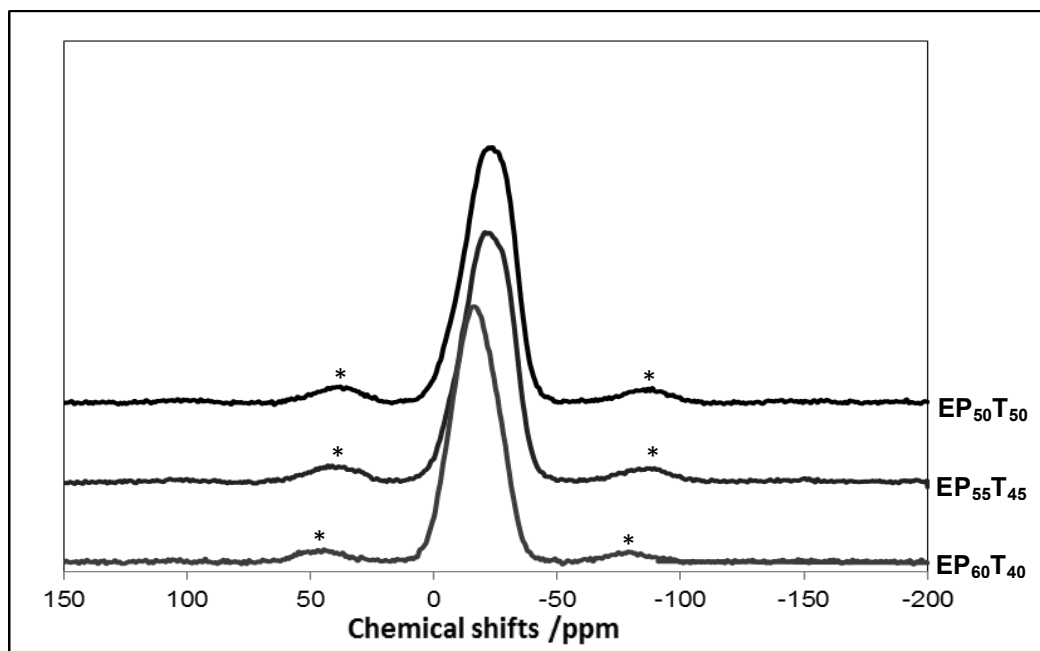


Figure 2.14. ^{31}P MAS-NMR spectra of binary $\text{P}_2\text{O}_5\text{-TiO}_2$ sol-gel derived glasses using triethyl phosphate as a phosphorus precursor. The peaks correspond to mainly Q^1 and Q^2 phosphate units. The asterisks denote spinning sidebands.

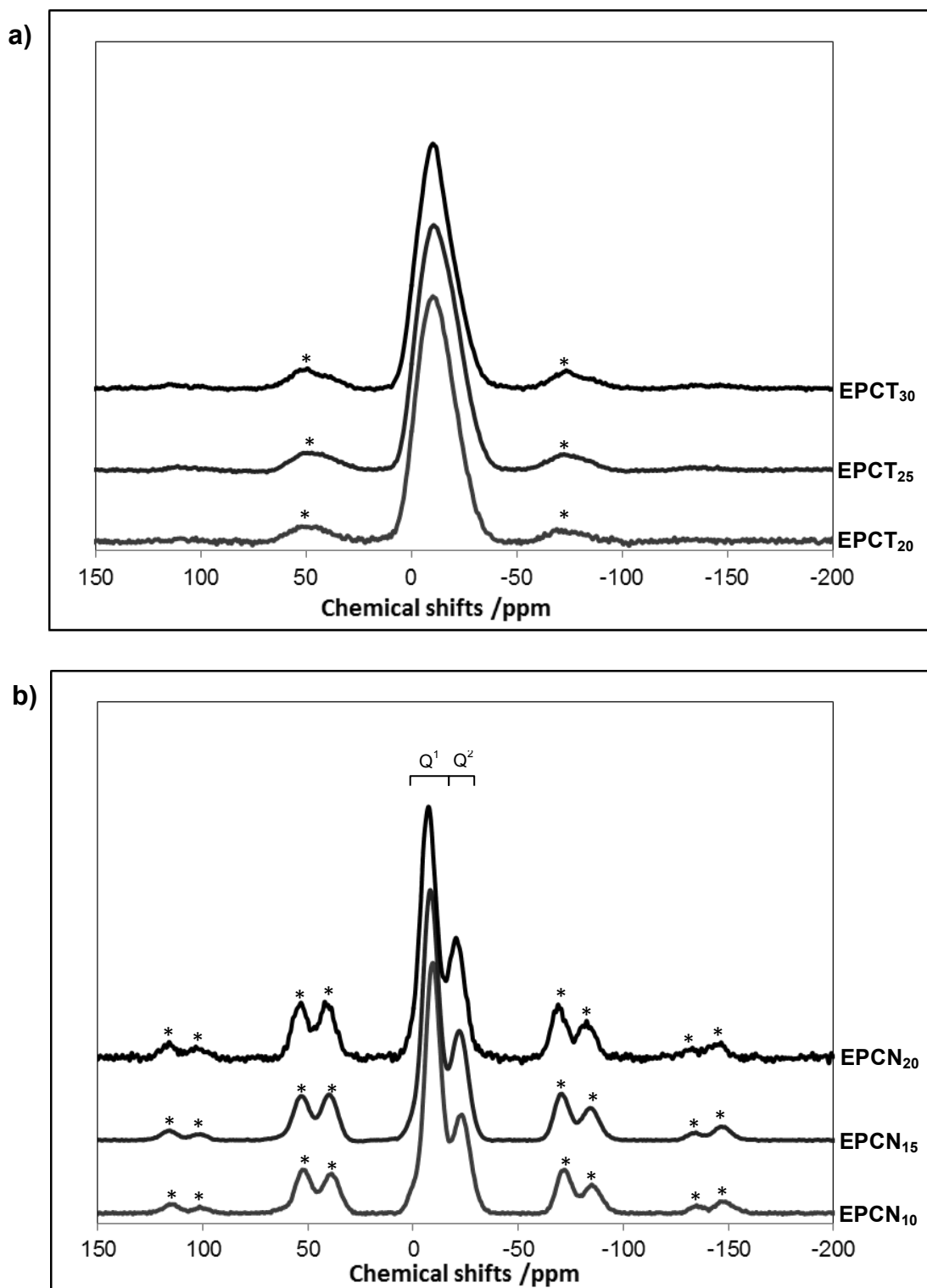


Figure 2.15. ^{31}P MAS-NMR spectra of ternary sol-gel derived glasses using triethyl phosphate as a phosphorus precursor in; (a) $\text{P}_2\text{O}_5\text{-CaO-TiO}_2$ and (b) $\text{P}_2\text{O}_5\text{-CaO-Na}_2\text{O}$ systems. The peaks correspond to mainly Q^1 and Q^2 phosphate units. The asterisks denote spinning sidebands.

Table 2.4. ^{31}P MAS-NMR peak parameters of binary and ternary phosphate-based sol-gel derived glasses using triethyl phosphate as a phosphorus precursor.

Sample code	Position (ppm, ± 0.2)	Q ⁱ species	Line width (ppm, ± 0.2)	Abundance (% , ± 1.0)
EP ₆₀ T ₄₀	1.3	0	3.9	8.4
	-8.8	1	6.4	24.3
	-15.2	1	9.7	46.5
	-24.3	2	12.3	20.8
EP ₅₅ T ₄₅	1.2	0	4.2	6.7
	-9.3	1	6.7	20.1
	-15.4	1	10.1	50.2
	-25.1	2	12.5	23.0
EP ₅₀ T ₅₀	0.9	0	4.6	5.8
	-9.4	1	6.8	17.4
	-15.7	1	10.4	52.7
	-25.4	2	12.6	24.1
EP ₅₅ CT ₂₀	-8.2	1	5.8	46.4
	-14.3	1	9.4	26.1
	-22.3	2	11.7	27.5
EP ₅₅ CT ₂₅	-8.3	1	6.4	39.1
	-14.5	1	9.5	29.8
	-22.8	2	12.1	32.0
EP ₅₅ CT ₃₀	-8.3	1	6.5	35.7
	-14.6	1	9.7	32.3
	-23.0	2	12.1	32.0
EP ₅₅ CN ₁₀	0.8	0	3.9	0.4
	-9.3	1	9.8	58.5
	-22.3	2	11.6	41.1
EP ₅₅ CN ₁₅	1.2	0	4.9	0.9
	-8.5	1	10.2	55.4
	-22.1	2	11.8	43.7
EP ₅₅ CN ₂₀	1.7	0	5.3	3.1
	-7.9	1	10.3	52.6
	-21.8	2	12.3	44.3

2.3.4.2. Quaternary P_2O_5 -CaO-Na₂O-TiO₂ glasses

Figure 2.16 shows ^{31}P MAS-NMR spectra of quaternary P_2O_5 -CaO-Na₂O-TiO₂ sol-gel derived glasses and peak parameters are given in **Table 2.5**. Peaks in the range of -0.4 to -1.1 ppm and -8.4 to -10.6 ppm are associated with Q^0 and Q^1 phosphate units, respectively. While, peaks in the range of -22.2 to -24.4 ppm are attributed to the Q^2 species (Lee et al., 2013, Montagne et al., 2003). Similarly, additional peaks in the range between -13.8 and -14.4 ppm can be related to the Q^1 (Ti-O-P) phosphate units (Abrahams et al., 2004, Foroutan et al., 2015).

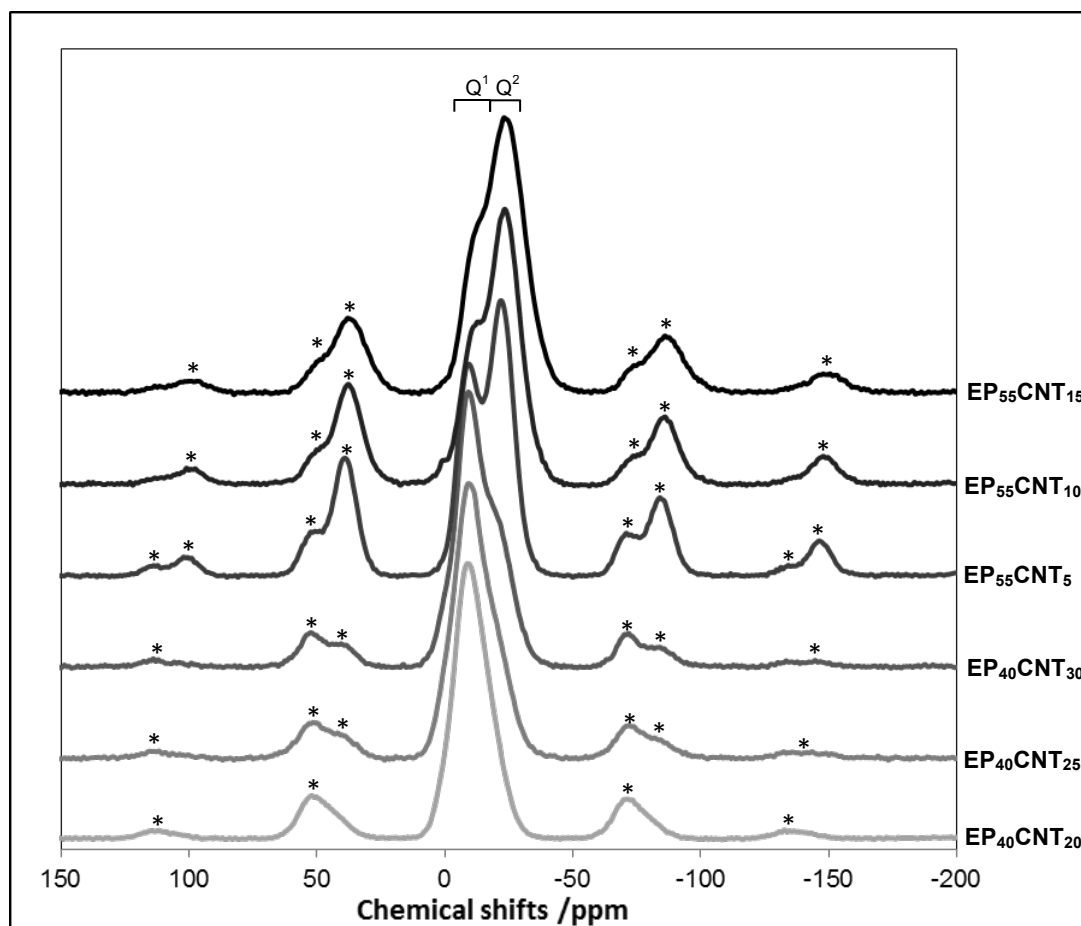


Figure 2.16. ^{31}P MAS-NMR spectra of quaternary P_2O_5 -CaO-Na₂O-TiO₂ sol-gel derived glasses using triethyl phosphate as a phosphorus precursor. The peaks correspond to mainly Q^1 and Q^2 phosphate units. The asterisks denote spinning sidebands.

Table 2.5. ^{31}P MAS-NMR peak parameters of quaternary $\text{P}_2\text{O}_5\text{-CaO-Na}_2\text{O-TiO}_2$ sol-gel derived glasses using triethyl phosphate as a phosphorus precursor.

Sample code	Position (ppm, ± 0.2)	Q^i species	Line width (ppm, ± 0.2)	Abundance (% , ± 1.0)
P ₄₀ CNT ₂₀	-0.4	0	5.3	4.6
	-8.4	1	6.2	54.5
	-13.9	1	9.1	29.2
	-22.3	2	10.5	11.7
P ₄₀ CNT ₂₅	-0.7	0	6.2	3.8
	-8.6	1	6.1	50.2
	-14.1	1	9.3	32.6
	-22.4	2	11.1	13.4
P ₄₀ CNT ₃₀	-1.1	0	6.7	3.6
	-8.9	1	5.9	46.2
	-14.4	1	9.4	33.9
	-22.7	2	11.4	16.3
P ₅₅ CNT ₅	-9.2	1	5.8	41.4
	-13.8	1	10.6	7.1
	-22.2	2	12.1	51.5
P ₅₅ CNT ₁₀	-10.4	1	6.2	37.1
	-14.0	1	10.7	9.5
	-23.7	2	12.5	53.4
P ₅₅ CNT ₁₅	-10.6	1	6.5	31.6
	-14.1	1	11.0	12.3
	-24.4	2	12.7	56.1

2.3.5. FTIR spectroscopy

Figures 2.17, 2.18, and 2.19 present FTIR data for $\text{P}_2\text{O}_5\text{-TiO}_2$, $\text{P}_2\text{O}_5\text{-CaO-TiO}_2$, $\text{P}_2\text{O}_5\text{-CaO-Na}_2\text{O}$, $\text{P}_2\text{O}_5\text{-CaO-Na}_2\text{O-TiO}_2$ sol-gel derived glass systems. Each spectrum was the result of summing 10 scans. Peaks assignments were acquired

according to the previous FTIR spectroscopy studies on phosphate-based glasses (Baia et al., 2007, Byun et al., 1995, Ilieva et al., 2001, Moustafa and El-Egili, 1998, Sene et al., 2004, Pickup et al., 2007). Peaks in the range of 730 to 740 cm^{-1} can be assigned to symmetrical stretching ν_s (P-O-P) mode, while peaks between 890 and 920 cm^{-1} can be assigned to asymmetrical stretching ν_{as} (P-O-P) mode that can be related to Q^2 phosphate species. Peaks between 1000 and 1120 cm^{-1} are associated with symmetrical stretching mode of ν_s (PO_3) $^{2-}$ (Q^1 phosphate units). Peaks in the range of 1100 to 1120 cm^{-1} and 1235 to 1250 cm^{-1} are assigned to asymmetrical ν_{as} (PO_3) $^{2-}$ and ν_{as} (PO_2) $^-$ modes which can be related to Q^1 and Q^2 phosphate units, respectively. For titanium-containing glasses, a small shift in the P-O-P band to higher wave numbers with an increase of TiO_2 content can be related to either smaller metallic cation size or shorter phosphate chain length (Shih, 2003). Infrared band assignment for phosphate-based sol-gel derived glasses are summarised in **Table 2.6**.

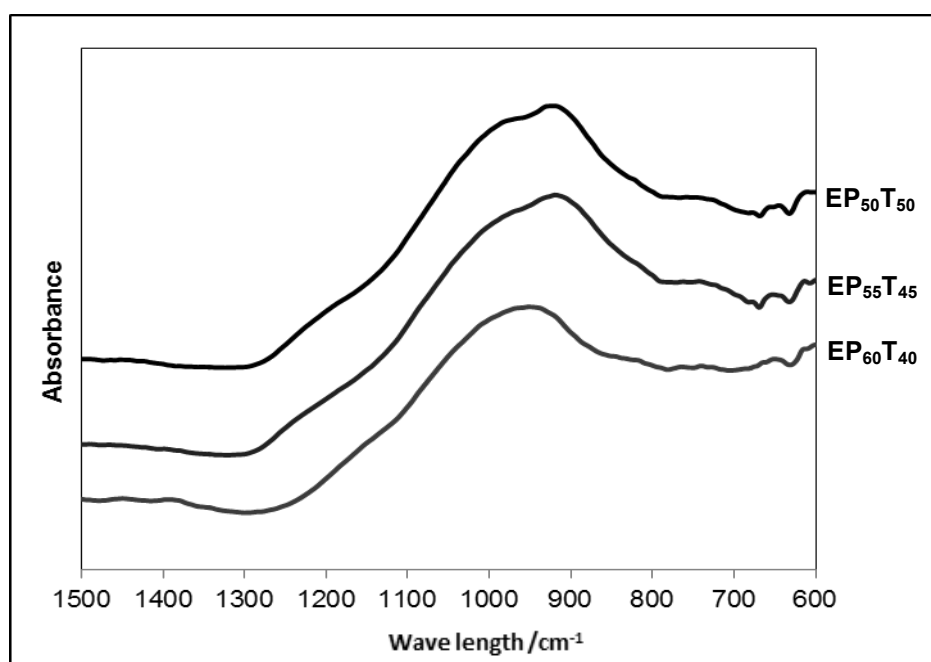


Figure 2.17. FTIR spectra of binary P_2O_5 - TiO_2 sol-gel derived glasses using triethyl phosphate as a phosphorus precursor.

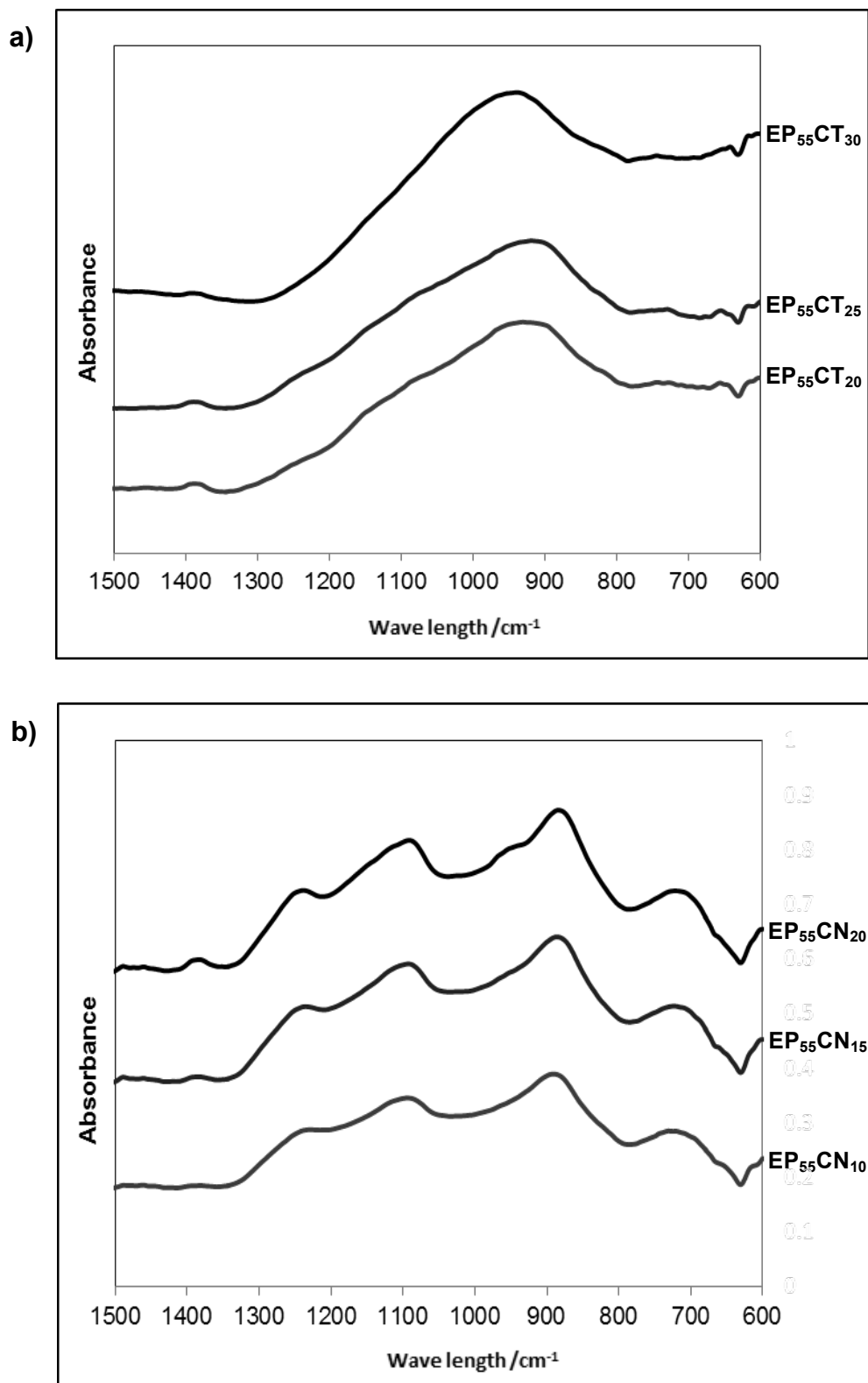


Figure 2.18. FTIR spectra of ternary sol-gel derived glasses using triethyl phosphate as a phosphorus precursor in; **(a)** P_2O_5 -CaO- TiO_2 and **(b)** P_2O_5 -CaO- Na_2O systems.

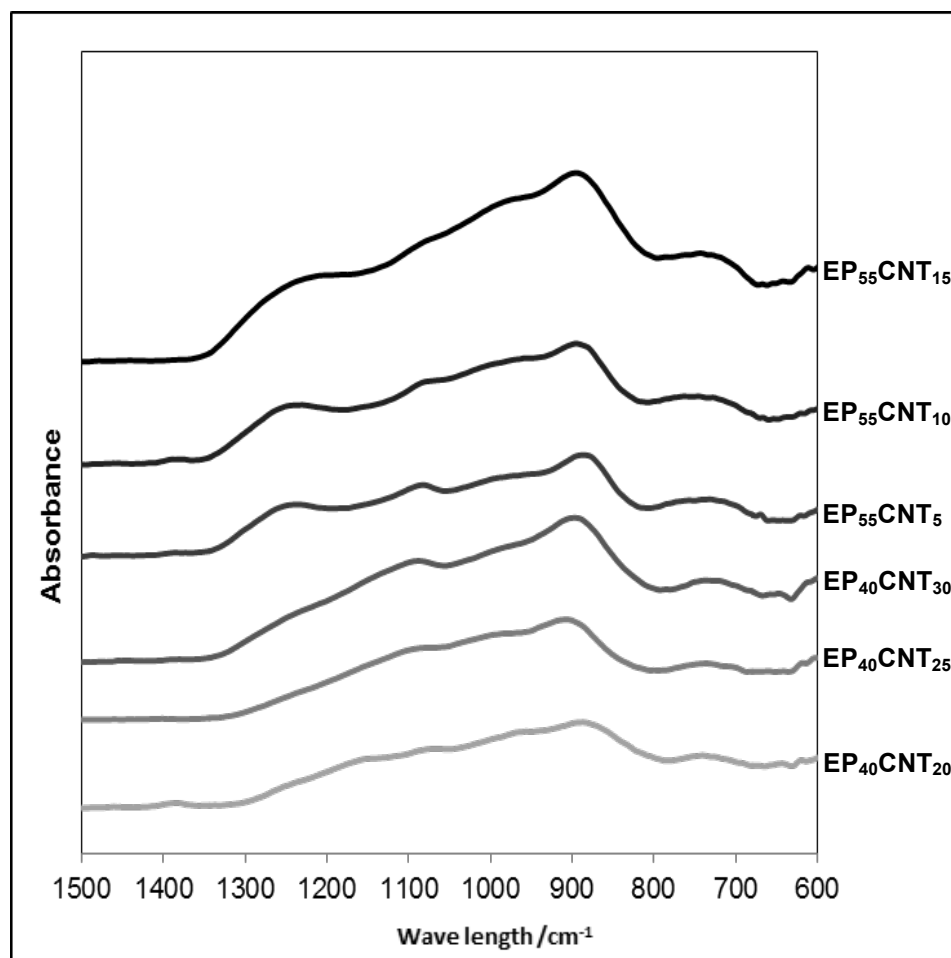


Figure 2.19. FTIR spectra of quaternary P_2O_5 -CaO- Na_2O - TiO_2 sol-gel derived glasses using triethyl phosphate as a phosphorus precursor.

Table 2.6. Infrared band assignment of phosphate-based sol-gel derived glasses using triethyl phosphate as a phosphorus precursor (ν , stretching; s, symmetric; as, asymmetric).

Wavenumber (cm^{-1})	Assignments	Associated Q^n
730-740	ν_s (P-O-P)	N/A
890-920	ν_{as} (P-O-P)	Q^2
985-1000	ν_s (PO_3) ²⁻	Q^1
1100-1120	ν_{as} (PO_3) ²⁻	Q^1
1235-1250	ν_{as} (PO_2) ⁻	Q^2

2.4. Discussion

The main objective of this chapter was to demonstrate the successful production of sol-gel derived phosphate-based glasses in the P_2O_5 - TiO_2 , P_2O_5 - TiO_2 - CaO , P_2O_5 - CaO - Na_2O , and P_2O_5 - CaO - Na_2O - TiO_2 systems. The sol-gel synthesis of phosphate-based glasses has been proven to be a challenging task since choosing the right precursors and also solvents with the capability of dissolving precursors and subsequent removal after the final heat treatment are essential. In this chapter, and in line with the previous study by Tang *et al.* (Tang *et al.*, 2005) who reported successful sol-gel synthesis of bulk titano-phosphate glasses, we used triethyl phosphate as a phosphorus precursor to sol-gel synthesise binary, ternary and quaternary phosphate-based glasses with a wide range of compositions. The maximum heat treatment temperature was set at 200 °C in order to not limit the potential use of these glasses for biomedical applications such as drug delivery systems. The chosen temperature was higher than the boiling point of the solvents used and it was selected to make sure there is no or minimal residual solvents (that can be very toxic for biomedical application purposes) exist in prepared samples after the final heat treatment.

Sample preparation results confirmed that the upper limit for the gel formation at room temperature for binary P_2O_5 - TiO_2 glasses is 60 mol% P_2O_5 . Bulk, transparent, and glassy-like specimens were successfully synthesised for samples contain 50 and 55 mol% P_2O_5 and XRD patterns for these samples were free from any detectable crystalline phase confirming the amorphous and glassy nature of these samples. For samples with $P_2O_5 > 60$ mol%, however, crystalline patterns were observed which corresponded to TiP_2O_7 structure. It should be noted that TiP_2O_7 ceramics have a great potential to be used in a variety of applications such as rechargeable batteries to replace with the current generation of rechargeable

lithium-ion-batteries (Rai et al., 2012, Wang et al., 2007a) and the sol-gel technique mentioned herein, may be a new, simplified and low temperature synthesis method to prepare these ceramics. However, this area was not in the scope of this study and were excluded from further investigation.

Ternary phosphate-based glasses in P_2O_5 -CaO- Na_2O and P_2O_5 -CaO- TiO_2 systems with fixed P_2O_5 content of 55 mol% were successfully synthesised *via* the sol-gel method. Bulk and transparent specimen was obtained for ternary titanium-containing glasses with high titanium dioxide content of 30 mol%. The same behaviour was observed for quaternary P_2O_5 -CaO- Na_2O - TiO_2 glasses at P_2O_5 content of 55 mol% when high titanium dioxide (15 mol% TiO_2) incorporated at the expense of sodium oxide that clearly indicates, incorporation of titanium into the phosphate-based glasses can make the phosphate network more interconnected due to the cross-linking effect of titanium (Abrahams et al., 2004, Brauer et al., 2010). However, it was not possible to make bulk glasses for quaternary P_2O_5 -CaO- Na_2O - TiO_2 sol-gel derived glasses at P_2O_5 content of 40 mol%, which might be related to the insufficient levels of P_2O_5 for these glasses to form a network. The XRD patterns for ternary and quaternary sol-gel derived glasses also confirmed the amorphous and glassy nature of these samples.

EDX results revealed a reduction of between 7 to 11 mol% P_2O_5 from the theoretical values with a concomitant increase in the percentage content of other oxides to compensate. This reduction was expected to be due to the slow reaction of triethyl phosphate and thus not all the P_2O_5 was incorporated into the glass network and could be lost by evaporation during the heat treatment cycle of the sol-gel process.

To confirm this, the evaporated gas from ternary $EP_{55}CN_{20}$ sol-gel derived sample that was heat treated up to 100 °C was analysed *via* FTIR spectroscopy during the heat treatment. This composition was chosen because of the high phosphorus loss of around 11 mol%, which was previously confirmed by EDX. For the heat

treatment cycle, differential thermal analysis (DTA) (Labsys, Setaram, Caluire, France) was used. Pure N₂ gas was used for the DTA inlet and the outlet connected to the FTIR spectroscopy chamber (2000, Perkin Elmer, Seer Green, UK) *via* PTFE tube to analyse the evaporated gas from the sample during the heat treatment cycle (**Figure 2.20**). The study was carried out on 50 mg of the powder sample and the heat treatment cycle was set at a heating rate of 20 °C.min⁻¹ from 100 to 220 °C, while the FTIR spectroscopy chamber was scanned in an absorbance mode in the range of 700-1500 cm⁻¹ at various time-points with the Timebase software supplied by Perkin Elmer Co. Each spectrum was baseline corrected prior to data analysis.

Figure 2.21 shows the FTIR spectroscopy data of the ternary EP₅₅CN₂₀ sol-gel derived sample that was confirmed an appearance of a broad peak at 1040 cm⁻¹ during the heat treatment cycle from 140 to 200 °C that can be attributed to the evaporation of unreacted phosphorus (PO₄³⁻) (Mobasherpour et al., 2007).

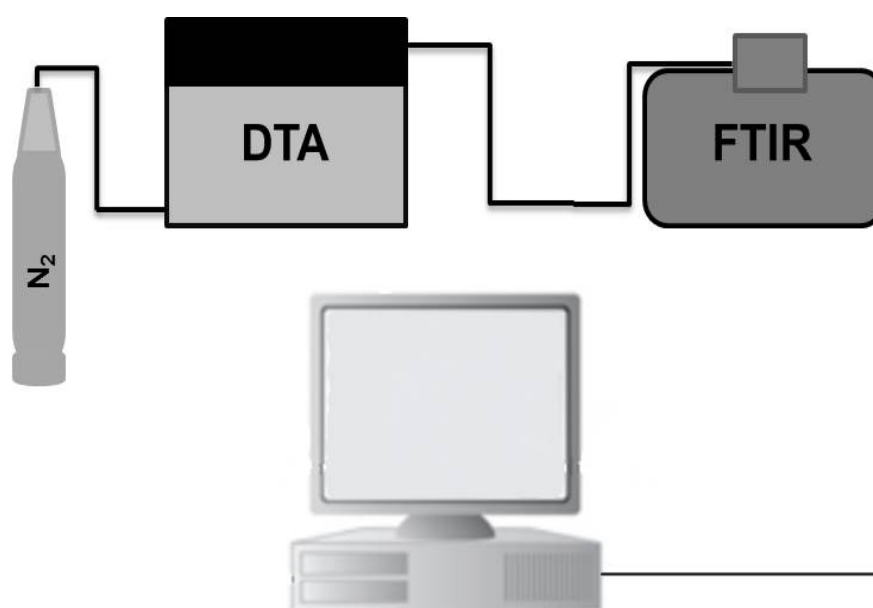


Figure 2.20. Schematic setup to analyse the evaporated gas from ternary EP₅₅CN₂₀ sol-gel derived sample *via* FTIR spectroscopy during the heat treatment cycle.

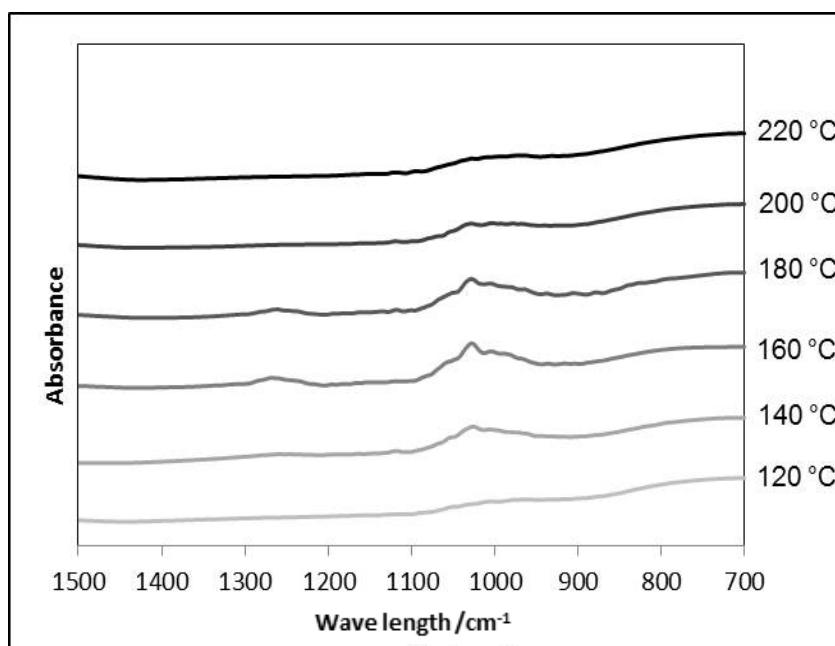


Figure 2.21. FTIR spectra of ternary EP₅₅CN₂₀ sol-gel derived sample during the heat treatment cycle from 100 to 220 °C.

Interestingly, substitution of titanium for calcium or sodium, reduced the phosphorus loss. This can be related to the cross-linking effect of titanium that makes the phosphate network more interconnected. ³¹P MAS-NMR results confirmed, the structure of the prepared phosphate-based glasses consists of mainly Q¹ and Q² phosphate units, indicating the structure has undergone polymerisation. In addition, substituting titanium for calcium or sodium improves the polymerisation of the phosphate network with a higher formation of Q² species. The FTIR measurements on the titanium-containing glasses were also in correlation with ³¹P MAS-NMR results that showed an increase in the intensity of the peaks in the range between 890 and 920 cm⁻¹ as titanium substituted in place of calcium or sodium.

These results suggested that titanium was acting as an ionic cross-linker and may increase the rigidity and durability of the phosphate network (Foroutan et al., 2015). Likewise, calcium can provide cross-links between the phosphate chains (but not as

strong as titanium, which has been shown to be), whereas, sodium can link to just one chain and therefore leads to depolymerisation of the phosphate network (Lee et al., 2013). The FTIR spectra of ternary glasses in the P_2O_5 -CaO- Na_2O system (**Fig. 2.17b**) were also in good correlation with the ^{31}P MAS-NMR data that revealed an increase in the intensity of the peaks at 900 and 1240 cm^{-1} as calcium substituted in place of sodium which is attributed to the Q^2 phosphate units.

In summary, to date, there have been no reports on sol-gel preparation of TiO_2 - P_2O_5 , P_2O_5 -CaO- TiO_2 , and P_2O_5 -CaO- Na_2O glasses with a wide range of compositions at relatively low processing temperatures as investigated here. We successfully synthesised these glass systems *via* a new and simplified sol-gel method. In this study for the first time, according to the knowledge of the author, the sol-gel preparation of quaternary P_2O_5 -CaO- Na_2O - TiO_2 glasses with high titanium dioxide content of up to 30 mol% was reported. While, incorporating a high amount of titanium into the phosphate network *via* melt-quench method is non-trivial and according to the literature the maximum percentage in quaternary phosphate-based glasses may only reach as high as 15 mol% TiO_2 since incorporation of higher amount of titanium either is not melt into the glass due to its sedimenting out or can causing immediate crystallisation of the glass upon removal from the furnace (Kiani et al., 2012). However, in this study, a relatively high amount of phosphorus was lost which might be related to the slow reaction of the phosphorus precursor used. In the next chapter, we investigated the use of a more reactive phosphorus precursor to increase the reaction rate and also reduce the amount of phosphorus lost during the sol-gel synthesis of these glasses.

References

- ABOU NEEL, E. A., PICKUP, D. M., VALAPPIL, S. P., NEWPORT, R. J. & KNOWLES, J. C. 2009. Bioactive functional materials: a perspective on phosphate-based glasses. *Journal of Materials Chemistry*, 19, 690-701.
- ABRAHAMS, I., HADZIFEJZOVIC, E. & DY GAS, J. R. 2004. Structural and electrical characterisation of Li₂O : TiO₂ : SnO₂ : P₂O₅ electrolyte glass. *Dalton Transactions*, 3129-3136.
- BAIA, L., MURESAN, D., BAIA, M., POPP, J. & SIMON, S. 2007. Structural properties of silver nanoclusters-phosphate glass composites. *Vibrational Spectroscopy*, 43, 313-318.
- BOSTMAN, O. & PIHLAJAMAKI, H. 2000a. Clinical biocompatibility of biodegradable orthopaedic implants for internal fixation: a review. *Biomaterials*, 21, 2615-2621.
- BOSTMAN, O. M. & PIHLAJAMAKI, H. K. 2000b. Adverse tissue reactions to bioabsorbable fixation devices. *Clinical Orthopaedics and Related Research*, 216-227.
- BRAUER, D. S., KARPUKHINA, N., LAW, R. V. & HILL, R. G. 2010. Effect of TiO₂ addition on structure, solubility and crystallisation of phosphate invert glasses for biomedical applications. *Journal of Non-Crystalline Solids*, 356, 2626-2633.
- BROW, R. K. 2000. Review: the structure of simple phosphate glasses. *Journal of Non-Crystalline Solids*, 263, 1-28.
- BYUN, J. O., KIM, B. H., HONG, K. S., JUNG, H. J., LEE, S. W. & IZYNEEV, A. A. 1995. Properties and Structure of R₂O-Na₂O-Al₂O₃-P₂O₅ (R=Mg, Ca, Sr, Ba) Glasses. *Journal of Non-Crystalline Solids*, 190, 288-295.
- CARTA, D., PICKUP, D. M., KNOWLES, J. C., AHMED, I., SMITH, M. E. & NEWPORT, R. J. 2007. A structural study of sol-gel and melt-quenched phosphate-based glasses. *Journal of Non-Crystalline Solids*, 353, 1759-1765.
- FOROUTAN, F., DE LEEUW, N., MARTIN, R., PALMER, G., OWENS, G., KIM, H.-W. & KNOWLES, J. 2015. Novel sol-gel preparation of (P₂O₅)_{0.4}-(CaO)_{0.25}-(Na₂O)_X-(TiO₂)_(0.35-X) bioresorbable glasses (X = 0.05, 0.1, and 0.15). *Journal of Sol-Gel Science and Technology*, 73, 434-442.
- GOLDSTEIN, J. 2003. Scanning Electron Microscopy and X-ray Microanalysis. *Springer US*, 1.

- ILIEVA, D., JIVOV, B., KOVACHEVA, D., TSACHEVA, T., DIMITRIEV, Y., BOGACHEV, G. & PETKOV, C. 2001. FT-IR and Raman spectra of Gd phosphate crystals and glasses. *Journal of Non-Crystalline Solids*, 293, 562-568.
- KIANI, A., LAKHKAR, N. J., SALIH, V., SMITH, M. E., HANNA, J. V., NEWPORT, R. J., PICKUP, D. M. & KNOWLES, J. C. 2012. Titanium-containing bioactive phosphate glasses. *Philosophical Transactions of the Royal Society a-Mathematical Physical and Engineering Sciences*, 370, 1352-1375.
- KIRKPATRICK, R. J. & BROW, R. K. 1995. Nuclear-Magnetic-Resonance Investigation of the Structures of Phosphate and Phosphate-Containing Glasses - a Review. *Solid State Nuclear Magnetic Resonance*, 5, 9-21.
- LE SAOUT, G., SIMON, P., FAYON, F., BLIN, A. & VAILLS, Y. 2002. Raman and infrared study of $(\text{PbO})_x(\text{P}_2\text{O}_5)_{(1-x)}$ glasses. *Journal of Raman Spectroscopy*, 33, 740-746.
- LEE, I. H., FOROUTAN, F., LAKHKAR, N. J., GONG, M. S. & KNOWLES, J. C. 2013. Sol-gel synthesis and structural characterization of $\text{P}_2\text{O}_5\text{-CaO-Na}_2\text{O}$ glasses. *Physics and Chemistry of Glasses-European Journal of Glass Science and Technology Part B*, 54, 115-120.
- MACKENZIE, K. J. D. & SMITH, M. E. 2002. Multinuclear Solid State NMR of Inorganic Materials. *Oxford, Pergamon*.
- MASSIOT, D., FAYON, F., CAPRON, M., KING, I., LE CALVE, S., ALONSO, B., DURAND, J. O., BUJOLI, B., GAN, Z. H. & HOATSON, G. 2002. Modelling one- and two-dimensional solid-state NMR spectra. *Magnetic Resonance in Chemistry*, 40, 70-76.
- MOBASHERPOUR, I., HESHAJIN, M. S., KAZEMZADEH, A. & ZAKERI, M. 2007. Synthesis of nanocrystalline hydroxyapatite by using precipitation method. *Journal of Alloys and Compounds*, 430, 330-333.
- MONTAGNE, L., DAVIERO, S. & PALAVIT, G. 2003. Glass network evolution with $\text{Bi}^{3+}/\text{Ti}^{4+}$ substitution in phosphate glasses formulated with a constant oxygen/phosphorus ratio. EXAFS, XANES, and P-31 double quantum MAS NMR. *Chemistry of Materials*, 15, 4709-4716.
- MOUSTAFA, Y. M. & EL-EGILI, K. 1998. Infrared spectra of sodium phosphate glasses. *Journal of Non-Crystalline Solids*, 240, 144-153.
- PICKUP, D. M., GUERRY, P., MOSS, R. M., KNOWLES, J. C., SMITH, M. E. & NEWPORT, R. J. 2007. New sol-gel synthesis of a $(\text{CaO})_{0.3}(\text{P}_2\text{O}_5)_{0.7}$ glass.

- Na₂O)(0.2)(P₂O₅)(0.5) bioresorbable glass and its structural characterisation. *Journal of Materials Chemistry*, 17, 4777-4784.
- RAI, A. K., GIM, J., SONG, J., MATHEW, V., ANH, L. T. & KIM, J. 2012. Electrochemical and safety characteristics of TiP₂O₇-graphene nanocomposite anode for rechargeable lithium-ion batteries. *Electrochimica Acta*, 75, 247-253.
- SENE, F. F., MARTINELLI, J. R. & GOMES, L. 2004. Synthesis and characterization of niobium phosphate glasses containing barium and potassium. *Journal of Non-Crystalline Solids*, 348, 30-37.
- SHIH, P. Y. 2003. Properties and FTIR spectra of lead phosphate glasses for nuclear waste immobilization. *Materials Chemistry and Physics*, 80, 299-304.
- TANG, A. J., HASHIMOTO, T., NASU, H. & KAMIYA, K. 2005. Sol-gel preparation and properties of TiO₂-P₂O₅ bulk glasses. *Materials Research Bulletin*, 40, 55-66.
- WANG, H., HUANG, K., ZENG, Y., YANG, S. & CHEN, L. 2007a. Electrochemical properties of TiP₂O₇ and LiTi₂(PO₄)₃ as anode material for lithium ion battery with aqueous solution electrolyte. *Electrochimica Acta*, 52, 3280-3285.
- WANG, H. B., HUANG, K. L., ZENG, Y. Q., YANG, S. & CHEN, L. Q. 2007b. Electrochemical properties of TiP₂O₇ and LiTi₂(PO₄)₃ as anode material for lithium ion battery with aqueous solution electrolyte. *Electrochimica Acta*, 52, 3280-3285.
- WARREN, B. E. 1969. X-Ray Studies of Glass Structure. *American Ceramic Society Bulletin*, 48, 872-&.

CHAPTER 3

Sol-Gel Synthesis and Characterisation of Phosphate-Based Glasses Using n-butyl Phosphate as a Phosphorus Precursor

3.1. Introduction

In the previous chapter, EDX results revealed a relatively high phosphorus reduction from the theoretical values (~7-11 mol%) that was due to the evaporation of unreacted phosphorus during the heat treatment cycle of sol-gel process. A range of more reactive phosphorus precursors have been investigated to increase the reaction rate and also reduce the amount of phosphorus loss during the sol-gel process such as phosphoric acid (H_3PO_4), phosphoryl chloride (POCl_3), and alkyl phosphates like n-butyl phosphate (Livage et al., 1992). The results showed that H_3PO_4 is too reactive and usually leads to precipitation, while POCl_3 and n-butyl phosphate seem to be better alternatives for the sol-gel synthesis of phosphate-based glasses (Pickup et al., 2007, Clayden et al., 2001). It was also confirmed that the phosphorus loss from POCl_3 during the sol-gel reaction is relatively higher than n-butyl phosphate (Carta et al., 2005, Lee et al., 1996).

In this chapter, n-butyl phosphate was used as a phosphorus precursor to synthesise ternary $\text{P}_2\text{O}_5\text{-CaO-Na}_2\text{O}$ and quaternary $\text{P}_2\text{O}_5\text{-CaO-NaO-TiO}_2$ glass systems *via* the sol-gel method. A similar preparation method that was explained in chapter 2, was used to make these glass systems with a wide range of compositions. The structure of the prepared samples was characterised using XRD, ^{31}P MAS-NMR, FTIR spectroscopy, and the elemental proportions were measured by EDX. The compositions of the starting solutions are shown in **Table 3.1**.

Table 3.1. Compositions of starting solutions for ternary P_2O_5 -CaO- Na_2O and quaternary P_2O_5 -CaO- Na_2O - TiO_2 sol-gel derived samples using n-butyl phosphate as a phosphorus precursor.

Sample code	Theoretical composition	Concentration (mol%)			
		P_2O_5	CaO	Na_2O	TiO_2
BP ₅₅ CN ₁₀	$(P_2O_5)_{55}-(CaO)_{35}-(Na_2O)_{10}$	55.0	35.0	10.0	0.0
BP ₅₅ CN ₁₅	$(P_2O_5)_{55}-(CaO)_{30}-(Na_2O)_{15}$	55.0	30.0	15.0	0.0
BP ₅₅ CN ₂₀	$(P_2O_5)_{55}-(CaO)_{25}-(Na_2O)_{20}$	55.0	25.0	20.0	0.0
BP ₄₀ CNT ₂₀	$(P_2O_5)_{40}-(CaO)_{25}-(Na_2O)_{15}-(TiO_2)_{20}$	40.0	25.0	15.0	20.0
BP ₄₀ CNT ₂₅	$(P_2O_5)_{40}-(CaO)_{25}-(Na_2O)_{10}-(TiO_2)_{25}$	40.0	25.0	10.0	25.0
BP ₄₀ CNT ₃₀	$(P_2O_5)_{40}-(CaO)_{25}-(Na_2O)_5-(TiO_2)_{30}$	40.0	25.0	5.0	30.0
BP ₅₅ CNT ₅	$(P_2O_5)_{55}-(CaO)_{25}-(Na_2O)_{15}-(TiO_2)_5$	55.0	25.0	15.0	5.0
BP ₅₅ CNT ₁₀	$(P_2O_5)_{55}-(CaO)_{25}-(Na_2O)_{10}-(TiO_2)_{10}$	55.0	25.0	10.0	10.0
BP ₅₅ CNT ₁₅	$(P_2O_5)_{55}-(CaO)_{25}-(Na_2O)_5-(TiO_2)_{15}$	55.0	25.0	5.0	15.0

3.2. Materials and methods

3.2.1. Materials

The precursors used have been reported in section 2.2.1. However, instead of triethyl phosphate, n-butyl phosphate (1:1 molar ratio of mono and di-n-butyl phosphate, 98%, Alfa Aesar, Heysham, UK) was used without further purification to prepare ternary P_2O_5 -CaO- Na_2O and quaternary P_2O_5 -CaO- Na_2O - TiO_2 glass systems. **Figure 3.1** shows the structural formula of n-butyl phosphate.

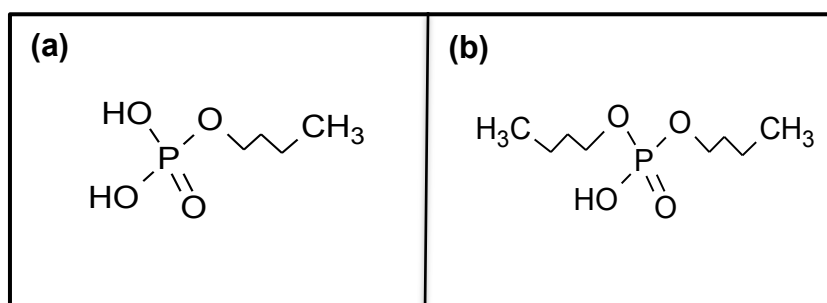


Figure 3.1. Structural formula of n-butyl phosphate; a mixture of **(a)** mono butyl phosphate ($C_4H_{11}O_4P$) and **(b)** di-butyl phosphate ($C_8H_{19}O_4P$).

3.2.2. Sol-gel synthesis methods

Similar sol-gel synthesis methods that were described previously in sections 2.2.2.3 and 2.2.2.4, were used to prepare ternary and quaternary phosphate-based glasses. The sol-gel preparation of ternary P_2O_5 -CaO- Na_2O and quaternary P_2O_5 -CaO- Na_2O - TiO_2 glass systems is outlined schematically in **Figure 3.2**.

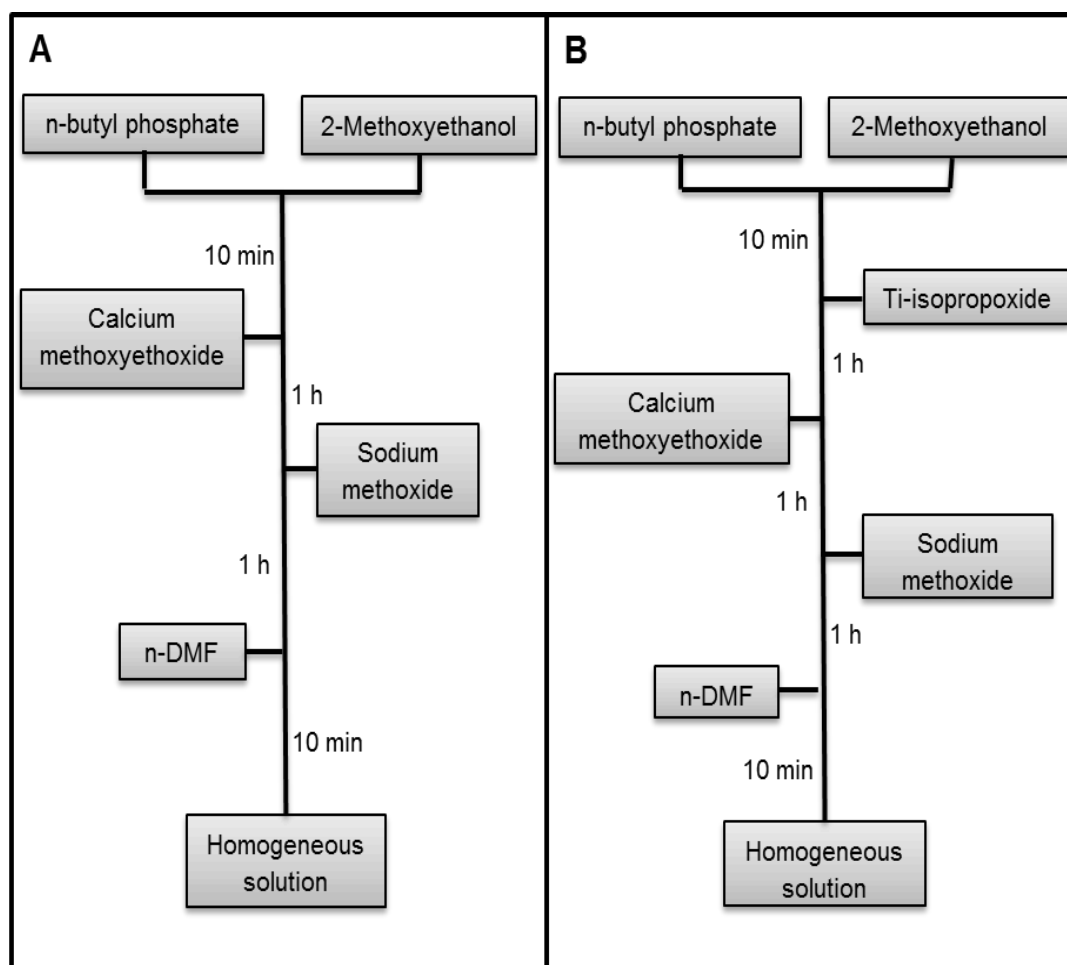


Figure 3.2. Schematic sol-gel synthesis of; **(A)** ternary P_2O_5 -CaO- Na_2O and **(B)** quaternary P_2O_5 -CaO- Na_2O - TiO_2 samples using n-butyl phosphate as a phosphorus precursor.

3.2.3. Drying procedure

The obtained homogeneous solutions were transferred into glass containers and heat treated similar to the previously explained method in section 2.2.3.

3.2.4. Structural characterisation methods

3.2.4.1. XRD and EDX

XRD and EDX characterisation methods were carried out on glass powders as previously reported in sections 2.2.4.1.1 and 2.2.4.2.1.

3.2.4.2. ^{31}P MAS-NMR and FTIR spectroscopy

^{31}P MAS-NMR and FTIR spectroscopy characterisation methods were carried out on glass powders as explained in sections 2.2.4.3.1 and 2.2.4.4.1

3.3. Results

3.3.1. Sample preparation

All samples in both ternary and quaternary systems turned to gel within the first 5 minutes at room temperature. Bulk, transparent and glassy-like specimens with few cracks were obtained for glasses with TiO_2 content of 15 mol% for glasses with 55 mol% P_2O_5 , and 25 or 30 mol% TiO_2 for glasses with P_2O_5 content at 40 mol% (**Fig. 3.3**). However, for ternary sol-gel synthesised glasses in the P_2O_5 -CaO- Na_2O system, it was not possible to make bulk specimens. A summary of the effect of the drying procedure in ternary and quaternary glasses is shown in **Table 3.2**.

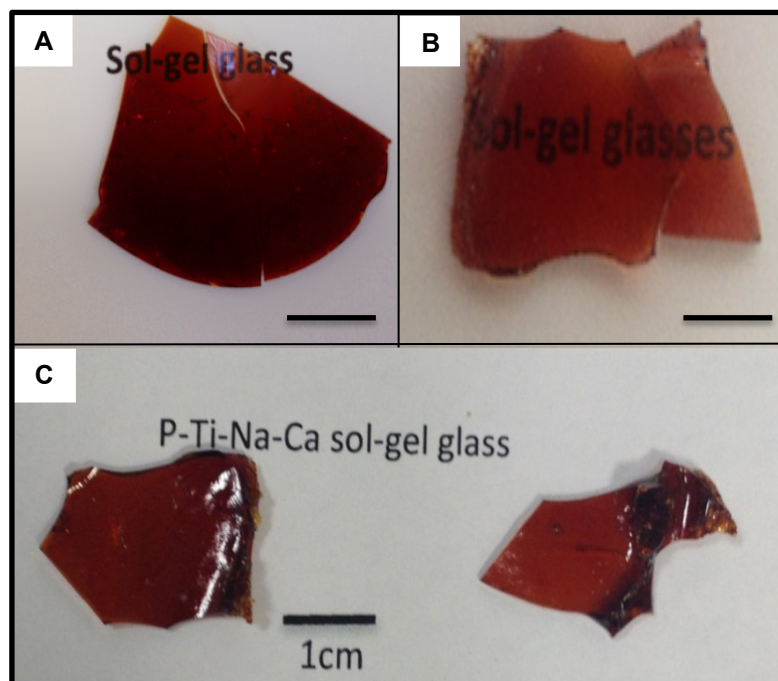


Figure 3.3. Photographs of; **A)** BP₄₀CNT₂₅, **B)** BP₄₀CNT₃₀, and **C)** BP₅₅CNT₁₅ sol-gel derived samples. The scale bar for **A**, **B**, and **C** is 1 cm.

Table 3.2. The effect of drying procedure in ternary P₂O₅-CaO-Na₂O and quaternary P₂O₅-CaO-Na₂O-TiO₂ sol-gel derived samples using n-butyl phosphate as a phosphorus precursor.

Sample code	Gelation at room temperature	Transparency	Bulk and crack-free sample
BP ₅₅ CN ₁₀	✓	✓	Heavily cracked
BP ₅₅ CN ₁₅	✓	✓	Heavily cracked
BP ₅₅ CN ₂₀	✓	✓	Heavily cracked
BP ₄₀ CNT ₂₀	✓	✓	Heavily cracked
BP ₄₀ CNT ₂₅	✓	✓	Few cracks
BP ₄₀ CNT ₃₀	✓	✓	Few cracks
BP ₅₅ CNT ₅	✓	✓	Heavily cracked
BP ₅₅ CNT ₁₀	✓	✓	Heavily cracked
BP ₅₅ CNT ₁₅	✓	✓	Few cracks

3.3.2. XRD

Figures 3.4 and 3.5 show the XRD patterns of ternary P_2O_5 -CaO- Na_2O and quaternary P_2O_5 -CaO- Na_2O - TiO_2 sol-gel derived samples, respectively. For both systems the XRD patterns were free from any detectable crystalline phases with a broad peak at 2θ values of between 20 and 40° that confirmed the amorphous and glassy nature of the prepared samples.

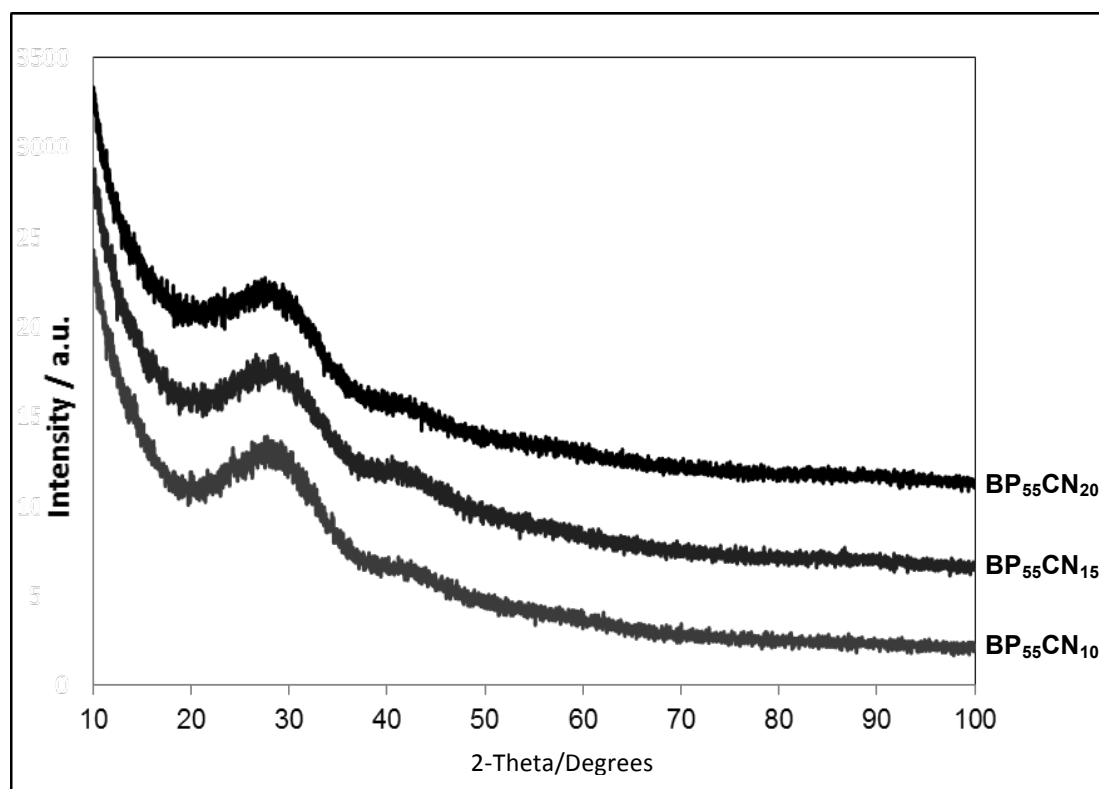


Figure 3.4. XRD patterns of ternary P_2O_5 -CaO- Na_2O sol-gel derived samples using n-butyl phosphate as a phosphorus precursor which are free from any detectable crystalline phases.

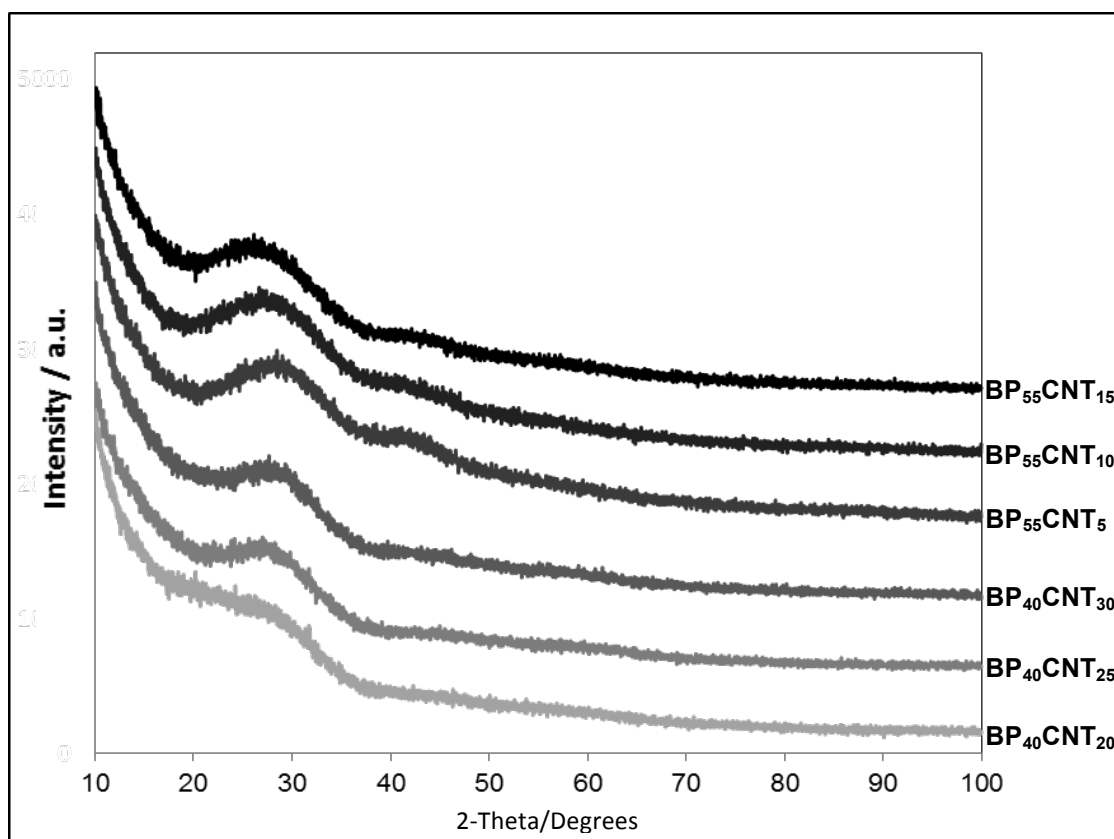


Figure 3.5. XRD patterns of quaternary P_2O_5 -CaO- Na_2O - TiO_2 sol-gel derived samples using n-butyl phosphate as a phosphorus precursor which showed no evidence of any detectable crystalline phases.

3.3.3. EDX

The EDX results were converted to mol% of oxides of the elements to allow a comparison to be made with the theoretical compositions and were reported in **Table 3.3**. A reduction of 5.7-8.0 mol% P_2O_5 from the theoretical values was observed for ternary glasses in the P_2O_5 -CaO- Na_2O system, with a concomitant increase in the percentage content of the other oxides to compensate. While, for quaternary glasses in the P_2O_5 -CaO- Na_2O - TiO_2 system, as titanium was substituted

in place of sodium, the amount of P_2O_5 loss decreased to 3.8-5.4 mol% from the theoretical values.

Table 3.3. Intended compositions and measured values of sol-gel derived glasses using n-butyl phosphate as a phosphorus precursor determined by EDX (in parentheses).

Sample code	P_2O_5 (mol%)	CaO (mol%)	Na_2O (mol%)	TiO_2 (mol%)
BP ₅₅ CN ₁₀	55.0 (49.3±1.1)	35.0 (38.6±1.2)	10.0 (12.1±0.7)	0.0
BP ₅₅ CN ₁₅	55.0 (48.1±1.3)	30.0 (34.6±1.4)	15.0 (17.3±0.8)	0.0
BP ₅₅ CN ₂₀	55.0 (47.0±1.0)	25.0 (30.8±0.9)	20.0 (22.2±0.6)	0.0
BP ₄₀ CNT ₂₀	40.0 (35.6±1.2)	25.0 (26.9±0.8)	15.0 (16.4±0.8)	20.0 (21.1±0.7)
BP ₄₀ CNT ₂₅	40.0 (35.9±1.3)	25.0 (26.9±1.0)	10.0 (11.2±0.9)	25.0 (26.0±0.8)
BP ₄₀ CNT ₃₀	40.0 (36.2±1.1)	25.0 (26.7±0.9)	5.0 (5.9±0.7)	30.0 (31.2±0.8)
BP ₅₅ CNT ₅	55.0 (49.6±1.0)	25.0 (27.2±0.7)	15.0 (16.7±0.8)	5.0 (6.5±0.9)
BP ₅₅ CNT ₁₀	55.0 (50.2±1.2)	25.0 (27.0±0.8)	10.0 (11.5±0.7)	10.0 (11.3±0.7)
BP ₅₅ CNT ₁₅	55.0 (50.9±1.1)	25.0 (26.5±0.6)	5.0 (6.1±0.6)	15.0 (16.5±1.0)

3.3.4. ^{31}P MAS-NMR

^{31}P MAS-NMR spectra of ternary P_2O_5 -CaO- Na_2O and quaternary P_2O_5 -CaO- Na_2O - TiO_2 sol-gel derived glasses are shown in **Figure 3.6** and peak parameters are summarised in **Table 3.4**. Peaks in the range of -9.9 to -10.8 ppm are attributed to Q^1 phosphate units, while peaks in the range of -21.9 to -23.9 ppm correspond to Q^2 species (Lee et al., 2013, Foroutan et al., 2015). Additional peaks in quaternary glasses in the range of -0.2 to -1.2 ppm and -13.6 to -14.8 ppm are attributed to Q^0 and $Q^1(Ti-O-P)$ phosphate units, respectively (Foroutan et al., 2015).

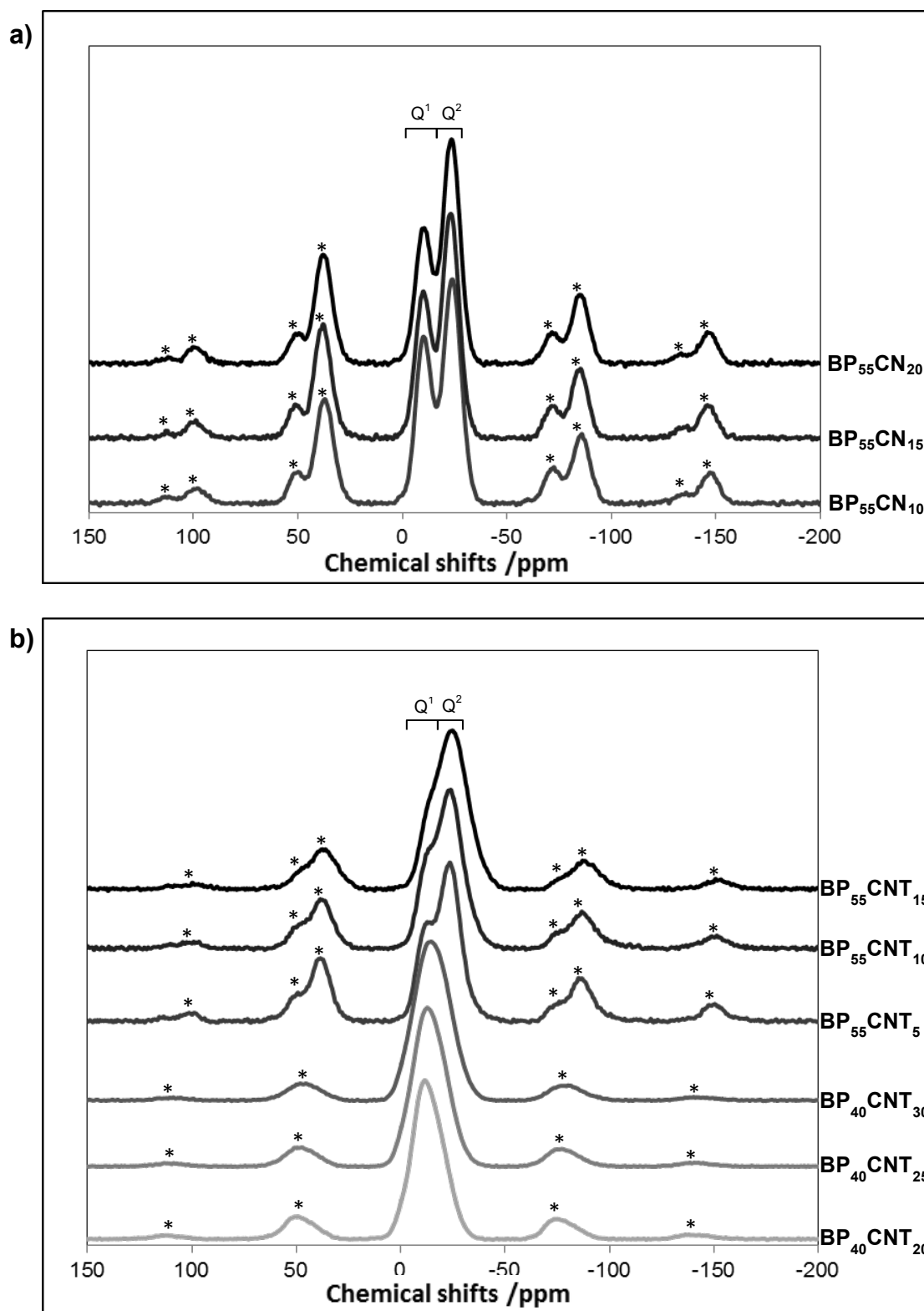


Figure 3.6. ^{31}P MAS-NMR spectra of; (a) ternary $\text{P}_2\text{O}_5\text{-CaO-Na}_2\text{O}$ and (b) quaternary $\text{P}_2\text{O}_5\text{-CaO-Na}_2\text{O-TiO}_2$ sol-gel derived glasses using n-butyl phosphate as a phosphorus precursor. The peaks correspond to mainly Q^1 and Q^2 phosphate units. The asterisks denote spinning sidebands.

Table 3.4. ^{31}P MAS-NMR peak parameters of ternary $\text{P}_2\text{O}_5\text{-CaO-Na}_2\text{O}$ and quaternary $\text{P}_2\text{O}_5\text{-CaO-Na}_2\text{O-TiO}_2$ sol-gel derived glasses using n-butyl phosphate as a phosphorus precursor.

Sample code	Position (ppm, ± 0.2)	Q^i species	Line width (ppm, ± 0.2)	Abundance (% , ± 1.0)
BP ₅₅ CN ₁₀	-10.2	1	8.0	32.9
	-22.8	2	9.2	67.1
BP ₅₅ CN ₁₅	-10.1	1	8.1	32.1
	-22.5	2	9.4	67.9
BP ₅₅ CN ₂₀	-9.9	1	8.3	30.4
	-22.3	2	9.4	69.6
BP ₄₀ CNT ₂₀	-0.2	0	6.8	4.1
	-10.0	1	9.5	41.3
	-14.1	1	9.6	33.2
	-21.9	2	11.2	21.4
BP ₄₀ CNT ₂₅	-0.8	0	7.4	3.4
	-10.1	1	9.7	37.4
	-14.4	1	9.9	35.7
	-22.5	2	11.7	23.5
BP ₄₀ CNT ₃₀	-1.2	0	7.7	2.0
	-10.3	1	9.8	29.1
	-14.8	1	9.9	40.8
	-22.8	2	11.8	28.1
BP ₅₅ CNT ₅	-9.9	1	8.5	21.3
	-13.6	1	8.3	4.3
	-23.2	2	12.4	74.4
BP ₅₅ CNT ₁₀	-10.1	1	8.9	12.5
	-14.0	1	8.4	7.9
	-23.2	2	13.1	79.6
BP ₅₅ CNT ₁₅	-10.3	1	9.4	6.1
	-14.1	1	9.6	9.7
	-23.8	2	13.6	84.2

3.3.5. FTIR spectroscopy

FTIR spectra of ternary P_2O_5 -CaO- Na_2O and quaternary P_2O_5 -CaO- Na_2O - TiO_2 sol-gel derived glasses are shown in **Figure 3.7**. Peak assignments were acquired and listed in **Table 3.5** according to the previous FTIR spectroscopy studies on phosphate-based glasses (Baia et al., 2007, Byun et al., 1995, Ilieva et al., 2001, Moustafa and El-Egili, 1998, Sene et al., 2004, Pickup et al., 2007). Peaks in the range between 720 and 730 cm^{-1} are assigned to symmetrical stretching ν_s (P-O-P) mode, while, peaks between 890 and 900 cm^{-1} are assigned to asymmetrical stretching ν_{as} (P-O-P) mode (Q^2 phosphate units). Peaks in the range between 980 to 990 cm^{-1} are assigned to symmetrical stretching ν_s (PO_3)²⁻ mode (Q^1 phosphate units). In addition, peaks in the range of 1090 to 1100 and 1230 to 1240 cm^{-1} are assigned to asymmetrical ν_{as} (PO_3)²⁻ and ν_{as} (PO_2)⁻ modes that can be related to Q^1 and Q^2 phosphate units, respectively.

Table 3.5. Infrared band assignment of phosphate-based sol-gel derived glasses using n-butyl phosphate as a phosphorus precursor.

Wavenumber (cm^{-1})	Assignments	Associated Q^i
720-730	ν_s (P-O-P)	N/A
890-900	ν_{as} (P-O-P)	Q^2
980-990	ν_s (PO_3) ²⁻	Q^1
1090-1100	ν_{as} (PO_3) ²⁻	Q^1
1230-1240	ν_{as} (PO_2) ⁻	Q^2

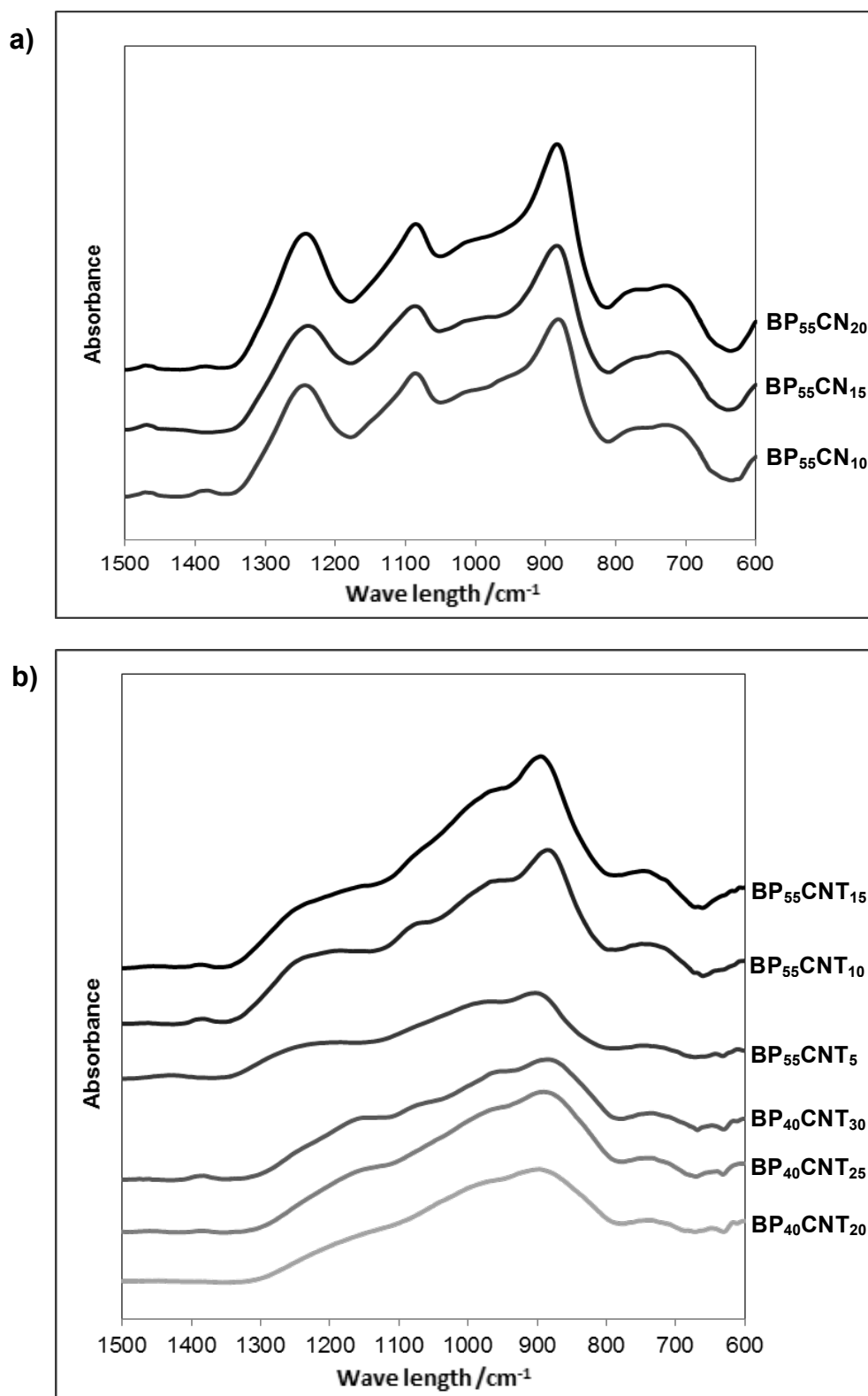


Figure 3.7. FTIR spectra of; **a)** ternary P₂O₅-CaO-Na₂O and **b)** quaternary P₂O₅-CaO-Na₂O-TiO₂ sol-gel derived glasses using n-butyl phosphate as a phosphorus precursor.

3.4. Discussion

In this chapter, phosphate-based sol-gel derived glasses in the P_2O_5 -CaO- Na_2O and P_2O_5 -CaO- Na_2O - TiO_2 systems were successfully synthesised by using n-butyl phosphate as a phosphorus precursor. The gelation time in the sol-gel reaction was much reduced compared to the sol-gel synthesised glasses with similar compositions in chapter 2. The high reactivity of n-butyl phosphate can be related to the -OH group which provided enough water for the sol-gel reaction. The XRD patterns for both systems were free from any detectable crystalline phase, which confirmed the amorphous and glassy nature of the prepared samples. This finding indicates a successful glass production by using n-butyl phosphate as a phosphorus precursor.

EDX results revealed a relatively lower phosphorus loss during the sol-gel synthesis compared to the previously synthesised glasses in chapter 2 with similar compositions. This can be related to the higher molecular weight and reactivity of n-butyl phosphate in comparison with triethyl phosphate as a phosphorus precursor. Substituting titanium in place of sodium also reduced the amount of phosphorus reduction that was due to the cross-linking effect of titanium in the phosphate network. The ^{31}P MAS-NMR study confirmed that the sol-gel synthesised glasses consist of mainly Q^1 and Q^2 phosphate units and as sodium was replaced with titanium, the glass network became more interconnected with higher levels of Q^2 species. Data for the chemical shifts also showed a change to more negative values as the Ti content increased. This is due to the formation of several cross-links between Ti^{4+} and oxygen sites, unlike Na^+ ions. As more cross-links are formed, the charge on the oxygen is displaced away from P-O bonds that leading to more shielded nuclei and producing a change in chemical shift. Analysis of the Q^2 species line width revealed an increase as titanium substituted in place of sodium indicating

a move to a more disordered structure that can be explained by the presence of a wider range of P environments in glasses containing cations with greater ionic potentials (Brow et al., 1991). FTIR spectroscopy data also in correlation with the ^{31}P MAS-NMR results that showed an increase in the peak intensity at about 900 and 1235 cm^{-1} indicating the level of Q^2 species increased as titanium substituted in place of sodium. Taken together, these results suggested titanium may act as a conditional network former in phosphate-based sol-gel derived glasses as presented here.

Previous *in vitro* and *in vivo* studies on titanium-containing phosphate-based glasses prepared *via* melt-quench method have shown significant potential for the use of these glasses in bone tissue engineering applications (Lakhkar et al., 2012, Kiani et al., 2012). In the next chapter, for the first time, we investigated the use of titanium-containing sol-gel derived glasses as a scaffold for bone tissue engineering applications. Low synthesis temperature and possibly a controllable degradation rate of these glasses may make them more favourable from the view point of cell attachment, growth, proliferation and differentiation. The sol-gel method also make it possible to fabricate phosphate-based glasses with different shapes, structure and diameter for various biomedical applications such as coating medical implants.

References

- BAIA, L., MURESAN, D., BAIA, M., POPP, J. & SIMON, S. 2007. Structural properties of silver nanoclusters-phosphate glass composites. *Vibrational Spectroscopy*, 43, 313-318.
- BROW, R. K., PHIFER, C. C., TURNER, G. L. & KIRKPATRICK, R. J. 1991. Cation Effects on P-31 Mas Nmr Chemical-Shifts of Metaphosphate Glasses. *Journal of the American Ceramic Society*, 74, 1287-1290.
- BYUN, J. O., KIM, B. H., HONG, K. S., JUNG, H. J., LEE, S. W. & IZYNEEV, A. A. 1995. Properties and Structure of $\text{Ro-Na}_2\text{o-Al}_2\text{o}_3\text{-P}_2\text{o}_5$ (R=Mg, Ca, Sr, Ba) Glasses. *Journal of Non-Crystalline Solids*, 190, 288-295.
- CARTA, D., PICKUP, D. M., KNOWLES, J. C., SMITH, M. E. & NEWPORT, R. J. 2005. Sol-gel synthesis of the $\text{P(2)O(5)-CaO-Na(2)O-SiO(2)}$ system as a novel bioresorbable glass. *Journal of Materials Chemistry*, 15, 2134-2140.
- CLAYDEN, N. J., ESPOSITO, S., PERNICE, P. & ARONNE, A. 2001. Solid state Si-29 and P-31 NMR study of gel derived phosphosilicate glasses. *Journal of Materials Chemistry*, 11, 936-943.
- FOROUTAN, F., DE LEEUW, N., MARTIN, R., PALMER, G., OWENS, G., KIM, H.-W. & KNOWLES, J. 2015. Novel sol-gel preparation of $(\text{P}_2\text{O}_5)_{0.4}-(\text{CaO})_{0.25}-(\text{Na}_2\text{O})_X-(\text{TiO}_2)_{(0.35-X)}$ bioresorbable glasses ($X = 0.05, 0.1,$ and 0.15). *Journal of Sol-Gel Science and Technology*, 73, 434-442.
- ILIEVA, D., JIVOV, B., KOVACHEVA, D., TSACHEVA, T., DIMITRIEV, Y., BOGACHEV, G. & PETKOV, C. 2001. FT-IR and Raman spectra of Gd phosphate crystals and glasses. *Journal of Non-Crystalline Solids*, 293, 562-568.
- KIANI, A., LAKHKAR, N. J., SALIH, V., SMITH, M. E., HANNA, J. V., NEWPORT, R. J., PICKUP, D. M. & KNOWLES, J. C. 2012. Titanium-containing bioactive phosphate glasses. *Philosophical Transactions of the Royal Society a-Mathematical Physical and Engineering Sciences*, 370, 1352-1375.
- LAKHKAR, N. J., PARK, J. H., MORDAN, N. J., SALIH, V., WALL, I. B., KIM, H. W., KING, S. P., HANNA, J. V., MARTIN, R. A., ADDISON, O., MOSSELMANS, J. F. W. & KNOWLES, J. C. 2012. Titanium phosphate glass microspheres for bone tissue engineering. *Acta Biomaterialia*, 8, 4181-4190.
- LEE, B. I., SAMUELS, W. D., WANG, L. Q. & EXARHOS, G. J. 1996. Sol-gel synthesis of phosphate ceramic composites .1. *Journal of Materials Research*, 11, 134-143.

- LEE, I. H., FOROUTAN, F., LAKHKAR, N. J., GONG, M. S. & KNOWLES, J. C. 2013. Sol-gel synthesis and structural characterization of P₂O₅-CaO-Na₂O glasses. *Physics and Chemistry of Glasses-European Journal of Glass Science and Technology Part B*, 54, 115-120.
- LIVAGE, J., BARBOUX, P., VANDENBORRE, M. T., SCHMUTZ, C. & TAULELLE, F. 1992. Sol-Gel Synthesis of Phosphates. *Journal of Non-Crystalline Solids*, 147, 18-23.
- MOUSTAFA, Y. M. & EL-EGILI, K. 1998. Infrared spectra of sodium phosphate glasses. *Journal of Non-Crystalline Solids*, 240, 144-153.
- PICKUP, D. M., GUERRY, P., MOSS, R. M., KNOWLES, J. C., SMITH, M. E. & NEWPORT, R. J. 2007. New sol-gel synthesis of a (CaO)(0.3)(Na₂O)(0.2)(P₂O₅)(0.5) bioresorbable glass and its structural characterisation. *Journal of Materials Chemistry*, 17, 4777-4784.
- SENE, F. F., MARTINELLI, J. R. & GOMES, L. 2004. Synthesis and characterization of niobium phosphate glasses containing barium and potassium. *Journal of Non-Crystalline Solids*, 348, 30-37.

CHAPTER 4

Titanium-Stabilised Sol-Gel Derived Glasses for Bone Tissue Engineering Applications

4.1. Introduction

Providing cells with an environment that they can continue their normal functionality is one of the most important issues in tissue regeneration. Bioactive and biodegradable materials are favourable due to their ability to break down and stimulate formation of novel extracellular matrix, and eventually tissue (Langer and Vacanti, 1993, Hench and Polak, 2002). Phosphate-based glasses, as explained previously, are bioresorbable materials with a controllable degradation rate that makes them an excellent choice for various biomedical applications (Knowles, 2003). These glasses offer an advantageous alternative to silica-based sol-gel derived glasses, with a more controllable degradation rate and easily metabolised dissolution products (Navarro et al., 2003, Hamadouche et al., 2001).

The biocompatibility and degradation rate of phosphate-based melt-derived glasses with the general formula of $P_2O_5-CaO-Na_2O$ and $P_2O_5-CaO-Na_2O-TiO_2$ have been extensively studied for a variety of biomedical applications (Navarro et al., 2002, Kiani et al., 2012, Franks et al., 2000). These studies confirmed that the addition of TiO_2 can significantly reduce the dissolution rate because of the formation of (Ti-O-P) bonds and the release of titanium may also enhance the biological response and make them a good choice in tissue engineering applications from the viewpoint of cell attachment, growth, proliferation and differentiation (Kiani et al., 2012, Lakhkar et al., 2012). The release of other ions such as Ca^{2+} can also stimulate cellular behaviour such as proliferation and bone formation (Knowles, 2003, Navarro et al., 2003, Franks et al., 2000). However, few studies exist concerning the preparation of titanium stabilised sol-gel derived phosphate glasses (Pickup et al., 2008b, Foroutan et al., 2015).

The sol-gel method allows more control over glass morphology in comparison with the melt-derived glasses, which is of fundamental importance in tissue regeneration

(Hench, 1997). In addition, the low processing temperature (200 °C) of the sol-gel synthesis enables incorporation of bioactive molecules for drug delivery applications, which is not possible with phosphate-based glasses formed by the melt-quench technique, as this requires higher processing temperatures (~1,000 °C) and therefore results in degradation of the organic components (Pickup et al., 2012, Lee et al., 2013, Kiani et al., 2012). However, to date, no studies have been published regarding the potential use of phosphate-based sol-gel derived glasses in tissue regeneration applications.

Phosphate-based sol-gel derived glasses with the general formula $(P_2O_5)_{55-x}-(CaO)_{25-x}-(Na_2O)_{(20-x)}-(TiO_2)_x$, where $X = 0, 5, 10$ or 15 were synthesised and the XRD, EDX, ^{31}P MAS-NMR, and FTIR spectroscopy results were reported in Chapter 3. Here, the pH change and ion release were quantified during the storage of samples in deionised water at 37 °C. Cytocompatibility was also assessed and cellular interaction with the surface of the glass particles was imaged using scanning electron microscopy (SEM) and confocal laser scanning microscopy (CLSM).

4.2. Aims

In this chapter, we investigated the potential use of titanium containing phosphate-based glasses for tissue regeneration applications. Since incorporation of titanium into the phosphate-based sol-gel derived glasses serves to stabilise the phosphate-network due to the cross-linking effect of titanium, greater control over the dissolution rate of these glasses would be expected, which could match with the bone tissue regeneration. In addition, the sol-gel method allows more control over glass morphology, which is of fundamental importance in tissue regeneration.

4.3. Materials and methods

4.3.1. Sol-gel synthesis

A total of four glass compositions (**Table 4.1**) were successfully synthesised as previously described in section 3.2. The obtained sol-gel derived glasses were ground to form microparticles (MM301 milling machine, Retsch GmbH, Hope, UK). Microparticles in the size range of 106–150 μm were obtained using test sieves (Endecotts Ltd, London, UK) and a sieve shaker (Spartan, Fritsch GmbH, Brackley, UK).

Table 4.1. The theoretical compositions of phosphate-based sol-gel derived glasses using n-butyl phosphate as a phosphorus precursor.

Sample code	Theoretical composition	Concentration (mol%)			
		P ₂ O ₅	CaO	Na ₂ O	TiO ₂
Ti0	(P ₂ O ₅) ₅₅ -(CaO) ₂₅ -(Na ₂ O) ₂₀	55.0	25.0	20.0	0.0
Ti5	(P ₂ O ₅) ₅₅ -(CaO) ₂₅ -(Na ₂ O) ₁₅ -(TiO ₂) ₅	55.0	25.0	15.0	5.0
Ti10	(P ₂ O ₅) ₅₅ -(CaO) ₂₅ -(Na ₂ O) ₁₀ -(TiO ₂) ₁₀	55.0	25.0	10.0	10.0
Ti15	(P ₂ O ₅) ₅₅ -(CaO) ₂₅ -(Na ₂ O) ₅ -(TiO ₂) ₁₅	55.0	25.0	5.0	15.0

4.3.2. pH change measurement

Specimens of each glass composition (25 mg, n = 3) were immersed in 5.5 mL deionised water (the pH adjusted to 7.0 ± 0.1 using NH₄OH or HCl) and stored at 37 °C (Compact Incubator, LEEC, Nottingham, UK) for up to 7 days. The pH of the solution was measured after 0, 1, 3 and 7 days (Orion pH Meter, Thermo scientific-Orion star, UK) fitted with a pH glass electrode. The pH meter was calibrated using standard solutions of pH 4, 7, and 10 before use. At each time-point, the particles were centrifuged at 4,000 rpm for 10 minutes, in order to separate them from the

solution. The supernatant was aspirated and the particles dried in an oven (IP100-LTE Scientific, Oldham, UK) at 60 °C for 3 hours, before they were resuspended in fresh deionised water.

4.3.3. Ion release measurement

Specimens of each glass composition (50 mg, n = 3) were immersed in 11 mL deionised water (pH 7.0 ± 0.1) and stored at 37 °C (Compact Incubator, LEEC, Nottingham, UK) for up to 7 days. At each time-point, glass suspensions were centrifuged at 4,000 rpm for 20 minutes, in order to separate them from the solution. The supernatant was collected and the particles dried in an oven (IP100-LTE Scientific, Oldham, UK) at 60 °C for 3 hours, before replenishment with fresh deionised water.

4.3.3.1. Cation release

The release of cations (Na⁺ and Ca²⁺) from glass microparticles was quantified after 0, 1, 3 and 7 days using an ICS-1000 ion chromatography system (Dionex, Surrey, UK) equipped with a 4 x 250 mm Ion Pac[®] CS12A column operating under suppressed conductivity, with 20 mM methanesulfonic acid (Fluka, Dorset, UK) eluent to separate cations based on their affinity to the ion exchanging resin. The sample solutions were passed through a Dionex OnGuard IIA filter (Dionex, Thermo Scientific, Hemel Hempstead, UK) prior injection through the column to eliminate anions that bind to the cation column. Also, before performing the analysis, the system was calibrated against a four-point calibration curve with a predefined calibration program from standard solutions provided by the manufacturer (Dionex,

Surrey, UK). Data analyses were performed in relation to standard solutions using the Chromeleon[®] software package (Dionex Surrey, UK).

4.3.3.2. Anion release

The release of anions (PO_4^{3-} , $\text{P}_2\text{O}_7^{4-}$, $\text{P}_3\text{O}_9^{3-}$, and $\text{P}_3\text{O}_{10}^{5-}$) from glass microparticles was quantified after 0, 1, 3 and 7 days using an ICS-2500 system (Dionex, Surrey, UK) equipped with a 4 x 250 mm Ion Pac[®] AS16 column which separating them based on their interaction with anion exchange resin. Isocratic separation was applied with a linear potassium hydroxide (KOH) gradient of between 30–50 mM over a 35 minute period provided by an EG50 eluent generator. Similar to the cation release measurement, the system was calibrated against a four-point calibration curve before carrying out the sample run for each time points from standard solutions. Standard solutions were prepared using sodium phosphate, trisodium trimetaphosphate, pentasodium tripolyphosphate (Sigma-Aldrich, Dorset, UK) and tetrasodium pyrophosphate (BDH, Poole, UK) as the reagents. Similar to the cation release measurements, the Chromeleon[®] software package was used for data analysis.

4.3.4. Cell studies

4.3.4.1. Cell culture

Human osteoblast-like osteosarcoma cell line (MG-63, European Collection of Cell Cultures, Porton Down, UK) was cultured under standard conditions (37 °C, 95 % air, 5 % CO_2 , 95 % relative humidity) in Dulbecco's modified Eagle medium that contains 4 mM L-glutamine, 4500 mg/L glucose, 1 mM sodium pyruvate, and 1500 mg/L sodium bicarbonate (DMEM, Gibco, Life Technologies, Paisley, UK)

supplemented with 10 % foetal bovine serum (Gibco Life Technologies, Paisley, UK). The growth process was carried out until the cells reached at 80-90 % confluency.

4.3.4.2. Cytocompatibility assay

In order to assess the effect of TiO₂ content of the sol-gel derived glasses on cytocompatibility, MG-63 cells were cultured on the microparticles. The materials were sterilised using dry heat at a temperature of 180 °C for 2 hours in a sealed glass vial with aluminium foil and left to cool overnight. The sol-gel glass particles (5 mg per specimen) were evenly distributed across permeable cell culture supports in 48 well plates (Transwell, Corning B.V. Lifesciences, Amsterdam, Netherlands), in order to enable facile processing of the specimens for SEM and confocal microscopy after the final time-point. Cells were seeded on the particles at a density of 30,000 cells/cm² (10,000 cells/well) and cell culture medium was added to the cell culture support and the bulk of the well (1.1 mL total). Controls consisted of cells seeded directly on cell culture supports. Each sample type was analysed in triplicate. Cytocompatibility was assessed after 1, 3 and 7 days. At each time-point, cells were seeded at various densities, 2 hours prior to the assay, for the preparation of standard curves. The medium was then aspirated from the samples and standards and replaced with 1 mL medium containing 10 vol% water soluble tetrazolium salt-8 (WST-8, Cell Counting Kit-8, Sigma Aldrich, Gillingham, UK). WST-8 is a pink substrate, which is metabolised in the mitochondria to form an orange formazan product. After 80 min incubation at 37 °C, absorbance at 460 nm (with a reference wavelength of 650 nm) was measured (Infinite M200, Tecan, Männedorf, Switzerland). The apparent cell density of the samples was extrapolated from the standard curves. The WST-8 containing medium was then

aspirated and replaced with fresh cell culture medium until the next time-point. Following the final time-point, cells residing on the microparticles were imaged by SLCM and SEM.

4.3.4.3. Cell and particle imaging

Specimens consisting of MG-63 cells cultured on the glass microparticles for 7 days were fixed by replacing the medium with a 3% glutaraldehyde (Sigma-Aldrich, UK) in 0.14 M sodium cacodylate buffer solution (pH 7.3, Sigma-Aldrich, UK) and kept at 4 °C overnight before dehydration through a graded series of ethanol solutions according to the following regimen: 50% ethanol for 10 minutes, 70% ethanol for 10 minutes, 90% ethanol for 10 minutes and 100% ethanol for 10 minutes (2 times). The final drying was done by hexamethyldisilazane (Sigma-Aldrich, UK) for 1-2 minutes and then the plate was left to dry overnight in a desiccator. It should be noted that all of the above mentioned steps were performed very carefully to minimise the detachment of cells from the glass microparticles. The membranes were carefully excised using a scalpel and mounted onto carbon adhesive discs attached to aluminium stubs. The specimens were then sputter-coated with gold-palladium alloy by a Polaron E5100 coating device (Polaron CVT, Milton Keynes, UK) and imaged using a scanning electron microscope (Philips-XL30 instrument, Netherland) with an accelerating voltage of 5 kV and working distance of 10 mm at various magnifications.

Cells residing on the glass microparticles were imaged using confocal laser scanning microscopy (CLSM) after 7 days culture. The cytoskeleton (actin filaments) and nuclei of the cells were fluorescently stained using Alexa Fluor 488 phalloidin (Invitrogen, UK) and propidium iodide (BD Biosciences, UK), respectively.

Specimens were prepared by fixation in 4% paraformaldehyde, followed by two washes using Dulbecco's phosphate buffered saline (D-PBS, Lonza, Slough, UK). Cells were then permeabilised using a 0.1 vol% solution of Triton X-100 (Sigma-Aldrich) in D-PBS for 5–10 minutes at room temperature. A 2.5 vol% solution of phalloidin methanolic stock solution in D-PBS was then added to each specimen and incubated for 20 minutes at room temperature in a dark environment, in order to minimise evaporation and photo-bleaching. After a further two washes with D-PBS, specimens were counter-stained using $1 \mu\text{g.mL}^{-1}$ propidium iodide (BD Biosciences, Oxford, UK) for 10 minutes, before visualisation by CLSM (Biorad, Hemel Hempstead, UK).

4.4. Results

4.4.1. pH change measurement

The pH of the dissolution products of all glass compositions reduced significantly over the first 24 hours, as shown in **Figure 4.1**. A more gradual decrease in pH progressed during the remainder of the immersion period. Increasing TiO_2 content reduced the extent and rate of pH decrease, although there was little difference between Ti5, Ti10 and Ti15.

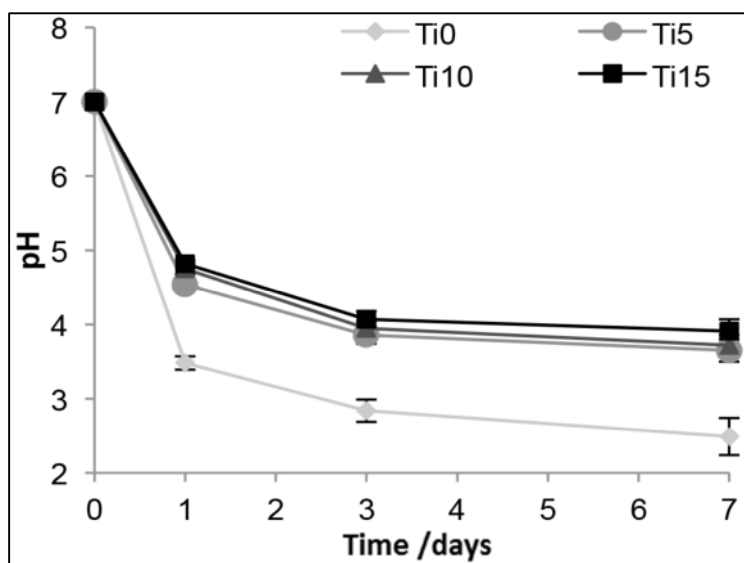


Figure 4.1. pH measurement after 0, 1, 3 and 7 days immersion of sol-gel derived glass microparticles in deionised water that shows significant decrease in pH after 24 hours. Error bars represent the standard deviation of three samples.

4.4.2. Ion release measurement

Figure 4.2 illustrates the release of cations (Ca^{2+} and Na^{+}) and anions ($\text{P}_2\text{O}_7^{4-}$, $\text{P}_3\text{O}_{10}^{5-}$, $\text{P}_3\text{O}_9^{3-}$ and PO_4^{3-}) from the sol-gel derived glass microparticles. As expected, higher concentrations of Ca^{2+} were detected in samples collected from Ti0 glass microparticles. There was a significant decrease in the Ca^{2+} release rate with an increase in the TiO_2 content from 0 to 15 mol%. Likewise, Na^{+} release showed a clear distinction between each glass composition. Glasses with lower Na^{+} content released less Na^{+} into solution. The release of Ti^{4+} was also investigated but was below the detectable range. Similarly, the release of $\text{P}_2\text{O}_7^{4-}$ and $\text{P}_3\text{O}_{10}^{5-}$ anions correlated directly with TiO_2 content, with increasing Ti resulting in decreasing release. $\text{P}_3\text{O}_9^{3-}$ and PO_4^{3-} release, however, followed trends that were distinct from a direct relationship with Ti content. Ti5 and Ti10 demonstrated higher $\text{P}_3\text{O}_9^{3-}$ release than Ti0 and Ti15. Conversely, the release of PO_4^{3-} from Ti0 and Ti5 was markedly lower than from Ti10 and Ti15.

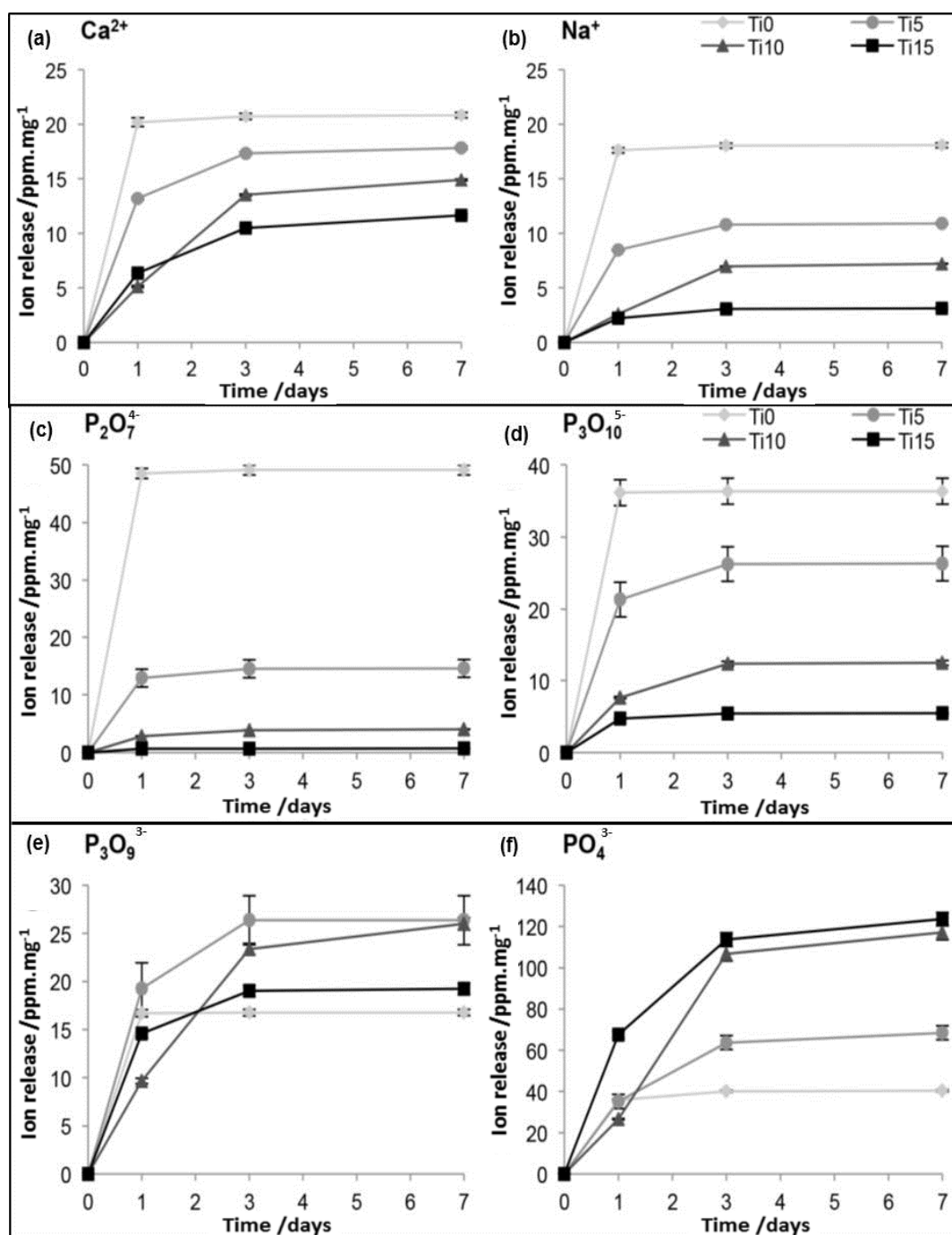


Figure 4.2. Cumulative release of (a) Ca²⁺ and (b) Na⁺ cations and (c) P₂O₇⁴⁻, (d) P₃O₁₀⁵⁻, (e) P₃O₉³⁻ and (f) PO₄³⁻ anions from sol-gel derived glass microparticles after 1, 3 and 7 days storage in deionised water. Error bars represent the standard deviation of three samples.

4.4.3. Cytocompatibility

The cytocompatibility of the sol-gel derived glasses is presented in **Figure 4.3**. The control (MG-63 on cell culture supports) approximately doubled in apparent cell density at each time-point, reaching 217,000 cells/cm² by day 7. The apparent density of cells cultured on glass particles remained low after 1 and 3 days. Ti0 caused cells to approximately halve in number within the first day, with little subsequent recovery. Cells cultured on Ti5 and Ti10 had a low apparent cell density after 1 and 3 days, but this recovered to 135,000 and 212,000 cells/cm² by day 7, respectively. Ti15, however, had poor cytocompatibility, with cells failing to recover even after 7 days.

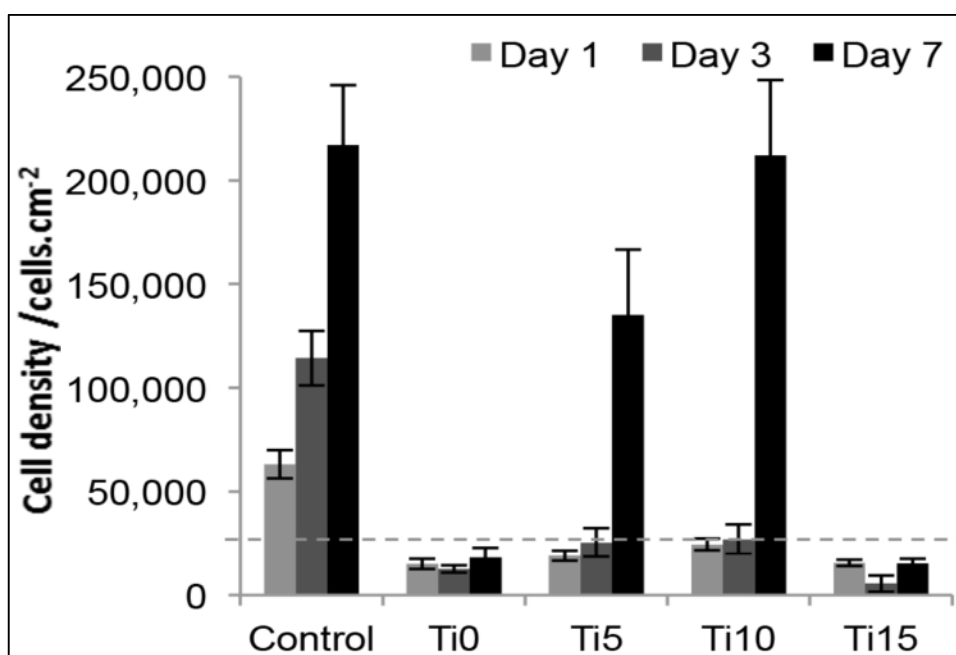
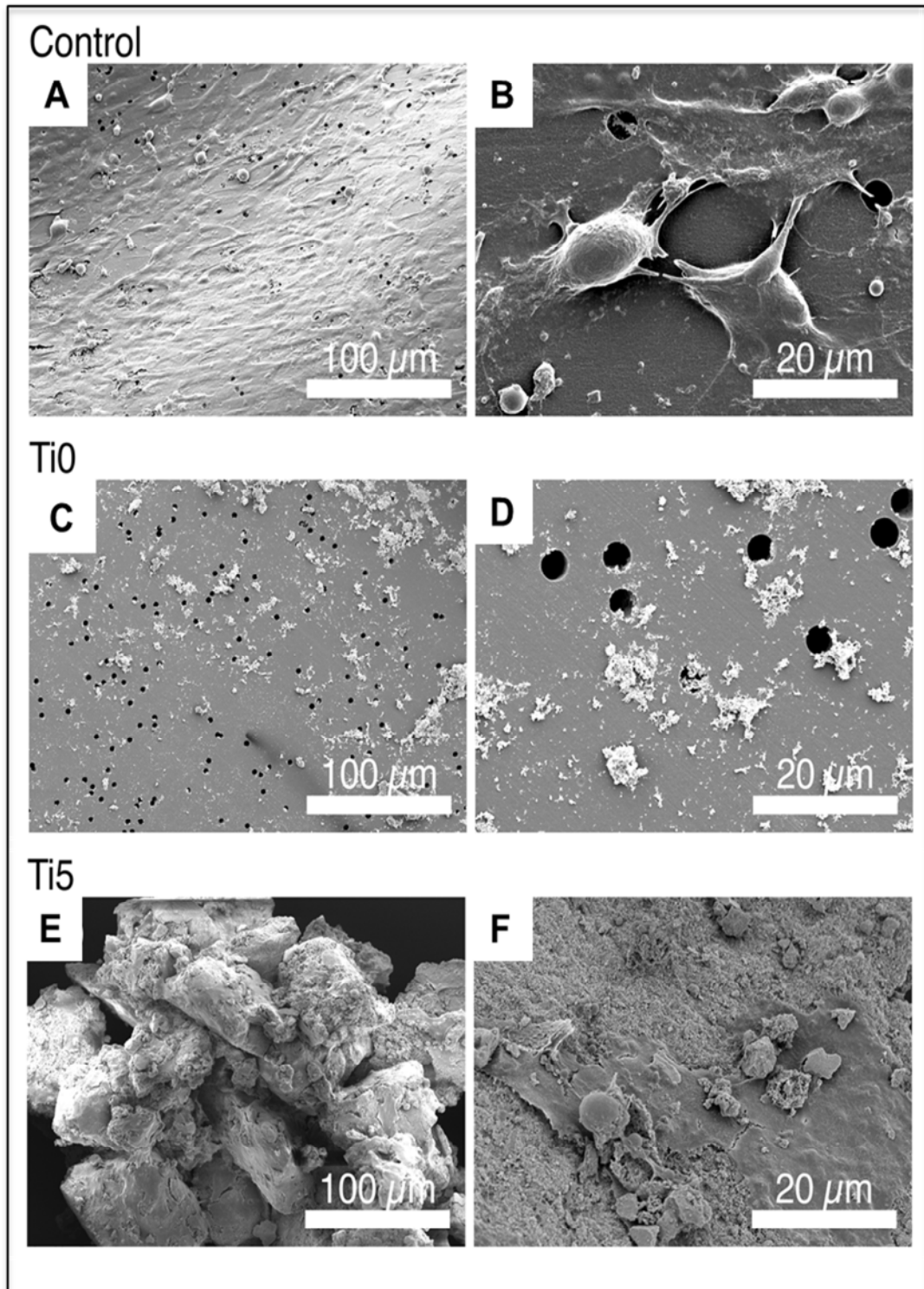


Figure 4.3. Cytocompatibility of glass microparticles containing 0, 5, 10 or 15 mol% Ti with MG-63 cells at 1, 3 and 7 days. Dotted line represents an initial seeding density. Error bars represent the standard deviation of three samples.

4.4.4. Cell and particle imaging

The morphology and size of the glass microparticles were identified by SEM (**Figure 4.4**) after 7 days in cell culture. All compositions had a similar morphology, with particles assuming a jagged but generally spherical form with diameters in the range of $\sim 0.5\text{--}2\ \mu\text{m}$ and a rough surface topography. The control (**A, B**) shows a monolayer of cells spread on the cell culture support (dark circular features are pores). After 7 days in culture, Ti0 particles (**C, D**) had almost fully degraded and therefore cells could not be visualised on the remaining small particles. Some cells were visible on the surface of Ti5 particles (**E, F**), though this was much more apparent on the surface of Ti10 (**G–I**). At high magnification, it was confirmed that cells were proliferating and forming a very flattened morphology on the surface of a Ti10 glass microparticles (**I**). Ti10 and Ti15 glass microparticles remained large, having degraded little, though no cells were visible on Ti15 (**J, K**). **Figure 4.5** shows cells attached to Ti5 and Ti10 microparticles. Cells were not observed on Ti0 or Ti15.



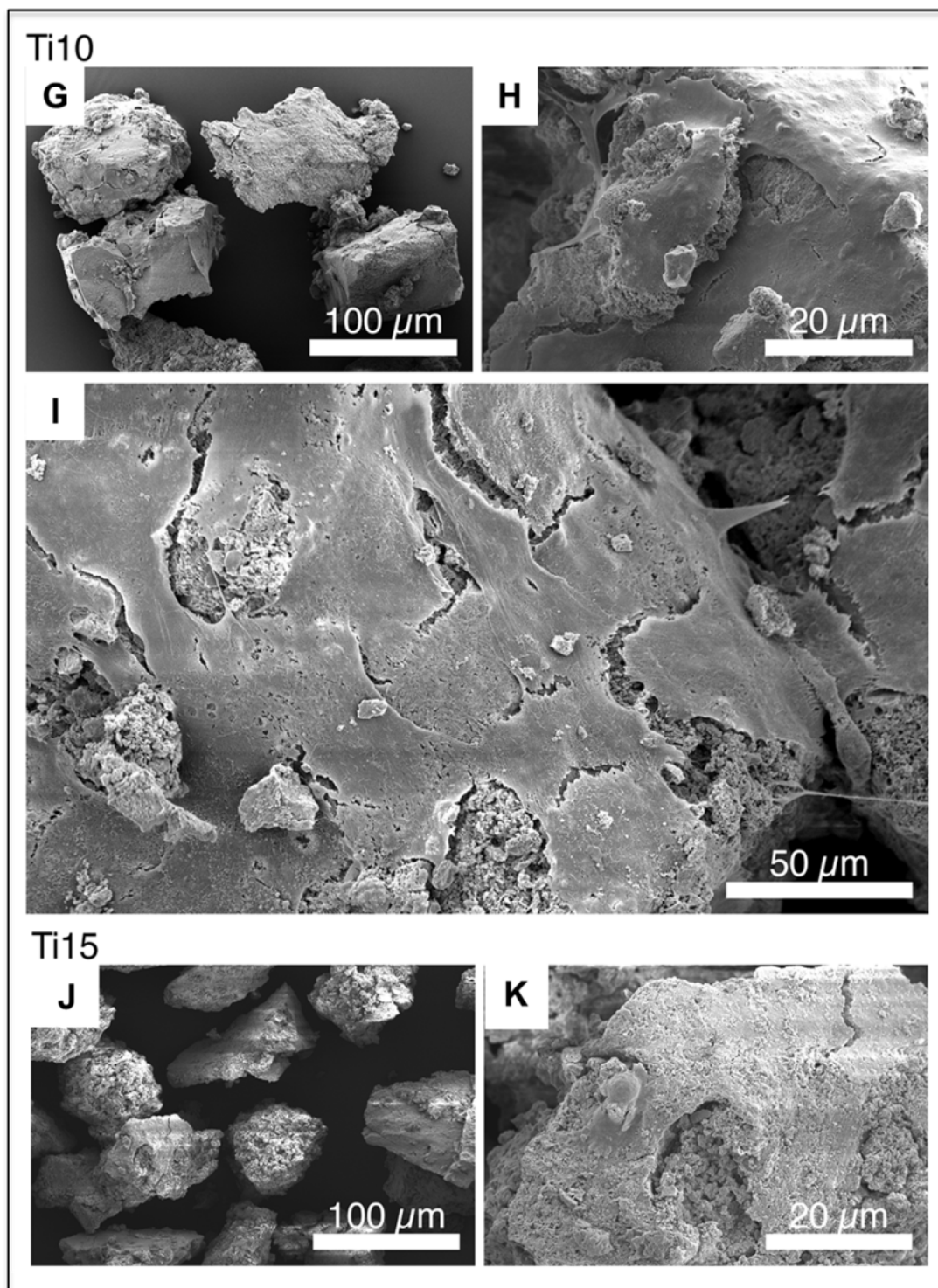


Figure 4.4. Scanning electron micrographs showing glass particles morphology and cell attachment. **(A, B)** Control (cells on cell culture support), **(C, D)** Ti0, **(E, F)** Ti5, **(G-I)** Ti10, and **(J, K)** Ti15.

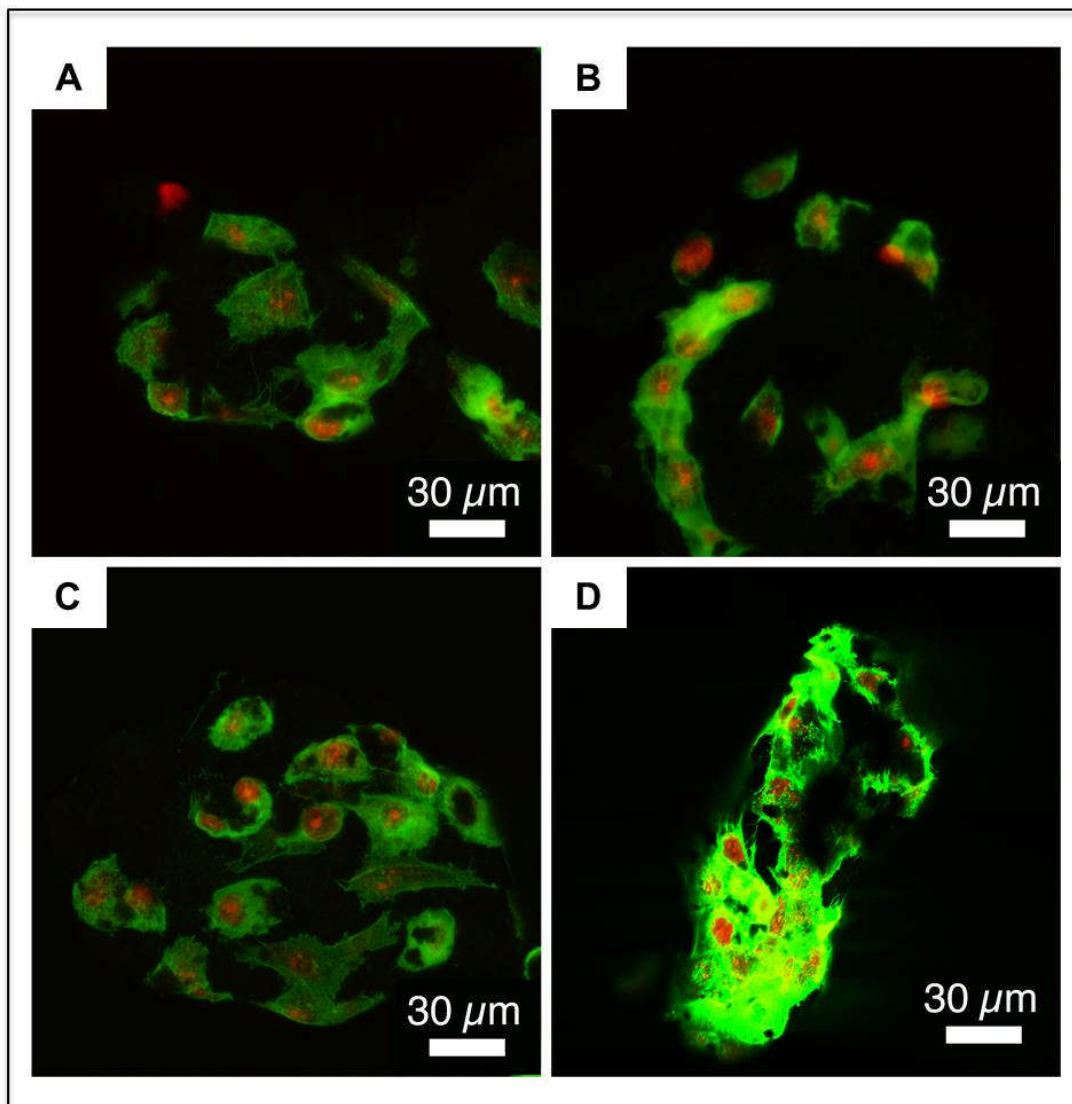


Figure 4.5. Confocal micrographs showing cells attached to glass microparticles containing (A, B) 5 or (C, D) 10 mol% TiO₂. The green fluorescent stain (phalloidin) shows filamentous actin and red (propidium iodide) shows nuclei.

4.5. Discussion

In this chapter, we reported the potential use of sol-gel synthesised glasses with the general formula $(P_2O_5)_{55}-(CaO)_{25}-(Na_2O)_{(20-x)}-(TiO_2)_x$ where $X = 0, 5, 10$ or 15 for bone tissue regeneration applications. Degradation studies revealed that immersion of glass microparticles in deionised water for 0, 1, 3 and 7 days resulted in a significant decrease in pH after 24 hours for all compositions, followed by a more gradual decrease at subsequent time-points. This suggested that increasing TiO_2 content reduced the rate of pH reduction, since titanium has a high charge/diameter ratio and can make the network more interconnected. As expected, the higher calcium release was associated with lower titanium content. Likewise, the release of sodium followed a similar pattern, which can be explained on the basis of substitution between sodium and titanium within the present glass compositions. A similar trend was observed for $P_2O_7^{4-}$ and $P_3O_{10}^{5-}$.

The detected levels of $P_3O_9^{3-}$ and PO_4^{3-} follow more complex trends. As $P_3O_9^{3-}$ release reached a maximum for Ti0, which was below that of the other compositions, this may reflect that the entire $P_3O_9^{3-}$ content of the glass had been released into solution. $P_3O_9^{3-}$ is a cyclic molecule composed of three phosphate units. In order to form, it can be reasoned that phosphate alkoxides would need to be in close proximity to each other at the point of synthesis without other network forming units. With the higher valency of Ti increasing network connectivity in comparison to Na, the amount of phosphate bonds that form with other phosphate units is expected to be reduced by increasing Ti (Pickup et al., 2008a). Hence, a lower degree of $P_3O_9^{3-}$ would be present within the Ti0 glass. PO_4^{3-} may also be released as a result of smaller phosphate units within the glass network. It should also be noted, however, that linear molecules lack the stability of cyclic structures. Taking this into consideration, variable trends in PO_4^{3-} release are to be reasonably

expected, as the PO_4^{3-} detected in solution thus represents the accumulation of PO_4^{3-} released directly from the glass and PO_4^{3-} formed by degradation of longer chain polyphosphates in solution. These results are also corroborated by the initial pH data collected. For example, highly acidic species such as $\text{P}_2\text{O}_7^{4-}$ and $\text{P}_3\text{O}_{10}^{5-}$ were released in the greatest amount from the Ti0 glass and this particular composition also induced the greatest pH reduction in solution (Montchamp, 2015). Likewise, less acidic PO_4^{3-} and $\text{P}_3\text{O}_9^{3-}$ species were released in proportionally greater amounts from those glasses which reduced the pH of the solution to a lesser extent (Fluck, 1978).

The apparent cell density of MG-63 cells cultured on a layer of glass microparticles was reduced in comparison to the cell culture support control after 1 and 3 days in the case of all compositions. This was likely caused by the rapid decrease in pH that occurred upon glass degradation. Although the pH change would have been partially buffered by the cell culture medium, the more extreme drop in pH in Ti0 explains why the cells failed to recover and reach an initial seeding density. As Ti content was increased from 0 to 5 or 10 mol%, the density of surviving cells increased in parallel, due to the decrease in glass degradation and lower drop in pH. The apparent density of cells residing on Ti5 after 7 days in culture had recovered to ~60% that of the control, whereas cells cultured on Ti10 had recovered to the same level as the control. Cells cultured on Ti15, however, failed to recover. No cells were visible in the SEM or CLSM images and only low cell densities were detected by WST-8.

Furthermore, of the anions investigated, only PO_4^{3-} contributes to apatite formation, whereas longer chain polyphosphates are known to inhibit crystal growth (Driessens, 1982). As apatite formation is believed to promote cellular attachment (Hu et al., 2013), the deposition of a mineral layer at the interface of the glass and it

environment is a plausible explanation of the high cytocompatibility of Ti10. The reduced survival of cells cultured on Ti15, however, requires further explanation. Titanium has been shown to inhibit hydroxyapatite mineralization (Blumenthal and Cosma, 1989). Higher release of Ti^{4+} from the Ti15 glass may have therefore exceeded the biocompatibility threshold, preventing the formation of a hydroxyapatite surface layer amenable to cellular growth. Alternatively, oxolation and subsequent olation of Ti^{4+} could serve to induce microtemporal pH shifts in the immediate vicinity of the glass surface. Again, higher release of Ti^{4+} from the Ti15 glass would exacerbate this effect. The other possibility can be related to the greater retention of toxic residual solvents by the more highly cross-linked composition. This possible explanation is beyond the scope of this study and would require further investigation.

It is also worth noting that water-soluble cell proliferation assays such as WST-8 measure mitochondrial metabolic activity and only give an indication of cell density. It is possible that the lower readings after 1 and 3 days may have been due to lower metabolic activity as the cells attached to the unfamiliar particles and spread across their surface. This would explain the large difference in apparent cell densities between days 3 and 7. It is also possible that the layer of glass microparticles on the cell culture support somewhat inhibited diffusion of nutrients across the membrane, compared to the control.

These results were also supported by SEM and CLSM images, which showed cells residing on Ti5 and Ti10 but not Ti0 or Ti15. Furthermore, scanning electron micrographs showed significant mineral formation on the surface of Ti5 and Ti10. Since bone cells strongly favour rough surface topographies for adhesion and proliferation (Walters and Gentleman, 2015), the mineral content and morphology of these compositions are likely to be the causes of their improved cytocompatibility.

References

- BLUMENTHAL, N. C. & COSMA, V. 1989. Inhibition of Apatite Formation by Titanium and Vanadium Ions. *Journal of Biomedical Materials Research-Applied Biomaterials*, 23, 13-22.
- DRIESENS, F. C. M. 1982. Mineral Aspects of Dentistry. *Monographs in Oral Science, Basel, Karger*, 10.
- FLUCK, E. 1978. Phosphor: Phosphorus. An Outline of its Chemistry, Biochemistry and Technology. Von D. E. C. Corbridge. Elsevier Scientific Publ. Comp., Amsterdam-Oxford-New York 1978. VIII, 456 S., geb. Dfl. 146,—. *Nachrichten aus Chemie, Technik und Laboratorium*, 26, 386-386.
- FOROUTAN, F., DE LEEUW, N., MARTIN, R., PALMER, G., OWENS, G., KIM, H.-W. & KNOWLES, J. 2015. Novel sol-gel preparation of $(P_2O_5)_{0.4}-(CaO)_{0.25}-(Na_2O)_X-(TiO_2)_{(0.35-X)}$ bioresorbable glasses ($X = 0.05, 0.1,$ and 0.15). *Journal of Sol-Gel Science and Technology*, 73, 434-442.
- FRANKS, K., ABRAHAMS, I. & KNOWLES, J. C. 2000. Development of soluble glasses for biomedical use Part I: In vitro solubility measurement. *Journal of Materials Science-Materials in Medicine*, 11, 609-614.
- HAMADOUCHE, M., MEUNIER, A., GREENSPAN, D. C., BLANCHAT, C., ZHONG, J. P. P., LA TORRE, G. P. & SEDEL, L. 2001. Long-term in vivo bioactivity and degradability of bulk sol-gel bioactive glasses. *Journal of Biomedical Materials Research*, 54, 560-566.
- HENCH, L. L. 1997. Sol-gel materials for bioceramic applications. *Current Opinion in Solid State & Materials Science*, 2, 604-610.
- HENCH, L. L. & POLAK, J. M. 2002. Third-generation biomedical materials. *Science*, 295, 1014-+.
- HU, H. J., QIAO, Y. Q., MENG, F. H., LIU, X. Y. & DING, C. X. 2013. Enhanced apatite-forming ability and cytocompatibility of porous and nanostructured $TiO_2/CaSiO_3$ coating on titanium. *Colloids and Surfaces B-Biointerfaces*, 101, 83-90.
- KIANI, A., LAKHKAR, N. J., SALIH, V., SMITH, M. E., HANNA, J. V., NEWPORT, R. J., PICKUP, D. M. & KNOWLES, J. C. 2012. Titanium-containing bioactive phosphate glasses. *Philosophical Transactions of the Royal Society a-Mathematical Physical and Engineering Sciences*, 370, 1352-1375.

- KNOWLES, J. C. 2003. Phosphate based glasses for biomedical applications. *Journal of Materials Chemistry*, 13, 2395-2401.
- LAKHKAR, N. J., PARK, J. H., MORDAN, N. J., SALIH, V., WALL, I. B., KIM, H. W., KING, S. P., HANNA, J. V., MARTIN, R. A., ADDISON, O., MOSSELMANS, J. F. W. & KNOWLES, J. C. 2012. Titanium phosphate glass microspheres for bone tissue engineering. *Acta Biomaterialia*, 8, 4181-4190.
- LANGER, R. & VACANTI, J. P. 1993. Tissue Engineering. *Science*, 260, 920-926.
- LEE, I. H., FOROUTAN, F., LAKHKAR, N. J., GONG, M. S. & KNOWLES, J. C. 2013. Sol-gel synthesis and structural characterization of P₂O₅-CaO-Na₂O glasses. *Physics and Chemistry of Glasses-European Journal of Glass Science and Technology Part B*, 54, 115-120.
- MONTCHAMP, J. L. 2015. *Phosphorus Chemistry I: Asymmetric Synthesis and Bioactive Compounds*, Springer International Publishing.
- NAVARRO, M., CLEMENT, J., GINEBRA, M. P., MARTINEZ, S., AVILA, G. & PLANELL, J. A. 2002. Improvement of the stability and mechanical properties of resorbable phosphate glasses by the addition of TiO₂. *Bioceramics* 14, 218-2, 275-278.
- NAVARRO, M., GINEBRA, M. P. & PLANELL, J. A. 2003. Cellular response to calcium phosphate glasses with controlled solubility. *Journal of Biomedical Materials Research Part A*, 67A, 1009-1015.
- PICKUP, D. M., ABOU NEEL, E. A., MOSS, R. M., WETHERALL, K. M., GUERRY, P., SMITH, M. E., KNOWLES, J. C. & NEWPORT, R. J. 2008a. TiK-edge XANES study of the local environment of titanium in bioresorbable TiO₂-CaO-Na₂O-P₂O₅ glasses. *Journal of Materials Science-Materials in Medicine*, 19, 1681-1685.
- PICKUP, D. M., NEWPORT, R. J. & KNOWLES, J. C. 2012. Sol-Gel Phosphate-based Glass for Drug Delivery Applications. *Journal of Biomaterials Applications*, 26, 613-622.
- PICKUP, D. M., WETHERALL, K. M., KNOWLES, J. C., SMITH, M. E. & NEWPORT, R. J. 2008b. Sol-gel preparation and high-energy XRD study of (CaO)_x(TiO₂)_(0.5-x)(P₂O₅)_(0.5) glasses (x=0 and 0.25). *Journal of Materials Science-Materials in Medicine*, 19, 1661-1668.
- WALTERS, N. J. & GENTLEMAN, E. 2015. Evolving insights in cell–matrix interactions: Elucidating how non-soluble properties of the extracellular niche direct stem cell fate. *Acta Biomaterialia*, 11, 3-16.

CHAPTER 5

**Sol-Gel Synthesis and Electrospinning of Ternary
(P₂O₅)_{0.55}-(CaO)_{0.30}-(Na₂O)_{0.15} Glass Nanospheres for
Diagnostic and Therapeutic Applications**

5.1. Introduction

Ultrasound imaging is a real time, non-ionising, effective, and low cost imaging tool. Yet it remains primarily an anatomic imaging tool versus positron emission tomography or bioluminescence. Ultrasound contrast agents can increase the signal specificity for molecular imaging by increasing backscattered echoes from the target site, however, the current generation of microbubbles is too large to be used outside of the vasculature or inside specific cells of interest (Goldberg and Liu, 1997, Benchimol et al., 2013, Nakatsuka et al., 2011, Willmann et al., 2008). The use of microbubbles as a contrast agent were first introduced in 1968 by injecting agitated saline into the ascending aorta and cardiac chambers during echocardiographic examination (Gramiak R and Shah PM, 1968). Strong echoes were produced within the heart due to the acoustic mismatch between free air microbubbles in the saline and the surrounding blood. However, microbubbles produced by agitation were both large and unstable and diffused into solution in a short period of time.

To overcome these limitations encapsulated gas bubbles were developed, however, these microbubbles were unstable in circulation even with polyethylene glycol surface treatment (Klibanov, 1999, Schutt et al., 2003, Kono et al., 2008). Furthermore, microbubbles require a careful choice of ultrasound frequency because they burst at low frequencies that can result in local microvasculature rupture and haemolysis (Klibanov, 2005). While nanotechnology and production of nanobubbles have made important improvements in this area, however, a complete solution has remained elusive (Xing et al., 2010, Shapiro et al., 2014, Krupka et al., 2010).

One alternative is the use of solid nanoparticles as backscatter contrast agents for ultrasound molecular imaging (Casciaro et al., 2010, Jokerst et al., 2013, Liberman

et al., 2013). These solid particles have been used to image cell surface proteins in cancer cells, visualising stem cells in cardiac regenerative medicine, and also for encapsulating drug molecules to transport them to specific cells (Jokerst et al., 2013, Casciaro et al., 2010). These particles are particularly attractive for cancer treatment due to their small size and potential for functionalising their surface which provide immense opportunity in drug delivery and cell imaging.

However, in order to be effective, the material properties of these agents are very critical. They must have acoustic impedance, be capable of strongly and stably backscattering incident acoustic energy, possess the ability to encapsulate drug molecules, and be able to be metabolised and removed safely from the body shortly after administration. In addition the particles must be small enough to extravasate through tumour vasculature due to the enhanced permeation and retention (EPR) effect or be phagocytosed by cells when growing in culture. While silica-based nanoparticles have shown some promises (Ta et al., 2012, Martinez et al., 2010, Malvindi et al., 2011), their degradation rate is very slow which may limit their applications (He et al., 2011a, Hudson et al., 2008).

Phosphate-based glasses are an attractive alternative since they offer a controllable degradation rate by varying their chemical compositions which gives rise to easily metabolised degradation components in the body (Knowles, 2003, Hench and Polak, 2002, Franks et al., 2001). In addition, phosphate-based glasses can be a good choice to encapsulate drug molecules as they could be a way to reduce the drug dose needed and the side effects associated with particular drugs (Pickup et al., 2012).

In our previous approach to prepare ternary phosphate-based glasses *via* the sol-gel method in the P_2O_5 -CaO- Na_2O system (section 2.2.2.3), we focused on preparing bulk glasses and for that reason, the drying procedure had to be done very carefully over three weeks (section 2.2.3). However, the long synthesis time

and the difficulty of preparing bulk glasses and tailoring their shape may limit their potential biomedical applications. Here, we used a similar sol-gel synthesis method to prepare a ternary $(\text{P}_2\text{O}_5)_{0.55}\text{-(CaO)}_{0.30}\text{-(Na}_2\text{O)}_{0.15}$ glass composition and subsequent electrospaying allowed us to prepare glass spheres in the nanometer size range at relatively low processing temperatures, with potential use as a contrast agent for ultrasound imaging or a carrier in drug delivery applications. The initial objectives of this chapter were to investigate the application of electrospaying to produce phosphate-based glass nanospheres (PGNs). To date, this is the first report of electrospaying phosphate-based sol-gel derived glasses to prepare PGNs and the first use of such system for diagnostic and therapeutic purposes. Synthesised PGNs were characterised by SEM, EDX, XRD, ^{31}P MAS-NMR, and FTIR spectroscopy. Biodegradation was then monitored *via* inductively coupled plasma mass spectroscopy (ICP-MS) to measure phosphorus, sodium, and calcium ion release into an aqueous medium. Cell cytotoxicity analysis was also performed to determine the biocompatibility. We used PGNs as a diagnostic probe to label mesenchymal stem cells for both *in vitro* and *in vivo* ultrasound imaging. The potential drug delivery application of drug-loaded PGNs was also determined by ultra performance liquid chromatography (UPLC). It should be noted that in this chapter; cytotoxicity study, and *in vitro* and *in vivo* ultrasound imaging was done in collaboration with Dr. Jesse Jokerst at Stanford University.

5.2. Aims

In this chapter, the initial aim was to use the electrospaying technique to prepare phosphate-based glass nanospheres in the diameter size range of below 500 nm for theranostic applications, which was discussed in chapter 1. Following that the potential application of phosphate-based glass nanospheres in the $\text{P}_2\text{O}_5\text{-CaO-Na}_2\text{O}$

system as a transient contrast agent for ultrasound imaging and as a carrier in drug delivery systems were investigated.

5.3. Materials and methods

5.3.1. Design of electrospraying

The experimental setup of the electrospraying system is shown in **Figure 5.1**. It consists of high voltage source, syringe pump, stainless steel hypodermic needle, and a counter electrode. Silicone oil (Sigma-Aldrich, Gillingham, UK) was used as a substrate and the temperature of the substrate was controlled *via* a hot plate located underneath. An electric field was generated by applying the voltage between the needle and the counter electrode while the syringe pump provided a constant flow rate. Surface charges, which are proportional to the resulting electric field, were formed on the surface of the sol-gel solution droplet at the tip of the needle. These charges exert an outward electrostatic pressure which is in opposition to the pressure developed by surface tension resulting in the formation of a Taylor cone at the tip of the needle. Above a critical value of the electric field, the electrostatic forces overcome the surface tension of the solution resulting in the extraction of a liquid jet. The extruded sol-gel solution was separated into small droplets and propelled into the heated silicone oil.

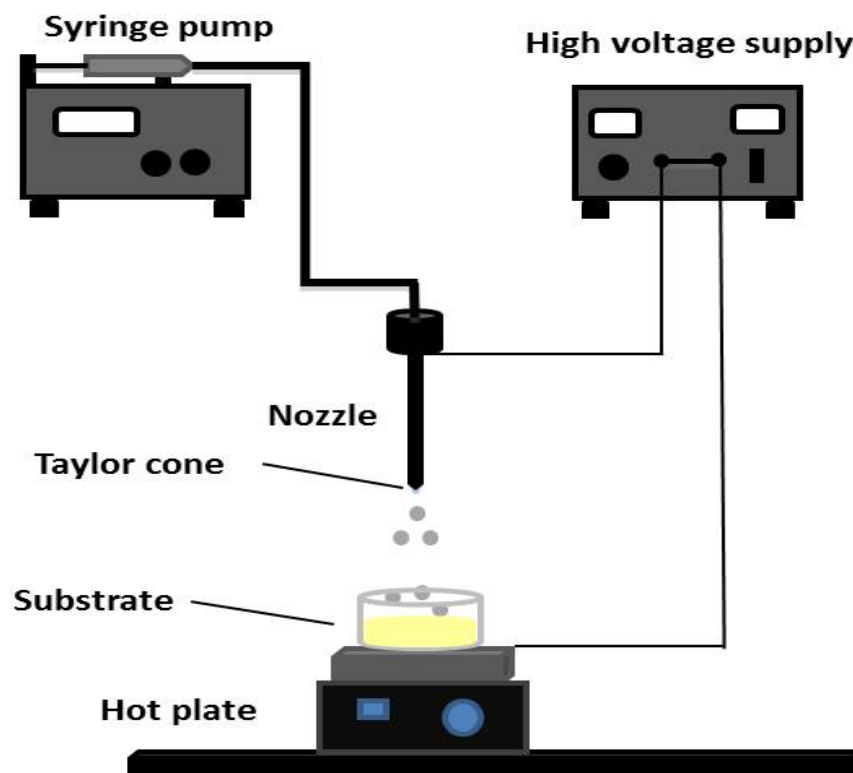


Figure 5.1. Schematic of the electrospaying setup including; syringe pump, stainless steel needle, high voltage supply, collection substrate, and a hot plate. The high voltage between the needle and the ground creates nanospheres from the needle tip and these are propelled toward the heated silicone oil as a substrate to obtain dried gel nanospheres.

5.3.2. Synthesis of the sol for subsequent electrospaying

The sol-gel preparation method of ternary $(P_2O_5)_{0.55}-(CaO)_{0.30}-(Na_2O)_{0.15}$ glass composition has been described previously in Section 2.2.2.3. To evaluate the potential diagnostic and therapeutic applications of PGNs, during the final stage of the sol-gel process 1 wt% fluorescein dye (Sigma-Aldrich, Gillingham, UK) or 1 wt% tetracycline hydrochloride (Sigma-Aldrich, Gillingham, UK) was added to a subset of the mixture and homogeneous solutions were obtained after mixing for about 10

minutes. The mixtures were aged overnight at 60 °C before being electrosprayed over the heated silicone oil.

A stainless steel hypodermic needle (18 gauge) with 10 cm distance from the substrate was used. The electrospraying setup was operated at room temperature and atmospheric pressure. The temperature of the substrate was controlled and kept at 150 °C using a hot plate. The flow rate of the syringe pump was set at 0.20 mL.h⁻¹ and a voltage of 20 kV was applied between the needle and the ground to provide a continuous and stable Taylor cone output. The sprayed particles were separated from silicone oil *via* centrifugation at 4600 rpm for 30 minutes and washed three times with acetone (99.5%, Alfa-Aesar, Heysham, UK) before drying at 180 °C for 2 hours in an oven (EV014-Townson & Mercer, Cheshire, UK) to evaporate the acetone and other remaining solvents.

5.4. Structural characterisation methods

5.4.1. SEM

The shape and morphology of the obtained particles were probed using scanning electron microscopy (SEM). SEM images were acquired using a Philips-XL30 instrument (Philips, Netherland) at a working distance of 10 mm and an accelerating voltage of 5 kV. The particles were mounted onto a stub using araldite and sputter-coated with gold/palladium alloy by a Polaron E5100 coating device (Polaron CVT, Milton Keynes, UK) and imaged at various magnifications. Particle size distribution was determined from the measurement of at least 100 particles using Image Pro Plus software (Medium Cybernetics, USA).

5.4.2. XRD and EDX

XRD and EDX analysis were carried out on PGNs as previously described in sections 2.2.4.1.1 and 2.2.4.2.1.

5.4.3. ^{31}P MAS-NMR and FTIR spectroscopy

^{31}P MAS-NMR and FTIR spectroscopy characterisation methods have been previously reported in sections 2.2.4.3.1 and 2.2.4.4.1.

5.4.4. Cell culture, labelling, and cytotoxicity

Human mesenchymal stem cells (MSCs) and culture medium were purchased from Lonza (p/n 2501 and 3001, respectively). Cells were seeded at a cell seeding density of 5000 cells/cm², and the medium was changed every 2-3 days. Cell labeling was carried out using MSCs plated at a cell seeding density of 5000 cells/cm² in a 225 cm² flask after reaching 80% confluence. For labeling optimisation studies, 12 well plates at the same cell seeding density were used. In order to investigate the application of PGNs as a contrast agent, they were incubated in PBS at 25 mg.mL⁻¹. To obtain an optimised concentration value for the labelling process using PGNs, the cells were exposed to a range of PGNs concentrations from 30 to 1000 µg.mL⁻¹. The PGNs were then incubated with the cells for 2 hours and then washed three times with PBS. To study the effect of time, 500 µg.mL⁻¹ of PGNs from 1 – 360 minutes was used. For labelling experiments, we used fluorescently-tagged PGNs. Cell fluorescence was measured with a plate reader (Bio-TEK), and EVOS-FI fluorescence microscopy (Invitrogen). Leica confocal microscope (TCS-SP5) was used for confocal microscopy with a 20x APO

objective (p/n 506147) seated on a Virbraplane air table. For z-stacking experiments, 20 slices were collected over $\sim 50 \mu\text{m}$.

For the cell counting experiments, we used the optimised protocol of 2 hours and $250 \mu\text{g.mL}^{-1}$. After labelling, the cells were washed three times with saline. We monitored the washes with absorbance spectroscopy to confirm that the third wash contained no more nanoparticles. The cells were then removed from the flask with TrypLE Express (Invitrogen), washed with complete medium to deactivate the trypsin, centrifuged at 1000 rpm at 4°C for 5 minutes and resuspended in saline. The cells were counted with an automated hemocytometer before being placed in a phantom and imaged.

For cell viability, cells were plated in a 96 well plate and allowed to adhere overnight. The next day, cells were incubated in contact with a range of PGNs concentration for 4 hours. For a positive control, we added $10 \mu\text{L}$ of 1 mg.mL^{-1} cetyl trimethylammonium bromide (CTAB) in phosphate buffered saline. Cell viability was assessed using the tetrazolium-based metabolic reagent compound 3-(4,5-dimethylthiazol-2-yl)-5-(3-carboxymethoxyphenyl)-(4-sulfophenyl)-2H-tetrazolium (MTS; Promega). The solution was used as received and $20 \mu\text{L}$ of MTS solution was added to each well in a 96 well plate containing cells and allowed to incubate for 3 hours. Absorbance at 490 nm was measured to estimate cell viability. Each condition was tested with at least four replicates.

To determine whether the particles generated any reactive oxygen species, we utilized 2',7' -dichlorofluorescein diacetate (DCFDA; Biotium). We first made a 1 mg.mL^{-1} stock solution of DCFDA in dimethyl sulfoxide (DMSO) and then $125 \mu\text{L}$ of the DMSO solution was diluted to 10 mL using Hanks Buffered Saline Solution (HBSS). Cells were washed with fresh HBSS and then $100 \mu\text{L}$ of the DCFDA solution in HBSS was added; the plate was incubated at 37°C for 1 hour. Next, the

labelling solution was aspirated and the cells again washed with fresh HBSS. Increasing concentrations of PGNs in 100 μ L HBSS were then added. Controls include 10 %H₂O₂ and wells with no cells. The fluorescence emission of each well was measured 1 hour later.

5.4.5. Biodegradation monitoring

Biodegradation was monitored *via* inductively coupled plasma mass spectroscopy (ICP-MS). The experiment used 0.1 mg.mL⁻¹ PGNs in deionised water at 37 °C with three replicates at the following time points: 0, 0.2, 0.5, 1, 3, 6, 12, 24, and 48 hours. The tubes were secured to a tube rotation device set to 5 rotations per minute. This device was in a 37 °C incubator (Compact Incubator, LEEC, Nottingham, UK) under ambient humidity. After each time point, the resulting suspension was centrifuged at 4600 rpm for 30 minutes to separate the PGNs from the solution. The liquid phase was then extracted and the PGNs were dried at 60 °C in an oven (IP100-LTE Scientific, Oldham, UK) before replenishing with fresh deionised water. The release of phosphorus, calcium, and sodium in solution was measured by using a Spectro Mass 2000 Analytical System (Kleve, Germany) calibrated across the predicted concentrations range of 0 - 4000 ppb by dilution of 100 ppm elemental standards. Calcium standard was obtained as part of a pre-made standard solution (Fluka, Gillingham, UK) whereas phosphorus and sodium standards were prepared from analytical grade K₂HPO₄ (Sigma-Aldrich, Gillingham, UK) and NaNO₃ (Sigma-Aldrich, Gillingham, UK) salts, respectively. Standards were first diluted in deionised water to the desired concentration range. Both samples and standards were diluted in 1:1 in 4% HNO₃ (Fluka, Gillingham, UK) and analysed against a blank (2% HNO₃) solution under standard operating conditions

(Power: 1350 W; Coolant Flow: 15 L.min⁻¹; Auxiliary Flow: 1 L.min⁻¹). Results were reported as a cumulative ion release over the full period of the degradation study.

5.4.6. *In vitro* ultrasound imaging

To measure the echogenicity of the nanoparticles, increasing concentrations of PGNs were placed in a 1% agarose phantom. Ultrasound backscatter mode (B-mode) images were collected with a Visualsonics 2100 scanner with a MS-550 transducer (Fuji, Ontario, Canada) for 40 MHz centre frequency imaging or a MS-250 transducer for 16 MHz. Other imaging parameters included 100% power, 35 dB gain and a 60 dB dynamic range. At least three frames were collected for each sample and were quantified with ImageJ software using region of interest analysis and 8-bit depth as the dependant variable (0-255) (Schneider et al., 2012).

5.4.7. *In vivo* ultrasound imaging

All animal studies were approved by the Administrative Panel for Laboratory Animal Care (APLAC) at Stanford University. Nude mice aged 10-14 weeks were anaesthetized with 2% isoflurane in oxygen at 2 L.min⁻¹. The PGNs were dissolved in 50:50 matrigel:PBS at 2.0, 0.25, and 0.1 mg.mL⁻¹. The injection volume was 100 µL that was subcutaneously implanted on the rear flank of the mice. The animals were imaged 10 minutes after implantation after the matrigel had solidified using 40 MHz centre frequency, 100% power, 35 dB gain, and a 60 dB dynamic range. At least three frames were collected for each sample and images were quantified with ImageJ. For longitudinal imaging the injection site was marked and the animal returned to the same position the next day for identical imaging conditions.

5.4.8. Drug release measurement

To measure the tetracycline hydrochloride (TCH) release from the drug-loaded PGNs, 1 mg.mL⁻¹ sample suspended in deionised water at 37 °C (Compact Incubator, LEEC, Nottingham, UK) with three replicates at the following intervals: 0, 0.2, 0.5, 1, 2, 4, 8, 16, and 24 hours. After each interval, the mixture was centrifuged at 4600 rpm for 30 minutes to separate the PGNs from the solution. The liquid phase was then extracted and the PGNs were dried at 60 °C in an oven (IP100-LTE Scientific, Oldham, UK) before they were resuspended in fresh deionised water. 6µL of the extracted solution diluted with 4 µL of methanol solution containing 0.1% formic acid and injected into the Hypersil Gold C₁₈ column (Thermo Scientific, Leicestershire, UK) using the Acquity Capillary UPLC system (Waters, Manchester, UK) and was monitored at 345 nm. The mobile phases were: A) 0.1% formic acid in 100% water, and B) 0.1% formic acid in 100% acetonitrile. The gradient program was started at 5% B and was gradually increased to 95% B over 4 minutes. The mobile phase composition was maintained at 95% B for a further 0.5 minutes before returning to 5% B in 6 seconds. The flow-rate was 600 µL.min⁻¹ and the column was then re-equilibrated for a further 24 seconds giving a total run time of 5 minutes. Before performing the analysis, the system was calibrated against a five point calibration curve from prepared TCH standard solutions.

5.5. Results

5.5.1. SEM and EDX

Nanoparticles were successfully synthesised with the electrospraying technique and the shape and size of the particles were characterised using SEM analysis. **Figure 5.2** shows nanospherical particles and measurement of the particle size for

more than 100 particles confirmed more than 80% of the particles had a diameter distribution of 200-500 nm with a mean diameter size of 320 nm. The EDX results are reported in **Table 5.1**. The P_2O_5 content was 12.5 mol% less than the theoretical value with a concomitant increase in the percentage content of the other oxides to compensate.

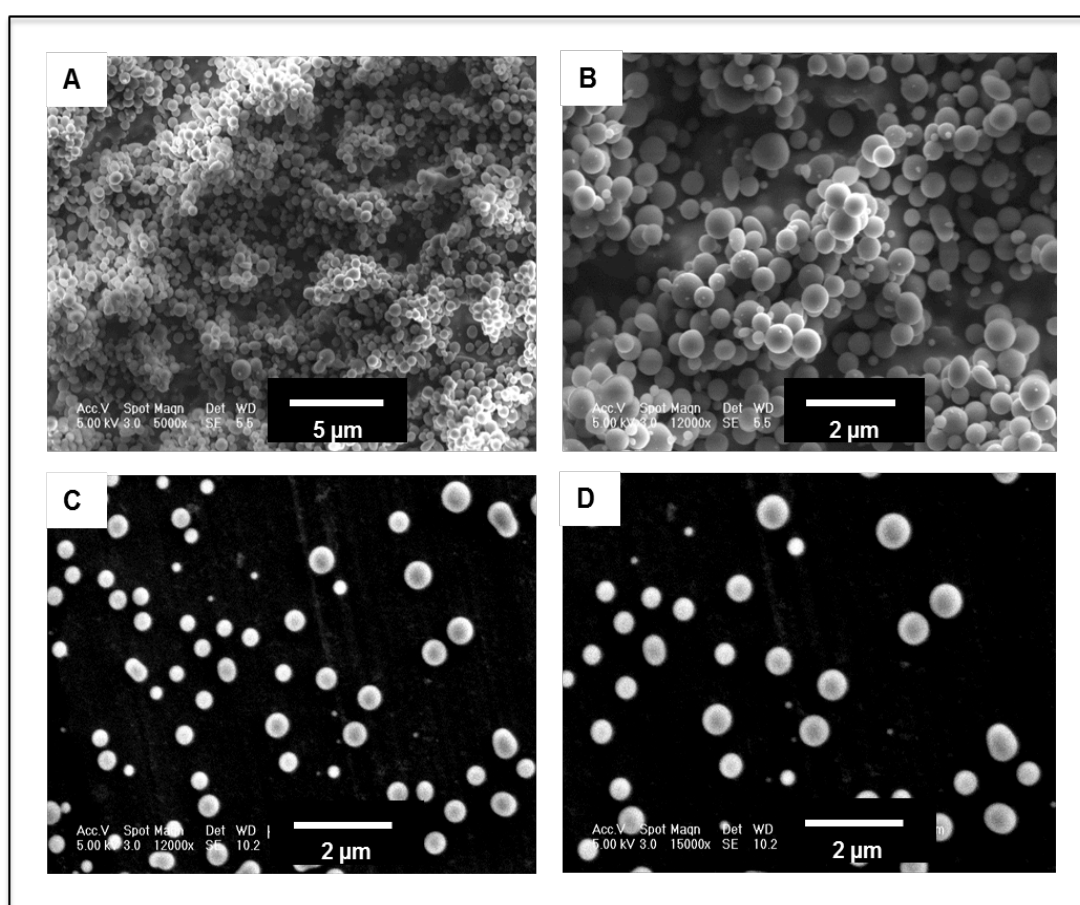


Figure 5.2. SEM images of **(A, B)** washed and heat-treated PGNs (the scale bars represent 5 and 2 μm) and **(C, D)** dispersed PGNs in anhydrous ethanol solution after heat-treatment (the scale bars represent 2 μm). The PGNs have an approximate size distribution of 200 - 500 nm with mean diameter of 320 nm based on measurement of more than 100 particles.

Table 5.1. Intended composition and measured values of sol-gel derived glasses, determined by EDX (in parentheses).

Sample code	Concentration (mol%)		
	P ₂ O ₅	CaO	Na ₂ O
PGN	55.0 (42.5±1.0)	30.0 (37.9±0.9)	15.0 (19.6±0.8)

5.5.2. XRD

The XRD pattern of the PGNs showed no evidence of any detectable crystalline phase (**Fig.5.3**). Only two broad peaks at 2θ values between 20 and 50° were observed. This confirmed the amorphous and glassy nature of the PGNs.

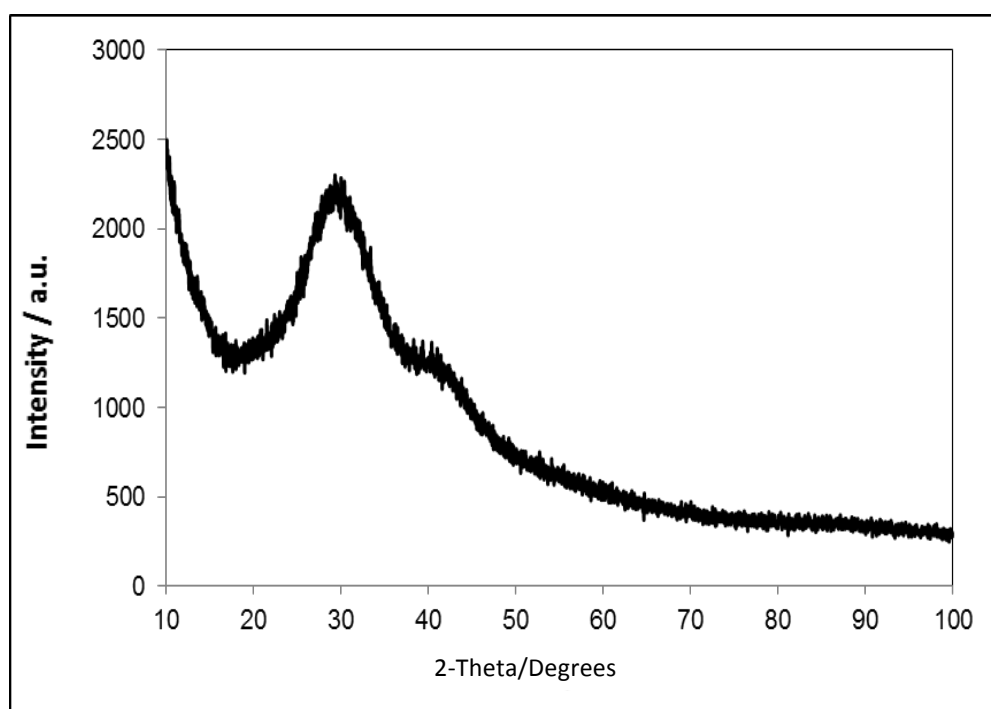


Figure 5.3. The XRD pattern of PGNs which is free from any detectable crystalline phase.

5.5.3. ^{31}P MAS-NMR

Figure 5.4 shows the ^{31}P MAS-NMR spectrum from PGNs. The peak at 1.7 ppm corresponds to Q^0 phosphate units, while the peaks with the chemical shifts at -8.3 and -21.9 ppm are assigned to Q^1 and Q^2 units, respectively (Lee et al., 2013, Carta et al., 2007). The peak parameters of the PGNs spectrum are listed in **Table 5.2**.

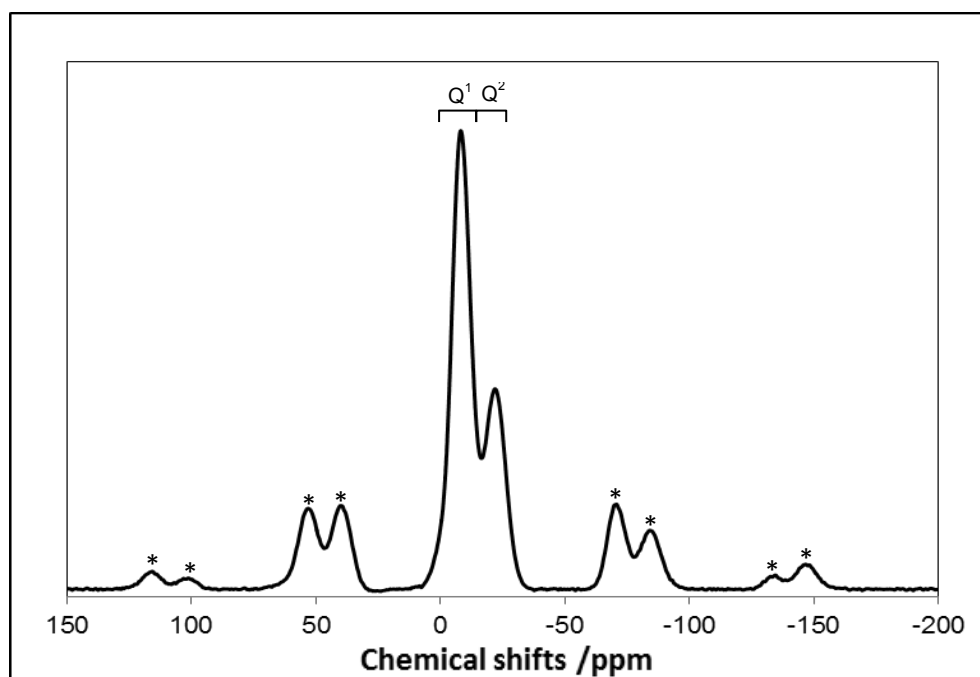


Figure 5.4. ^{31}P MAS-NMR spectrum of PGNs that correspond to mainly Q^1 and Q^2 phosphate units. The asterisks denote spinning sidebands.

Table 5.2. ^{31}P MAS-NMR peak parameters of phosphate-based glass nanospheres.

Sample code	Position (ppm, ± 0.2)	Q^i species	Line width (ppm, ± 0.2)	Abundance (% , ± 1.0)
	1.7	0	6.7	1.9
PGN	-8.3	1	10.1	59.5
	-21.9	2	12.5	38.6

5.5.4. FTIR spectroscopy

Figure 5.5 presents FTIR spectroscopy data for PGNs that allow assignment of peaks according to the previous FTIR spectroscopy studies on phosphate-based glasses (Baia et al., 2007, Byun et al., 1995, Ilieva et al., 2001, Moustafa and El-Egili, 1998, Sene et al., 2004, Pickup et al., 2007). The peak at 730 cm^{-1} can be assigned to symmetrical stretching ν_s (P-O-P) mode, while the peak at 900 cm^{-1} can be assigned to asymmetrical stretching ν_{as} (P-O-P) mode (Q^2 phosphate units). Peaks at 1100 and 1235 cm^{-1} are also assigned to asymmetrical $\nu_{as}(\text{PO}_3)^{-2}$ and $\nu_{as}(\text{PO}_2)^-$ modes that can be related to Q^1 and Q^2 phosphate units, respectively.

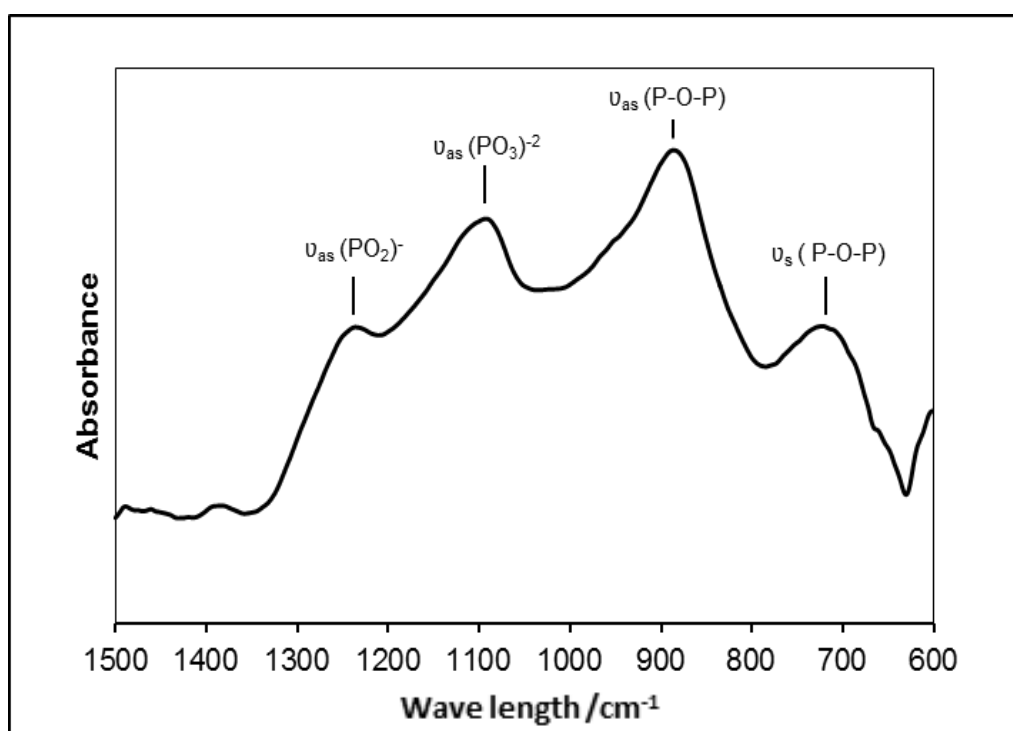


Figure 5.5. FTIR spectrum and band assignment for PGNs (ν , stretching; s, symmetric; as, asymmetric).

5.5.5. Ion release study

The concentration of phosphorus, sodium, and calcium that released into solution at different time points are presented in **Figure 5.6**. It can be seen that the highest rate of ion release occurs within the first 4 hours over the entire length of the study for all the elements. It should be noted that there is a small difference between the obtained data from EDX and ICP that can be related to the dissolution behaviour of phosphorus that requires the hydrolysis of P-O-P bonds prior to release, whereas other elements may be released *via* diffusion (Bunker et al., 1984).

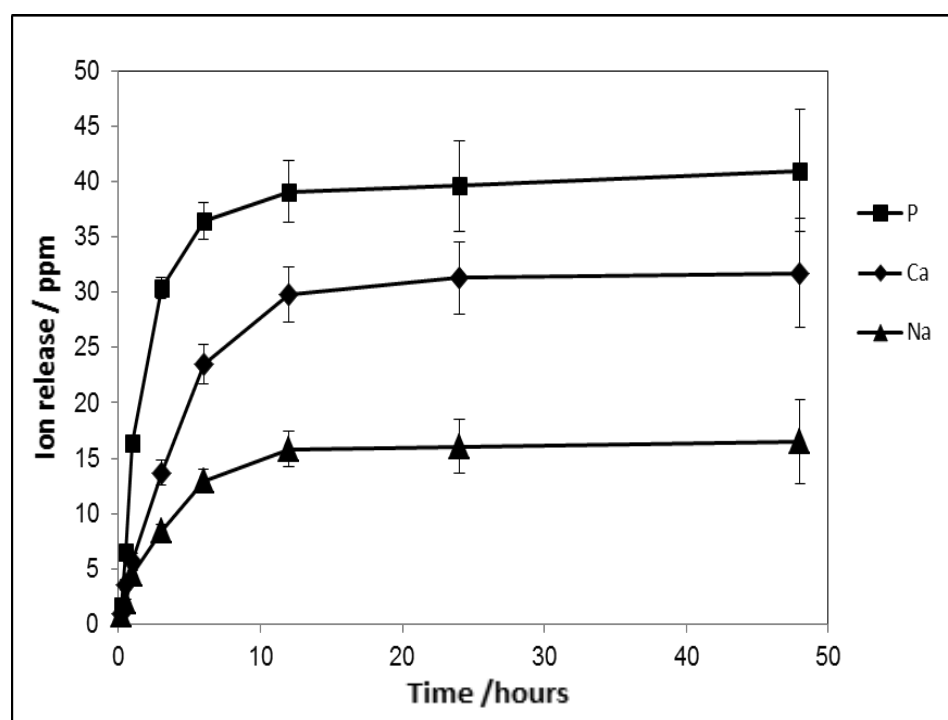


Figure 5.6. Cumulative release of phosphorus, calcium, and sodium in deionised water as a function of time for the investigated PGNs. Error bars represent the standard deviation of three samples.

5.5.6. Cytotoxicity study

MTS and DCFDA assays were used to measure the cell viability and to study whether reactive oxygen species (ROS) were generated (**Fig. 5.7**). MSCs were used for both applications because of the utility of ultrasound in cardiac stem cell therapy (Hare et al., 2012b, Jokerst et al., 2013). The cells were positive for CD105, CD166, CD29, CD44, CD14, CD34, and CD45 and were below passage number 5. The DCFDA assay was first validated with both positive and negative controls. The negative control was used well with no cells plated, and the positive control was a well with MSCs stimulated by 10% hydrogen peroxide. The negative control had a fluorescence value of 297 ± 76 which is attributed to auto-fluorescence from the plastic well plate. The MSCs in medium with neither PGNs nor H_2O_2 had a value of 869 ± 118 . The H_2O_2 positive control validated the assay and was 2.2-fold higher than the control cells. The experiments with PGNs added to the MSCs showed no increase in DCFDA signal except at $1000 \mu\text{g}\cdot\text{mL}^{-1}$. Here, the signal increased 1.6-fold to 1372 ± 41 —a value that was significant at $p < 0.0001$ versus the $0 \mu\text{g}\cdot\text{mL}^{-1}$ control. All other PGNs concentrations had p values greater than 0.05 indicating no generation of ROS (**Fig. 5.7A**).

We also used the MTS assay to measure any effects on cell viability. Two fractions of PGNs were analysed; freshly dissolved PGNs in PBS (**Fig. 5.7B**, Fresh) and PGNs that had been in PBS overnight (**Fig. 5.7B**, Degraded). In both cases, cells were treated with increasing concentrations of PGNs. The positive control was the known cytotoxic agent CTAB. Cells without stimulation had an optical density at 490 nm of 0.85 ± 0.06 for the fresh sample and 0.90 ± 0.05 for the degraded sample. No concentrations had a statistically significant change to baseline except the positive control, which suppressed the signal 4.3-fold and 4.1-fold for the fresh and degraded samples, respectively.

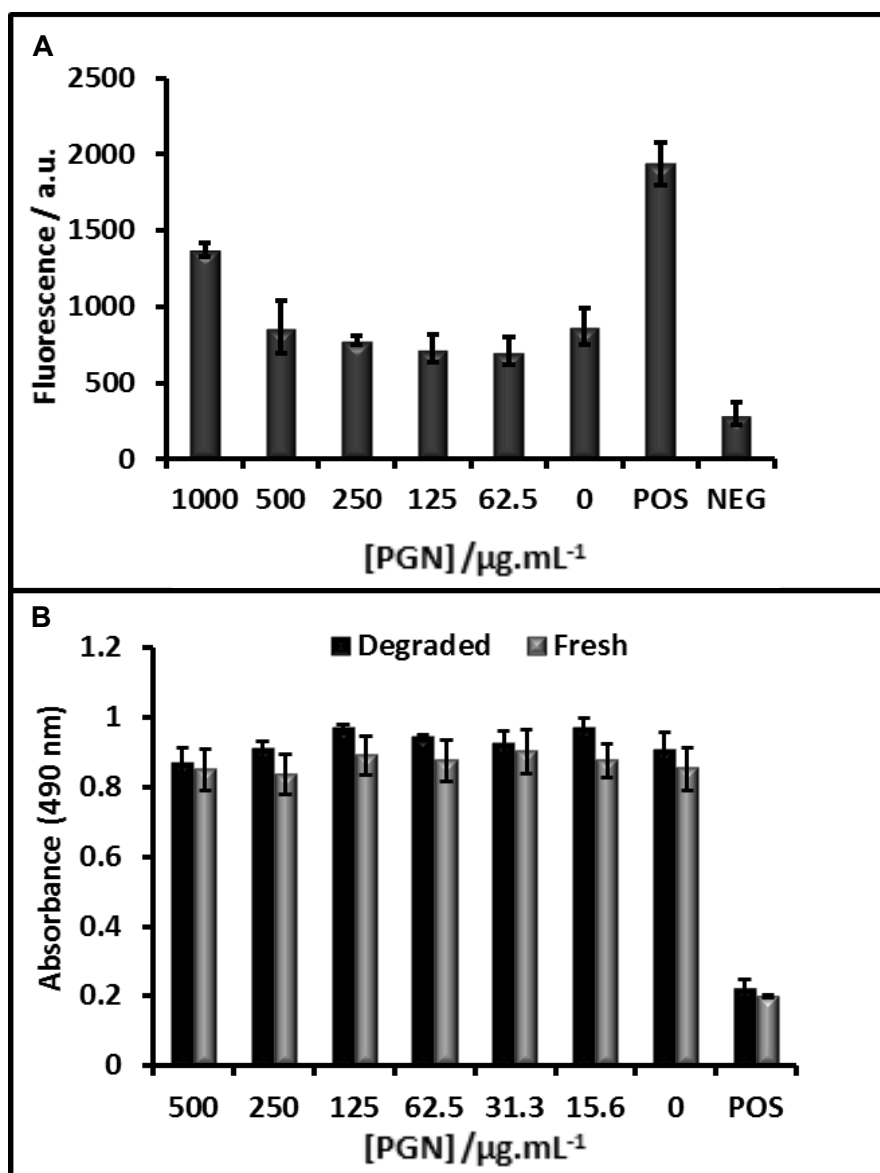


Figure 5.7. Increasing concentrations of PGNs were used to label MSCs for 4 hours followed by treatment with different markers of cytotoxicity. All experiments were validated with a positive control (POS). **A)** Cells were plated, tagged with DCFDA, and then perturbed with PGNs. Any ROS generation resulted in fluorescence from the DCFDA probe. Only the $1000 \mu\text{g.mL}^{-1}$ sample significantly upregulated ROS. A hydrogen peroxide positive control validated the assay. The negative control was wells with no cells. **B)** The MTS reagent measures cell metabolism and showed no decrease at any concentration studied. Here, we used both freshly dissolved PGNs (fresh) and PGNs that had been in solution for 24 hours (degraded). No concentration decreased metabolism. Error bars represent the standard deviation of 6 wells.

5.5.7. *In vitro* ultrasound imaging

The ability of the PGNs to backscatter acoustic energy was tested with phantoms. Inclusions contained increasing concentrations of PGNs were added to the agarose support and imaged at 40 MHz (**Fig. 5.8**). In **Figure 5.8A**, the echogenicity of a 0 mg.mL⁻¹ PGNs is seen. The outline of the well can be seen clearly due to the presence of air bubbles that became trapped on the side of the well (dashed lines). A much more intense signal is seen when a specific well was loaded with 1 mg.mL⁻¹ PGNs (**Fig. 5.8B**). The mean intensity of this image and at least three replicate images was measured to be 81.5 ± 1.3 a.u. This value and the value determined for the other concentrations of PGNs is plotted in **Figure 5.8C**. Using the best fit line ($R^2 > 0.99$) and the background value of 5.3 ± 0.4 , we estimated the limit of detection to be 5 $\mu\text{g.mL}^{-1}$ at three standard deviations above the mean of the background.

To understand how biodegradation affects the ultrasound signal was also measured using 0.25 mg.mL⁻¹ PGNs after different periods of dissolution in standard PBS (**Fig. 5.8D**). It was found that the signal has a maximum near 10 minutes, but remains elevated at least 4 hours after wetting. Interestingly, the increase from 2 minutes to 10 minutes was significant ($p < 0.05$) and suggests that the wetting of the PGNs may induce hydration that increases backscatter.

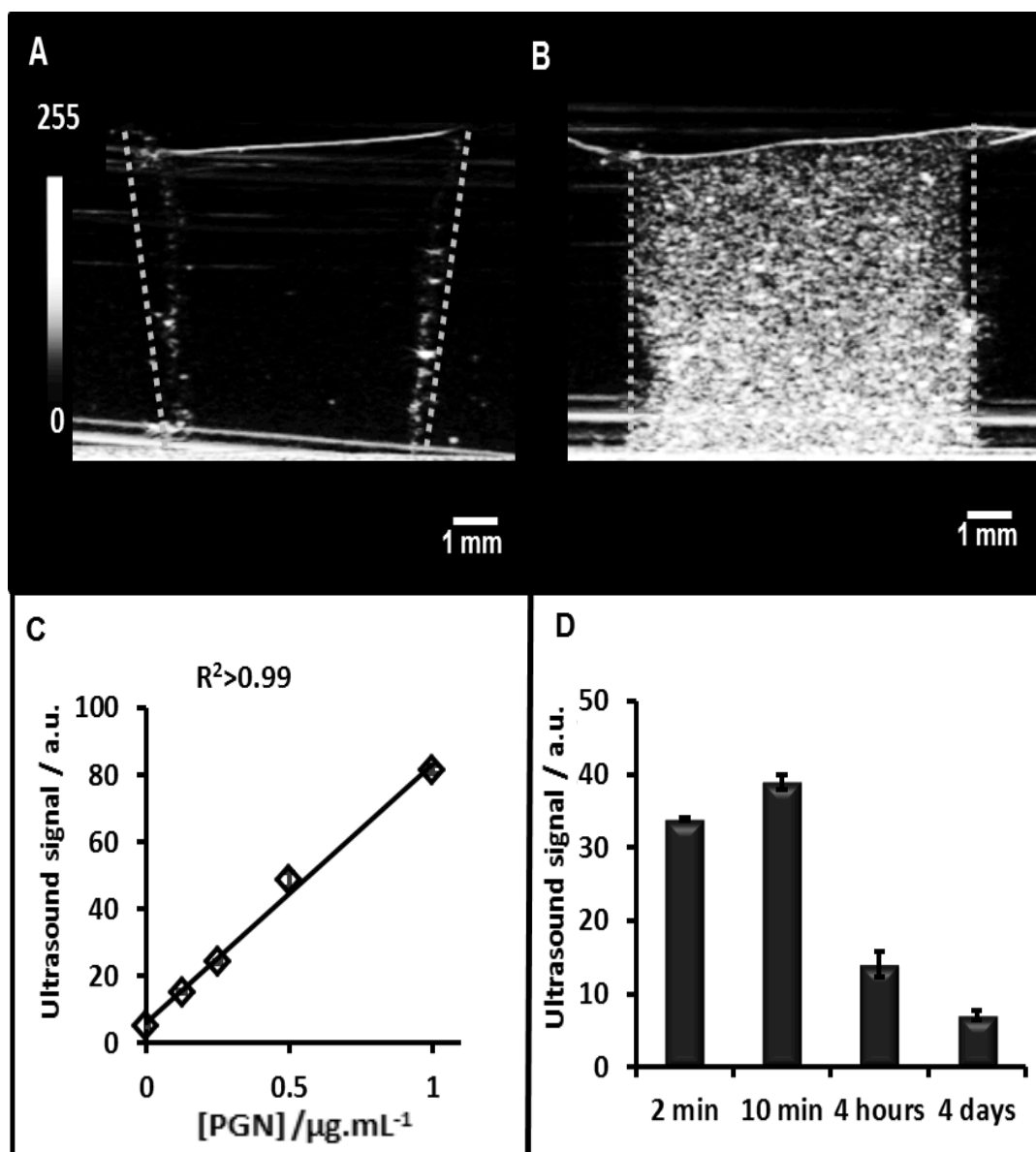


Figure 5.8. Ultrasound images in the z-axis for inclusions with 0 mg.mL⁻¹ PGNs (A) and 1 mg.mL⁻¹ PGNs at 40 MHz (B). The increased backscatter results from the increasing number of particles that was further quantified for multiple fields of view in (C). PGNs (0.25 mg.mL⁻¹) at various time points were imaged with ultrasound to understand how signal changes as a function of time (D). These data indicate that ultrasound signal decreases as the PGNs degrades because of decreased acoustic impedance. The imaging window is within the first four hours of dissolution.

The frequency of imaging is also an important parameter. Higher frequencies have better resolution, but lower depth of penetration and the echogenicity of the material may change as a function of frequency. To understand how the PGNs behave in both clinical and pre-clinical frequencies, we also imaged nanoparticles at 16 MHz (**Fig. 5.9A**). The signal of a 1 mg.mL^{-1} PGNs solution was measured as well as the background signal of agar. Both the signal and signal-to-background (S/B) are plotted and are shown in **Figure 5.9B**. While the signal was 36% higher at 40 MHz, the signal-to-background at 16 MHz was 4.6-fold higher than 40 MHz, because of a lower background signal. These data indicate that the PGNs are suitable for imaging at both clinical and pre-clinical frequencies.

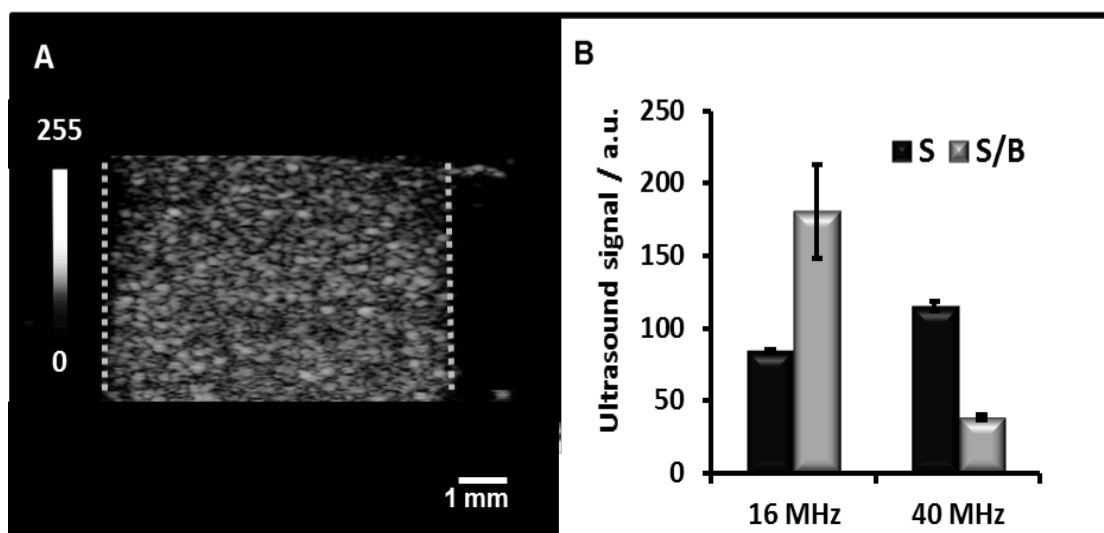


Figure 5.9. Panel **A** is an ultrasound image in the z-axis for 1 mg.mL^{-1} PGNs at 16 MHz, and **B** is signal and signal-to-background for both 16 and 40 MHz. Here, the signal was defined as echogenicity of the sample and background was adjacent agar. While the signal was higher at 40 MHz, the signal-to-background at 16 MHz was 4.6-fold higher than 40 MHz because of a lower background signal. These data indicate that the PGNs are suitable for imaging in both clinical and pre-clinical frequencies.

5.5.8. *In vivo* ultrasound imaging

To understand the capability of PGNs for *in vivo* imaging and biodegradation, 100 μL boluses of increasing concentrations of PGNs were implanted into the rear flank of nude mice (**Fig. 5.10A**). These samples were in a 50% matrigel carrier and this vehicle served as the negative control (0 $\text{mg}\cdot\text{mL}^{-1}$ PGNs). Each implant was imaged at 40 MHz and the backscatter was quantified for various concentrations in **Figure 5.11A**. The calculated limit of detection *in vivo* is 9 $\mu\text{g}\cdot\text{mL}^{-1}$ of PGNs with a value nearly 2-fold higher than *in vitro* analysis. This is because of the increased background signal in *in vivo* imaging.

We also studied the capability for *in vivo* biodegradation. Mice implanted with 2 $\text{mg}\cdot\text{mL}^{-1}$ PGNs were imaged immediately after implantation (**Fig. 5.10A**) and one day later (**Fig. 5.10B**). As expected, the matrigel and saline carriers were largely resorbed into circulation and extracellular matrix. Concurrently, the PGNs implanted began to degrade as we observed a 3.5-fold decrease in signal-to-background after one day (**Fig. 5.11B**).

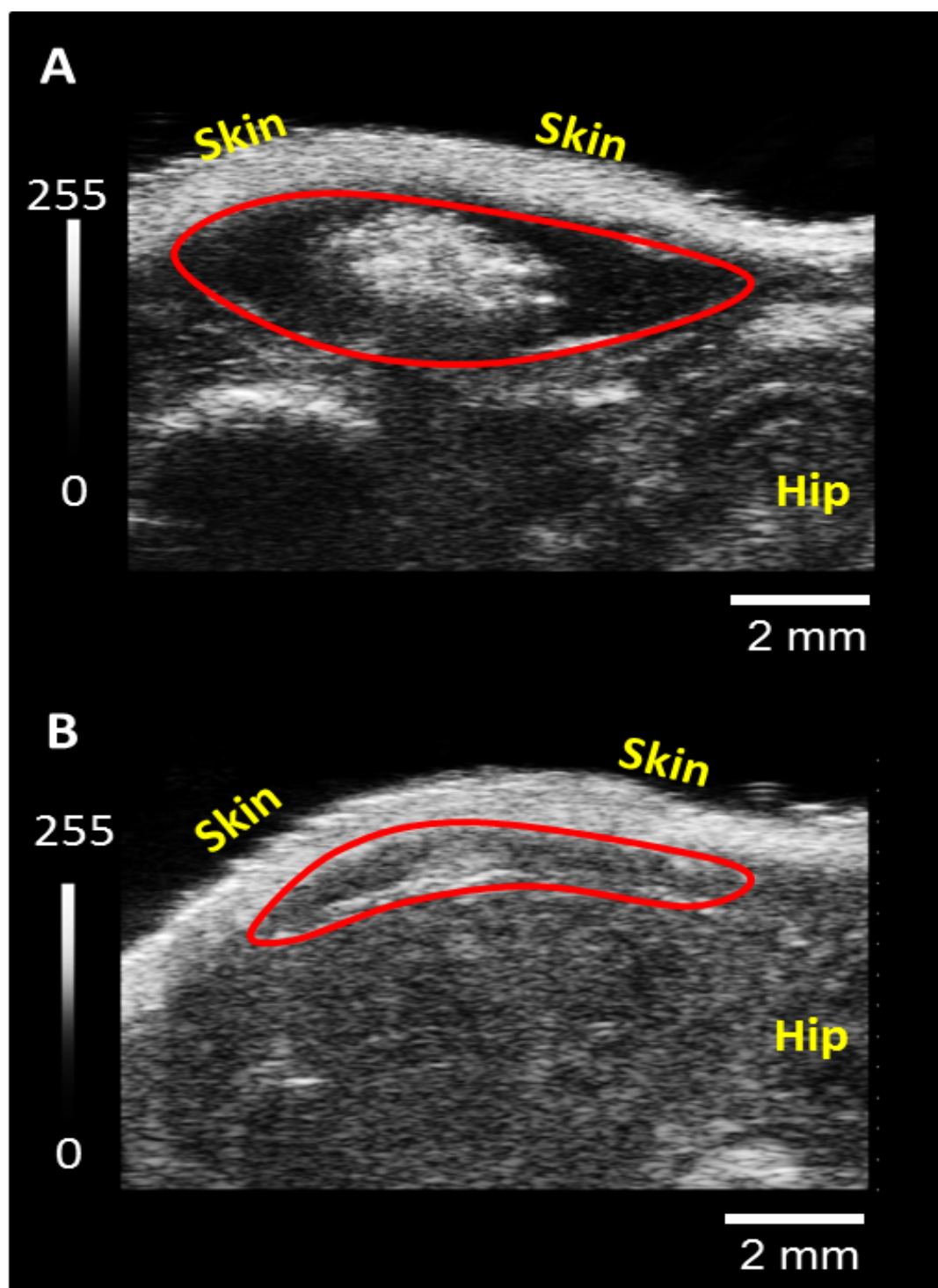


Figure 5.10. Nude mice received 100 μL boluses of 2 $\text{mg}\cdot\text{mL}^{-1}$ PGNs in 1:1 matrigel:PBS and imaged at 40 MHz immediately after implantation (**A**) and 1 day after (**B**). Red outlines in **A** and **B** indicate the region of implantation.

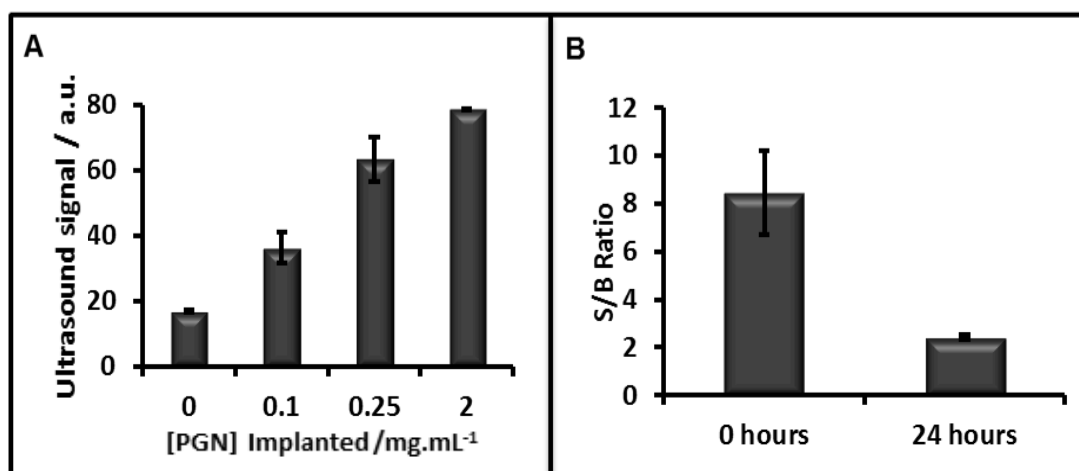


Figure 5.11. Decreasing concentrations of PGNs were also implanted to calculate the limit of detection and variance between animals **(A)**. Error bars represent the standard error of measurement. Changes in ultrasound backscatter for PGNs indicates a 3.5-fold decrease in signal-to-background ratio (SBR) **(B)**. Error bars represent the standard deviation.

5.5.9. Ultrasound cellular imaging

A final imaging study was carried out on labelled MSCs with the PGNs. We first optimised the labelling protocol using the cell fluorescence to monitor labelling. There was a linear relationship ($R^2=0.98$) between the starting concentration and the resulting cell fluorescence from 30 to 1000 $\mu\text{g.mL}^{-1}$ of PGNs at 2 hours of incubation (**Fig. 5.12A**). When the incubation time was changed from 1 to 360 minutes at 500 $\mu\text{g.mL}^{-1}$, a marked plateau effect was noted after 1 hour of incubation (**Fig. 5.12B**). Further incubation with cells did not significantly increase the signal from the cells ($p>0.05$). Even 30 minutes of incubation gave a signal from the cells that was 70% of maximum. These conditions were used to label MSCs and then imaged them with ultrasound (**Fig. 5.12C**) and fluorescence microscopy (**Fig. 5.13A**).

Next microscopy was used to understand the interaction between the PGNs and the MSC's. Epifluorescence microscopy indicated low non-specific binding of PGNs to the culture flasks. Less than 5% of the fluorescent pixels did not correspond to a cell in **Figure 5.13B** with many regions of increased signal seen throughout the MSC's.

Different numbers of cells were placed in a 100 μ L inclusion in an agar phantom and imaged at 40 MHz. This cell volume was used because it is similar to the injection volume used in trials of non-human primates and would likely be used in human. A linear relationship was noted between the number of cells and the ultrasound backscatter ($R^2 > 0.99$; **Fig. 5.12C**), which is important for studies in which unknown numbers of cells may need to be quantified. The calculated limit of detection for ultrasound imaging was 4000 MSCs at three standard deviations above the mean of the background.

Finally, confocal microscopy was used to study the distribution of the PGNs. Our goal was to determine whether the nanoparticles were on the cells or inside the cells. This is important because nanoparticles that were only on the surface could become detached after implantation and incorrectly be considered as a cell. The confocal data in **Figure 5.13F** showed that the nanoparticles are located throughout the cell in the cytoplasm and are not simply on the cell surface.

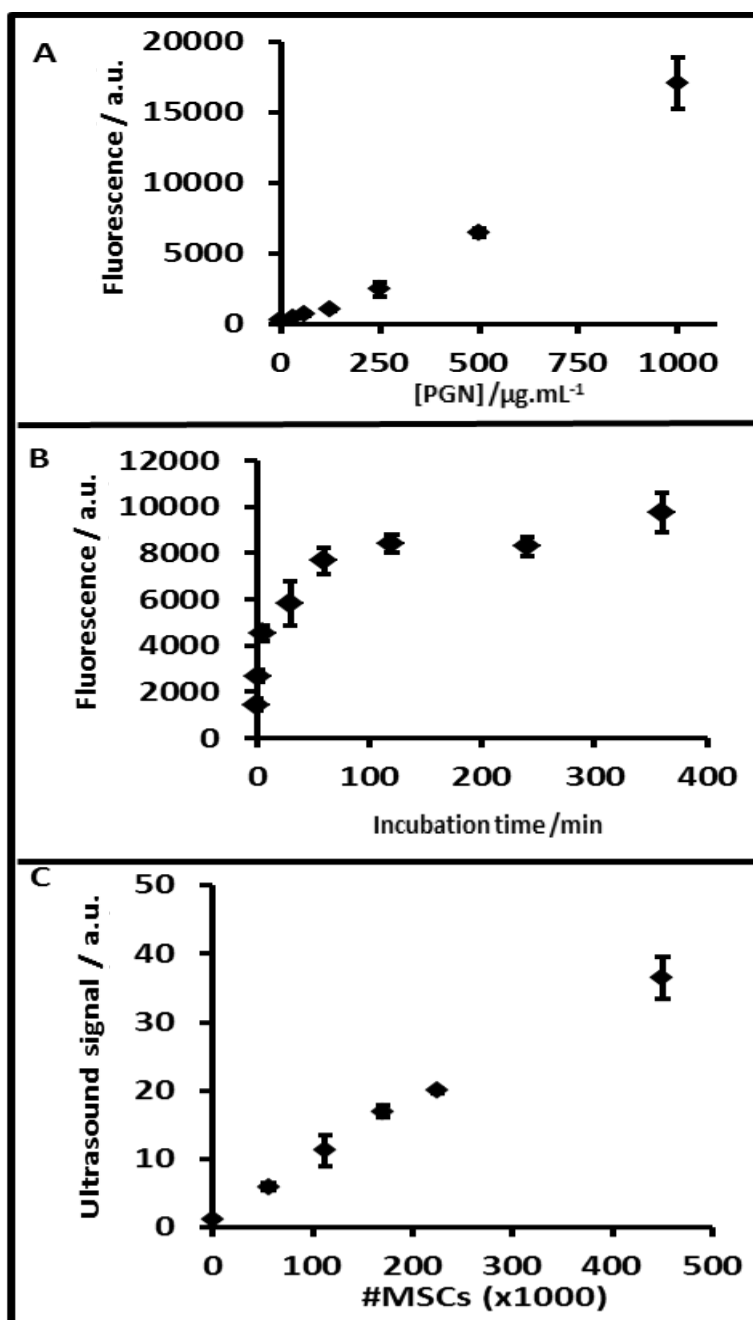


Figure 5.12. The optimal labeling conditions were tested empirically including starting concentration of PGNs (**A**) and incubation time (**B**). We found a nearly linear relationship between starting concentration and cell fluorescence (**A**). These concentrations used 2 hours of labeling. In **B**, we studied the effect of time and found that incubation times beyond 2 hours offered no additional signal. (**C**) MSCs labelled with these conditions ($500 \mu\text{g.mL}^{-1}$ and 2 hours) were imaged with 40 MHz ultrasound—the limit of detection is 4000 MSCs.

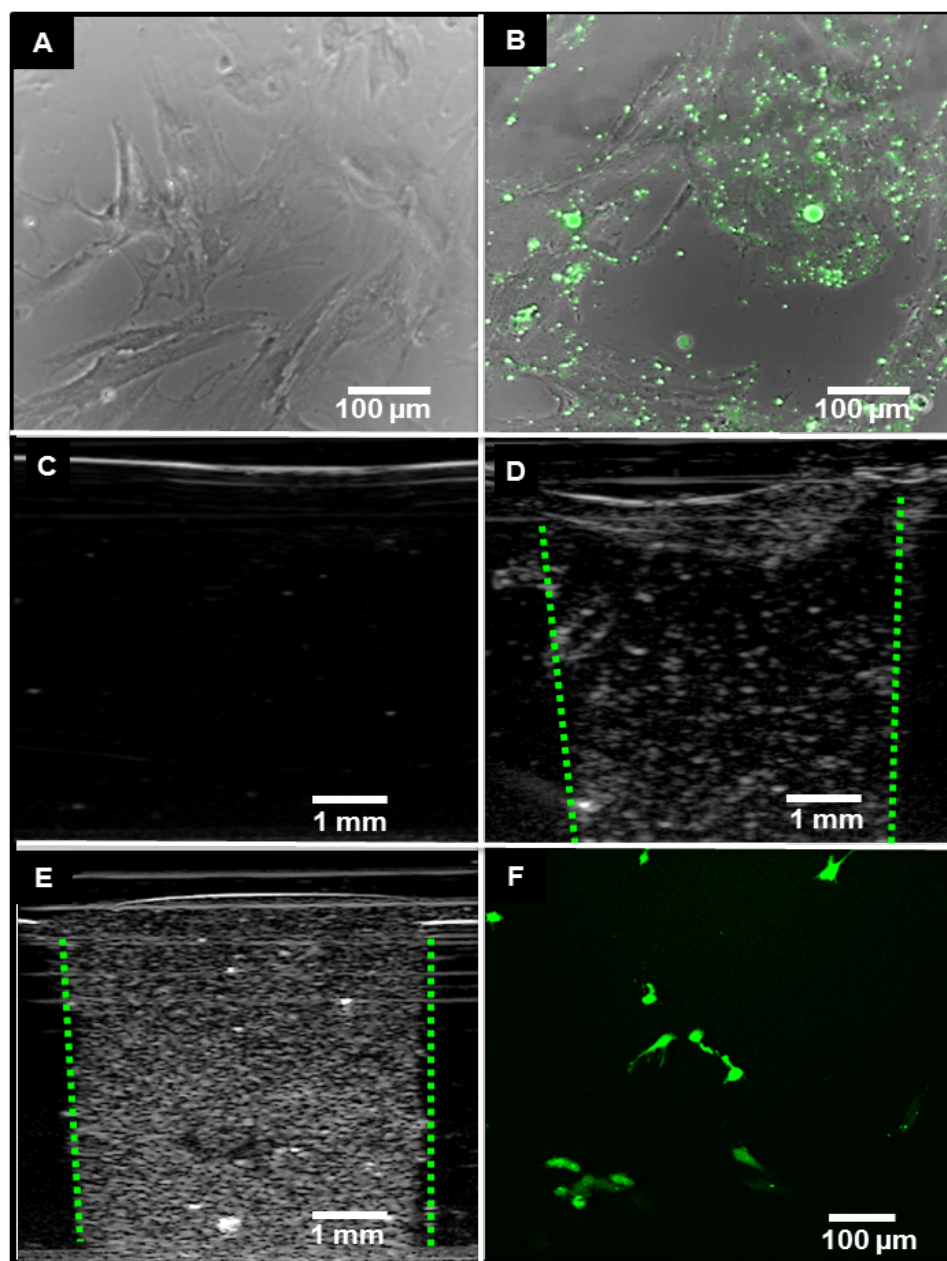


Figure 5.13. Phase contrast/fluorescence microscopy of naive MSCs (A) and MSCs labelled with PGNs shows that fluorescence only corresponds to the cells (low non-specific binding) (B). Panel C is ultrasound image of blank agarose phantom (no cells), panel D is the ultrasound backscatter from 225,000 MSCs, and panel E is the same number MSCs labeled with PGNs in an agar phantom. The PGNs increased the backscatter two-fold versus unlabeled cells. Panel F is a confocal image through the medial slice of adherent cells labelled with fluorescently tagged PGNs. The image shows that the nanoparticles are located throughout the cell and are localised in the cytoplasm and are not simply on the cell surface.

5.5.10. Drug release measurement

Figure 5.14 shows the cumulative TCH release profile measured *via* UPLC from the drug-loaded PGNs. It can be seen that the highest TCH release occurs within the first 4 hours of study period (~ 55% TCH). These results matching with the data that was obtained from the ICP and ultrasound imaging analysis. The release reached to around 60% TCH theoretical total after 12 hours and appeared to have been saturated. This can be related to the existence of the TCH molecules on the surface of the PGNs that washed out during the preparation of PGNs.

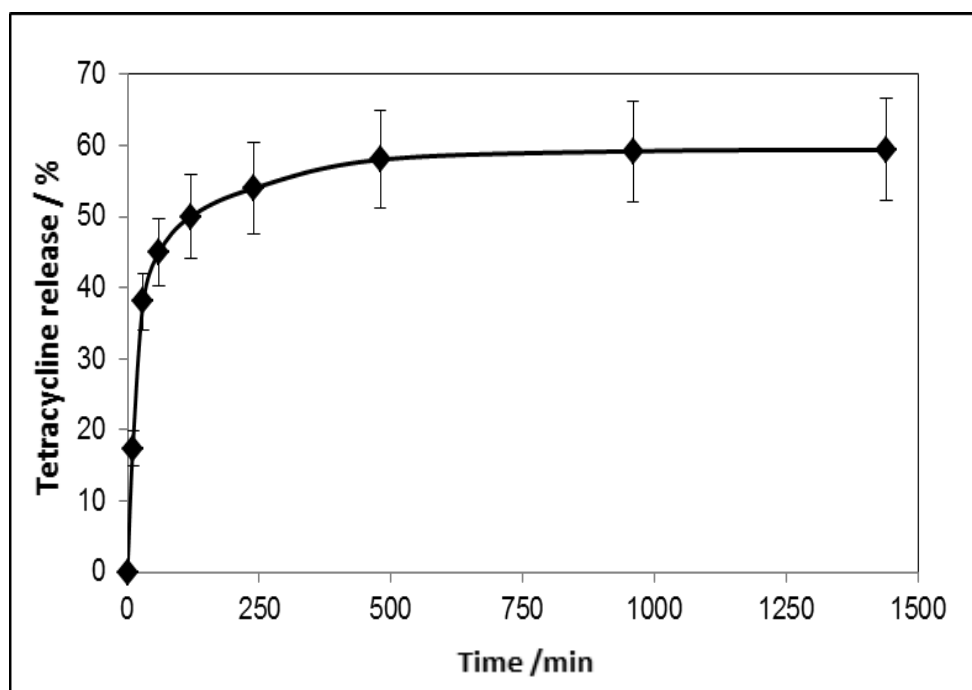


Figure 5.14. Cumulative release measurement of TCH from the drug-loaded PGNs determined *via* UPLC. Highest release occurred within the first 4 hours of the entire study. Error bars represent the standard deviation of three samples.

5.6. Discussion

In this chapter, the sol-gel preparation method and the subsequent application of electrospraying was utilised to prepare ternary phosphate-based glass nanospheres in the diameter size range of 200-500 nm at relatively low temperature. Previous approaches to prepare these glasses have been focused on preparing bulk sol-gel glasses. However, the difficulties in manufacturing bulk glasses have led to their limited biomedical applications. In this study, the electrospraying technique was used to tailor the shape of these sol-gel derived glasses in the range of nanometers.

The amorphous and glassy nature of the PGNs was confirmed by XRD data analysis. The ^{31}P NMR and FTIR spectroscopy results also showed the structure of these PGNs consists of mainly Q^1 and Q^2 phosphate units. The Q^0 and Q^1 percentages for the PGNs are slightly higher than the previously synthesised glass with the same composition in section 2.2.2.3 that can be related to the shorter ageing time period and also evaporation of unreacted phosphorus precursors during the heating stage that was confirmed by EDX measurement which showed an approximately 12.5 mol% P_2O_5 loss, post processing.

The PGNs have strong ultrasound backscattering capabilities both *in vivo* and *in vitro*. Phantom experiments indicated a limit of detection of $5 \mu\text{g}\cdot\text{mL}^{-1}$ with linear behaviour below $1000 \mu\text{g}\cdot\text{mL}^{-1}$ (**Fig. 5.8A**). The imaging window of this material is below 4 hours. The ICP data show the highest rate of dissolution within the first 4 hours of immersion in distilled water (**Fig. 5.6**), and our time course study shows that by 4 hours the signal has decreased more than 2-fold with even further reduction the next day (**Fig. 5.8D**). This is particularly important because it bridges a gap between the minutes of stability of microbubbles and the months of stability of Stober silica particles (Hudson et al., 2008, He et al., 2011b).

One potential concern is that the high local ionic concentrations could perturb cellular function. For 0.1 mg.mL^{-1} of PGNs, over the 48 hours of dissolution study and assuming no diffusion, cells would be exposed to 41 ppm $(\text{PO}_4)^{3-}$, 32 ppm Ca^{2+} , and 16 ppm Na^+ (**Fig. 5.6**). These values are well within the standard physiological range of serum chemistries (Bishop, 2010). For example, the reference range of Ca^{2+} is $8.5 - 10 \text{ mg.dL}^{-1}$ or 85 - 100 ppm. The additional calcium due to the contrast agents is within the reference range and should not unduly perturb cell metabolism. Furthermore, diffusion and normal circulation may contribute to equilibration of any locally disturbed ionic concentrations.

To further confirm the cytocompatibility, we performed a series of cell toxicity assays. While we did find that very high doses ($1000 \text{ }\mu\text{g.mL}^{-1}$) increased ROS (hydroxyl, peroxy, etc.) activity within the cell, this is much higher than the concentrations needed for imaging, which are usually $250 \text{ }\mu\text{g.mL}^{-1}$ for MSC imaging and $>9 \text{ }\mu\text{g.mL}^{-1}$ for subcutaneous imaging (**Fig. 5.7A**). All materials—even water—are toxic over certain concentration ranges, our goal here was to discover above which concentration PGNs began to dysregulate metabolism. After PGNs implantation into animals, we noticed no changes in posture, behaviour, gait, or feeding pattern according to observation up to two weeks.

We also used the MTS assay to study cell metabolism and viability *via* mitochondrial reductase activity (**Fig. 5.7**). MTS is a colorimetric, water-soluble tetrazolium dye that indicates the activity of oxidoreductase enzymes. One concern was that the degradation products may increase the sodium, calcium, and phosphorus concentration to levels inconsistent with cell survival. Thus, it was important to study both fresh and degraded PGNs in this assay. Fortunately, we noticed no cytotoxicity in either sample group at concentrations below $500 \text{ }\mu\text{g.mL}^{-1}$ (**Fig. 5.7**).

Although we did not investigate tumour imaging here, the PGNs implantation experiments (**Fig. 5.11**) indicated that concentrations as low as $9 \mu\text{g.mL}^{-1}$ could be imaged *in vivo*. This is important because nanoparticle contrast agents must overcome significant competition from the reticuloendothelial system to reach the target tissue. Values near 4 \%ID.g^{-1} are common for nanoparticle contrast agents. Thus, a 1 g tumour would need at least 225 μg of material injected into the 2.5 mL murine blood pool to achieve 4 \%ID.g^{-1} accumulation. Importantly, this concentration is well below the concentration that increases ROS generation.

Our primary goal was cell imaging, which is critical to understand the location of implanted stem cells in regenerative medicine. We achieved cell counting below 5000 cells in 100 μL volumes (**Fig. 5.12**). While we did not achieve the single cell counts which is possible with some MRI techniques (Shapiro et al., 2006), the cell counts described here is more than sufficient for clinical trials that will likely use millions of cells (Chong et al., 2014, Hare et al., 2012a, Makkar et al., 2012). These low detection limits would be useful because it would allow analysis without requiring all cells in a given population be labelled. The 4 hour imaging window would be useful for imaging the immediate implantation events in cells. Long term imaging could utilize a reporter gene (Yaghoubi et al., 2006).

The detection limits reported here are higher than that achieved with perfluorocarbon microbubbles. Indeed, these can be detected even at the single microbubble level (Klibanov et al., 2004). The PGNs could not be detected at the single particle level, but did have detection levels down to $50 \mu\text{g.mL}^{-1}$, which is on par with the $20 \mu\text{g.mL}^{-1}$ detection limits that have been reported previously with silica nanoparticles (Jokerst et al., 2013). These materials also have lower overall signal intensity than perfluorocarbon microbubbles. However, perfluorocarbon microbubbles are approximately the same size as cells and their application for ultrasound cell imaging can be difficult. Importantly, the PGNs are approximately

10-fold smaller in diameter (and 1000-fold smaller in volume) and thus have a significant advantage for ultrasound cell imaging. Also, the time stability of the PGNs (~4 hours), is much longer than *in vivo* stability of perfluorocarbon microbubbles which is reported to be in the range of a few minutes.

The low processing temperature allowed us to incorporate organic dye (fluorescein) or drug molecules (TCH) during PGNs processing which cannot be achieved for phosphate-based glasses synthesised *via* the melt-quench technique (Franks et al., 2000). The UPLC results from the drug-loaded PGNs showed a linear release of drug molecules during the first 4 hours of the study period (**Fig. 5.14**). This shows the potential of these nanoparticles for applications as an efficient vehicle for the local delivery of antibiotics with lower active doses which can reduce systemic cytotoxicity and side effects.

References

- BAIA, L., MURESAN, D., BAIA, M., POPP, J. & SIMON, S. 2007. Structural properties of silver nanoclusters-phosphate glass composites. *Vibrational Spectroscopy*, 43, 313-318.
- BENCHIMOL, M. J., HSU, M. J., SCHUTT, C. E., HALL, D. J., MATTREY, R. F. & ESENER, S. C. 2013. Phospholipid/carbocyanine dye-shelled microbubbles as ultrasound-modulated fluorescent contrast agents. *Soft Matter*, 9, 2384-2388.
- BISHOP, M. L. 2010. *Clinical Chemistry*.
- BUNKER, B. C., ARNOLD, G. W. & WILDER, J. A. 1984. Phosphate-Glass Dissolution in Aqueous-Solutions. *Journal of Non-Crystalline Solids*, 64, 291-316.
- BYUN, J. O., KIM, B. H., HONG, K. S., JUNG, H. J., LEE, S. W. & IZYNEEV, A. A. 1995. Properties and Structure of $R\text{-Na}_2\text{O-Al}_2\text{O}_3\text{-P}_2\text{O}_5$ (R=Mg, Ca, Sr, Ba) Glasses. *Journal of Non-Crystalline Solids*, 190, 288-295.
- CARTA, D., KNOWLES, J. C., SMITH, M. E. & NEWPORT, R. J. 2007. Synthesis and structural characterization of $\text{P}(2)\text{O}(5)\text{-CaO-Na}(2)\text{O}$ sol-gel materials. *Journal of Non-Crystalline Solids*, 353, 1141-1149.
- CASCIARO, S., CONVERSANO, F., RAGUSA, A., MALVINDI, M. A., FRANCHINI, R., GRECO, A., PELLEGRINO, T. & GIGLI, G. 2010. Optimal Enhancement Configuration of Silica Nanoparticles for Ultrasound Imaging and Automatic Detection at Conventional Diagnostic Frequencies. *Investigative Radiology*, 45, 715-724.
- CHONG, J. J. H., YANG, X. L., DON, C. W., MINAMI, E., LIU, Y. W., WEYERS, J. J., MAHONEY, W. M., VAN BIBER, B., COOK, S. M., PALPANT, N. J., GANTZ, J. A., FUGATE, J. A., MUSKHELI, V., GOUGH, G. M., VOGEL, K. W., ASTLEY, C. A., HOTCHKISS, C. E., BALDESSARI, A., PABON, L., REINECKE, H., GILL, E. A., NELSON, V., KIEM, H. P., LAFLAMME, M. A. & MURRY, C. E. 2014. Human embryonic-stem-cell-derived cardiomyocytes regenerate non-human primate hearts. *Nature*, 510, 273-+.
- FOROUTAN, F., DE LEEUW, N., MARTIN, R., PALMER, G., OWENS, G., KIM, H.-W. & KNOWLES, J. 2015. Novel sol-gel preparation of $(\text{P}_2\text{O}_5)_{0.4}\text{-(CaO)}_{0.25}\text{-(Na}_2\text{O)}_X\text{-(TiO}_2\text{)}_{(0.35-X)}$ bioresorbable glasses (X = 0.05, 0.1, and 0.15). *Journal of Sol-Gel Science and Technology*, 73, 434-442.

- FRANKS, K., ABRAHAMS, I., GEORGIU, G. & KNOWLES, J. C. 2001. Investigation of thermal parameters and crystallisation in a ternary CaO-Na₂O-P₂O₅-based glass system. *Biomaterials*, 22, 497-501.
- FRANKS, K., ABRAHAMS, I. & KNOWLES, J. C. 2000. Development of soluble glasses for biomedical use Part I: In vitro solubility measurement. *Journal of Materials Science-Materials in Medicine*, 11, 609-614.
- GOLDBERG, B. B. & LIU, J. B. 1997. Contrast agents in abdominal ultrasound. *Current Trends in Digestive Ultrasonography*, 24, 323-341.
- GRAMIAK R & SHAH PM 1968. Echocardiography of the aortic root. *Investigative Radiology*, 3, 356-366.
- HARE, J., FISHMAN, J. & GERSTENBLITH, G. 2012a. The POSEIDON Randomized Trial. *JAMA*, 308, 2369-2379.
- HARE, J. M., FISHMAN, J. E., GERSTENBLITH, G., VELAZQUEZ, D. L. D., ZAMBRANO, J. P., SUNCION, V. Y., TRACY, M., GHERSIN, E., JOHNSTON, P. V., BRINKER, J. A., BRETON, E., DAVIS-SPROUL, J., SCHULMAN, I. H., BYRNES, J., MENDIZABAL, A. M., LOWERY, M. H., ROUY, D., ALTMAN, P., FOO, C. W. P., RUIZ, P., AMADOR, A., DA SILVA, J., MCNIECE, I. K. & HELDMAN, A. W. 2012b. Comparison of Allogeneic vs Autologous Bone Marrow-Derived Mesenchymal Stem Cells Delivered by Transendocardial Injection in Patients With Ischemic Cardiomyopathy The POSEIDON Randomized Trial. *Jama-Journal of the American Medical Association*, 308, 2369-2379.
- HE, Q. J., GAO, Y., ZHANG, L. X., ZHANG, Z. W., GAO, F., JI, X. F., LI, Y. P. & SHI, J. L. 2011a. A pH-responsive mesoporous silica nanoparticles-based multi-drug delivery system for overcoming multi-drug resistance. *Biomaterials*, 32, 7711-7720.
- HE, Q. J., ZHANG, Z. W., GAO, F., LI, Y. P. & SHI, J. L. 2011b. In vivo Biodistribution and Urinary Excretion of Mesoporous Silica Nanoparticles: Effects of Particle Size and PEGylation. *Small*, 7, 271-280.
- HENCH, L. L. & POLAK, J. M. 2002. Third-generation biomedical materials. *Science*, 295, 1014-+.
- HUDSON, S. P., PADERA, R. F., LANGER, R. & KOHANE, D. S. 2008. The biocompatibility of mesoporous silicates. *Biomaterials*, 29, 4045-4055.
- ILIEVA, D., JIVOV, B., KOVACHEVA, D., TSACHEVA, T., DIMITRIEV, Y., BOGACHEV, G. & PETKOV, C. 2001. FT-IR and Raman spectra of Gd

- phosphate crystals and glasses. *Journal of Non-Crystalline Solids*, 293, 562-568.
- JOKERST, J. V., KHADEMI, C. & GAMBHIR, S. S. 2013. Intracellular Aggregation of Multimodal Silica Nanoparticles for Ultrasound-Guided Stem Cell Implantation. *Science Translational Medicine*, 5.
- KLIBANOV, A. L. 1999. Targeted delivery of gas-filled microspheres, contrast agents for ultrasound imaging. *Advanced Drug Delivery Reviews*, 37, 139-157.
- KLIBANOV, A. L. 2005. Ligand-carrying gas-filled microbubbles: Ultrasound contrast agents for targeted molecular imaging. *Bioconjugate Chemistry*, 16, 9-17.
- KLIBANOV, A. L., RASCHE, P. T., HUGHES, M. S., WOJDYLA, J. K., GALEN, K. P., WIBLE, J. H. & BRANDENBURGER, G. H. 2004. Detection of individual microbubbles of ultrasound contrast agents - Imaging of free-floating and targeted bubbles. *Investigative Radiology*, 39, 187-195.
- KNOWLES, J. C. 2003. Phosphate based glasses for biomedical applications. *Journal of Materials Chemistry*, 13, 2395-2401.
- KONO, Y., HOLSCHER, T. & MATTREY, R. F. 2008. Use of Ultrasound Microbubbles for Vascular Imaging. *Nanoparticles in Biomedical Imaging: Emerging Technologies and Applications*, 311-325.
- KRUPKA, T. M., SOLORIO, L., WILSON, R. E., WU, H. P., AZAR, N. & EXNER, A. A. 2010. Formulation and Characterization of Echogenic Lipid-Pluronic Nanobubbles. *Molecular Pharmaceutics*, 7, 49-59.
- LEE, I. H., FOROUTAN, F., LAKHKAR, N. J., GONG, M. S. & KNOWLES, J. C. 2013. Sol-gel synthesis and structural characterization of P2O5-CaO-Na2O glasses. *Physics and Chemistry of Glasses-European Journal of Glass Science and Technology Part B*, 54, 115-120.
- LIBERMAN, A., WU, Z., BARBACK, C. V., VIVEROS, R., BLAIR, S. L., ELLIES, L. G., VERA, D. R., MATTREY, R. F., KUMMEL, A. C. & TROGLER, W. C. 2013. Color Doppler Ultrasound and Gamma Imaging of Intratumorally Injected 500 nm Iron-Silica Nanoshells. *Acs Nano*, 7, 6367-6377.
- MAKKAR, R. R., SMITH, R. R., CHENG, K., MALLIARAS, K., THOMSON, L. E., BERMAN, D., CZER, L. S., MARBÁN, L., MENDIZABAL, A. & JOHNSTON, P. V. 2012. Intracoronary cardiosphere-derived cells for heart regeneration after myocardial infarction (CADUCEUS): a prospective, randomised phase 1 trial. *The Lancet*, 379, 895-904.

- MALVINDI, M. A., GRECO, A., CONVERSANO, F., FIGUEROLA, A., CORTI, M., BONORA, M., LASCIALFARI, A., DOUMARI, H. A., MOSCARDINI, M., CINGOLANI, R., GIGLI, G., CASCIARO, S., PELLEGRINO, T. & RAGUSA, A. 2011. Magnetic/Silica Nanocomposites as Dual-Mode Contrast Agents for Combined Magnetic Resonance Imaging and Ultrasonography. *Advanced Functional Materials*, 21, 2548-2555.
- MARTINEZ, H. P., KONO, Y., BLAIR, S. L., SANDOVAL, S., WANG-RODRIGUEZ, J., MATTREY, R. F., KUMMEL, A. C. & TROGLER, W. C. 2010. Hard shell gas-filled contrast enhancement particles for colour Doppler ultrasound imaging of tumors. *Medchemcomm*, 1, 266-270.
- MOUSTAFA, Y. M. & EL-EGILI, K. 1998. Infrared spectra of sodium phosphate glasses. *Journal of Non-Crystalline Solids*, 240, 144-153.
- NAKATSUKA, M. A., HSU, M. J., ESENER, S. C., CHA, J. N. & GOODWIN, A. P. 2011. DNA-Coated Microbubbles with Biochemically Tunable Ultrasound Contrast Activity. *Advanced Materials*, 23, 4908-4912.
- PICKUP, D. M., GUERRY, P., MOSS, R. M., KNOWLES, J. C., SMITH, M. E. & NEWPORT, R. J. 2007. New sol-gel synthesis of a (CaO)(0.3)(Na₂O)(0.2)(P₂O₅)(0.5) bioresorbable glass and its structural characterisation. *Journal of Materials Chemistry*, 17, 4777-4784.
- PICKUP, D. M., NEWPORT, R. J. & KNOWLES, J. C. 2012. Sol-Gel Phosphate-based Glass for Drug Delivery Applications. *Journal of Biomaterials Applications*, 26, 613-622.
- SCHNEIDER, C. A., RASBAND, W. S. & ELICEIRI, K. W. 2012. NIH Image to ImageJ: 25 years of image analysis. *Nature Methods*, 9, 671-675.
- SCHUTT, E. G., KLEIN, D. H., MATTREY, R. M. & RIESS, J. G. 2003. Injectable microbubbles as contrast agents for diagnostic ultrasound imaging: The key role of perfluorochemicals. *Angewandte Chemie-International Edition*, 42, 3218-3235.
- SENE, F. F., MARTINELLI, J. R. & GOMES, L. 2004. Synthesis and characterization of niobium phosphate glasses containing barium and potassium. *Journal of Non-Crystalline Solids*, 348, 30-37.
- SHAPIRO, E. M., SHARER, K., SKRTIC, S. & KORETSKY, A. P. 2006. In vivo detection of single cells by MRI. *Magnetic Resonance in Medicine*, 55, 242-249.

- SHAPIRO, M. G., GOODWILL, P. W., NEOGY, A., YIN, M., FOSTER, F. S., SCHAFFER, D. V. & CONOLLY, S. M. 2014. Biogenic gas nanostructures as ultrasonic molecular reporters. *Nature Nanotechnology*, 9, 311-316.
- TA, C. N., LIBERMAN, A., MARTINEZ, H. P., BARBACK, C. V., MATTREY, R. F., BLAIR, S. L., TROGLER, W. C., KUMMEL, A. C. & WU, Z. 2012. Integrated processing of contrast pulse sequencing ultrasound imaging for enhanced active contrast of hollow gas filled silica nanoshells and microshells. *Journal of Vacuum Science & Technology B*, 30.
- WILLMANN, J. K., PAULMURUGAN, R., CHEN, K., GHEYSENS, O., RODRIGUEZ-PORCEL, M., LUTZ, A. M., CHEN, I. Y., CHEN, X. & GAMBHIR, S. S. 2008. US imaging of tumor angiogenesis with microbubbles targeted to vascular endothelial growth factor receptor type 2 in mice. *Radiology*, 246, 508-518.
- XING, Z. W., WANG, J. R., KE, H. T., ZHAO, B., YUE, X. L., DAI, Z. F. & LIU, J. B. 2010. The fabrication of novel nanobubble ultrasound contrast agent for potential tumor imaging. *Nanotechnology*, 21.
- YAGHOUBI, S. S., COUTO, M. A., CHEN, C.-C., POLAVARAM, L., CUI, G., SEN, L. & GAMBHIR, S. S. 2006. Preclinical safety evaluation of ¹⁸F-FHBG: a PET reporter probe for imaging herpes simplex virus type 1 thymidine kinase (HSV1-tk) or mutant HSV1-sr39tk's expression. *Journal of Nuclear Medicine*, 47, 706-715.

CHAPTER 6

General Discussion and Future Directions

In the presented study, the successful sol-gel synthesis of phosphate-based glasses at a relatively low processing temperature using triethyl phosphate as a phosphorus precursor in the P_2O_5 - TiO_2 , P_2O_5 - CaO - TiO_2 , P_2O_5 - CaO - Na_2O and P_2O_5 - CaO - Na_2O - TiO_2 systems was reported. The synthesised glasses, were characterised in terms of structural properties including XRD, ^{31}P MAS-NMR, EDX, and FTIR spectroscopy that indicated the successful production of phosphate-based glasses. However, there were some limitations such as synthesis compositional ranges with an upper limit of about 60 mol% P_2O_5 for binary P_2O_5 - TiO_2 glasses and also phosphorus loss of up to 11 mol% during the sol-gel reaction was seen. To overcome the high phosphorus loss, triethyl phosphate was replaced with n-butyl phosphate to sol-gel synthesise ternary P_2O_5 - CaO - Na_2O and quaternary P_2O_5 - CaO - Na_2O - TiO_2 glass systems. The EDX results of these glasses revealed relatively lower phosphorus loss during the sol-gel synthesis of these glasses. In addition, substituting titanium in place of sodium or calcium reduced the amount of phosphorus loss during the sol-gel reaction and bulk, transparent and glassy-like specimens were obtained for the glasses with high titanium contents. These results indicated, incorporation of titanium into the phosphate-based glasses serves to stabilise the phosphate-network due to the cross-linking effect of titanium. This effect was confirmed by ^{31}P MAS-NMR results that showed the formation of $Q^1(Ti-O-P)$ species with a slight increase in the amount of Q^2 phosphate units. FTIR spectroscopy data also correlated with the NMR results that suggesting Ti may act as a conditional network former in phosphate-based sol-gel derived glasses.

We used sol-gel derived glasses with the general formula of $(P_2O_5)_{55}-(CaO)_{25}-(Na_2O)_{(20-x)}-(TiO_2)_x$, where $X = 0, 5, 10$ or 15 as a scaffold for bone tissue engineering applications. The degradation studies revealed that the dissolution rate of these glasses significantly reduced as titanium substituted in place of sodium

because of the cross-linking effect of titanium and gave an indication of how the solubility of phosphate-based glasses can be controlled for various biomedical applications. Cell culture studies were carried out on these glasses that showed the degradation rate has a significant effect on the activity of the cells. The substitution of Na₂O with 5 or 10 mol% TiO₂ improved cytocompatibility that was also supported by SEM and CLSM images that showed significant mineral formation and cells residing on the glass microparticles surface. However, cells cultured on Ti15 failed to recover and higher heat treatment temperature might be needed to evaporate the remaining toxic solvents in the glass structure.

The electrospaying technique was applied, for the first time to these sol-gel derived glasses, according to the author's knowledge, and was designed and developed to prepare ternary P₂O₅-CaO-Na₂O glass nanospheres in the diameter size range of 200-500 nm. The amorphous and glassy nature of these nanosphere particles was confirmed *via* XRD, ³¹P NMR, and FTIR analysis. This probe was used to label mesenchymal stem cells with an *in vitro* and *in vivo* detection limit of 5 and 9 µg.mL⁻¹, respectively. Cell counts down to 4000 were measured by ultrasound imaging with no cytotoxicity at doses needed for imaging. Also, due to the relatively low synthesis temperature, these phosphate-based glass nanospheres (PGNs) offered the potential to incorporate therapeutic molecules for drug delivery application. The UPLC results from the drug-loaded PGNs in an aqueous medium revealed a constant and linear release of TCH molecules within the first 4 hours of the study period with easily metabolised degradation components in the body that make them an attractive choice in drug delivery applications. Together, these results suggested, PGNs are useful for both *in vivo* and *in vitro* ultrasound imaging and have the utility for cell tracking and as a drug delivery system that can make them a

promising candidate for theranostic applications (serve dual roles as diagnostic and therapeutic agents) especially in cancer treatment.

From the synthesis point of view, further work could be focused on alternative solvents and precursors to be able to synthesise phosphate-based glasses at even lower temperatures. There is also a possibility to incorporate other metal oxides such as iron, copper or silver into the phosphate-based glasses for various biomedical applications. For example, iron-containing phosphate-based glasses have been prepared *via* melt-quench method and showed high durability and controllable degradation rate that can make them a good choice for tissue engineering applications (Abou Neel et al., 2005). However, to date, no study has been published regarding the possibility to synthesise these glasses *via* a sol-gel method that might be related to the limitation in access to the right Fe precursor. Our preliminary work on iron-containing sol-gel derived glasses confirmed iron (III) isopropoxide (2.55% in isopropanol, Alfa Aesar, Heysham, UK) can be used as a Fe precursor to synthesise quaternary glasses with the general formula of $(P_2O_5)_{50}-(CaO)_{30}-(Na_2O)_{(15-x)}-(Fe_2O_3)_x$, where $X = 0, 2.5$ or 5 . Initial XRD results confirmed the amorphous and glassy nature of the prepared samples. Further works could be focused on evaluation of their structural property and potential biomedical applications.

Cell culture studies on titanium-containing glasses offer several avenues for the future research on biomedical applications of these glasses, such as a coating for medical implants to provide a high degree of biocompatibility and promote the healing response without side effects. Initial studies showed that there is a possibility to deposit titanium-containing sol-gel derived glasses on metallic implants *via* the electrospraying technique. Low processing temperatures of the sol-gel synthesis also enables incorporation of bioactive molecules that can promote

bone formation or antimicrobial compounds that can subsequently be released in a localised and controlled manner to reduce the risk of bacterial infection of medical implants.

The electro spraying technique has allowed us to prepare nano-size glass spheres for both therapeutic and diagnostic applications. Future work may focus on reducing the degradation rate of the glass nanospheres by introducing Ti into the glass structure to increase the imaging window and therapeutic release of a drug molecule for longer periods (Lakhkar et al., 2012, Kiani et al., 2012, Foroutan et al., 2015). The surface of these glass nanospheres may also be functionalised with specific ligands for tasks beyond regenerative medicine, including targeted drug delivery and tumour imaging after i.v injection that can make them an attractive candidate for simultaneous diagnostic and therapeutic applications especially in cancer treatment (Cheng et al., 2010).

The other limitation in drug delivery applications of the prepared glass nanospheres is related to the heat treatment temperature that was applied during the sol-gel synthesis and subsequent electro spraying. While the processing temperature is significantly lower than the previous studies on the sol-gel preparation of phosphate-based glasses (Carta et al., 2005, Pickup et al., 2007, Carta et al., 2007), however, still just a few numbers of drug molecules show stability at the chosen synthesis temperature (200 °C). The idea of spraying the sol over the liquid nitrogen instead of heated silicone oil can be an alternative. Following that the obtained particles are transferred into a freeze dryer to evaporate the solvents. Our preliminary work showed the possibility of using this novel technique and future work may be focused on the development of this technique to prepare a wide range of drug-loaded nanoparticles for drug delivery purposes.

References

- ABOU NEEL, E. A., AHMED, I., BLAKER, J. J., BISMARCK, A., BOCCACCINI, A. R., LEWIS, M. P., NAZHAT, S. N. & KNOWLES, J. C. 2005. Effect of iron on the surface, degradation and ion release properties of phosphate-based glass fibres. *Acta Biomaterialia*, 1, 553-563.
- CARTA, D., PICKUP, D. M., KNOWLES, J. C., AHMED, I., SMITH, M. E. & NEWPORT, R. J. 2007. A structural study of sol-gel and melt-quenched phosphate-based glasses. *Journal of Non-Crystalline Solids*, 353, 1759-1765.
- CARTA, D., PICKUP, D. M., KNOWLES, J. C., SMITH, M. E. & NEWPORT, R. J. 2005. Sol-gel synthesis of the P(2)O(5)-CaO-Na(2)O-SiO(2) system as a novel bioresorbable glass. *Journal of Materials Chemistry*, 15, 2134-2140.
- CHENG, S. H., LEE, C. H., CHEN, M. C., SOURIS, J. S., TSENG, F. G., YANG, C. S., MOU, C. Y., CHEN, C. T. & LO, L. W. 2010. Tri-functionalization of mesoporous silica nanoparticles for comprehensive cancer theranostics-the trio of imaging, targeting and therapy. *Journal of Materials Chemistry*, 20, 6149-6157.
- FOROUTAN, F., DE LEEUW, N., MARTIN, R., PALMER, G., OWENS, G., KIM, H.-W. & KNOWLES, J. 2015. Novel sol-gel preparation of (P2O5)0.4-(CaO)0.25-(Na2O)X-(TiO2)(0.35-X) bioresorbable glasses (X = 0.05, 0.1, and 0.15). *Journal of Sol-Gel Science and Technology*, 73, 434-442.
- KIANI, A., LAKHKAR, N. J., SALIH, V., SMITH, M. E., HANNA, J. V., NEWPORT, R. J., PICKUP, D. M. & KNOWLES, J. C. 2012. Titanium-containing bioactive phosphate glasses. *Philosophical Transactions of the Royal Society a-Mathematical Physical and Engineering Sciences*, 370, 1352-1375.
- LAKHKAR, N. J., PARK, J. H., MORDAN, N. J., SALIH, V., WALL, I. B., KIM, H. W., KING, S. P., HANNA, J. V., MARTIN, R. A., ADDISON, O., MOSSELMANS, J. F. W. & KNOWLES, J. C. 2012. Titanium phosphate glass microspheres for bone tissue engineering. *Acta Biomaterialia*, 8, 4181-4190.
- PICKUP, D. M., GUERRY, P., MOSS, R. M., KNOWLES, J. C., SMITH, M. E. & NEWPORT, R. J. 2007. New sol-gel synthesis of a (CaO)(0.3)(Na2O)(0.2)(P2O5)(0.5) bioresorbable glass and its structural characterisation. *Journal of Materials Chemistry*, 17, 4777-4784.

APPENDICES

Appendix I:

A1. Indirect calculation of phosphate units

Instead of using ^{31}P MAS-NMR data, the amount of phosphate units can be obtained indirectly by assumption of exclusively network modifying roles for CaO and Na₂O. For example, in chapter 5, (P₂O₅)₅₅ - (CaO)₃₀ - (Na₂O)₁₅ sol-gel derived glasses may be written as Na_{39.2}Ca_{37.9}P₈₅O₂₇₀ according to the EDX results. The O/P ratio is 3.18 that suggests the phosphate species will be predominantly Q¹ and Q². The average formula for Q¹ and Q² phosphate species are (PO_{3.5})²⁻ and (PO₃)⁻ and in order to maintain electroneutrality the total cation charge of +115 must be balanced by a combination of these species:

$$115 = 2Q^1 + Q^2$$

And since there are a total of 85 phosphorus atoms per formula unit:

$$85 = Q^1 + Q^2$$

By using these two equations it can be found the Q¹ and Q² amount of 35 and 65 % respectively. These results show higher polymerisation in comparison with the obtained data from the ^{31}P MAS-NMR spectrum. These results suggested that may be higher synthesis temperature is needed to evaporate the remaining solvents and to make the phosphate network more interconnected. However, it would limit the potential biomedical applications of the phosphate-based sol-gel derived glasses that was the main aim of this project. Future work may focus on the effect of various heat treatment temperature on the polymerisation rate of the phosphate-based glasses.

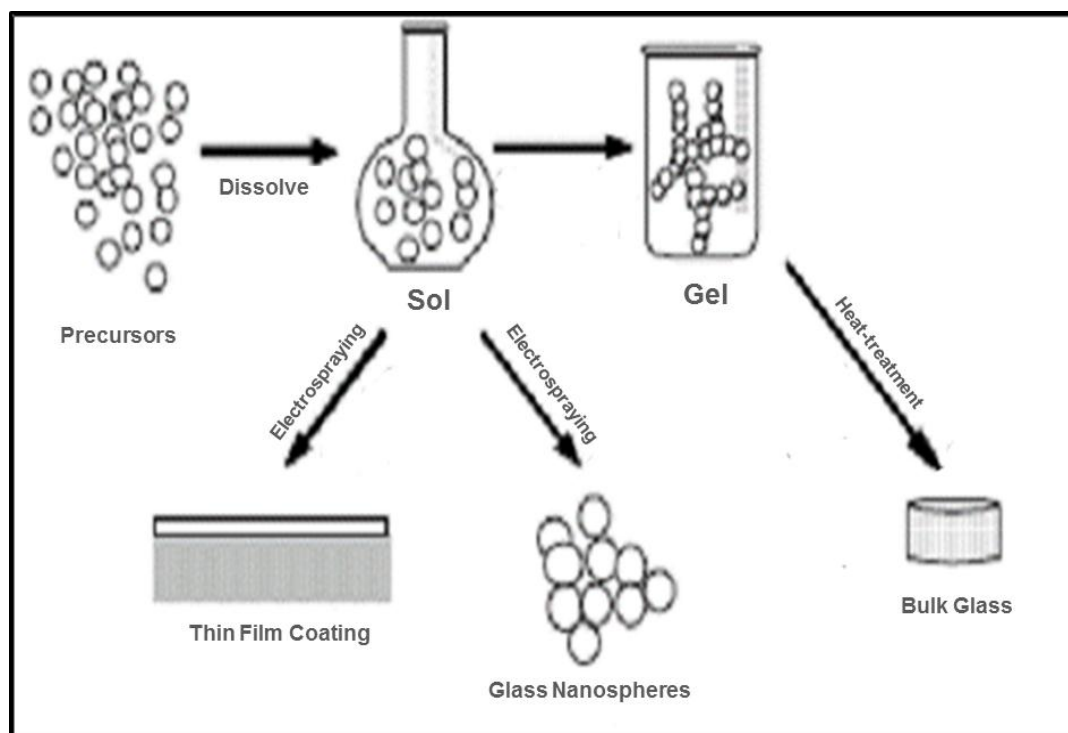


Figure A.1. Schematic of sol-gel synthesis of phosphate-based glasses to prepare thin film coating and glass nanospheres *via* electrospraying or to obtain bulk glasses *via* controlled heat-treatment of the gel over three weeks.

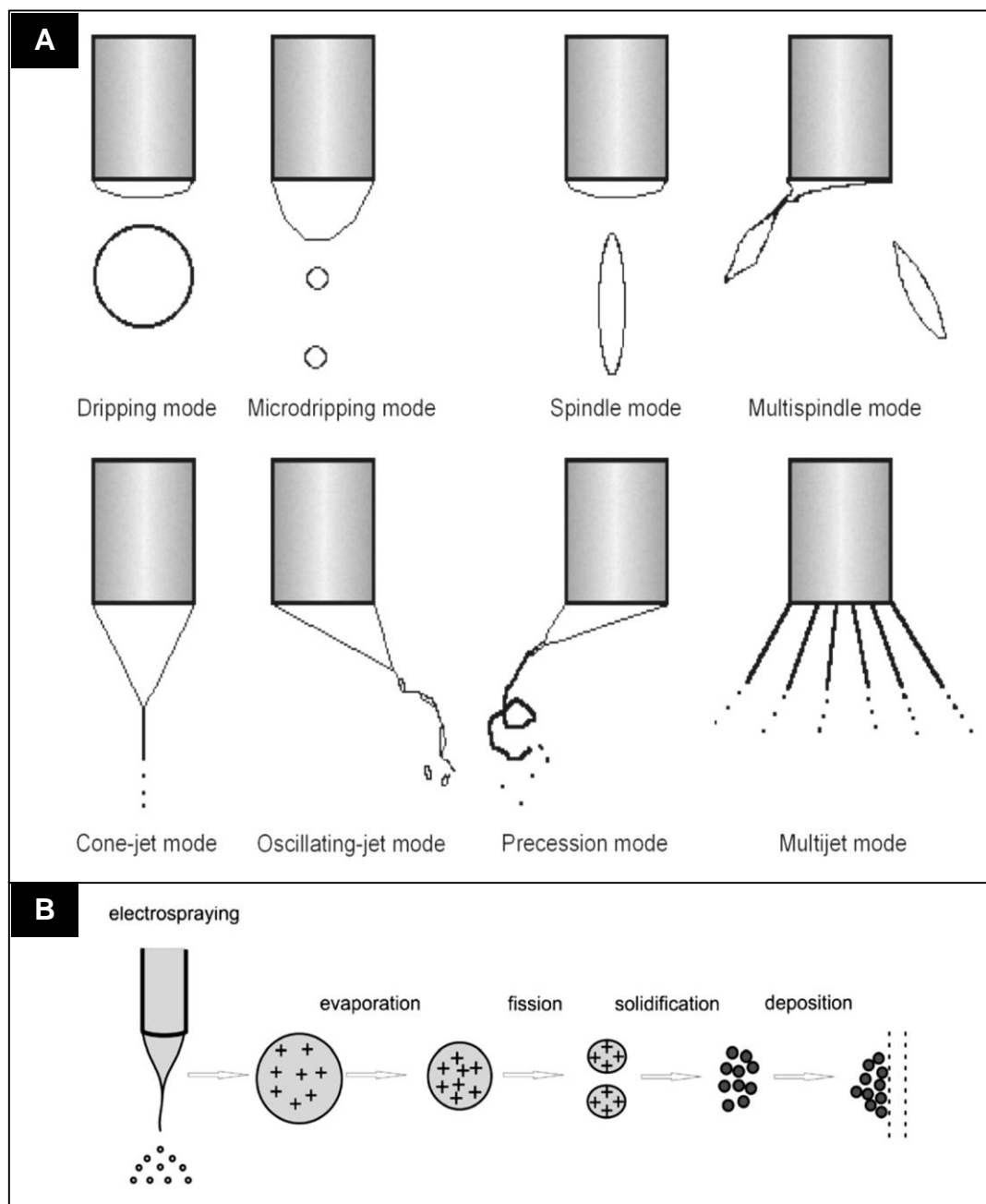


Figure A.2. Various electrospaying modes **(A)** and steps of nanospheres production *via* electrospaying **(B)** (Jaworek and Sobczyk, 2008).

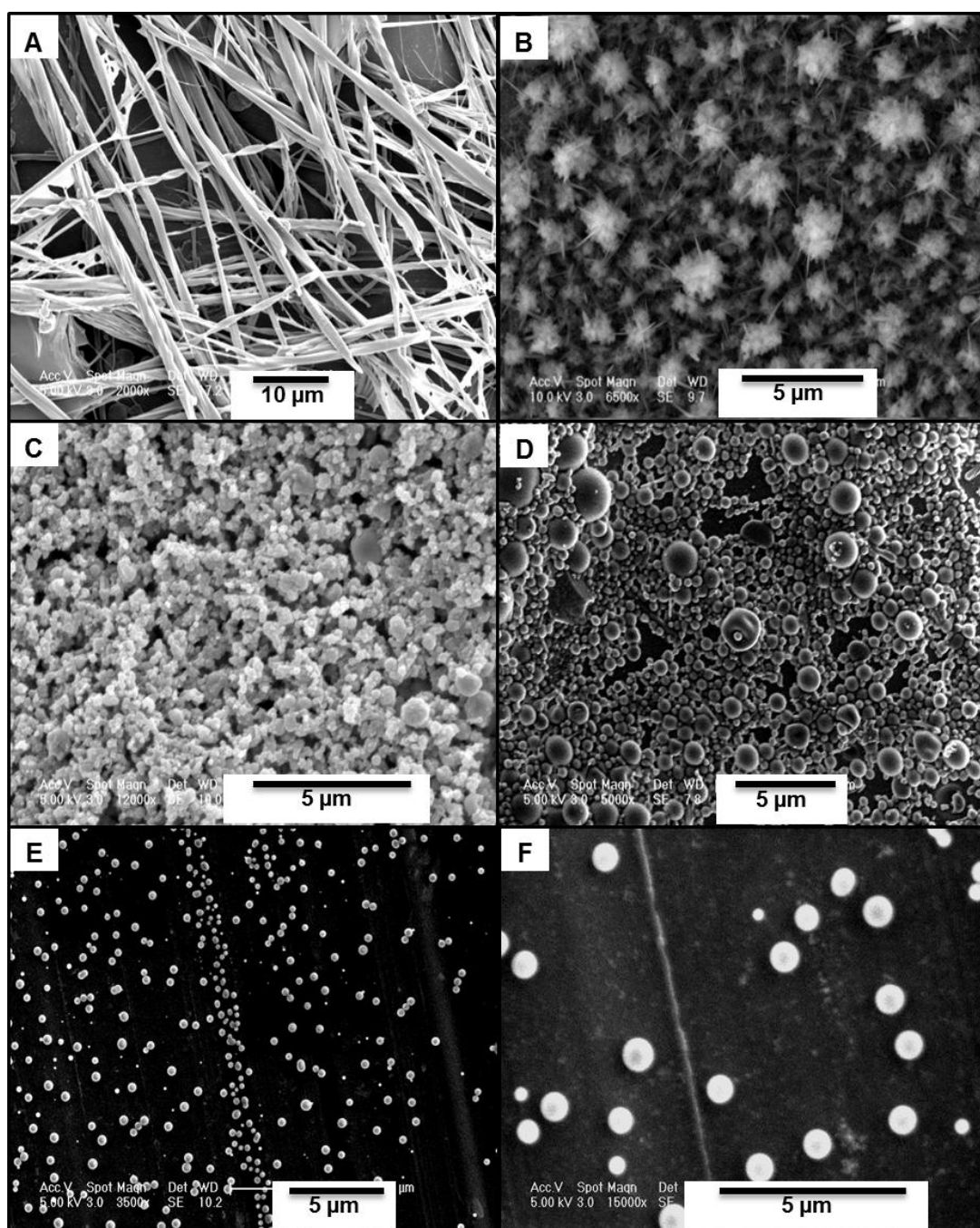


Figure A.3. SEM images of sol-gel derived glasses (after heat-treatment) created by electrospinning at; **A)** voltage of 12 kV and flow rate of 1 mL.h⁻¹, **B)** voltage of 15 kV and flow rate of 0.5 mL.h⁻¹, **C)** voltage of 18 kV and flow rate of 0.5 mL.h⁻¹, **D)** voltage of 20 kV and flow rate of 0.4 mL.h⁻¹, and voltage of 20 kV and flow rate of 0.2 mL.h⁻¹ (**E** and **F**).

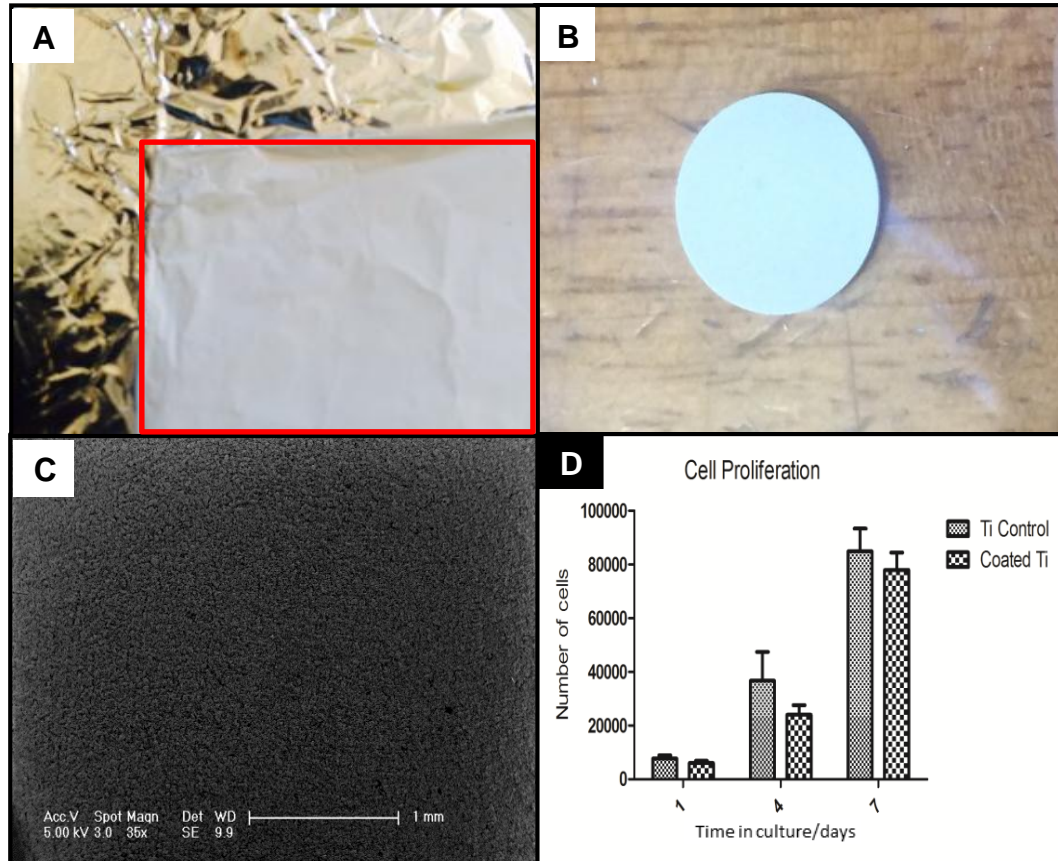


Figure A.4. Photographs of; electrodepositon of quaternary $(P_2O_5)_{55}-(CaO)_{25}-(Na_2O)_{10}-(TiO_2)_{10}$ glass on **(A)** aluminium foil and **(B)** titanium disc. Panel **C** is SEM image of coated titanium disc after heat-treatment at 200 °C. Initial cell proliferation study (MG-63 cells) results on Ti coated discs (n=3) is shown in panel **D**. Error bars represent the standard deviation.

Appendix II: List of publications

1. LEE, I. H., **FOROUTAN, F.**, LAKHKAR, N. J., GONG, M. S. & KNOWLES, J. C. 2013. Sol-gel synthesis and structural characterization of P2O5-CaO-Na2O glasses. *Physics and Chemistry of Glasses-European Journal of Glass Science and Technology Part B*, 54, 115-120.
2. LEE, I. H., SHIN, S. H., **FOROUTAN, F.**, LAKHKAR, N. J., GONG, M. S. & KNOWLES, J. C. 2013. Effects of magnesium content on the physical, chemical and degradation properties in a MgO-CaO-Na2O-P2O5 glass system. *Journal of Non-Crystalline Solids*, 363, 57-63.
3. **FOROUTAN, F.**, DE LEEUW, N., MARTIN, R., PALMER, G., OWENS, G. J., KIM, H.-W. & KNOWLES, J. C. 2015. Novel sol-gel preparation of (P2O5)0.4-(CaO)0.25-(Na2O)X-(TiO2)(0.35-X) bioresorbable glasses (X = 0.05, 0.1, and 0.15). *Journal of Sol-Gel Science and Technology*, 73, 434-442.
4. **FOROUTAN, F.**, JOKERST, J. V., GAMBHIR, S. S., VERMESH, O., KIM, H.-W. & KNOWLES, J. C. 2015. Sol-Gel Synthesis and Electrospinning of Biodegradable (P2O5)55-(CaO)30-(Na2O)15 Glass Nanospheres as a Transient Contrast Agent for Ultrasound Stem Cell Imaging. *ACS Nano*, 9, 1868-1877.
5. **FOROUTAN, F.**, WALTER, N. J., OWENS, G. J., MORDAN, N. J., KIM, H.-W. DE LEEUW, & KNOWLES, J. C. 2015. Sol-gel synthesis of quaternary (P2O5)55-(CaO)25-(Na2O)(20-X)-(TiO2)X bioresorbable glasses for bone tissue engineering applications (X = 0, 5, 10, or 15). *Biomedical Materials Journal*, accepted.
6. AL QAYSI, M., WALTER, N. J., **FOROUTAN, F.**, OWENS, G. J., & KNOWLES, J. C. 2015. Strontium- and titanium-containing phosphate-based glasses with prolonged degradation for bone tissue engineering. *Journal of Biomaterials Applications*, DOI: 10.1177/0885328215588898, (MQ, NW & FF contributed equally).
7. KNOWLES, J. C., OWENS, G. J., RAJENDRA, S., **FOROUTAN, F.**, AL QAYSI, M., LEE, E. J., HAN, M. N., MAHAPATRA, C., & KIM, H. W. Sol-gel Based Materials for Biomedical Applications: A Review. *Progress in Materials Science*, submitted.

Appendix III: List of conferences

1. **FOROUTAN, F., DE LEEUW, N., & KNOWLES, J.** *Novel sol-gel preparation of binary $(\text{TiO}_2)_x-(\text{P}_2\text{O}_5)_{(100-x)}$ nanospheres via electrospraying for biomedical applications ($x=40, 45, 50$). 4th International Conference on Nanotek, December 1-3, 2014, San Francisco, USA.*
2. **FOROUTAN, F., DE LEEUW, N., & KNOWLES, J. C.** *Sol-gel synthesis of $(\text{P}_2\text{O}_5)_{0.4}-(\text{CaO})_{0.25}-(\text{Na}_2\text{O})_{10}-(\text{TiO}_2)_{25}$ for drug delivery applications. 25st European Conference on Biomaterials, September 8-12, 2013, Madrid, Spain.*
3. **FOROUTAN, F., DE LEEUW, N. & KNOWLES, J. C.** *Novel sol-gel synthesis of $(\text{P}_2\text{O}_5)_{50}-(\text{CaO})_{30}-(\text{Na}_2\text{O})_{15}-(\text{Fe}_2\text{O}_3)_5$ glasses for biomedical applications. 26st European Conference on Biomaterials, September 1-4, 2014, Liverpool, UK.*